Unraveling the dynamic of MITF stability and nuclear localization and its role in regulating PRDM7

Hong Nhung Vu

Thesis for the degree of Philosophiae Doctor

June 2023

School of Health Sciences

FACULTY OF MEDICINE

UNIVERSITY OF ICELAND

Thesis title

Unraveling the dynamic of MITF stability and nuclear localization and its role in regulating PRDM7

Hong Nhung Vu

Thesis for the degree of Philosophiae Doctor

Supervisor(s)

Eiríkur Steingrímsson

Doctoral committee

Larue Lionel
Margrét Helga Ögmundsdóttir
Zophonías Oddur Jónsson
Hans Tómas Björnsson

June 2023

School of Health Sciences

FACULTY OF MEDICINE

UNIVERSITY OF ICELAND

Stöðugleiki og kjarnaflutningur MITF umritunarþáttarins og hlutverk við stjórnun á tjáningu PRDM7

Hong Nhung Vu

Ritgerð til doktorsgráðu

Leiðbeinandi/leiðbeinendur

Eiríkur Steingrímsson

Doktorsnefnd

Larue Lionel
Margrét Helga Ögmundsdóttir
Zophonías Oddur Jónsson
Hans Tómas Björnsson

Júní 2023

Heilbrigðisvísindasvið
LÆKNADEILD
HÁSKÓLI ÍSLANDS

ISBN 978-9935-9732-1-4

Printing by Háskolaprent.

ORCID: 0000-0002-8262-900X

Reykjavik, Iceland 2023

Ágrip

Umritunarþátturinn MITF (microphthalmia associated transcription factor) er mikilvægur fyrir sérhæfingu, fjölgun og lifun nokkurra frumugerða, þar með talið lifrumur í húð og augum, mastfrumur og beinátsfrumur. MITF gegnir einnig hlutverki í sortuæxlum þar sem það virkar sem rofi sem ákvarðar hvort frumurnar skipta sér eða ekki og hvort þær geta ferðast og myndað meinvörp. Ritgerð þessi fjallar um tvær spurningar: i) Hverjar eru sameindalíffræðilegar afleiðingar bælibreytingarinnar Mitfmi-sl í mús; og ii) Hvert er hlutverk PRDM7 gensins í sortuæxlum? Bælibreytingin Mitfmi-sl er breyting í Mitf geninu sem bælir svipgerðir annarra stökkbreytinga í Mitf geninu. Breytingin setur stopptákna í stað tákna K316, en það er þekkt SUMOyleringar-set í MITF. Þrátt fyrir að breytingin hafi verið þekkt í tvo áratugi hefur reynst erfitt að finna sameindalíffræðileg áhrif hennar. Með próteintjáningu, stökkbreytingum og western-blettun hefur mér tekist að sýna að breyting þessi hefur áhrif á bæði stöðugleika MITF próteinsins og staðsetningu þess í kjarna. Stökkbreytta MITFmi-sl próteinið getur dregið önnur prótein sem það getur myndað tvenndir með (villigerðar MITF, stökkbreytt MITF og TFE3) inn í kjarnann og þannig aukið eigin stöðugleika. MITFmi-sl próteinið getur bundið DNA og þegar það losnar úr ofangreindum tvenndum geta MITFmi-sl einstvenndir bundist DNA og örvað umritun. Auk þess hef ég sýnt að E318K stökkbreytingin sem eykur líkur á sortuæxlum í mönnum hefur einnig áhrif á stöðugleika MITF og staðsetningu í kjarna, en einungis ef S409 er ekki fosfært. Í seinna verkefninu sýndi ég að MITF stjórnar tjáningu PRDM7 en það er tjáð sérhæft í sortuæxlum og einungis að finna í prímötum. Ég sýndi að genið hefur áhrif á skiptingar og útlit sortuæxlisfruma auk þess sem það hefur áhrif á tjáning MITF próteinsins. Áhugavert er að bæði MITF og PRDM7 genin hafa svipuð áhrif á umbreytingar históna í sortuæxlisfrumum. Niðurstöðurnar benda til þess að áhrif MITF próteinsins fari að hluta í gegnum áhrif þess á PRDM7.

Lykilorð: Mitf, stöðugleiki, flutningur úr kjarna, bælibreyting, PRDM7, umbreytingar históna.

Abstract

Microphthalmia-associated transcription factor (MITF) is known as an essential regulator of melanocyte differentiation, proliferation, survival, and differentiation of multiple cell lineages, including neural crest-derived melanocytes, pigmented epithelial cells of the eye, mast cells, and osteoclasts. In melanoma cells, it plays a critical role as a lineage-survival oncogene. MITF may act as a switch that determines whether cells proliferate or become quiescent, thus allowing migration and formation of metastases. In this thesis, I investigated two questions: i) What are the molecular consequences of a suppressor mutation in mouse Mitf, $Mitf^{mi\text{-}sl}$ and ii) What is the role of PRDM7 in melanoma. The $Mitf^{mi\text{-}sl}$ suppressor mutation is an intragenic suppressor mutation discovered over two decades ago, but the molecular effects have been elusive. Using protein expression, mutagenesis, and western blotting, I have shown that this mutation affects both protein stability and nuclear localization of MITF. Interestingly, the $Mitf^{mi\text{-}sl}$ mutant protein can drag its dimerization partner proteins, including wild-type MITF, mutant MITF, or TFE3, into the nucleus, thus improving its own stability. This is likely to explain the suppressor phenotype. In addition, I have shown that the E318K mutation, which predisposes melanoma in humans, also affects stability and nuclear localization in concert with S409, providing information about the molecular mechanism involved. This is a novel way of action for suppressor mutation and for cancer predisposition. In the second project, I have shown that MITF regulates the expression of PRDM7, a primate-specific gene specifically expressed in melanoma. This gene, in turn, affects cell morphology and proliferation and MITF protein expression level. Interestingly, both MITF and PRDM7 mediate changes in the distribution of histone marks. Our results suggest that MITF mediates its role in regulating extracellular matrix organization, proliferation, and histone modification partially through PRDM7.

Keywords: Mitf, stability, nuclear export, suppressor mutation, Prdm7, histone modification.

Acknowledgments

All of the above, I would like to express my greatest appreciation to my supervisor Prof. Eiríkur Steingrímsson, colleagues, friends, and family for everything you did to make this dissertation possible.

I owe my deepest gratitude to my supervisor Prof. Eiríkur Steingrímsson for his continuous support, caring, and patience during the planning and development of the projects. It is a pleasure to thank his willingness to give his time so generously for guiding, inspiring, and making me what I am today. I will never forget that he is the only person who gave me the opportunity to return to the lab, where I think I truly belong. Thanks to him for letting me work on the PRDM7 project, which taught me much about being patient, and the suppressor project, which gave me an excellent opportunity to learn and understand how exciting science is! I will always cherish the memory of him being the nicest Icelander who was always there to protect me from the negative and encourage me toward the future. I feel a sense of assurance just by seeing the light on in his office. No words can fully express my deep appreciation for all he has done for me. I wish him the feeling of love, good time, and good cheer in the coming days.

I would also like to thank my Ph.D. committee members, Prof. Larue Lionel, Prof. Margrét Helga Ögmundsdóttir, Prof. Zophonías Oddur Jónsson, Prof. Hans Tómas Björnsson for their guidance and suggestions through my studies and this dissertation. Especially to Larue Lionel, I am grateful for his endless questions and comments, which inspire me a lot, and to be honest, I love his questions so much. I wish for a full day to discuss my project with him and answer all his challenging questions.

My sincere appreciation is extended to administrators and staff at the Department of Biochemistry and Molecular Biology at the BioMedical Center of the University of Iceland, Reykjavik, Iceland, especially Erikur's Lab members. My special thanks are sent to Dr. Sara Sigurbjörnsdóttir and Dr. Ramile Dilshat for their tutoring, critical comments, suggestions, encouragement, and kindness. May they continue to shine and achieve great things in everything they do.

I am also indebted to my friends, who always stand by me. I would like to thank Clem, Evangeline, Thejus, Abbi, Teitur, Kevin, and Romain for the fun times, their candies, everything they support, and for being wonderful members of our

"complaining club". Without them, my life in the lab would be boring. Especially to Clem, more than being a friend, I would like to send my appreciation to her for being with me at a special moment in my life and supporting me unconditionally. Also, I would thank Matti for the intense discussions on protein structures and for teaching me a lot about thinking about them. Wishing all of them a fulfilling and rewarding journey ahead. You have my full support!

To my family, thanks, mom and dad, for letting me know that I always have a home to come back to and, importantly, never asking me what I have been researching or what MITF and PRDM7 are. That simply makes my life easier and more comfortable since I do not need to make complicated things become simple. Bố Giang, mẹ Ninh và mẹ Tâm, những năm tháng con sống ở đây thực sự đã rất vui vẻ! Tất cả mọi người ở trong lab giúp đỡ và dạy con rất nhiều. Dù cũng có những điều có thể chưa hài lòng, thỉ nh thoảng vẫn cằn nhằn chỗ này chỗ kia, nhưng con thấy mãn nguyện khi được sống trọn vẹn trong suốt 3 năm qua và rất sẵn sàng cho hành trình tiếp theo của gia đình thỏ!

Chú thỏ yêu quý, cảm ơn anh đã luôn ủng hộ, yêu thương và động viên em. Mong chúng ta sớm được "đoàn tụ", cả nhà mình trộm vía sẽ được đón em bé yêu thương! Chúng mình cùng cố gắng như đã từng và cùng nhau học những điều thú vị ở một đất nước khác nhé! Vẫn là câu nói kinh điển: Không sao đâu, chúng mình có nhau mà!

Last but not least, I would like to thank myself, Nhung's version_2018-2023, when you were strong enough to give up on time and when you tried your best and enjoyed your time in the lab. Thanks to your love in MITF and endless Western blots. For Nhungs's version 2023, sometimes you need to slow down to learn what you can not know when running! I hope I can make a good choice for the future!

Once again, thanks for all!

Vu Hong Nhung

Contents

List of abbreviations

5hmC	Hydroxymethyl-cytosine
5mC	Methyl-cytosine
ACTH	Adrenocorticotropic hormone
bHLH-Zip	Basic helix-loop-helix leucine zipper
cAMP	Cyclic adenosine monophosphate
CDH1	Cadherin 1/E-cadherin
CDK4	Cyclin dependent kinase inhibitor 4
CDKN2A	Cyclin dependent kinase inhibitor 2A
cDNA	Complementary deoxyribonucleic acid
Dapi	4′ ,6-diamidino-2-phenylindole
DCT	Dopachrome Tautomerase
DEGs	Differentially expressed genes
DMSO	Dimethyl sulfoxide
DNA	Deoxyribonucleic acid
ECM	Extracellular matrix
EMT	Epithelial to mesenchymal transition
EZH2	Zeste homolog 2
FAMMM	Familial atypical multiple mole-melanoma syndrome
GNAT	GCN5-related N-acetyltransferase
GO	Gene Ontology
h	hour
H3K27ac	Histone 3 Lysine 27 acetylation
H3K27me3	Histone 3 Lysine 27 trimethyl
H3K36me3	Histone 3 Lysine 36 trimethyl
H3K4me1	Histone 3 Lysine 4 monomethyl
H3K4me3	Histone 3 Lysine 4 trimethyl
H3K79me3	Histone 3 Lysine 79 trimethyl
H3K9me3	Histone 3 Lysine 9 trimethyl
H4K20me3	Histone 3 Lysine 20 trimethyl
HATs	Histone acetyltransferases

HDACs	Histone deacetylases
HMTs	Histone methyltransferases
KD	Knock down
KMTs	Lysine methyltransferases
KO	Knock-out
MAPK	Mitogen-activated protein kinase
MAS	Melanoma-astrocytoma syndrome
MC1R	Melanocortin-1 receptor
miRNA	MicroRNA
MITF	Microphthalmia-associated transcription factor
MLANA	Melanocyte antigen A
mRNA	Messenger RNA
MSCs	Melanocyte stem cells
OE	Overexpression
PAX	Paxillin
PcG	Polycomb group
PRC2	Polycomb repressive complex 2
PRDM7	PR domain-containing Protein 7
PRMTs	Arginine methyltransferases
PTMs	Post translational modification
qPCR	Quantitative reverse transcription PCR
RB	Retinoblastoma protein
RHC	Red hair color
RNA	Ribonucleic acid
RNA	seq RNA sequencing
SA-β-gal	Senescence-associated beta-galactosidase
SDS-PAGE	Sodium dodecyl-sulfate polyacrylamide gel electrophoresis
SETDB1	SETDB2 SET domain bifurcated 1
siRNA	Small interfering RNA
TFEB	Transcription factor EB
TGFa	Transforming growth factor alpha
TGFβ	Transforming growth factor beta
THBS1	Thombospondin-1
TYR	Tyrosinase
TYRP1	Tyrosinase-related protein 1

TYRP2	Tyrosinase-related protein 2
UV	Ultraviolet
ZEB1	Zinc finger E-box binding homeobox 1
ZEB2	ZEB2 Zinc finger E-box binding homeobox 2
α-MSH	α-melanocyte-stimulating hormone
µL	Microliter
µM	Micromolar
µM	Micrometer

List of Figures

List of tables

List of papers

This thesis is partly based on the following original publications and manuscripts:

I. Vu HN, Dilshat R, Fock V, Steingrímsson E. **User guide to MiT-TFE isoforms and post-translational modifications**. Pigment Cell Melanoma Res. Jan 2021;34(1):13-27. doi:10.1111/pcmr.12922

II. Vu HN, Arnheiter H, Valdimarsson MM, Bergsteinsdóttir K, Debbache J, Keren Bismuth, Skuntz S, Swing DA, Hallsson JH, Larue L, Heidarsson PO, Copeland NG, Jenkins NA, Steingrímsson E. **An induced suppressor mutation in mouse MITF unravels the effects of the melanoma-predisposing E318K mutation in humans.** *Manuscript in preparation*.

III. Vu HN, Dilshat R, Steingrímsson E. **Functional roles of PRDM7 and its regulation by MITF.** *Manuscript in preparation*.

Papers to which I contributed:

IV. Dilshat R, Vu HN, Steingrímsson E. **Epigenetic regulation during melanocyte development and homeostasis.** Exp Dermatol. Aug 2021;30(8):1033-1050. doi:10.1111/exd.14391

Declaration of contribution

I designed the experiments described in the first part of the thesis with the assistance of my supervisor Prof. Eiíkur Steingrímsson. Prof. Eiríkur Steingrímsson carried out the original screen for suppressor mutations in mice. I performed all the experiments involving characterizing the effect of MITF mutations on localization and stability, effects on dimerization, and on gene transcription.

All the experiments described in the PRDM7-part of the thesis were designed and performed by me in collaboration with my supervisor, Prof. Eiíkur Steingrímsson, and Dr. Ramile Dilshat, a previous Ph.D. student and postdoc in the Steingrímsson lab. I generated the PRDM7 knock-out cells and conducted experiments to characterize the functional roles of PRDM7 in melanoma. In addition, I performed RNA-seq bioinformatic analysis to study the transcriptomic of PRDM7 knock-out cells and their corresponding control cell lines. I further carried out Cut&Run for the H3K4me3, H3K9me3, and H3K27me3 histone marks in PRDM7 and MITF knock-out cells and analyzed the data to study the epigenetic alteration upon deletion of PRDM7 and MITF, respectively.

I prepared all the figures and wrote the text for the review all post-translational modifications and isoforms in MITF and the related transcription factors TFEB, TFE3, and TFEC (Paper I) together with my supervisor. I wrote the manuscript (in preparation) on the MITF suppressor paper (Paper II) together with my supervisor and prepared all the figures except the mouse figures. I have written an early draft of a manuscript on PRDM7 and prepared all the figures for that manuscript. In addition, I searched for references and designed Figure 2 and Table 1 in the review paper on epigenetic regulation during melanocyte development (*Dilshat R. el., al 2021* - Paper III) and contributed to the writing together with the other authors.

1 Introduction

1.1 Melanocytes and melanogenesis

Melanocytes are the melanin-producing cells that can be primarily found in the epidermis, hair, eyes/iris, inner ear, nervous system, heart, and other tissues (Brito and Kos, 2008; Le Douarin et al., 1999; Tachibana, 1999; Yajima and Larue, 2008). The development of melanocytes starts with the differentiation of melanoblasts which originate directly from the neural crest (Figure 1). Specification of melanoblasts occurs during neural crest delamination, after which the cells migrate into the migration staging area (MSA), an extracellular matrix-rich wedge-shaped area that is located between the somite and the dorsal neural tube. Melanoblasts then migrate between the somites and epidermis (the dorsolateral pathway) and proliferate during the migration process. While, in mice, most of the melanoblasts enter the epidermis and then occupy the hair bulb, most of the melanoblasts in humans remain in the epidermis except in the palm of the hand and feet (Bertrand et al., 2020; Dilshat et al., 2021b). When moving toward the hair follicle, some of the melanoblasts enter the hair matrix, where they differentiate into melanocytes, whereas other melanoblasts enter the bulge of the hair and form quiescent melanocyte stem cells (MSCs), which eventually differentiate into melanocytes during the hair cycle (Bertrand et al., 2020; Dilshat et al., 2021b). Briefly, during the anagen phase of the hair growth cycle, MSCs differentiate into immature melanocytes and produce melanin, while in catagen and telogen, the melanocyte population in the hair follicle is reduced, and MSCs maintain a pool of undifferentiated melanocyte precursors that can be activated to regenerate the melanocyte population in the next anagen phase (Nishimura, 2011). A second wave of melanoblast development has also been described, particularly for melanocytes in the skin of the trunk and limbs, which originate from derivatives from neural crest-derived Schwann cells through the ventral pathway (between somites and neural tubes) (Figure 1) (Bertrand et al., 2020; Cichorek et al., 2013; Dilshat et al., 2021b). In the skin, a mature melanocyte, together with approximately 30-40 of its surrounding keratinocytes, forms a pigmentary unit.

Melanin synthesis in melanocytes is stimulated by the binding of either α-melanocyte-stimulating hormone (α-MSH) or adrenocorticotropic hormone

(ACTH), secreted by neighboring cells, including keratinocytes, to melanocortin-1 receptor (MC1R) on melanocytes. MC1R then activates the cyclic adenosine monophosphate (cAMP) pathway, which subsequently upregulates the expression of the MITF transcription factor, often termed the master regulator of melanocyte development. MITF, in turn, activates the expression of pigment genes involved in melanin synthesis, including the enzymes tyrosinase (TYR), tyrosinase-related protein 1 (TYRP1), and dopachrome tautomerase (DCT) (Meyle and Guldberg, 2009). Two basic forms of melanin, reddish-yellow pheomelanin, and black photoprotective eumelanin, are the final products of this melanin synthesis process. Those two forms, which differ in color and way of synthesis, are synthesized in specialized cytoplasmic organelles called melanosomes (Sturm, 2009). The pigment phenotype of an individual is determined by the ratio of these two types of melanins (Sturm, 2009). Although both humans and mice produce eumelanin and pheomelanin, their relative amounts and distribution differ; human skin contains mainly eumelanin, while mouse skin has a higher proportion of pheomelanin (Ito and Wakamatsu, 2003). Melanosomes are subsequently transferred to neighboring keratinocytes and benefit the body by acting like a shield and protecting the genetic material in the nuclei from ultraviolet (UV) light. Melanosomes also play important roles in ion storage (Bush and Simon, 2007; Costin and Hearing, 2007; Riley, 1997).

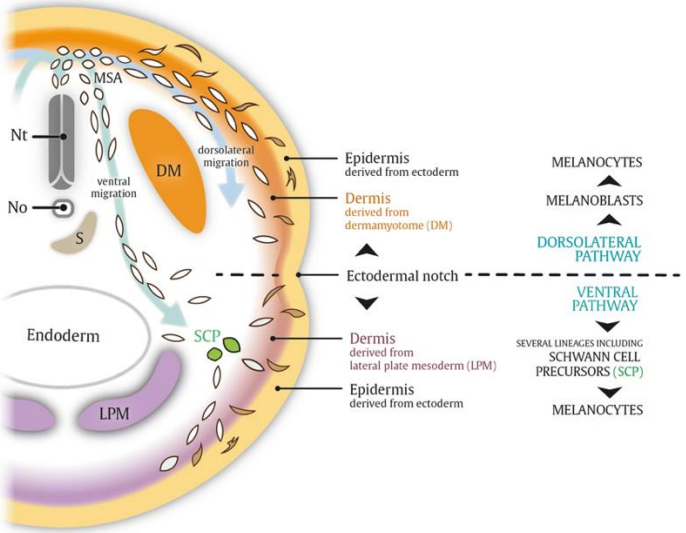

Figure 1. Neural crest migration and melanocyte development model. Figure obtained with permission from Springer Nature according to permit number 5513590971375 (Vandamme et al., 2019)

1.2 Melanoma Epidemiology and risk factors

Melanoma is the malignancy of melanocytes (Mc), melanocyte stem cells (McSC), or transit-amplifying cells (TACs). While cutaneous melanoma arises from melanocytes in the epidermis and is the most common form of melanoma, melanoma can also arise in mucosal surfaces, the uveal tract, and leptomeninges (Leonardi et al., 2018). Unfortunately, the incidence of cutaneous melanoma has been rising worldwide much faster than other types of cancer (Leonardi et al., 2018). In addition, melanoma is the most frequent neoplasm in young adults, especially in women (Rastrelli et al., 2014).

The environment, host factors, and their interplay have been identified as major risk factors for melanoma (Ali et al., 2013; Leonardi et al., 2018). Exposure to UV radiation, particularly UV-A and UV-B radiation from both sun exposure and artificial sources, is a major environmental risk factor for cutaneous melanoma. UV radiation can cause DNA damage and mutations in skin cells, as well as suppress the immune system's ability to detect and destroy cancer cells, contributing to the development of melanoma (Anna et al., 2007; Falzone et al., 2016; Gilchrest et al., 1999; Pennello et al., 2000). Interestingly, intermittent (rather than chronic) and high levels of sun exposure during childhood increases the risk of melanoma (Bertrand et al., 2020). In addition, alcohol, heavy metals, and pesticides are environmental factors that have been linked with melanoma development, although the mechanism behind their contribution is still unknown (Bertrand et al., 2020).

Host factors, including melanocytic nevi, genetic susceptibility, and family history, have also been associated with melanoma predisposition (Leonardi et al., 2018). It has been shown that the size and the number of melanocytic nevi positively correlate with melanoma risk (Bertrand et al., 2020; Grob et al., 1990; Halpern et al., 1991; Watt et al., 2004). The risk of melanoma is also increased in families susceptible to familial atypical multiple mole-melanoma syndrome (FAMMM syndrome) and the melanoma-astrocytoma syndrome (MAS) (Soura et al., 2016), which has been described with typical phenotypic features including high nevi count and multiple precancerous dysplastic nevi. While FAMMM syndrome is commonly associated with the alteration of p16 (*CDKN2A*) and rarely with *CDK4* and *MITF* mutations (Truderung et al., 2021), MAS syndrome is caused by mutations in *CDKN2A* gene. Various syndromes and conditions also contribute to the incidence of melanoma, including retinoblastoma, Werner syndrome, xeroderma pigmentosum, neurofibromatosis, and immunosuppression conditions (e.g., iatrogenically or HIV infections) (de Snoo and Hayward, 2005; Saginala et al., 2021).

Previous work has also indicated that 10% of cutaneous melanoma is due to mutations in various genes (Bertrand et al., 2020). The genetic susceptibility can be traced to changes in DNA sequence (mutation, amplification, or translocation) or epigenetic modifications (DNA methylation, chromatin alterations, or histone modification) (Giunta et al., 2021; Sarkar et al., 2015; Truderung et al., 2021). These genetic alterations act as melanoma genetic drivers through biasing the cell homeostasis, proliferation, metabolism, apoptosis, cell cycle control, and replicate lifespan (Akbani et al., 2015; Hodis et al., 2012; Leonardi et al., 2018). This will be described in the following chapters.

1.3 Germline mutations in melanoma

1.3.1 CDKN2A and CDK4

Germline mutations in approximately 20 genes are found to be associated with an increase in the risk of melanoma (Bertrand et al., 2020). By using different reading frames, the CDKN2A locus encodes two different functional and structural tumor suppressor proteins, called $p14^{ARF}$ and $p16^{INK4a}$ (Meyle and Guldberg, 2009). Therefore, mutations, deletions, or promoter hypermethylation of *CDKN2A* may affect both $p14^{ARF}$ and $p16^{INK4a}$ or each gene independently. The mediator roles of $p16^{INK4a}$ and $p14^{ARF}$ in melanocyte senescence and melanoma suppression have been well-described (Bennett, 2003; Meyle and Guldberg, 2009). On the one hand, the loss of $p14^{ARF}$ due to mutations might activate ubiquitin ligase activity of the MDM2 protein, leading to the inactivation of the p53 senescence barrier and, in turn, inhibit of the cyclin-dependent kinase inhibitor p21 (Meyle and Guldberg, 2009). On the other hand, $p16^{INK4a}$ inhibits the cyclin-dependent kinases *CDK4* and *CDK6*, leading to the activation of retinoblastoma protein (RB) by preventing it from phosphorylation. Hypo-phosphorylation of the RB protein subsequently inhibits the E2F protein from regulating the expression of genes required for entering the S-phase. Loss-of-function variants in the $p14^{ARF}$ and $p16^{INK4a}$ genes stop the cell cycle from going from the G1 phase to the S phase. Inactivation of $p16^{INK4a}$ has been found in the majority of melanoma specimens. Loss-of-function variants in CDKN2A are a critical factor in bypassing senescence in melanocytes and keeping them from undergoing growth arrest (Bennett, 2008; Bertrand et al., 2020; Dahl and Guldberg, 2007; de Snoo and Hayward, 2005). However, some *CDKN2A* and *CDK4* mutation carriers are free of melanoma (Meyle and Guldberg, 2009), suggesting that environmental factors may be involved. The importance of environmental exposure, co-genetic susceptibility, and host-phenotype in

modulating the penetrance of melanoma has been further suggested (Ali et al., 2013). Although *CDKN2A* mutations are found in melanoma families (Berwick et al., 2006; Goldstein et al., 2007), they have also been frequently identified among kindreds with pancreatic and neural system tumors (Borg et al., 2000; Randerson-Moor et al., 2001).

Mutations in *CDK4* have also been found in melanoma families. Only two mutations are known in the *CDK4* gene, namely R24H and R24C. Carriers of the *CDK4* variants showed an increased incidence of early onset malignant melanoma (Read et al., 2016). Interestingly, mutations in *CDKN2A, CDK4*, and *RB1* occur mutually exclusive, suggesting that they encode critical elements for suppressing melanoma development (Bartkova et al., 1996; Walker et al., 1998).

1.3.2 MITF

As the key regulator in the proliferation and survival of melanocytes and an important factor in melanoma development, both loss-of-function and gain-of-function mutations in *MITF* might significantly affect melanocyte homeostasis and proliferation, eventually initiating melanoma progression. Previous studies have shown that the germline E318K mutation in MITF protein increases the risk of melanoma by 2 to 5-fold. In an Australian case-control study of 2,059 cases, it increased the risk by 2.33-fold, whereas in a UK case-control study of 1,929 cases, this mutation increased the risk of melanoma by 2.09-fold (Yokoyama et al., 2011). The risk was increased 4.8-fold in a French study of 586 melanoma patients (Bertolotto et al., 2011) and 2.9-fold in a study of 667 Italian melanoma patients (Ghiorzo et al., 2013). The MITF-E318K mutation not only increases the risk of melanoma but also raises the incidence of pancreatic cancer (PC) and renal cell carcinoma (RCC) (Bertolotto et al., 2011; Ghiorzo et al., 2013). Surprisingly, MITF-E318K mutation carriers showed no skin pigmentation defects and no association with hair color or freckling. However, carriers had higher nevus count and non-blue eye color and suffered from multiple primary melanomas (Bertolotto et al., 2011; Sturm et al., 2014; Yokoyama et al., 2011). Non-blue eye color is likely influenced by the gain-of-function activity of MITF-E318K mutation and may also reflect the transition from pheomelanin to eumelanin. Interestingly, amelanotic melanoma occurs with higher frequency in MITF-E318K carriers (30.7%) than in general melanoma patients (2–8%) (Sturm et al., 2014). Heterozygous mice carrying the $Mitf^{E318K}$ mutation had no signs of nevi or melanoma development. However, on the $Braf^{V600E/+}$ background, $Mitf^{E318K/+}$ mice showed an increase in the number of nevi. The $Mitf^{E318K/+}$, $BRaf^{V600E/+}$ mouse model did not increase melanoma progression unless Pten was also deleted. Furthermore, the $Mitf^{E318K/+}$, $BRaf^{V600E/+}$, $Pten^{-/-}$ mice showed earlier

and faster onset of pigmented lesions and reduced survival time compared to $BRaf^{V600E/+}$, $Pten^{-/-}$ (Bonet et al., 2017). Unfortunately, none of the previous work has investigated the link between MITF-E318K and $BRAF^{V600E}$ mutations in melanoma patients. In previous studies, *CDKN2A* mutation carriers were not included in the cohort to avoid the masking effect of *CDKN2A* on the MITF-E318K mutation (Bertolotto et al., 2011; Ghiorzo et al., 2013). Hence, the interplay between *CDKN2A* variants and MITF-E318K was not studied. Also, no evidence indicates an interaction between *MC1R* loss-of-function variants and the MITF-E318K mutation (Berwick et al., 2014).

At the molecular level, the MITF-E318K mutation is located in a SUMO consensus site (ΨKXE) (Figure 2), and consistent with that, the E318K mutation impaired SUMOylation of MITF at the K316 residue; SUMOylation still can take place at K182 (Bertolotto et al., 2011; Bonet et al., 2017; Yokoyama et al., 2011). The E318K mutation has some but limited effects on the transcriptional activity of a limited subset of its target genes. Bertolotto et al., (2011) did not detect any difference between the transcriptional activity of MITF-E318K and MITF-WT from the *MET*, *TYR*, and *CDKN2A* promoters using reporter assays in 501Mel cells. However, MITF-WT showed less efficiency in activating the HIF1A promoter than the E318K mutant protein (Bertolotto et al., 2011). Transcriptomic analysis showed that in RCC4 renal carcinoma cells, the MITF-E318K protein increased the expression of genes involved in cell growth, proliferation, and inflammation. However, in A375 melanoma cells, no differences were observed in genes regulated by MITF-WT and MITF-E318K proteins (Bertolotto et al., 2011). In the transcriptomic analysis performed by Yokoyama et al. (2011), the MITF-E318K protein led to an increase in the expression of pigment genes as well as in melanin content compared to the MITF-WT protein (Yokoyama et al., 2011). Inconsistent with that, it has been reported that heterozygous and homozygous $Mitf^{E318K}$ mice are slightly hypopigmented compared to $Mitf^{wt}$ (Bonet et al., 2017). ChIP-seq analysis of cells overexpressing the MITF-E318K-HA fusion protein in 501Mel cells showed a significant increase in the number of binding sites compared to that observed upon overexpressing MITF-WT. Although the higher number of binding sites upon MITF-E318K overexpression is mostly due to weakly occupied sites, some of the binding sites are preferentially occupied by MITF-E318K (Bertolotto et al., 2011). Interestingly, IHC analysis using anti-MITF antibodies on melanoma samples from MITF-E318K and MITF-WT suggested that MITF is intensively stained in the nucleus, and no significant differences were observed in nuclear/cytoplasmic MITF staining ratio between MITF-WT and MITF-E318K carriers. Fewer MITF-E318K tumor samples showed cytoplasmic staining (3 out of 19), hypothesizing that the mutant protein may accumulate mainly in the

nucleus and, in distinct circumstances, did not present in the cytoplasm (Sturm et al., 2014).

Forced expression of the BRAF^{V600E} protein in Mel-ST melanocytes stimulated SA-β-gal activity, which was suppressed in the presence of the MITF-E318K mutant protein but not in the presence of MITF-WT protein (Bonet et al., 2017). BRAF^{V600E} reduced the incorporation of BrdU in cells overexpressing MITF-WT. However, the effect on BrdU incorporation in cells expressing MITF-E318K and BRAF^{V600E} was not observed (Bonet et al., 2017). This work suggests that MITF-E318K suppresses BRAF^{V600E}-induced senescence, but the underlying mechanism remains unclear. Further, the MITF-E318K mutation increases migration and invasion in 501Mel and VHL-deficient RCC4 cells but not in A375P cells (Bonet et al., 2017). It is known that A375P cells express a low level of endogenous MITF compared to that of 501Mel and VHL-deficient RCC4 cells. The expression of MITF-E318K resulted in an increased number of colonies in melan-a and RCC cells; however, it did not affect the proliferation of those cells (Bertolotto et al., 2011). This suggests a potential role of MITF-E318K in phenotype switching of melanoma cells. However, the exact mechanism of how the MITF-E318K variant leads to melanoma remains unknown.

Figure 2. Protein sequence alignment from Human to Tetraodon shows that the ΨKXE sumoylation motif is highly conserved. Figure obtained with permission from Springer Nature according to permit number 5514171050106 (Bertolotto et al., 2011)

1.3.3 MC1R

The melanocortin-1 receptor *(MC1R),* a seven-transmembrane G-protein coupled receptor, has been proposed to act as a melanoma susceptibility factor. Among 60 nonsynonymous *MC1R* variants, some (e.g., ins86-87A, D84E, R142H, R151C, R160W, R294H) have been shown to result in a decrease in cAMP activation upon α-MSH stimulation. These mutations reduce the production of eumelanin and therefore determine the melanoma-associated red hair color (RHC) phenotype (Beaumont et al., 2007), which is characterized by fair skin,

red hair, freckles, poor tanning response, and solar lentigines (Raimondi et al., 2008). Previous meta-analyses have shown that the frequency of some *MC1R* variants is positively correlated with both melanoma incidence and melanogenesis, while other variants are only associated with melanogenesis (Raimondi et al., 2008). It has also been suggested that the risk of melanoma upon *MC1R* mutations might go beyond their effect on pigmentation (Meyle and Guldberg, 2009). Remarkably, the association between inherited risk factors and acquired variants in melanoma development is observed in the case of *MC1R*, with a significantly higher rate of BRAF mutations observed in *MC1R* variant carriers than in non-MC1R carriers (Dhomen and Marais, 2007). The *MC1R* mutations have also been shown to increase the penetrance of *CDKN2A* mutations, which are highly associated with melanoma, possibly together with environmental factors (e.g. UV light and geographic variants) that affect the onset of melanoma (Box et al., 2001). *MC1R* mutations have also been suggested to be linked with Parkinson's disease (Chen et al., 2017). Since agouti-signaling protein (ASIP) enables elevation of pheomelanin production by antagonizing the binding of α-MSH to MC1R, gained function of *ASIP* mutations might show a similar pattern as loss-of-function variants in *MC1R* and could therefore be considered as low-penetrance melanoma susceptibility alleles (Bastian and Pinkel, 2008). Variants in other pigment genes, including *TYRP1*, *TYR, OCA2, MATP, OCA4, KIT, and PARP1,* also slightly increase the risk of melanoma (Bertrand et al., 2020).

1.3.4 Others

Germline mutations in *TERT, POT1, ACD*, and *TERF2IP* also increase the risk of melanoma. Mutations in *TERT* (telomerase reverse transcriptase) promoter and coding regions, *POT1, ACD*, and *TERF2IP* (all of which encode proteins of the shelterin complex) caused longer telomeres and favored senescence bypass (Aoude et al., 2015; Harland et al., 2016; Horn et al., 2013; Robles-Espinoza et al., 2014). Additionally, loss-of-function mutations in *BAP1,* nonsense-mutation in *RAD51B*, and a missense-mutation in *POLE* (p.W347C) lead to the impairment of the DNA repair response and have also been identified in melanoma families (Aoude et al., 2015; Wiesner et al., 2011).

1.4 Somatic mutations in melanoma

In addition to the germ-line mutations discussed above, numerous somatic mutations have been shown to act as drivers in melanoma. Typically, the somatic mutations are known as the main melanoma genetic drivers belonging to the MAPK and (PI3K)/AKT signaling pathways (Chappell et al., 2011). The MAPK

pathway is a RAS/RAF/MEK/ERK signaling cascade in which RAS activates the serine-threonine-specific kinase RAF, which can subsequently activate MEK and, in turn, activate ERK. Mutations in BRAF, NRAS, and NF1, which elevate the MAPK kinase activity and lead to the loss of cell proliferation control, are the most frequent genetic abnormalities identified in melanoma (Akbani et al., 2015).

Approximately 50 percent of melanomas harbor the $BRAF^{V600E}$ mutation (Cheng et al., 2018; Davies et al., 2002). This particular mutation represents over 90% of BRAF mutations found in somatic tumors (Platz et al., 2008). Interestingly, the $BRAF^{V600E}$ mutation is not a characteristic of the UV-signature mutation (Thomas et al., 2006). Mutations in *BRAF* might be acquired during the melanoma progression (Bauer et al., 2011). *NRAS* is found to be mutated in 15-30% of melanoma cases, whereas that number was 10-15% for *NF1*. The *NF1* mutations were observed to co-occur with *BRAF* and *NRAS* (Gibney and Smalley, 2013). In contrast, *BRAF* and *NRAS* mutations occur mutually exclusively at the single melanoma cell level, although the *BRAF* and *NRAS* mutations have been shown to co-exist in the same melanoma specimens (Fedorenko et al., 2013). Both the *BRAF* and *NRAS* gain-of-function mutations have been shown to be efficient in activating the MEK-ERK pathway.

The oncogene *KIT* can also lead to the activation of the MAPK and PI3K pathways to mediate melanoma proliferation and survival (Curtin et al., 2006). *KIT* mutations are detected in 2-8% of melanomas. Both *NF1* and *KIT* variants are usually associated with sun-exposed skin (Handolias et al., 2010; Krauthammer et al., 2015). *PTEN* is another melanoma genetic driver, with 10-30% of melanomas harboring *PTEN* mutations (Hodis et al., 2012; Wu et al., 2003). PTEN converts PIP3 into PIP2, resulting in the inactivation of the oncogenic phosphatidylinositol-3-kinase (PI3K) signaling pathway, which is fundamental for cell growth and survival (Cully et al., 2006). It has been suggested that *PTEN* is critical for melanoma progression since *PTEN* mutations are rarely found in primary melanoma biopsies (Birck et al., 2000). Interestingly, *PTEN* loss-of-function and *NRAS* gain-of-function mutations occur in a mutually exclusive manner, whereas the co-occurrence of *BRAF* gain-of-function and *PTEN* loss-of-function mutations is frequently observed. Similar to the *BRAF* gain-of-function and *PTEN* loss-of-function mutation, the *NRAS* gain-of-function mutation enables the activation of both MAPK and PI3K pathways. Furthermore, it has been suggested that $BRAF^{V600E}$ and *PTEN* mutations are found more in non-CSD (non-chronic sun-damaged) skin, whereas *NF1* and *TP53* mutations are more frequent in CSD (chronic sun-damaged) skin, suggesting that the genetic aberrations influencing

melanomagenesis in CSD and non-CSD skin are different (Damsky and Bosenberg, 2017). Additionally, the hyperactivate PI3K-AKT signaling pathway in metastatic melanoma might also be caused by oncogenic mutations in PIK3CA, a catalytic subunit of PI3K (Wittig et al., 2006).

Interestingly, several somatic mutations in MITF (e.g. E87R, L135V, L142F, G244R, and D380N) have been reported in melanoma samples (Cronin et al., 2009). Surprisingly, most of these MITF melanoma mutations, except the G244R mutation, are located outside of the DNA binding bHLHzip domain, suggesting that these alterations do not affect DNA binding ability but may affect signaling or the function of the intrinsically disordered domains of MITF possibility through protein-MITF interaction or post-translational modifications.

The overexpression of matrix metalloproteinases (MMPs), particularly MMP9 and MMP2, which are regulated by genetic alterations and dysregulation of (NF)-κB pathways, has been shown to play a role in melanoma progression and metastasis (Moro et al., 2014). Apart from the burdens of somatic genetic alterations mentioned above, somatic mutations in *CDKN2A, CDK4*, *POT1, TERT*, *PPP6C*, *RAC1*, *SNX31*, *TACC1*, *BAP1,* and *STK19* are also linked with melanoma (Akbani et al., 2015; Hodis et al., 2012; Leonardi et al., 2018; Van Raamsdonk et al., 2009). However, the roles of mutations in melanoma development and their interlink with the environment remain to be further investigated.

1.5 Epigenetics in melanoma

As mentioned above, genetic aberrations in melanoma can be caused by epigenetic modifications, including aberrant DNA methylation, histone modifications, histone variants, chromatin remodeling, and non-coding RNA regulation. The epigenetic modifications may initiate or promote melanoma progression and involve drug resistance (Giunta et al., 2021; Sarkar et al., 2015; Truderung et al., 2021). Below I briefly summarize what is known about the role of the different epigenetic processes in melanoma.

1.5.1 DNA methylation

Silencing of tumor suppressor genes due to DNA hypermethylation or activation of oncogenes through DNA demethylation has been reported as a tumorigenesis factor in melanoma (Sarkar et al., 2015). DNA methylation is catalyzed by DNA methyltransferases (DNMTs), in which cytosine in the DNA is methylated. The *RAR-β2 (RARB)* gene is frequently hypermethylated in melanoma, leading to its silencing and contributing to the development and progression of the disease. *RARB* is methylated in 70% of malignant melanoma specimens (Hoon et al.,

2004). The reduction of RARB expression contributes to an increase in melanoma growth (Fan et al., 2010). Interestingly, silencing of *RARB* is not only due to the hypermethylation status but also through histone hypoacetylation, suggesting that different epigenetic mechanisms might be involved in regulating tumor suppressor genes at different stages of melanoma progression (Fan et al., 2010).

Hypermethylation of *RASSF1A* is apparent in approximately 55% of melanoma samples (Hoon et al., 2004). RASSF1A regulates ASK1, which in turn activates the p38 MAPK to modulate cell-cycle progression and induce apoptosis. Hence, decreasing *RASSF1A* expression through DNA methylation suppresses apoptosis and increases the risk of melanoma (Yi et al., 2011). Interestingly, hypermethylation of *RASSF1A* is different depending on the stage of melanoma and is highest at stage IV but is not seen at stages I and II (Tanemura et al., 2009), suggesting that it may be an epigenetic marker of malignant melanoma.

DNA methylation at *CDKN2A* is also well-studied during melanomagenesis. Ten to twenty percent of melanoma samples lose $p16^{INK4A}$ expression due to methylation, which in turn is associated with a decrease in survival rate and a rise of the Ki-67 index, an indicator of proliferation (Straume et al., 2002). Interestingly, *CDKN2A*/$p16^{INK4A}$ promoter methylation is frequently overrepresented in *NRAS*-mutant melanoma samples (Lahtz et al., 2010). Silencing of $p16^{INK4A}$ upon hypermethylation is similar to the *CDKN2A*/$p16^{INK4A}$ loss-of-function variants, which lead to a deficiency of p53-mediated apoptosis and melanoma progression (Schinke et al., 2010).

In addition to the deletion or loss-of-function mutations in *PTEN*, *PTEN*-silencing is also due to promoter methylation, which has been identified in 62% of sera samples from melanoma patients (Mirmohammadsadegh et al., 2006). Besides, the methylation-mediated silencing of *KIT, HOXB13, SYK, TERT,* and *LXN* has also been described in melanoma (Karami Fath et al., 2022; Micevic et al., 2017). A number of hypermethylated genes have been identified in melanoma cells. However, the mechanism of hypermethylation in regulating melanoma development remains to be further investigated. Some hypermethylated genes in melanoma, e.g., *CDH1, CDK8*, and *PTEN*, have been considered independent predictors of poor outcomes (Sigalotti et al., 2010). Furthermore, the link between genetic mutations and DNA methylation and their role in the initiation and progression of melanoma must be considered since it has been shown that the $BRAF^{V600E}$-mutation leads to increased DNMT1 expression, which in turn catalyzes and promotes hypermethylation (Hou et al., 2012).

On the other hand, DNA hypomethylation is generally associated with oncogene activation, chromosomal instability, and drug resistance (Giunta et al., 2021). In primary and metastatic melanoma, the abundance of 5-hydroxymethylcytosine (5hmC) is decreased compared to that in melanocytes. However, the impact of DNA hypomethylation in melanoma development still needs further investigation. It has been shown that in melanoma, the ten-eleven-translocase (TET) family of dioxygenase enzymes is responsible for converting methyl-cytosine (5mC) to hydroxymethyl-cytosine (5hmC). The loss of TET-family enzymes, particularly TET2, was more frequent in melanoma than in nevi (Gambichler et al., 2013; Lian et al., 2012). Therefore, TET has been proposed as a novel epigenetic marker.

1.5.2 Chromatin remodeling

As a chromatin remodeling complex, SWI/SNF (also known as BAF) impacts the recruitment of regulators to gene promoter regions through remodeling nucleosomes. The complex is composed of an ATPase (e.g., BRG1 known as SMARCA4 or BRM known as SMARCA2) and a DNA binding domain subunit (e.g., ARID1A, ARID1B or ARID2) (Reisman et al., 2009). The chromatin-remodeling SWI/SNF complex is known for its roles in sustaining DNA stability and repairing double-stranded DNA breaks in response to UV. Changes to the SWI/SNF subunit have been linked to melanoma, with loss-of-function mutations in ARID2, ARID1A, ARID1B, or SMARCA4 present in 13% of melanomas (Hodis et al., 2012; Mehrotra et al., 2014; Saginala et al., 2021; Vinod Saladi et al., 2010). Besides, it has been reported that SOX10 and MITF can recruit SMARCA4 (subunit of SWI/SNF complex) and BPTF (subunit of the NURF complex) to MITF-associated regulator region for mediating MITF genomic occupancy (Cancer Genome Atlas, 2015; Laurette et al., 2015). As a result, the abnormal SMARCA4 and BPTF expression significantly impacted the expression of MITF target genes. Furthermore, loss-of-function mutations in ATRX, another SWI/SNF chromatin remodeling protein, have also been associated with melanoma progression (Qadeer et al., 2014).

The involvement of bromodomain and extra-terminal domain (BET) proteins (BRD2, BRD3, BRD4, and BRDT) in melanoma development has also been reported. Through binding to acetylated lysine residues of histones, BET proteins permit the travel of RNA polymerase II, thus allowing elongation of the mRNA (LeRoy et al., 2008). Increased expression of BRD2 and BRD4, which control cell cycle and survival signaling pathways, has been shown in melanoma (Giunta et al., 2021). Meanwhile, using an inhibitor of the bromodomain-containing protein resulted in the activation of NF-κB signaling pathway resulting in activation of

genes associated with cell cycle regulation (e.g., *CDK6*), inflammation (e.g., *VEGF* and *CCL-20*), cytokine production (IL-6 and IL-8), and induction of apoptosis (Gallagher et al., 2014a; Gallagher et al., 2014b).

Through affecting S-phase regulation and the DNA repair processes, overexpression of p60, a subunit of the chromatin assembly factor-1 (CAF-1), has also been linked to melanoma progression via promoting the incorporation of histones into chromatin (Mascolo et al., 2010).

The roles of Polycomb group (PcG) proteins in both development and cancer have been reported (Sarkar et al., 2015). PcG proteins consist of two separate complexes called PRC1 and PRC2. While PRC2 is brought to the chromatin and adds a trimethyl group to lysine 27 on the histone H3 tail, PRC1 recognizes this mark and contributes to the formation of heterochromatin. The enhancer of zeste homolog 2 (EZH2), a subunit of the polycomb repressive complex 2 (PRC2), has been shown to catalyze H3K27me3 and be involved in melanoma progression. This will be discussed further in the following chapter.

1.5.3 Histone modifiers

Chromatin is a highly organized structure consisting of histones and DNA packed into nucleosomes where 146 base pairs of DNA are wrapped around an octamer histone protein complex (e.g., two of each histone H2A, H2B, H3, and H4 (Strub et al., 2020). In addition to modifying chromatin access through ATP-dependent chromatin remodeling, the changes in chromatin structure due to histone post-translational modifications (PTMs) or histone variants also affect histone-DNA and histone-histone interactions and eventually enable the mediation of transcription activity (Zentner and Henikoff, 2013).

PTMs of histones are important for regulating chromatin structure which subsequently impacts the transcriptional and replication machinery without changing the DNA nucleotide sequence (Alaskhar Alhamwe et al., 2018). Various forms of histone PTMs, including acetylation, methylation, phosphorylation, and ubiquitination, have been well studied and shown to regulate chromatin structure and activity (Bannister and Kouzarides, 2011; Peterson and Laniel, 2004; Swygert and Peterson, 2014). Interestingly, individual or combinatorial histone PTMs, placed on both tails and core of the different histones, affect nucleosome dynamics (Bowman and Poirier, 2015).

Histone methylation

Histone methylation status is controlled by histone methyltransferases (HMTs) which transfer up to three methyl groups to either arginine or lysine of histones. HMTs have been classified into two groups, including lysine methyltransferases (KMTs) and arginine methyltransferases (PRMTs). To date, 50 KMTs have been described, which fall into two subfamilies based on catalytic domain sequence: SET domain-containing and the DOT1-like protein. KMTs are generally recruited to a specific lysine residue, leading to more specificity than that of HATs. For example, KMT1A/SUV39H1, KMT1B/ SUV39H2, KMT1C/G9a, or KMT1D/EuHMTase/GLP methylate H3K9 histone (Morera et al., 2016). Interestingly, it has been shown that specific DNA sequences, long non-coding RNAs (lncRNAs), and small non-coding RNAs can direct histone-modifying enzymes to the target genome location (Greer and Shi, 2012). Different methylated lysine residues on histones have different turnover rates (Zee et al., 2010). Besides arginine or lysine methylation, monomethylated histidine has been shown to be present in histones (Borun et al., 1972; Gershey et al., 1969). However, histidine methylation is rare and has not been well studied (Greer and Shi, 2012).

Different forms of histone methylation have been classified. The location and level of methylation play a critical role in regulation. Different degrees of methylation of histone lysine residues (e.g., mono-, di- or tri-methylation) have been identified in different gene regulatory regions. While H3K4me1 (mono-methylated lysine 4 at histone 3) is enriched at enhancers, H3K4me3 (tri-methylated lysine at histone 3) is mainly found at promoters of active genes. (Heintzman et al., 2007). The methylation at different lysine residues is also suggested to play different roles. For instance, H3K4me3, H3K36me3, or H3K79me3 are active transcription histone marks. In contrast, H3K9me3, H3K27me3, or H4K20me3 are associated with repression (Lawrence et al., 2016).

Histone demethylation is performed by histone demethylases (HDMs). Regarding HDMs, amine-oxidase type lysine-specific demethylases (LSDs or KDM1s) and JumonjiC (JMJC) domain-containing HDMs are two subclasses of HDMs that have been separated due to differences in sequence homology and catalytic mechanism. While the catalytic activity of LSDs/KDM1s (KDM1A/LSD1/AOF2 and KDM1B/LSD2/AOF1) is the demethylation of only mono- and dimethylated H3K4, JumonjiC (JMJC) domain-containing HDMs (KDM2-8) eliminate methyl groups from various mono-, di-, and trimethylated lysine histones (Alaskhar Alhamwe et al., 2018).

Abnormal histone methylation has been reported to be involved in melanoma (Giunta et al., 2021; van den Hurk et al., 2012). Through catalyzing tri-methylation of lysine 9 on histone 3, SETDB1 has been known as a silencing mediator (Schultz et al., 2002). While an increase in SETDB1 activity is associated with melanoma initiation and progression, *SETDB1*-silencing in SETDB1^{high} melanoma cell lines reduces melanoma cell viability (Ceol et al., 2011; Orouji et al., 2019). The expression of *SETDB1* is also increased in tumors harboring BRAF^{V600E} mutation and implicated in tumor development (Ceol et al., 2011), suggesting an interplay between genetic mutations and epigenetic events in promoting melanoma progression. The interplay between DNA methylation and histone modification has also been observed where SETDB1 is recruited to methylated CpG islands through its methyl-CpG-binding domain. Subsequently, the H3K9me3 histone mark is introduced at the specific loci and thus acts as a double layer to control repression (Sarraf and Stancheva, 2004). In addition to the gene repression effect, SETDB1 has also been suggested to influence the H3K4 active mark. SETDB1 has been shown to alter the enrichment of H3K4me1 at the thombospondin-1 (THBS1) enhancer region and induce its expression (Strub et al., 2020). However, genome-wide histone modifications by SETDB1 in melanoma remain unknown.

As mentioned before, elevated levels of both *EZH2* and H3K27me3 have been observed in aggressive melanoma cells, leading to suppression of the tumor suppressors RUNX3 and E-cadherin, allowing the cells to evade senescence (Sengupta et al., 2016). Meanwhile, reduced *EZH2* expression leads to an increase in *CDKN2A* and *CDKN1A* expression, resulting in the inhibition of proliferation and restoration of apoptosis (Fan et al., 2011; Wu et al., 2010). The somatic gain-of-function EZH2^{Y646N} mutation represses gene expression by triggering an enrichment of the H3K27me3 histone mark and reorganization of chromatin structure, which favors melanoma progression (e.g., bypass of senescence through the NF-kB pathway or by promoting tumorigenicity through WNT/β-catenin signaling) (Strub et al., 2020). Furthermore, the interplay between Ezh2^{Y641F} (equivalent to EZH2^{Y646N} in humans) and BRAF^{V600E} in melanomagenesis has been reported in the mouse model (Souroullas et al., 2016).

G9a methyltransferase regulates the levels of H3K9me2 and is known as an important factor in various developmental processes and decisions related to cell fate (Tachibana et al., 2002). It has also shown that gain-of-function mutations in G9a are frequently found in melanomas and other cancer types (Kato et al., 2020). The activation mutations in G9a can drive oncogenesis by promoting

cell proliferation and survival, as well as suppressing immune responses through repressing DKK1, an antagonist of WNT pathway (Kato et al., 2020).

Changes in global H3K4me3 levels were noticed in zebrafish by comparing melanoma to normal skin (Anelli et al., 2009). The histone demethylase H3K4me3 JARID1B (i.e. KDM5B) was reported to play roles in melanoma tumor growth. Knocking down JARID1B accelerated tumor growth, followed by exhaustion (Roesch et al., 2010). Demethylation at histone H3 lysine 9 at the E2F target gene promoters by LSD1 (i.e. KDM1A) and JMJD2C (i.e. KDM4C) promotes the senescence bypass that is induced by $HRas^{G12V}$- or $Braf^{V600E}$ and favors melanoma development (Yu et al., 2018). Meanwhile, an increase in the H3K27-specific demethylase KDM6B has been described to be associated with melanoma progression and metastasis through upregulating genes in the NF-κB and BMP (Bone Morphogenic Protein) pathways (Park et al., 2016). Additionally, the role of KMT2D in gene regulation has been identified through its mono-methylation of H3K4 (Guo et al., 2013). The inactivation of KMT2D results in a decrease in H3K4me1 and H3K27ac histone marks in the enhancer region, which eventually reduces the expression of genes associated with cell migration (e.g., *MFGE8* and *RPL39L)* and deregulates tumorigenesis (Bossi et al., 2016).

Histone acetylation: acetyltransferases and deacetylase

There are two groups of enzymes, namely histone acetyltransferases (HATs) and histone deacetylases (HDACs), that participate in acetylating and deacetylating histones, respectively (Alaskhar Alhamwe et al., 2018). HATs catalyze the transfer of the acetyl groups from acetyl-CoA to target lysine residues in histones, whereas HDACs catalyze their removal. Acetylation of a lysine leads to the loss of a positive charge on the histone, which weakens the interaction between histones and DNA. This, in turn, increases gene expression due to the relaxation of the chromatin and increases the accessibility of DNA to transcription factors (Alaskhar Alhamwe et al., 2018). Histone acetylation also affects transcription by serving as a binding site for histone reader proteins (Gallagher et al., 2015). Lysine residues on H3 and H4 histone tails are the most widely studied targets of histone acetylation; however, other residues, like H3K56, which is located in the H3 histone core domain, can also be acetylated (Gallagher et al., 2015). To date, three subfamilies of HATs have been described, namely GCN5-related N-acetyltransferase (GNAT), MYST, p300/CBP. The GNATs subfamily is one of the major subfamilies of histone acetyltransferases (HATs) in humans. GNATs consisting of at least 12 genes, including *KAT2-KAT14,* have been suggested to modulate cell cycle, DNA replication, and DNA repair by contributing to the acetylation of histones and transcription factors (Alaskhar Alhamwe et al., 2018)

and to maintain genome stability by preserving the correct centrosome numbers (Fournier and Tora, 2017). Similar to GNATs, the MYST subfamily (i.e., *KAT6A, KAT6B, KAT8, MYST2)* is also involved in transcription regulation and DNA repair (Alaskhar Alhamwe et al., 2018). On the other hand, there are 18 enzymes in the family of HDACs, and they are classified into four groups. Group I (HDAC 1, 2, 3, and 8) is primarily expressed in the nucleus in all tissues. While group IIa (HDAC4, 5, 7, and 9) is mainly in the cytoplasm, group IIb (HDAC6 and 10) is present both in the nucleus and cytoplasm. Little is known about the subcellular localization of group III, NAD-dependent sirtuins (SIRTs; SIRT 1–7), and group IV (HDAC11) (Alaskhar Alhamwe et al., 2018; Seto and Yoshida, 2014).

Deregulation of acetylation resulting in melanomagenesis has been reported (Strub et al., 2020). It has been shown that loss of histone acetylation in regulatory regions of genes associated with cell signaling pathways that drive melanoma (e.g. *PI3K, ITGβ1, TGFβ, PDGF*) (Fiziev et al., 2017). In this context, the expression of PIB5PA or BCL2, both of which play roles in apoptosis resistance by blocking PI3K/AKT signaling, is also usually reduced in melanoma upon hypoacetylation (Giunta et al., 2021; Ye et al., 2013). Additionally, it has been shown that *CDKN2A* ($p14^{AFK}$) *and CDKN1A* (p21) expression was reduced upon histone deacetylation, resulting in senescence bypass and melanoma progression (Fiziev et al., 2017; Flørenes et al., 2004).

Although the understanding of HDAC expression in melanoma is still limited, it has been shown that the percentage of nuclear HDAC3 and cytoplasmic HDAC8 positively correlate with survival in melanoma (Wilmott et al., 2015). However, HDAC1 and HDAC8 are also connected to increased levels of phosphorylated p65, a subunit of the NF-κB complex that has been linked to resistance to MAPK inhibitors (Konieczkowski et al., 2014; Wilmott et al., 2015). Notably, another study also described the function of HDACs on other proteins rather than histones. Particularly, HDAC8 was shown to deacetylate c-JUN to activate c-Jun transcriptional activity, which subsequently affects MAPK and AP-1 signaling regulation and eventually conveys resistance to BRAF inhibition (Emmons et al., 2019).

Histone variants

Histone variants have been shown to play a key role in modifying chromatin structure and gene expression since variant histones differ from canonical histones in sequence and properties. H2A and H3 variants are the most common and are placed in specific genomic locations by histone chaperones (Vardabasso et al., 2014). The expression of H2A.Z variants, including H2A.Z.1

and H2A.Z.2, is increased in melanoma as well as other cancers (Kapoor et al., 2010). An increase in H2A.Z.2 expression has been associated with poor patient survival (Vardabasso et al., 2015). In fact, H2A.Z.2 stabilizes the histone reader protein BRD2, leading to the activation of genes, especially E2F targets, that advance the cell cycle (Vardabasso et al., 2015). Meanwhile, the H3.3 variant is linked to the expression of E2F target genes. An increase in H3.3 results in the suppression of E2F target genes and induced senescence (Duarte et al., 2014). The histone variant MacroH2A, known as transcriptionally repressive, suppresses CDK8 expression, resulting in a slower proliferation of melanoma cells (Kapoor et al., 2010). Overexpression of histone variant H2A.Z.2 has been reported to lead to poor melanoma progression (Kapoor et al., 2010; Vardabasso et al., 2015).

Histone modification in key genomic regions

While the pattern of histone modifications can indicate a gene activation state, the location of these modifications in the genome can provide further specific information about their role and the underlying mechanism. In general, the histone modifications H3K4me1/2/3, H3K9ac, H2A.Z, H3.3, and H3K27ac are found at active promoters, whereas H3K27me3, H3K9me3, and DNA methylation are usually found at inactive promoters (Tollefsbol, 2017). It has been shown that some genes have bivalent promoters, in which both the H3K4me3 and H3K27me3 or the H3K4me3 and H3K9me3 histone marks are found. The H3K4me3 and H3K27me3 marks at bivalent promoters are mostly identified on adjacent histones within a homodimer. Interestingly, genes containing bivalent promoters are silent and only switch to activation mode during differentiation and development (Tollefsbol, 2017). In melanoma, it has been suggested that the bivalent states are impacted by the NRAS and BRAF genotypes (Terranova et al., 2021). Additionally, the broad H3K4me3 domain, which can span thousands of kilobases at promoters, might be involved in pro-metastatic melanoma, suggesting an epigenetic feature of melanoma development (Terranova et al., 2021). Particularly, *SOX9*, *PDGFA*, *PDGFRA*, and *MYCN*, which are important metastasis drivers, showed a transition from a bivalent state to active transcription with broad H3K4me3 modification upon switching towards mesenchymal/invasive state (Terranova et al., 2021). Compared to melanocytes, in melanoma tumors, reduced H3K4me3 domains (<2 kb) were observed at the promoter regions of melanocyte-specific cell-identity genes (e.g., *PMEL*, *PAX3*, *MITF*, and *TFAP2A*), leading to decreased gene expression (Terranova et al., 2021).

Active genes are often associated with active enhancers, which usually present both the H3K4me1 and H3K27ac histone marks and contain of H3.3 and H2A.Z histone variants. The H3K4me1 mark primes active enhancer regions. Active enhancers are also defined by other histone acetylation marks, such as H2BK20ac, H3K122ac, and H4K16ac. Meanwhile, inactive enhancers have increased H3K9me2/3 marks, and surprisingly, inactive enhancers lack TF binding. A different enhancer state referred to as prime enhancer has been discovered, marked by the presence of H3K4me1 but not H3K27ac. Nevertheless, the H3K4me1 mark is much reduced in prime enhancers compared to active enhancers (Tollefsbol, 2017).

Histone modification has also been identified in the gene body. The H3K36me3 and H3K79me2 methylations are found in the body of active genes since these two histone modifications are favorable for RNAPII traveling through the genes. Although H2BK120ub1, H3K9me2/3, H3K27me2, and H3K27me3 are also located within the gene bodies, they play roles in transcriptional elongation through pausing the traveling RNAPII (Tollefsbol, 2017).

1.6 The Microphthalmia-associated transcription factor

The Microphthalmia-associated transcription factor (MITF) regulates the specification, proliferation, survival, and differentiation of multiple cell lineages, including neural crest-derived melanocytes, pigmented epithelial cells of the eye, mast cells, and osteoclasts (Arnheiter, 2010; Goding and Arnheiter, 2019; Steingrimsson et al., 2004). In melanoma cells, it plays a critical role as a lineage-survival oncogene (Garraway et al., 2005). It may act as a switch that determines whether cells proliferate or become quiescent, thus allowing migration and formation of metastases (Hoek and Goding, 2010). Its protein product, MITF, is a member of the basic-Helix-Loop-Helix-leucine zipper (bHLHZip) transcription factor family that binds to the E- (CACGTG) and M- (TCATGTG) box motifs as homodimers or heterodimers with its closest relatives TFE3, TFEB and TFEC (Hodgkinson et al., 1993; Strub et al., 2011); a unique 3-amino acid domain EQQ[260–262] restricts dimerization of these proteins such that they do not dimerize with other bHLHZip proteins (Pogenberg et al., 2020; Pogenberg et al., 2012).

The human *MITF* gene is located on chromosome 3 and is about 230,000 base pairs long, while the mouse Mitf gene is located on chromosome 6 and is 215,000 base pairs long. Both genes have multiple promoters and tissue-specific first exons which are all spliced to the common exons 2-9, leading to the production of various mRNA and protein forms through alternative promoter

usage and splicing (Goding and Arnheiter, 2019; Vu et al., 2021). Multiple MITF mRNA and protein isoforms (e.g. MITF-A, -B, -C, -D, -E, -J, -H, -Mc, and -M), therefore, differ at the amino terminus and are regulated by specific promoters (Goding and Arnheiter, 2019). While human MITF and mouse Mitf genes are remarkably conserved and share overall gene organization, in zebrafish, there are two Mitf genes encoding two Mitf proteins, named *Mitfa* and *Mitfb*. These zebrafish genes are considered homologs of mouse and human MITF-M and MITF-A, respectively (Lister et al., 2001). MITF proteins are further grouped into MITF(+) (referred to as MITF-WT in this thesis), containing the six amino acids encoded by exon 6A and MITF(-) (referred to in this thesis as $MITF^{mi\text{-}sp}$) lacking these residues.

The various MITF isoforms are expressed in different tissues (Figure 3). For instance, MITF-M is found mostly in melanocytes and melanoma cells, while MITF-Mc only occurs in mastocytoma cell lines. MITF-E is abundant in mastcells, and MITF-D is expressed in cells of the RPE, macrophages, mast cells, and osteoclasts. On the other hand, MITF-A, MITF-B, MITF-H, and MITF-J are expressed in multiple cell types, with MITF-H being prominent in the heart and MITF-A and -J in RPE cells. MITF-C, although present in many cell lines, is absent in cells of the melanocyte lineage. The specific functional roles of the different MITF isoforms have not been clarified, and in fact, most of the work on MITF has focused on the MITF-M isoform, which is predominant in melanocytes and melanoma (Goding and Arnheiter, 2019; Hershey and Fisher, 2005; Hodgkinson et al., 1993; Yasumoto et al., 1998).

1.6.1 Regulation of MITF expression

The transcription of MITF is regulated by a collection of transcription factors, including MITF itself, as well as signaling events that are important in melanocyte development and homeostasis (Goding and Arnheiter, 2019; Levy et al., 2006). It has been reported that MITF expression is positively governed by the transcription factors SOX10 (Bondurand et al., 2000), PAX3 (Yang et al., 2008), the EMT transcription factor ZEB2 (Denecker et al., 2014), ONECUT-2 (Jacquemin et al., 2001), as well as by LEF1 (lymphoid enhancer-binding factor 1) (Eichhoff et al., 2011; Saito et al., 2002), and CREB (Huber et al., 2003). MITF is also suppressed by PAX3 (Eccles et al., 2013), GLI2 (Javelaud et al., 2011), BRN2 (Pinner et al., 2009; Thurber et al., 2011), and signaling pathways like TGFβ and WNT (Hartman et al., 2014).

Figure 3. The alternative exon 6A has been described in human MITF-A, MITF-H, and MITF-M proteins. Translation starts and stops codons are indicated by the (▼) symbol and (*) symbol, respectively. The (▽) symbol shows the alternative start codon of the MITF-B isoform. The numbers indicate amino acid residues. The cell lines exhibiting the major expression of the human MITF isoforms according to the FANTOM database are presented. Figure obtained with permission from John Wiley and Sons according to permit number 5514180354498 (Vu et al., 2021).

PAX3 is a paired-box homeodomain transcription factor that plays a crucial role in melanocyte development and melanocyte stem cell activation regulation. This is achieved through its ability to control MITF-M expression and activity (Lang et al., 2005; Medic and Ziman, 2010). While PAX3 has been shown to activate the transcription of MITF-M in melanocytes and melanoma (Watanabe et al., 1998), PAX3 promotes the activation of the BRN2 promoter via PI3K, which might eventually repress the expression of MITF (Bonvin et al., 2012; Eccles et al., 2013). PAX3 not only controls MITF expression but also regulates TYRP1 expression. In melanoblasts, PAX3 competes with MITF for binding to the enhancer region of the DCT (Lang et al., 2005). Working together with PAX3, SOX10, a key player in both neural crest development and melanocyte biology, also positively regulates the MITF expression (Elworthy et al., 2003; Lee et al., 2000; Verastegui et al., 2000). It is further suggested that SOX10 plays a crucial role in melanoma initiation and development, in which a high expression level of SOX10 was found in melanoma samples but not frequently mutated (Cronin et al., 2013; Shakhova et al., 2012). A decline in the transcriptional proficiency of SOX10 due to increased ERK activity may also cause alteration in MITF expression since ERK-mediated phosphorylation inhibits the transcriptional activity of SOX10 by impeding its SUMOylation, which is typically necessary for its transcriptional function (Han et al., 2018). In contrast, by blocking PAX3 from the MITF promoter, FOXD3 indirectly repressed the MITF expression (Thomas and Erickson, 2009). FOXD3 is also widely expressed in melanoma and has been linked to conferring resistance to BRAF inhibitors, partly through its ability to suppress MITF expression and activation of ERBB3/HER3 (Abel et al., 2013).

Known as a bZIP transcription factor, CREB activates MITF expression in response to elevated cAMP levels through its binding to a TGACGTCA motif (CRE element) in the MITF promoter (Huber et al., 2003). The regulation of MITF expression by CREB is dependent on SOX10 and is involved in controlling hair and skin pigmentation through the regulation of downstream genes implicated in the pigmentation process (Huber et al., 2003). Furthermore, the cAMP-CREB-MITF activation pathway has also been shown to play an important role in the UV-suntanning response (Kawakami and Fisher, 2017). In addition to cAMP-CREB-MITF, the SIK-CRTC-CREB axis in regulating MITF expression was also reported. In detail, SIK kinases phosphorylate cAMP-regulated transcriptional co-activator (CRTC) proteins, which inhibits their translocation to the nucleus where phosphorylated CRTC typically co-activates CREB and causes an inhibition MITF expression (Nguyen and Fisher, 2019). In this context, the ATF4 transcription factor can suppress MITF mRNA expression by competing with CREB for binding to the MITF promoter (Falletta et al., 2017; Ferguson et al., 2017). This means

that any upstream activator of ATF4 (e.g., TNFα) that increases its expression could also lead to decreased MITF transcription and eventually to melanoma de-differentiation (Falletta et al., 2017).

WNT/beta-catenin also plays an important role in regulating MITF expression by activating the MITF promoter through the LEF1/TCF transcription factors, which are essential for the specification of melanoblasts from neural crest cells and for melanocyte formation. The functional role of WNT/β-catenin in activating melanocyte stem cells in adult hair follicles has also been reported, likely through increasing MITF expression to promote cell differentiation (Rabbani et al., 2011). In melanoma, the activation of WNT/beta-catenin pathway has been shown to decrease tumor proliferation *in vivo*. (Chien et al., 2009).

Despite the fact that both ZEB1 and ZEB2 belong to the Zinc-Finger-E-box binding transcription factor family, they regulate MITF in different ways and significantly impact the switching from epithelial to mesenchymal cells (Vandewalle et al., 2009). In particular, ZEB2 activates MITF expression, whereas ZEB1 has been reported to repress MITF expression in retinal pigment epithelium cells (Denecker et al., 2014).

Also known as a MITF regulator, the homeodomain transcription factor ONECUT-2 is expressed in melanocytes and enables to bind to the MITF promoter. A mutation in the binding site of ONECUT-2 decreases MITF promoter activity by about 75% (Jacquemin et al., 2001). However, the specific function of ONECUT-2 in melanocyte differentiation and melanoma development remains to be investigated.

Additionally, BRG1, a component of SWI-SNF chromatin remodeling complex, has also been shown to positively regulate MITF expression through its direct binding to the MITF promoter (Vachtenheim and Borovanský, 2010). Interestingly, while BRN2 has been shown to regulate MITF directly by binding to MITF promoter, BRN2 has been shown to mediate both increased and decreased MITF expression, depending on the control of $BRAF^{V600E}$ mutation on BRN2 expression and the BRN2 phosphorylation status (Berlin et al., 2012; Goodall et al., 2008; Goodall et al., 2004; Wellbrock et al., 2008). BRN2 is a transcription factor that is regulated by three different signaling pathways involved in both melanocyte development and melanoma, namely BRAF/MAPK, PI3K through PAX3, and WNT/β-catenin. BRN2 expression is commonly increased in melanoma and is important in driving melanoma invasion (Goding and Arnheiter, 2019).

Although the activity of ALX3 in melanocytes and melanoma is still limited, according to CHIP-seq data, ALX3 has been reported to repress MITF expression and is involved in regulating pigmentation patterning in rodents through binding to the MITF promoter (Mallarino et al., 2016). The GLI2 transcription factor, which is downstream of Hedgehog signaling, also has a significant role in melanoma, e.g., by promoting invasion and resistance to BRAF inhibitors through its binding to MITF promoter regions and inhibiting the expression of MITF (Alexaki et al., 2010; Faiao-Flores et al., 2017; Javelaud et al., 2011).

1.6.2 MITF target genes

MITF is known as the master regulator of melanocyte differentiation, melanoma proliferation, and invasion. Consistent with that, MITF has been shown to bind to the regulatory regions of many genes involved in the indicated pathways and regulate their expression.

MITF can stimulate differentiation-related processes in both melanocytes and melanoma (Goding and Arnheiter, 2019) by positively regulating the expression of pigmentation-associated genes cell adhesion or epithelial-to-mesenchymal transition genes (Goding and Arnheiter, 2019). In addition, MITF has been shown to play a role in autophagy regulation (Möller et al., 2019). It has been shown that the depletion of MITF reduced the autophagy response to starvation, whereas overexpression of MITF increased the number of autophagosomes. A subset of genes involved in autophagy has been shown to be regulated by MITF (Möller et al., 2019). Particularly, MITF can regulate the expression of the lysosomal acid ceramidase *ASAH1*, which manages sphingolipid metabolism (Leclerc et al., 2019). Notably, the cell cycle arrest caused by the depletion of MITF was rescued by overexpression of ASAH1, suggesting that ASAH1 plays an important role proliferation of melanoma cells (Realini et al., 2016).

Previous studies also reported that MITF sustains both cell growth and survival during melanoma development. The role of MITF in mediating the cell cycle is particularly interesting. It has been shown that MITF positively regulates the expression of genes associated with DNA replication and DNA repair, including *BRCA1, AURKB,* and *TERT* (Strub et al., 2011). A reduction in MITF protein expression, therefore, causes genomic instability and increases the expression of DNA damage markers such as γH2AX and p53. MITF depletion in melanoma cell lines, therefore, leads to cell cycle arrest and senescence (Giuliano et al., 2010; Strub et al., 2011; Wellbrock and Marais, 2005). Reduced MITF protein expression has also been linked to a senescence-associated secretome driven by PARP and NFκB, which leads to the dedifferentiation of melanoma cells (Ohanna

et al., 2013; Ohanna et al., 2011). On the other hand, the cell cycle arrest upon MITF depletion is also explained by its direct binding and activation of the cyclin genes (e.g. *CDK2, CDK4, CDKN2A, CCNB1*, and *CCND1)* (Du et al., 2004; Loercher et al., 2005; Šestáková et al., 2010; Strub et al., 2011; Wellbrock et al., 2008). In melanoma cells, MITF also indirectly represses *CDKN2B* (p27kip1) through a regulator of the actin cytoskeleton termed Dia1 (Carreira et al., 2006). As another layer to control the cell cycle, high MITF protein expression also halts cell proliferation through regulating genes associated with mitosis, such as PLK1, a crucial player in M-phase progression. MITF further regulates components of the CENPA and NDC80 complexes, which link mitotic spindle microtubules to kinetochores. (Du et al., 2004; McGill et al., 2006; Strub et al., 2011; Wellbrock et al., 2008). However, MITF also activates the expression of genes that inhibit proliferation. For example, MITF cooperates with the RB1 protein to mediate cell cycle progression by activating *CDKN1A* expression (Carreira et al., 2005). The opposing functions of MITF in mediating the cell cycle could be explained by the MITF rheostat model, which is explained below.

MITF is also known to mediate cell invasion. On the one hand, MITF depletion in melanoma cell lines has been linked to the promotion of invasion (Carreira et al., 2006; Cheli et al., 2011; Javelaud et al., 2011). The loss of MITF has been shown to increase intracellular GTP levels by mediating the expression of the Guanosine Monophosphate Reductase (GMPR), which then enabled the elevation of the expression of the actin cytoskeleton regulators *RAC1, RHO-A,* and *RHO-C* (Bianchi-Smiraglia et al., 2017; Carreira et al., 2006). Furthermore, MITF also regulates the expression of the actin polymerization-associated gene *DIAPH1*, thus consolidating the observation that a reduction in MITF activity enhances invasion (Carreira et al., 2006). In contrast, the decrease of MITF expression has been also reported not to induce invasion (Falletta et al., 2017).

The observation that MITF depletion can both reduce and increase invasion and proliferation has been a confusing paradox (Goding and Arnheiter, 2019). However, this paradox was explained by the MITF rheostat model, which links the level of MITF protein expression or activity to effects on the phenotype (Figure 4). According to this model, low MITF activity results in the dedifferentiation of melanocytes/melanoma cells, promotes invasion, and slows down the proliferation through increased cell cycle inhibitor expression, which are favorable conditions for malignant transition. However, the severe replication and mitotic defects observed upon reduction below a specific threshold of MITF expression/activity result in cell senescence. In contrast, intermediate levels of MITF promote proliferation through the activation of genes associated with cell

cycle regulators and repression of genes that promote invasion. High levels of MITF stimulate cell cycle arrest and induce differentiation (Figure 4) (Rambow et al., 2019; Strub et al., 2011).

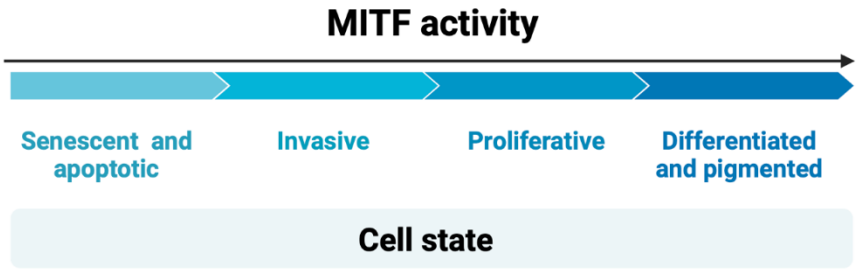

Figure 4. MITF rheostat model MITF expression level has been hypothesized to link with cell phenotype

1.6.3 MITF post-translational modifications (Paper I)

Post-translational modifications (PTMs) are defined as the chemical changes of proteins following the translation process (Bürkle, 2001). Many different types of PTMs have been shown to occur on a wide range of proteins in every cellular compartment. PTMs serve as a tightly regulated and highly dynamic mechanism in response to different physiological conditions, including nutrient availability, hormone stimulation, cell differentiation, and cell cycle controls (Fan et al., 2015). PTMs play critical roles in regulating protein activity, conformation, location inside the cell, and interaction with DNA/RNA or other proteins (Bowman and Poirier, 2015). There are over 400 different types of PTMs, including phosphorylation, ubiquitination, acetylation, sumoylation, and glycosylation, among others (Ramazi and Zahiri, 2021).

The activity of MITF is regulated by several post-translational modifications, including phosphorylation, SUMOylation, ubiquitination, acetylation, and proteolytic cleavage that affect its transcriptional activity, localization, protein stability, and interaction with partner proteins (Goding and Arnheiter, 2019; Larribere et al., 2005; Vu et al., 2021) (Figure 5). Below I review what is currently known about PTMs in the MITF protein.

While phosphorylation is catalyzed by kinases that add phosphate groups to proteins, phosphatases are responsible for removing the phosphate groups (Skamnaki et al., 1999). The amino acids serine, threonine, tyrosine, and histidine can all be phosphorylated (Panni, 2019). Phosphorylation is a highly dynamic and reversible process. It has been reported that phosphorylation

regulates cellular processes such as signal transduction, metabolism, and gene expression through modulating protein activity by altering their conformation and interactions with other proteins. As a result, phosphorylation plays a key role in many physiological processes and is also involved in many diseases, such as cancer, diabetes, and neurological disorders (Ramazi and Zahiri, 2021). Notably, phosphorylation of MITF has been shown to affect the subcellular localization of the protein. Phosphorylation at Y22, Y35, and Y90 by SRC (Phung et al., 2016), S69 by GSK3β (Ngeow et al., 2018), S73 by ERK (Hemesath et al., 1998; Wu et al., 2000) and S173 by C-TAK1 (Bronisz et al., 2006) has been shown to lead to the retention of MITF in the cytosol. The phosphorylation at S173 of MITF leads to the accumulation of the protein in the cytoplasm due to the formation of complexes with 14-3-3 proteins which are chaperone-like adaptor molecules and play important roles in many cellular processes. However, S73A, S298A, S307A, and S409A mutations did not impact the binding of MITF to 14-3-3 proteins (Bronisz et al., 2006). This suggests that Ser173 is specifically involved in 14-3-3 interactions. In contrast, phosphorylation at the S298, S397, S401, and S405 residues did not affect MITF subcellular localization (Ngeow et al., 2018). Phosphorylation of MITF has also been suggested to affect transcription. For example, phosphorylation at S73 affects transcription activation through stimulating the interaction between MITF and p300 (Hemesath et al., 1998; Xu et al., 2000). While phosphorylation at S298 by GSK3β has been suggested to increase the binding of MITF to the TYR promoter (Takeda et al., 2000), this site does not fit the GSK3β consensus sequence. Phosphorylation of S409 has been shown to alter the expression of the *CDKN1A* and *TYR* genes (Wang et al., 2016).

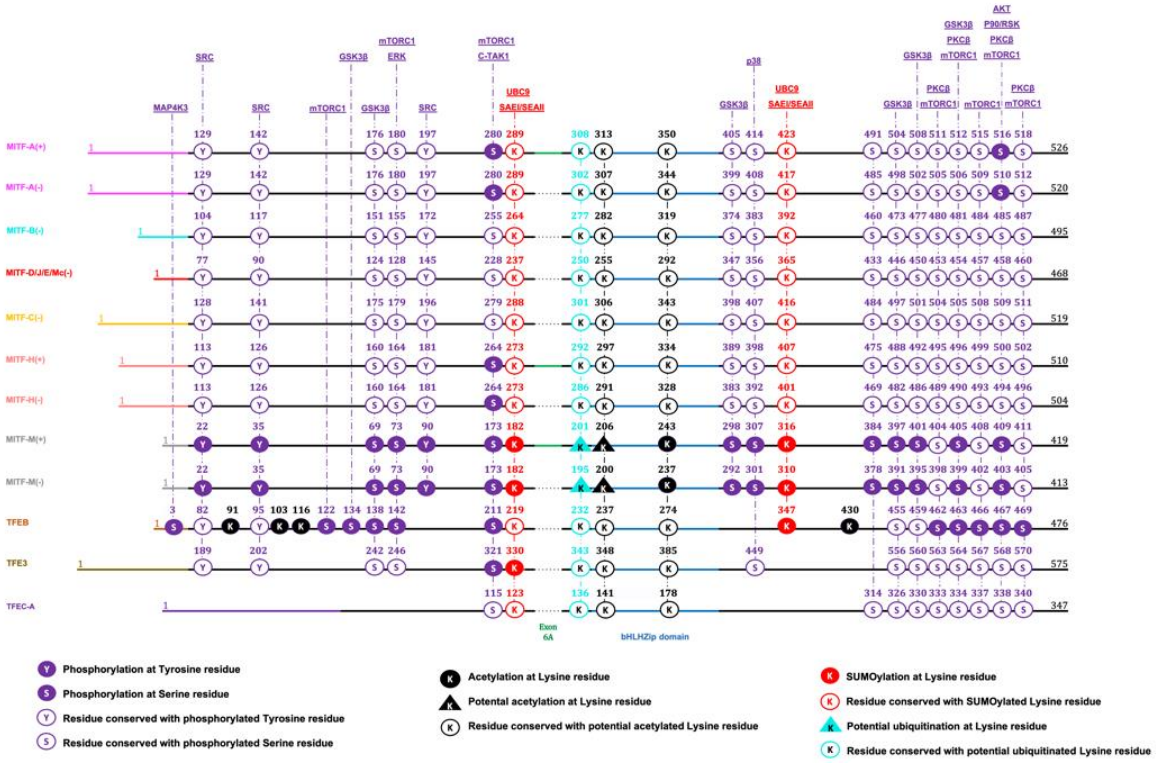

Figure 5. A schematic showing all known post-translational modifications (PTMs) of zebrafish *mitf, tfeb,* and *tfe3* isoforms. Human MITF-A(+) and MITF-*M*(+) are aligned with zebrafish Mitfa (NP_570998.1), Mitfb (NP_571922.2), Tfeb (NP_001244121.1), Tfe3a (NP_571923.2), and Tfec (NP_001025276.2) to map the conserved post-translationally modified residues in zebrafish MiT-TFE factors. Figure obtained with permission from John Wiley and Sons according to permit number 5514180354498 (Vu et al., 2021).

In addition to nuclear localization and transcription activity, phosphorylation has also been proposed to mediate the stability of the MITF protein (Goding and Arnheiter, 2019; Vu et al., 2021). Initially, phosphorylation at S73 was suggested to be required for MITF degradation, and the S73/409A double mutant protein was reported to be significantly more stable than the human MITF-WT protein (Wu et al., 2000; Xu et al., 2000). However, Wellbrock et al. (Wellbrock and Marais, 2005) later found that S73 phosphorylation is not the only mechanism regulating MITF stability since MITF-S73A protein was significantly increased upon MG132 proteasomal inhibitor treatment. Importantly, phosphorylation of S397, S401, S405, and S409 sites has been shown to improve the stability of the MITF protein; when these residues are mutated to alanine protein, stability is also increased (Ploper et al., 2015; Wang et al., 2016).

SUMOylation is a type of post-translational modification (PTM) found in MITF. SUMOylation is a process in which the small ubiquitin-like modifier (SUMO) protein is covalently attached to target proteins at lysine residues. Like phosphorylation, it is a reversible modification. While the SUMO-activating enzyme (E1), SUMO-conjugating enzyme (E2), and SUMO-ligase (E3) are responsible for catalyzing the reaction, SUMO proteases remove SUMO from target proteins. SUMOylation has been shown to affect protein structure, localization, activity, and stability (Flotho and Melchior, 2013). In the case of MITF, SUMOylation has been shown to take place at the K182 and K316 residues (Miller et al., 2005). The enzymes SAE I/SAE II and UBC9 have been suggested to be involved in this SUMOylation process. Interestingly, it has been shown that the single mutation K182R or K316R did not alter the nuclear distribution; and the double K182/316R double mutation did not impact DNA binding, stability, or nuclear localization. However, transcriptional activation by the double mutant was shown to depend on the number of MITF binding sites in the promoter region of its target genes (Murakami and Arnheiter, 2005), such that the K182/316R double mutation is better at activating promoters with multiple binding sites compared to single mutation K182R or K316R or MITF-WT. This suggests that SUMOylation has specific effects on transcription.

Although phosphorylation and SUMOylation of MITF have been well studied, MITF ubiquitination and acetylation are less understood. The K201 residue has been reported as a potential ubiquitination site. While the UCHL1 enzyme has been suggested to act as a ubiquitin ligase for MITF and decrease its stability (Seo et al., 2017), the ubiquitin-specific protease 13 (USP13) deubiquitinates MITF, eventually increasing MITF protein expression leading to an induced expression of genes involved in the proliferation and growth of melanoma cell

lines (Zhao et al., 2011). Multiple lysine residues in MITF can undergo acetylation, including K21, K33, K43, K243, and K248. Acetylation at K243 has been demonstrated to impact its binding to low-affinity binding sites (Louphrasitthiphol et al., 2020). Although these modifications have been mapped, the exact biological function of these PTMs and the interplay between different types of PTMs are still unknown.

1.6.4 MITF mutations in mouse and human

Mutations in *Mitf* have been found in organisms ranging from zebrafish to humans. In humans, as mentioned above, the germline mutation E318K increases the incidence of melanoma. (Bertolotto et al., 2011; Yokoyama et al., 2011). The somatic mutations E87R, L135V, L142F, G244R, and D380N in MITF have also been found in melanoma (Cronin et al., 2009). MITF mutations have also been associated with the Waardenburg type 2A, Tietz syndromes, and the more serious COMMAD syndrome (Amiel et al., 1998; George et al., 2016; Smith et al., 2000; Tassabehji et al., 1994). WS2 is characterized by pigmentary abnormalities in the irides, skin, and hair and partial or bilateral loss of sensorineural hearing (Pingault et al., 1998; Tassabehji et al., 1994). Meanwhile, Tietz syndrome also reduces pigmentation and is characterized by partial albinism and congenital deafness (Léger et al., 2012). The more severe COMMAD syndrome is characterized by coloboma, osteopetrosis, microphthalmia, macrocephaly, albinism, and deafness and is associated with biallelic MITF mutant alleles (George et al., 2016). More than 18 MITF mutations (R203K, K206Q, N210K, I212M, I212S, E213D, R214X, R216K, R217del, R217I, R217G, I224S, S250P, Y253C, R259X, N278D, L283P, and S298P) have been identified in WS2A and TS patients. Consistent with their location in the bHLHzip domain of MITF, most of these mutations, except R203K and S298P, are defective in DNA binding and fail to regulate MITF target genes (Cronin et al., 2009; Grill et al., 2013).

In mice, there are over 40 different alleles that can be arranged in an allelic series according to the severity of their phenotypic effects. The original and most severe allele, $Mitf^{mi}$, leads to a white coat, severe microphthalmia, and osteopetrosis, and results in death at 3-4 weeks of age (Table 1). $Mitf^{Mi\text{-}White}$ ($Mitf^{Mi\text{-}Wh}$) is characterized by a point mutation changing residue 212 from isoleucine to asparagine (Steingrimsson et al., 1994) (Table 1). This residue lies in the middle of the DNA-binding basic region of the protein, is conserved in MiT-TFE family members, and is crucial in the binding of MITF to the M-box motif (Pogenberg et al., 2012). Homozygotes carrying the $Mitf^{Mi\text{-}Wh}$ mutation are white and have small eyes but are less severely affected than the $Mitf^{mi}$ mutation (Steingrimsson, 2010).

Mitf$^{Mi\text{-}Wh}$ heterozygotes have a relatively severe phenotype characterized by dilute coat color and a white belly spot; of all Mitf mutations, the *Mitf*$^{Mi\text{-}Wh}$ mutation leads to the most severe phenotype in heterozygous condition. The *Mitf*$^{mi\text{-}eyeless\text{-}white}$ (*Mit*$^{mi\text{-}ew}$) mutation, which lacks amino acids 187-212, has a white coat and severe microphthalmia but no osteopetrosis (Table 1). The mildest *Mitf* mutation, *Mitf*$^{mi\text{-}spotted}$ (*Mitf*$^{mi\text{-}sp}$), creates no visible phenotype even when homozygous. The *Mitf*$^{mi\text{-}sp}$ mutation is characterized by an extra cytosine in the alternatively spliced 18 bp exon 6A that encodes six amino acids just upstream of the DNA-binding basic domain and, when present in mature mRNA, leads to a premature stop codon in the adjacent exon 6B (Steingrimsson et al., 1994) (Table 1). While typically, the mRNAs encoding or lacking the alternative 6A domain are made in approximately equal proportion in most cell types, *Mitf*$^{mi\text{-}sp}$ homozygotes lack the 6A+ version and the overall *Mitf* mRNA levels are reduced. The DNA binding ability and stablity of MITF(-) homodimers are reduced compared to that of MITF(+) (hereafter referred to as MITF-WT) homodimers (Hemesath et al., 1994; Pogenberg et al., 2012). The combination of reduced mRNA levels and reduced DNA binding of the MITF$^{mi\text{-}sp}$ protein may explain why the pigment enzyme encoded by the *Mitf* target gene *Tyrosinase* and the survival of melanocytes are impaired in *Mitf*$^{mi\text{-}sp}$ homozygotes (Boissy and Lamoreux, 1995; Wolfe and Coleman, 1964). Nevertheless, this latter allele is named "*mi-spotted*" because it induces or enhances a white spotting phenotype when combined with other mutations at the locus (Arnheiter, 2010; Steingrimsson et al., 2004). For example, when the *Mitf*$^{mi\text{-}sp}$ allele is mated to the *Mitf*$^{Mi\text{-}Wh}$ or *Mitf*$^{mi\text{-}ew}$ allele, the resulting offspring is light grey/tan with white spots (Figure 6A). The offspring are white with light grey pigment spots when *Mitf*$^{mi\text{-}sp}$ is mated to the original *Mitf*^{mi} mutation (Figure 6A). And when mated to the *Mit*$^{mi\text{-}ew}$ mutation, the offspring exhibit a "salt-and-pepper" body color with a white head, belly, and feet.

1.6.5 The Mitf$^{mi\text{-}sl}$ suppressor mutation

The intermediate coat pigmentation alterations obtained in compound heterozygotes with *Mitf*$^{mi\text{-}sp}$ made this allele ideal for an N-ethyl-N-nitrosourea (ENU) mutagenesis screen for suppressors of the Mitf phenotype (Appendix 1A). Using this approach, the Steingrímsson group expected to find mutations in novel genes participating in the molecular pathways through which *Mitf* regulates pigment cell development and melanogenesis. Although the group was able to isolate a suppressor mutation, intriguingly, it turned out to be a derivative of the *Mitf*$^{mi\text{-}sp}$ allele, named *Mitf*$^{mi\text{-}spotless}$ (*Mitf*$^{mi\text{-}sl}$), that lacks 104 residues of the carboxyl end of MITF (Figure 6B-C).

Table 1. List of mouse Mitf mutants mention in this study

			Phenotype*		
Allele	**Symbol**	**Mode of induction**	**Heterozygote**	**Homozygote**	**Lesion**
micropthalmia	*Mitf^{mi}*	X-irradiation	Iris pigment less than in wild type; occasional spots on belly, head, or tail	White coat, eyes small and red; deficiency of mast cells, incisors fail to erupt, osteopetrosis; inner ear defects	3 bp deletion in basic domain
oak ridge	*Mitf$^{mi\text{-}or}$*	Gamma-irradiation	Pale ears and tail; belly streak or head spot	White coat, eyes small and red; incisors fail to erupt, osteopetrosis	R216K
white	*Mitf$^{Mi\text{-}Wh}$*	spontaneous or X-irradiation	Coat color lighter than dilute *(d/d)*; eyes dark ruby; spots on feet, tail and belly	White coat; eyes small and slightly pigmented; inner ear defects	I212N
brownish	*Mitf$^{Mi\text{-}b}$*	spontaneous	Fur diluted brownish with pale ears and tail	White coat, reduced eye pigment, eyes of normal size	G244E
eyeless-white	*Mitf$^{mi\text{-}ew}$*	spontaneous	Normal	White coat, eyes almost absent, eyelids never open	25 amino acid deletion (splicing)
VGA-9	*Mitf$^{mi\text{-}vga9}$*	transgene insertion	Normal	White coat, eyes red and small; inner ear defects	transgene insertion and 882 bp deletion
red-eyed	*Mitf$^{mi\text{-}rw}$*	white spontaneous	Normal	White with pigmented spot on head and rump; eyes small and red	Upstream genomic deletion
spotted	*Mitf$^{mi\text{-}sp}$*	spontaneous	Normal (reduced tyrosinase activity in skin)	Normal (reduced tyrosinase activity in skin). MitfMi-Wh/Mitfmi-sp animals are light yellow with white spots on coat; eyes are pigmented	Additional cytosine in polypyrimidine tract; 18 bp exon missing
spotless	*Mitf$^{mi\text{-}sl}$*	ENU	Normal	"Brownish" coat color. Compound heterozygotes with other Mitf mutations show a more normal coat color than is seen with Mitfmi-sp mice.	Additional cytosine in polypyrimidine tract; 18 bp exon missing. In addition, Lys316STOP

In combination with other alleles of MITF, the *Mitf$^{mi\text{-}sl}$* mutation led to reduced effects on the phenotype when compared to the same alleles in combination with the *Mitf$^{mi\text{-}sp}$* mutation. For example, the *Mitf$^{mi\text{-}ew}$/Mitf$^{mi\text{-}sl}$* and *Mitf$^{Mi\text{-}Wh}$/Mitf$^{mi\text{-}sl}$* mice have the darkly pigmented phenotype whereas the *Mitf$^{mi\text{-}ew}$/Mitf$^{mi\text{-}sp}$* and *Mitf$^{Mi\text{-}Wh}$/Mitf$^{mi\text{-}sp}$* compound hereozygotes have major pigmentation defects (Figure 6A). The color was even darker than *Mitf$^{Mi\text{-}Wh}$/Mitf^{+}* mice, suggesting that the *Mitf$^{mi\text{-}sl}$* mutant represents a gain-of-function compared to the Mitf^{WT}. Similar effects were also seen when animals carrying the *Mitf$^{mi\text{-}sl}$* mutation were crossed to the dominant-negative *Mitf^{mi}* (Figure 6A), *Mitf$^{Mi\text{-}or,}$* and *Mitf$^{Mi\text{-}b}$* mutations (Appendix 1B) or the null mutation *Mitf$^{mi\text{-}vga9}$* (Figure 6A). In all cases the coat was more pigmented than when the respective mutations were crossed to the original *Mitf$^{mi\text{-}sp}$* mutation (Figure 6A). These observations showed that the suppressor effects of the *Mitf$^{mi\text{-}sl}$* mutation did not depend on the genetic background. However, *Mitf$^{mi\text{-}sl}$* did not affect the coat color of the recessive *Mitf$^{mi\text{-}rw}$* allele when compared to *Mitf$^{mi\text{-}rw}$/Mitf$^{mi\text{-}sp}$* animals (Figure 6A), reflecting the fact that the latter animals are already black and no further improvement in coat color is therefore possible. Similarly, no effects were observed on eye size or bone development in any of the combinations since both phenotypes are normal in *Mitf$^{mi\text{-}sp}$* homozygotes or their compound heterozygotes.

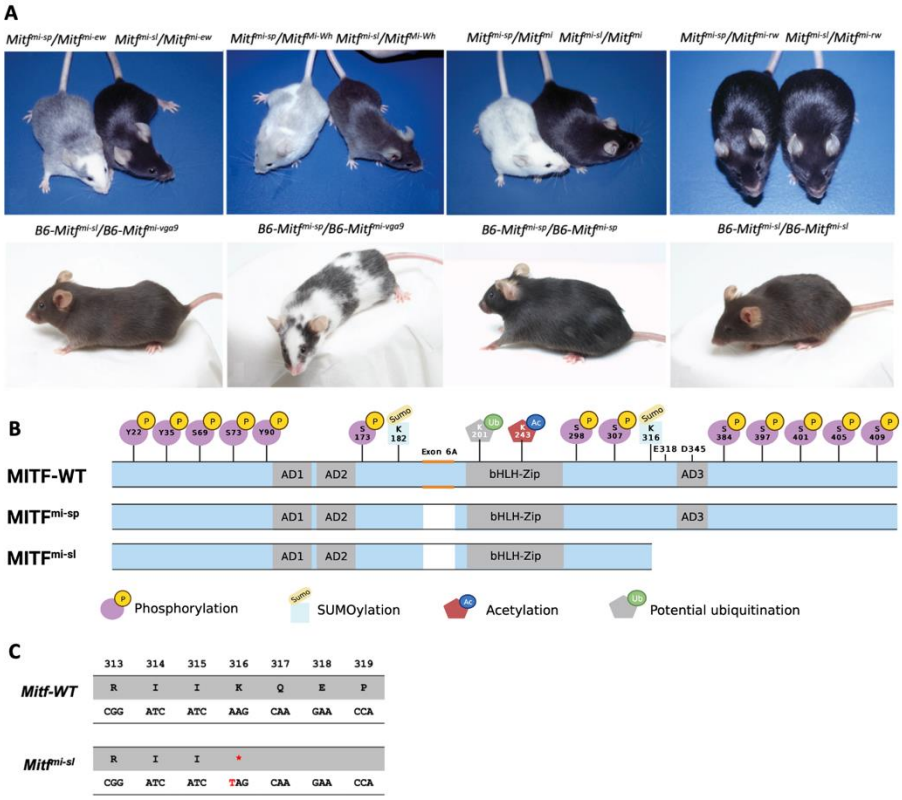

Figure 6. Phenotypes and molecular alteration associated with the induced suppressor mutation (*Mitf^{mi-sl}*). (A) From left to right in the upper pannel: NAW-Mitf^{mi-ew}/B6-Mitf^{mi-sp} and NAW-Mitf^{mi-ew}/B6-Mitf^{mi-sl} compound heterozygotes. B6-Mitf^{Mi-Wh}/B6-Mitf^{mi-sp} and B6-Mitf^{Mi-Wh}/B6-Mitf^{mi-sl} compound heterozygotes. B6-Mitf^{mi-sp}/B6-Mitf^{mi} and B6-Mitf^{mi-sl}/B6-Mitf^{mi} compound heterozygotes. Notice the dramatic suppression of the phenotype from near-white to black coat color. B6-Mitf^{mi-sp}/B6-Mitf^{mi-rw} and B6-Mitf^{mi-sl}/B6-Mitf^{mi-rw} animals. From left to right in the lower pannel: B6-Mitf^{mi-sl}/B6-Mitf$^{mi-vga9}$. B6-Mitf^{mi-sp}/B6-Mitf$^{mi-vga9}$. B6-Mitf^{mi-sp}/Mitf^{mi-sp}. B6-Mitf^{mi-sl}/Mitf^{mi-sl} (B) Compared to MITF-WT, the MITF^{mi-sl} protein lacks 104 residues of the carboxyl end, including a SUMOylation site at K316, a transcription activation domain 3 (AD3), a caspase cleavage site at D345, and phosphorylation sites at S384, S397, S401, S405, and S409. Like the Mitf^{mi-sp} mutation, the Mitf^{mi-sl} RNA also lacks the alternative 18 bp exon 6A. (C) The Mitf^{mi-sl} mutation is an A to T transversion at nucleotide 1075, replacing K316 with a stop codon.

Importantly, in the homozygous condition, the *Mitf^{mi-sl}* mutation affects coat color such that instead of the normally black coat, the animals have a brown color. The "brownish" color of homozygotes carrying the *Mitf^{mi-sl}* mutation might be explained by the observed delay in the onset of pigmentation (Appendix 1C-F).

However, the delay in pigmentation is not due to either an extended period of cell proliferation that would delay the beginning of differentiation, nor does it impair melanoblast development. Interestingly, the total *Mitf* RNA expression was shown to be affected by the $Mitf^{mi\text{-}sl}$ mutation. While expression of *Mitf* RNA is reduced to 65.7% in $Mitf^{mi\text{-}sp}$ in hearts and skin compared to wild-type controls, it remains above wild-type levels (115.8%) in $Mitf^{mi\text{-}sl}$ hearts (Appendix 1G). Importantly, however, the fundamental rescue mechanism at the molecular level of the $Mitf^{mi\text{-}sl}$ was still unknown.

1.7 The PR domain-containing Protein (PRDM) family and PRDM7

The human PR domain-containing Protein (PRDM) family of proteins consists of 17 members (PRDM1-17) with a conserved N-terminus PR domain followed by a variable number of Cys2-His2 (C2H2) zinc fingers towards the C-terminus (Hohenauer and Moore, 2012). The PR domain, which was first noted as the *PRDI-BF1-RIZ1* homologous region, has been suggested to be a derivative of the SET (Su(var)3–9, enhancer of zeste, and trithorax) domain (Buyse et al., 1995; Huang et al., 1998). Although many residues associated with catalytic activity in the PR domain are not conserved in the SET domain, the NMR structure of PR and SET domains are closely similar and both of them potentially have potential methyltransferase activity (Clifton et al., 2014). Regarding location, the PR and SET domains are localized at different parts of the respective protein, with the former mostly located at the N-terminus and the latter primarily at the C-terminus (Huang, 2002). Proteins containing the PR domain typically also have zinc-finger domains. In contrast, SET domains are linked to various motifs, for instance, A/T hooks, zinc fingers, PHD fingers, and GTP binding motifs (Huang, 2002; Jenuwein et al., 1998). It has also been shown that the PR domain of human PRDM4, -6, -7, -9, -10, -11, and -15 is preceded by a short motif with consensus sequence **C**-X2-**C**-X7-**C**-X2-**HG**-P where X can be any amino acid (Briknarová et al., 2011). This short motif is a zinc knuckle motif that participates in protein-protein interactions (Briknarová et al., 2011).

PRDM proteins contain a variable number of zinc fingers except for PRDM11, which has no zinc finger domain (Fumasoni et al., 2007). It has been suggested that differences in the number of C2H2 zinc finger repeats in PRDM proteins can influence specific interactions of PRDMs with either DNA or other proteins (Brayer and Segal, 2008; Ma et al., 2011) and may play an important role in nuclear import (Choi et al., 2014). The interactions of PRDMs with either DNA or other proteins may involve methyltransferase activity or recruitment of

transcription factors to the target promoters (Fog et al., 2012). Particularly, it was shown that PRDMs could recognize a specific DNA sequence and then mediate transcription factors to the target gene promoter. For instance, PRDM1 recruits the Groucho transcription factors to repress the INFβ promoter (Ren et al., 1999).

PRDMs are not present in fungi or plant genomes but originated in metazoans, expanded in vertebrates, and were further duplicated in primates (Fumasoni et al., 2007). PRDMs have been shown to be important players in cell-cycle regulation, apoptosis, cell differentiation, and chromatin-mediated gene expression (He et al., 1998; Hohenauer and Moore, 2012). It has also been found that PRDM genes act as tumor repressors (Huang, 2002). PRDMs are reported to be associated with a wide range of diseases. For instance, genetic variants of PRDM1 have been linked to the risk of rheumatoid arthritis (Raychaudhuri et al., 2009), and a SNP in PRDM9 correlates with human sterility (Miyamoto et al., 2008).

Among the 17 PRDM family members, PRDM2, -3, -6, -8, -9, and -16 show methyltransferase activity (Eom et al., 2009; Eram et al., 2014; Pinheiro et al., 2012; Wu et al., 2008). Particularly, both PRDM2 and PRDM8 catalyze di-methylation of lysine 9 of histone H3 (H3K9me2) (Eom et al., 2009; Kim et al., 2003). However, histones may not be the sole target for the methylation activity of PRDMs (Fog et al., 2012). Since only a few members of the PRDM family present catalytic activity, it has been suggested that the PR domain may have evolved from a catalytic domain to a protein interaction module. Subsequently, PRDMs may have acquired roles in regulating their interaction partners (Fog et al., 2012). Definitely, some members of the PRDM family have been shown to play indirect roles by recruiting chromatin remodeling enzymes (Ancelin et al., 2006; Davis et al., 2006). Particularly, PRDM1 binds to PRMT5, an arginine-specific histone methyltransferase, to provoke di-methylation of arginine 3 on histone H2A and/or H4 tails (H2A/H4R3me2s) in germ cells (Ancelin et al., 2006). PRDM6 is associated with H4K20 methylation in endothelial cells (Wu et al., 2008) and interacts with p300 histone acetyltransferase (HAT) to acetylate histones in smooth muscle cells (Davis et al., 2006).

PRDM proteins have been found at different protein complexes and play distinct roles in different cell types and promoter-dependent manners. For example, PRDM1, -5, and -6 function as transcriptional repressors by recruiting histone methyltransferase G9a and class I histone deacetylases HDAC1-3 to their target gene promoters (Davis et al., 2006; Duan et al., 2007; Gyory et al., 2004; Yu et al., 2000). PRDM2, -5, and -9 regulate cell-cycle (Deng and Huang, 2004;

Hayashi et al., 2005; He et al., 1998), while PRDM6 is suggested to regulate vascular proliferation by repressing genes associated with a differentiated phenotype (Davis et al., 2006). Although the enzymatic activity of PRDM14 remains to be clarified, this protein has critical roles in the maintenance and differentiation of human embryonic stem cells by regulating the expression of the key pluripotency gene POU5F1 directly and integrating into the core transcriptional regulatory network with other key transcription factors such as OCT4, NANOG and SOX2 (Chia et al., 2010; Tsuneyoshi et al., 2008). PRDM16 is a master regulator of brown fat differentiation (Kajimura et al., 2010).

Interestingly, it has been shown that PR domain-containing protein 7 (PRDM7) arose from a PRDM9 duplication event during the primate evolution (Fumasoni et al., 2007; Heerschop et al., 2021). PRDM7 may have originated in the *Catarrhine* branch before the separation of *Cercopithecoidea* and *Hominoidea*. However, why *Hominoidea* representatives need PRDM7 still needs to be further investigated. Because of the duplication event, PRDM9 and PRDM7 are highly homologous, with only three amino acid residues of the PR/SET domain of PRDM7 being different from that of PRDM9 (residues 244–358 in both proteins) (Blazer et al., 2016). These three different residues may lead to different catalytic activities and substrate specificity between PRDM7 and PRDM9. Although the biological roles of PRDM7 remain elusive, it is generally suggested to be a histone methyltransferase, with the SET domain enabling trimethylation of H3 lysine 4 (H3K4) both in vitro and in vivo (Blazer et al., 2016). Compared with PRDM7, the catalytic activity of PRDM9 is mono-, di- and trimethylation of H3K36 and H3K4 in vitro and in cells (Eram et al., 2014; Hayashi et al., 2005). While PRDM9 is only found in germ cells and plays roles in meiotic recombination (Baudat et al., 2010), PRDM7 is more widely expressed in non-meiotic tissues. However, limited information has been reported on its function. PRDM7 has been suggested to be expressed highly in melanocytes, suggesting its specific contribution to regulating melanocyte function (Fumasoni et al., 2007).

PRDM9 contains three functional domains, namely an N-terminus KRAB domain, a central PR/SET domain, and a terminus zinc finger (ZF) domain of C2H2 type (cysteine2-histidine2) (Parvanov et al., 2010). While an N-terminus KRAB domain promotes protein-protein interactions, the central PR/SET domain catalyzes histone trimethylation, and a terminus zinc finger (ZF) domain of C2H2 type determines DNA binding specificity (Parvanov et al., 2010). The PRDM7 gene has undergone a massive structural rearrangement compared with the PRDM9 gene. The number of encoded zinc fingers in PRDM7 is reduced compared to PRDM9, and the pattern of gene splicing is altered (Fumasoni et al., 2007).

Indeed, the PRDM7 protein contains only four Zn-Fingers domains in contrast to 14 Zn-Fingers in PRDM9 upon the partial deletion of the last exon coding for Zn-Fingers (Fumasoni et al., 2007). Moreover, an 89-nucleotide long segment coding for the PR-domain C-terminus part is duplicated in PRDM7 compared to PRDM9 (Fumasoni et al., 2007). The tandem duplication causes splicing variants (Appendix 2). In theory, the genomic locus of PRDM7 could code for a long isoform with the KRAB, SET, and Zn-figures domains, but the mRNA sequences published so far correspond to a short variant containing either KRAB and SET domains (isoform A – dominant isoform) or SET and Zn-Figures (isoform B) only (Figure 7). The above-mentioned rearrangements may be involved in changing the function of PRDM7 compared with PRDM9 (Blazer et al., 2016; Fumasoni et al., 2007).

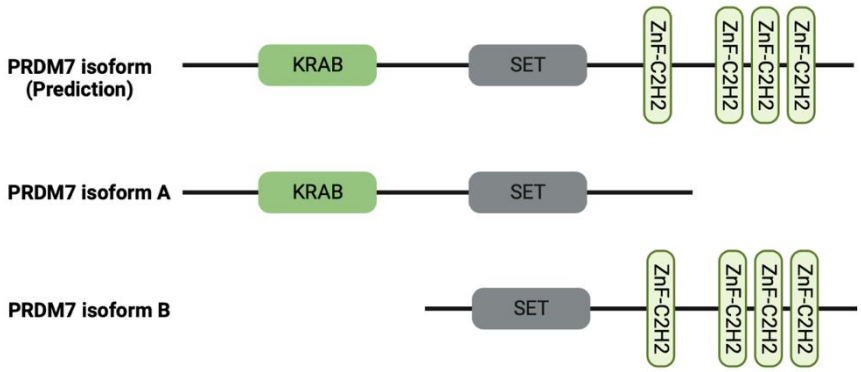

Figure 7. Domain architecture of PRDM7 isoform A and isoform B

2 Aims

2.1 Characterize the molecular mechanism involved in the genetic suppression of the Mitf$^{mi\text{-}sl}$ mutation

i. Study the molecular effects of the Mitf$^{mi\text{-}sl}$ mutation
ii. Unravel the mechanism of E318K mutation in melanoma

2.2 The functional roles of PRDM7 in melanoma

i. Functional characterization of Skmel28 and 501Mel melanoma upon PRDM7 depletion

ii. Analysis of the transcriptome profile of PRDM7 knock-out cells to map the regulatory network of PRDM7 and MITF

iii. Analyze the alteration of H3K4me3, H3K9me3, H3K27me3 histone modifications upon PRDM7 and MITF knock-out

3 Materials and methods

3.1 Cell culture, reagents, and antibodies

The cell lines HEK293, A375P (CRL-3224), and SkMel28 (HTB-72) were purchased from ATCC. 501Mel melanoma cells were obtained from the lab of Dr. Ruth Halaban (Yale University). The cells were maintained in RPMI 1640 medium (Gibco, (#5240025) supplemented with 10% FBS (Gibco #10270–106) at 5% CO_2 and 37°C in a humidified incubator. Cycloheximide (CHX - 50mg/ml) (Sigma, #66819), 20mg/ml MG132 (Sigma, #474790), 10mg/ml Doxycycline (Dox – Sigma, #324285), 10mg/ml TPA (Merck, #P1585), 1mg/ml Baf-A1 (Merk, #88899-55-2), 5mM Leptomycin B (Merk, #L2913), 5mM PLX4032 (Selleckchem, #S1267) stock solutions were prepared in DMSO. The primary antibodies used for all Western blot (WB) experiments and their dilutions were as follows: Anti-Flag (Sigma, #F3165) at 1:5000 dilution; Anti-β-Actin (Cell Signaling, #4970) at 1:1000 dilution; Anti-γH2AX (Abcam, #ab2251) at 1:2000 dilution, Anti-GAPDH (Cell Signaling, #), at 1:1000 dilution; Anti-H3K27me3 (Cell Signaling, #9733) at 1:1000 dilution; Anti-GFP (Abcam, #ab290) at 1:2500 dilution; Vimentin (Cell signaling, #5741) at 1:2000 dilution; CDC2 (Cell signaling, #9111) at 1:1000 dilution; CyclinB1 (Abcam, #ab32053) at 1:2000 dilution; Actin (Millipore, #Mab1501) at 1:5000 dilution; and MITF (Millipore, #Mab3747) at 1:2000 dilution. The primary antibodies used for the immunostaining experiments and their dilutions were as follows: Vimentin (Cell signaling, #5741) at 1:250 dilution, phospho-Paxillin (Tyr118) (Cell Signaling, #2541) at 1:100 dilution, MITF (Millipore, #Mab3747) at 1:200 dilution. The antibodies used for the Cut&Run are listed as follows: Anti-H3K4me3 (Cell Signaling, #9751S), Anti-H3K9me3 (Active-MO, #39161), Anti-H3K27me3 (Cell Signaling, #9733), and Rabbit IgG (Cell Signaling, #3900S).

3.2 Generation of plasmid constructs for stable doxycycline-inducible overexpression and knockdown

Fusions of wild-type and mutant mouse MITF-M cDNA with the 3XFLAG-HA tag at the C- or N-terminus or fusion with the GFP-tag at the C terminus were generated in the piggy-bac vector pPB-hCMV1. PRDM7 isoforms fusions with the 3XFLAG-HA tag at the C-terminus were also constructed in the same piggy-bac vector.

The cDNAs were subcloned downstream of a tetracycline response element (TRE) using the Gibson Assembly Cloning kit (New England Biolabs # E5510S). Mutations were introduced by in vitro mutagenesis using Q5 Site-directed Mutagenesis Kit (New England Biolabs) according to the manufacturer's instructions.

The BLOCK-iT RNAi designer was used to design microRNAs (miR1-PRDM7 and miR2-PRDM7) both targeting exon 10 of PRDM7. A non-targeting control (miR-CTRL) was used as a negative control. The microRNAs targeting PRDM7 and miR-CTRL (Table 2), including the required sequence for the terminal loop, were cloned downstream of a tetracycline response element (TRE) in the pPB-hCMV1 vector using the Gibson Assembly Cloning kit (New England Biolabs # E5510S following a similar protocol as mentioned above. A non-targeting control (miR-CTRL) was used as a negative control. All clones were sequence verified (Table 3).

Table 2. List of miR-PRDM7

Name	pre-miRNA sequences
miR-NTC	5'-TTTCGCTAAATGTACTGCGCGTGGAGACTTTTGGCCACTGACTGACTCTGAGGTCTTCAGCGAAA-3'
miR1-PRDM7-1	5'-TTTCGCTGAAGCCACCTCAGAGTTTTGGCCACTGACTGACTCTGAGGTCTTCAGCGAAA-3'
miR2-PRDM7-2	5'- TTTCCGATCTCTTTACACTCTGTTTTGGCCACTGACTGACAGAGTGTAGAGATCGGAAA -3'

Table 3. List of generated pPB-hCMV1 plasmids in this study

Expressing protein	Fusion tag	Expressing protein	Fusion tag
PRDM7-isoformA	3XFlag-HA	MITF$^{mi\text{-}sp}$-del326-378	3XFlag-HA
PRDM7_28kDa_PC1	3XFlag-HA	MITF$^{mi\text{-}sp}$-S73E	3XFlag-HA
PRDM7_28kDa_PC2	3XFlag-HA	MITF$^{mi\text{-}sp}$ -S73A	3XFlag-HA
miR1_PRDM7	3XFlag-HA	MITF$^{mi\text{-}sp}$-K316R	3XFlag-HA
miR2_PRDM7	3XFlag-HA	MITF$^{mi\text{-}sp}$-E318K	3XFlag-HA
Empty (EV)	3XFlag-HA	MITF$^{mi\text{-}sp}$-S409A-K316R	3XFlag-HA
Empty	GFP	MITF$^{mi\text{-}sp}$-S409A-E318K	3XFlag-HA
MITF-WT	3XFlag-HA	MITF$^{mi\text{-}sp}$-K182R-K316R	3XFlag-HA
MITF-WT	GFP	MITF$^{mi\text{-}sp}$-S325A	3XFlag-HA
MITF-WT-S73E	3XFlag-HA	MITF$^{mi\text{-}sp}$-K316R-S325A	3XFlag-HA
MITF-WT-K316R	3XFlag-HA	MITF$^{mi\text{-}sp}$-E318K-S325A	3XFlag-HA
MITF-WT-E318K	3XFlag-HA	MITF$^{mi\text{-}sp}$-S384A	3XFlag-HA
MITF-WT-S409A-K316R	3XFlag-HA	MITF$^{mi\text{-}sp}$-S397A	3XFlag-HA
MITF-WT K182R-K316R	3XFlag-HA	MITF$^{mi\text{-}sp}$-S401A	3XFlag-HA
MITF-WT	3XFlag-HA -(N-ter)	MITF$^{mi\text{-}sp}$-S405A	3XFlag-HA
MITF$^{Mi\text{-}Wh(+)}$	3XFlag-HA	MITF$^{mi\text{-}sp}$-S409A	3XFlag-HA
MITF$^{Mi\text{-}Wh(-)}$	3XFlag-HA	MITF$^{mi\text{-}sp}$-4A	3XFlag-HA
MITF^{mi}-316X	3XFlag-HA	MITF$^{mi\text{-}sp}$-E318K-S384A	3XFlag-HA
MITF^{mi}-326X	3XFlag-HA	MITF$^{mi\text{-}sp}$-E318K-S397A	3XFlag-HA
MITF^{mi}-378X	3XFlag-HA	MITF$^{mi\text{-}sp}$-E318K-S401A	3XFlag-HA
MITF^{mi}-del316-326	3XFlag-HA	MITF$^{mi\text{-}sp}$-E318K-S405A	3XFlag-HA
MITF^{mi}-S73A	3XFlag-HA	MITF$^{mi\text{-}sp}$-E318K-4A	3XFlag-HA
MITF$^{mi\text{-}ew}$	3XFlag-HA	MITF$^{mi\text{-}sp}$-K316R-S384A	3XFlag-HA

MITF$^{mi\text{-}ew}$-316X	3XFlag-HA	MITF$^{mi\text{-}sp}$-K316R-S397A	3XFlag-HA
MITF$^{mi\text{-}ew}$-326X	3XFlag-HA	MITF$^{mi\text{-}sp}$-K316R-S401A	3XFlag-HA
MITF$^{mi\text{-}ew}$-378X	3XFlag-HA	MITF$^{mi\text{-}sp}$-K316R-S405A	3XFlag-HA
MITF$^{mi\text{-}ew}$-del316-326	3XFlag-HA	MITF$^{mi\text{-}sp}$-K316R -4A	3XFlag-HA
MITF$^{mi\text{-}ew}$-S73A	3XFlag-HA	MITF$^{mi\text{-}sl}$	3XFlag-HA
MITF$^{mi\text{-}sp}$	3XFlag-HA	MITF$^{mi\text{-}sl}$	3XFlag-HA -(N-ter)
MITF$^{mi\text{-}sp}$	3XFlag-HA -(N-ter)	MITF$^{mi\text{-}sl}$	GFP
MITF$^{mi\text{-}sp}$	GFP	MITF$^{mi\text{-}sl}$(+)	3XFlag-HA
MITF$^{mi\text{-}sp}$-del316-326	3XFlag-HA	MITF$^{mi\text{-}sl}$-K182R	3XFlag-HA
MITF$^{mi\text{-}sp}$-326X	3XFlag-HA	MITF$^{mi\text{-}sl}$-S73E	3XFlag-HA
MITF$^{mi\text{-}sp}$-326X-K316R	3XFlag-HA	MITF$^{mi\text{-}sl}$-S73A	3XFlag-HA
MITF$^{mi\text{-}sp}$ -326X-E318K	3XFlag-HA	TFEB	3XFlag-HA
MITF$^{mi\text{-}sp}$-378X	3XFlag-HA	TFE3	3XFlag-HA
MITF$^{mi\text{-}sp}$ -378X-K316R	3XFlag-HA	ζ-14-3-3	3XFlag-HA
MITF$^{mi\text{-}sp}$ -378X-E318K	3XFlag-HA	ε-14-3-3	3XFlag-HA

3.3 Generation of stable doxycycline-inducible MITF, PRDM7 overexpression, and PRDM7-knockdown cell lines

Inducible A375P, SKmel28, and 501Mel cells were generated as described before (Dilshat et al., 2021a). Briefly, the wild-type and mutant mouse MITF fusion constructs with the 3XFLAG-HA at the C- or at N-terminus or fusion with GFP at C-terminus or PRDM7 fusion constructs with the 3XFLAG-HA at C-terminus or a pPB-hCMV1-miR-PRDM7 or a pPB-hCMV1-EV-3XFLAG-HA empty vector were transfected into 70—80% confluent A735P, 501Mel or SKMel28 cells using Fugene HD reagent (Promega, Ref#E2311) together with the py-CAG-pBase and pPB-CAG-rtTA-IRES-Neo plasmids at a 10:10:1 ratio. After 48 hours of transfection, the transfected cell lines were selected with 0.5mg/ml of G418 (Gibco, #10131-035) for two weeks. A 'mock plate' of no transfected cells was

also included in each case. To equalize the expression of MITF proteins, the dox-inducible A375P, 501Mel, and SKmel28 melanoma cell lines were treated with varying concentrations of doxycycline and the dox concentrations leading to similar MITF protein levels were used for future experiments. For overexpressing or knocking down PRDM7, the dox-inducible PRDM7 overexpression or knock-down cell lines were treated with doxycycline at 1ug/ml final concentration.

3.4 Knockdown of genes using siRNA

Cells were seeded at the density of $8x10^4$ per well in 24-well plates before transfection with the appropriate siRNAs. The siRNAs were obtained from ThermoFisher and were the following: siPRDM7 #AM16708 ID: 35655, siAKIRIN2 #4392420 ID: s30222). Cells were reverse transfected with 5pmol siRNA at the final concentration using Lipofectamine RNAiMAX (Invitrogen, #13778030) according to the manufacturer's instructions. For the protein degradation assay, cells were cultured with siRNA for 24 hours before inducing MITF expression by doxycycline. In order to prepare RNA from the samples, cells were treated with corresponding siRNA two days before harvesting.

3.5 Subcellular fractionations

The stable doxycycline-inducible MITF cells were seeded on 6-well plates at a density of $3.5x10^5$ cells per well. The next day, cells were treated with doxycycline at a different concentration depending on the cell lines to induce the expression of MITF protein. Upon 24 hours of dox treatment, the cells were either directly harvested or continuously treated with TPA at 200nM for 1 hour, 4 hours, or treated with TPA (200nM) for 1 hour and MG132 (40ug/ml) for the next 3 hours in the presence of TPA before harvesting by trypsinization. Cells were washed with PBS before washing twice with swelling buffer, which consisted of 10 mM HEPES, pH 7.9, 1.5 mM $MgCl_2$, 10 mM KCl, 0.5 mM DTT, and freshly added protease and phosphatase inhibitors. The cells were then lysed by incubated at 4°C for 15min in Cell lysis buffer (10mM HEPES, pH 7.9, 1.5 mM $MgCl_2$, 10 mM KCl, 0.5mM DTT, 0.1% NP40). Approximately 30% of the sample was collected and set aside as whole cell lysate. The remaining cell lysate was spun down at 3000 rpm for 5min at 4°C, and the supernatant was collected as the cytoplasmic fraction. At the same time, the pellet, representing the nuclear fraction, was washed with cold PBS before resuspension in RIPA buffer (20mM Tris-HCl, pH7.4, 50mM NaCl, 2mM MgCl2, 1%(v/v) NP40, 0.5%(m/v) sodium deoxycholate, and 0.1% (m/v) sodium dodecyl sulfate, and freshly added protease and phosphatase inhibitors) for further experiments including Western blot and immunoprecipitation.

3.6 Immunoprecipitation

Cells were seeded on 6-well plates at a density of $3.5x10^5$ cells per well the day before transfection. The following day, FuGENE HD reagent (Promega # E2311) was used to conduct the co-transfection of MITF-WT, $MITF^{mi\text{-}sp}$ or $MITF^{mi\text{-}sl}$-GFP-tagged constructs together with $MITF^{mi}$, $MITF^{mi\text{-}ew}$, $MITF^{Mi\text{-}Wh}$, ε-14-3-3 or ζ-14-3-3)-Flag-tagged proteins. After 24 hours, the cells were washed twice with ice-cold PBS and lysed by adding 200ul of RIPA buffer (20mM Tris-HCl, pH7.4, 50mM NaCl, 2mM MgCl2, 1%(v/v) NP40, 0.5%(m/v) sodium deoxycholate, and 0.1% (m/v) sodium dodecyl sulfate), with freshly added protease and phosphatase inhibitors. The cell lysate was then ready for immunoprecipitation (IP); 30% of the sample was collected as an input fraction.

For each IP sample, 20ul of Dynabeads Protein G magnetic beads (Invitrogen, # 10004D) were washed twice with 1ml PBS using a magnetic stand before resuspending in 300ul of PBS containing 0.01% Tween 20. The magnetic beads were then conjugated with anti-Flag antibodies by adding 1ug anti-Flag antibody (Sigma, #F3165), followed by a 30-minute incubation at RT with rotation. The magnetic beads were then washed twice with PBS containing 0.01% Tween 20 to eliminate non-conjugated antibodies and then resuspended with 20ul of PBS containing 0.01% Tween 20. The IP samples were incubated with the coated beads overnight at 4°C with rotation. Samples were then placed on the magnetic stand, and supernatants were removed and saved as an unbound fraction (UnB) in each case. The beads were washed twice with 1ml PBS containing 0.01% Tween 20. The protein was eluted from the beads by incubating with 150 ng/µL 3X Flag peptide in PBS containing 0.01% Tween 20 for 30 minutes at 4°C with rotation. The samples were placed on the magnetic stand, and supernatants were saved as an immunoprecipitation fraction (IP). The collected fractions were then subjected to Western blot analysis.

3.7 Protein degradation assay

The dox-inducible A375P cells were treated with doxycycline to express MITF-WT and MITF mutant proteins for 24 hours and then treated with 40µg/ml cycloheximide (Sigma #66819), in the presence or absence of 200nM TPA, 2uM PLX, or 5nM LMB for 0, 1, 2, and 3 hours before harvesting. For protein degradation pathway analysis, the dox-inducible A375P cells were treated with doxycycline to express the respective MITF constructs for 24 hours at a density of $8x10^4$ cells and then treated with either 40ug/ml MG132 or 2ug/ml Baf-A1 in the presence or absence of 40ug/ml CHX for 3 hours before harvesting. For determining where protein degradation takes place, the dox-inducible A375P

cells were seeded at a density of $8x10^4$ cells and treated with siAKIRIN2 for 24 hours before inducing the expression of either MITF-WT or $MITF^{mi\text{-}sl}$ proteins with dox in the next 6 hours. The cells were then treated with 40µg/ml cycloheximide for 0, 1, 2, and 3 hours before harvesting.

FuGENE HD reagent (Promega # E2311) was used for the co-transfection of $MITF^{mi\text{-}sl}$ and other MITF mutant proteins. After 24 hours, the cells were treated with 55µg/ml cycloheximide (Sigma #66819) for 0, 1, 2, and 3 hours. The cells were finally lysed in SDS sample buffer (2% SDS, 5% 2-mercaptoethanol, 10% glycerol, 63 mM Tris-HCl, 0.0025% bromophenol blue, pH 6.8), and the expression of the MITF protein determined by Western blot using Flag antibodies.

3.8 Western blot analysis

Cell lysates in SDS sample buffer (2% SDS, 5% 2-mercaptoethanol, 10% glycerol, 63 mM Tris-HCl, 0.0025% bromophenol blue, pH6.8) were boiled for 5 minutes at 95°C. Proteins were separated by SDS-PAGE and then transferred to 0.2 µm PVDF membranes (Thermo Scientific #88520). To minimize background staining, the membranes were blocked in T-TBS (20mM Tris, pH 7.4; 150mM NaCl; 0.01% Tween 20) containing 5% BSA. The membranes were probed with specific primary antibodies. Following incubation with the primary antibody the blots were washed three times with T-TBS for 10 minutes each, the membrane was then incubated for 1 hour at room temperature with either DyLight 800 anti-mouse (Cell Signaling, #5257) or DyLight 580 anti-rabbit IgG (Cell Signaling, #5366) secondary antibodies (Cell Signaling Technology). The protein bands were detected using Odyssey CLx Imager (LICOR Biosciences) and Image Studio version 2.0. The band intensities were quantified using the open-access ImageJ software (https://imagej.nih.gov/ij/).

3.9 Generation of PRDM7 knock-out cell lines

In order to generate knock-out mutation in the PRDM7 gene, CRISPR-Cas9 technology was used. Recombinant Alt-R *S.p.* Cas9 Nuclease V3 (Cat# 1081059), sequence-specific CRISPR RNA (crRNA) (5'-CCGATGAAGAATGGACCT-3', Ref#225403159) and Alt-RCRISPR-Cas9 tracrRNA ATTO 550 (tracrRNA) (IDT, t#1077024) were obtained from Integrated DNA Technologies (USA). The tracrRNA and pre-designed crRNA with the highest on-target and off-target scores targeting exon 3 of PRDM7 were ordered in the Alt-R format. The proprietary chemically modified Alt-R RNA protects the RNA oligos from degradation by cellular RNAase and further improves on-target

editing performance. The Cas9:crRNA:trRNA Alt-R ribonucleoprotein (RPN) complex was formed according to the manufacturer's instructions. Firstly, the crRNA and trRNA were resuspended to 2uM in Nuclease-Free Duplex Buffer (IDT, Cat#1072570) before forming the crRNA:trRNA duplex. Oligos were mixed at equimolar concentrations in a sterile microcentrifuge tube before annealing by heating at 95°C for 5 min in a PCR thermocycler. The mixture was then slowly cooled to room temperature. Before producing the transfection complex, (1:1:1, Cas9:crRNA:tracrRNA) Alt-R RNP complex was prepared 5 mins prior to mixing 1uM crRNA:tracrRNA and 1uM Cas9 nuclease with 1:1 volume ratio in Opti-MEM media (Gibco, Cat#11858-021). After that, 1.2ul per well Lipofectamine RNAiMAX lipid transfection reagent (Invitrogen, #13778-075) was incubated with 30nM (1:1:1, Cas9:crRNA:tracrRNA) Alt-R RNP complex in a final 50ul total volume for 20 min at room temperature. All transfections in SKmel28 and 501Mel cell lines were reverse transfected in a 96-well cell culture plate using 4.10^4 cells suspended in 100ul RPMI with 10% FBS per transfection. The cells were incubated for 48 hours post-transfection at 37°C in a 5% CO_2 humidified incubator. The transfected SKmel28 and 501Mel cells were serially diluted in 96-well plates to form single colonies. Following five weeks in stepwise expansion culture, single-cell colonies were trypsinized and divided in half. Half of the cells were sub-cultured in 6-well plates for further growth, and the other half was subjected to DNA isolation. Mutations were then detected by using T7 Endonuclease I (NEB, Cat#M0302S) and Sanger sequencing. As a result, we obtained PRDM7 knock-out cell lines (501Mel-PRDM7-KO and SKmel28-PRDM7-KO) targeting exon 3. The respective control cell lines, termed Skmel28-Control and 501Mel-Control, were generated by transfecting the cell without crRNA:trRNA duplex.

3.10 Preparation for Sanger sequencing

Genomic DNA was isolated from the PRDM7 knock-out cell lines. Approximately 2.10^5 cells were trypsinized and spun down at 1500 rpm for 2 min in an Eppendorf 5418 Centrifuge. The supernatant was removed. The cell pellet was resuspended in 25 µL of PBS before suspending in 250 µL Tail buffer (50mM Tris pH8, 100 mM NaCl, 100 mM EDTA, 1% SDS and 0.2mg/mL Proteinase K ThermoFisher, #EO0491) and incubating at 56°C overnight. At the next stage, 50ul of 5M NaCl was mixed with the suspension collected from the above step on a shaker for 5 minutes and spun at 12000 rpm for 5min in an Eppendorf 5418 Centrifuge 5418. The resulting supernatant was mixed with 300µL isopropanol by inversion and centrifuged at 12000 rpm for 5min in an Eppendorf 5418 Centrifuge. The collected pellet was washed with 70% Ethanol

and air-dried at room temperature. Finally, the dried pellet was dissolved in nuclease-free water for at least 2 hours at 37 °C.

PCR was performed to amplify the genomic region around exon 3 of PRDM7 using specific primers (Table 4). PCR mixture consisted of 500ng of gDNA, 10µl of 5X Q5 reaction buffer (NEB, #B9027S), 2.5µl of each specific forward and reverse primers (10pmol/µl), 1ul of 10mM dNTPs, 0.5ul of Q5 Hot start High-Fidelity DNA polymerase and nuclease-free water to the final volume of 50µl. After heating at 98°C for 30 seconds, the PCR amplification was programmed on the Veriti 96-Well Thermal Cycler (ThermoFisher, #4375786) for 31 cycles at 98°C for 10 seconds, 68°C for 12 seconds, 72°C for 30 seconds, and final elongation at 72°C for 5 mins. After PCR, the sizes of the resulting PCR products were confirmed by running the samples on 1.5% agarose gels at 90V for 30min. Subsequently, the PCR product was purified using the GeneJET PCR Purification Kit (ThermoFisher, #K0702). The concentration and purity of DNA were measured using the NanoDrop One Microvolume UV-Vis Spectrophotometer (ThermoFisher Scientific). The purified DNA was stored at −20°C or used immediately. The amplified regions were then subjected to Sanger sequencing, and the percent of insertions and deletions (indels) in the DNA of the targeted region relative to control cells was further determined using the ICE CRISPR Analysis Webtool (https://www.synthego.com/).

Table 4. Primers used for amplifying genomic regions of exon 3 of PRDM7 and exon 4 of PRDM9

Target	Primer name	Sequence	Amplicon size
Exon 3 -PRDM7	PRDM7_CRISPR-F	GAGAAGCTGAGGTGGGAGAA	958bp
	PRDM7_CRISPR-R	ATGGGCAGAAATGGGAGACT	
Exon 4-PRDM9	PRDM9-CRISPRscreen-F	TTAGTTCTCAGGTGGTGGCA	619bp
	PRDM9-CRISPRscreen-R	GAGACCAGCTTGACCAACAC	

3.11 Identifying alternative splicing and novel PRDM7 isoforms by PCR amplification and test digest

cDNA isolated from SKmel28 melanoma cells was used as the template to identify novel PRDM7 isoforms using PCR amplification. The common PCR was performed to amplify the target region using specific primers (Tables 5 and 6).

The sizes of PCR products were confirmed by running samples on 1.5% agarose gels at 90V for 30min. To screen novel PRDM7 isoforms, PCR products were cloned into pUC19 using the Gibson Assembly Cloning kit (New England Biolabs # E5510S). Before sending to sequencing the pUC19_PRDM7 plasmids, we conducted the test digested using BamHI (NEB, #R3136) and HindII (NEB, #R3104) restriction enzymes to confirm the size of the insert. For understanding alternative splicing events, primers in table 6 were used to amplify the target regions. The resulting PCR products were excised from agarose gels and purified by using GeneJET Gel Extraction Kit (ThermoFisher, #K0692) before sending to sequencing.

Table 5. Primers used for identifying novel PRDM7 isoforms

Primer name	Sequence
PRDM7_Predicted_GibpUC19_fwd	gcttgcatgcctgcaggtcgGATCTTGACTCACTGCAAC
PRDM7_Predicted_GibpUC19_rev	acccggggatcctctagagtAGAGTTTGGACCTTTCTTTG

Table 6. Primers used for identifying alternative splicing in PRDM7

Primer name	Sequence
PRDM7_PCR_Exon1_Fwd	ATGAGCCCTGAAAGGTCCCAAGA
PRDM7_PCR_Exon3_Rev	TCTTCTGTGTCATCCACCTGGAGTTT
PRDM7_PCR_Exon5_Rev	AGGAGGGGACACTGGTTTCTGAGCC
PRDM7_PCR_Exon6_Rev	TGTGGCTCGCTGATCTCTTTGTATG
PRDM7_PCR_Exon5_Fwd	GAGAGAATTGTCAGGAACGCCA
PRDM7_PCR_Exon9_Rev	TGAGCTCTTTCTTCCACTTGCTG
PRDM7_PCR_Exon7_Fwd	ATTTGTAAAGGACAGTGCAGTGG
PRDM7_PCR_Exon10_Rev	GACTTGAAAAGGCCAGACAGCATG

3.12 Immunostaining

For immunohistochemistry, cells were seeded in 8-chamber polystyrene vessel tissue culture-treated glass slides (Falcon, #354108) at 70% confluence. First, the

culture media were aspirated, and cells were then fixed with 4% paraformaldehyde (PFA) diluted in warm PBS for 15 minutes. After three washes with PBS for 5 min each, the blocking buffer (1xPBS, 5% Normal Goat Serum (Gibco, #6210-064) 0.3% Triton X-100) was added to each chamber and incubated for 1 hour at room temperature. After that, the cells were incubated with the appropriate primary antibody diluted in antibody dilution buffer (1xPBS, 1% BSA, 0.3% Triton™X-100) at 4°C overnight. After three washes with PBS for 5min each, the cells were then incubated for 2 hours at room temperature with the appropriate secondary antibody diluted in antibody dilution buffer. The secondary antibodies used for immunostaining were listed as follows: Alexa Flour 488 (ThermoFisher, #A11008) at 1:1000 dilution or Alexa Flour 546 (ThermoFisher, #1-11003) at 1:1000 dilution. Finally, the cells were washed three times in 1X PBS for 5min each before mounting in SlowFade Gold Antifade Reagent with DAPI (ThermoFisher, #8961,) and covering with a cover slide. The slides were then stored at 4°C in the dark.

3.13 Incucyte live cell imaging

Dox-inducible A375P melanoma cells overexpressing MITF-WT, $MITF^{mi\text{-}sp}$, and $MITF^{mi\text{-}sl}$ or PRDM7-KO cells and their corresponding control were seeded at 2000 cells per well in triplicate onto a 96-well cell culture plate (Falcon, #353072). Images were recorded with Incucyte S3 Live-Cell Analysis System (Sartorius, Essen BioScience) every 2 hours for four days. Collected images were then analyzed using the Incucyte software by measuring the percentage of cell confluency.

3.14 Single-cell movement assy

PRDM7-KO cells and their corresponding control were seeded at 100 cells per well in triplicate onto a 96-well cell culture plate (Falcon, #353072). Images were recorded with Incucyte S3 Live-Cell Analysis System (Sartorius, Essen BioScience) every 20 mins for 24 hours. Collected images were then analyzed using the Tracmate/ImageJ software by measuring the movement of single cells.

3.15 Scratch assay

Each cell line was seeded at $2x10^4$ cells per well in triplicate onto a 96-well cell culture plate (Sartorius, #4379). When the culture reached 100% confluency, scratches were made with Incucyte 96-well WoundMaker (Essen Bioscience, #4563). Images were recorded with Incucyte S3 Live-Cell Analysis System (Sartorius, Essen BioScience) every hour for a maximum of four days. The

recorded images of the scratches were analyzed with Incucyte software to quantify gap closure by measuring relative wound density (%) and wound width (µm). The migration rate was calculated with the following formula: (Wound Width[T_0] - Wound Width [T_i])/((T_i -T_0)x2).

3.16 Colony formation assay

Each cell line was seeded at 200 cells per well in triplicate onto a six-well cell culture plate. These cells were allowed to grow for another 11 days with or without constant treatment with 0.5uM Vemurafenib PLX4032 (Selleckchem, #S1267). Cells were then fixed by ice-cold 100% methanol for 30mins at -20°C and stained by staining solution (0.5% crystal violet, 25% methanol) for 20 mins at room temperature. Cells were washed with water to remove the excess dye. The number of colonies was counted using the ImageJ software.

3.17 Apoptosis assay

Each cell line was seeded at 3000 cells per well in triplicate onto a 96-well cell culture plate (Falcon, #353072). After 24 hours, the cells were treated with the IncuCyte Caspase-3/7 Green Reagent for Apoptosis (Essen BioScience, #4440) with 1:1000 dilution in culture media, for a final assay concentration of 5 µM. Phase-contrast and fluorescent images were recorded with Incucyte S3 Live-Cell Analysis System (Sartorius, Essen BioScience) every 2 hours for four days. Collected images were then analyzed using the Incucyte software by measuring the percentage of cell and fluorescent object confluency per well. The confluence of fluorescent objects (%) was a measurement of apoptosis.

3.18 qPCR and sequencing

The day before inducing MITF expression by doxycycline, cells were seeded on 12-well plates at a density of $1.2x10^5$ cells per well. MITF expression was induced for 6, 12, 24, and 36 hours and harvested for RNA isolation using TRIzol reagent (ThermoFisher, #15596–026). Regarding the PRDM7-KO, the cells were seeded on 12-well plates at a density of $1.2x10^5$ cells per well for 48 hours before being isolated by TRIzol reagent (ThermoFisher, #15596–026). High-Capacity cDNA Reverse Transcription Kit (#4368814, Applied Biosystems) was used for cDNA synthesis according to the manufacturer's instructions. The SensiFAST SYBR Lo-ROX Kit (Bioline, #BIO-94020) was utilized for the qPCR. qPCR reactions were performed using 0.4 ng/µl cDNA in triplicates. The relative fold-change in gene expression was calculated using the D-ΔΔCt method

(Livak and Schmittgen, 2001). The geometrical mean of β-actin and hARP expression was used to normalize target gene expression.

3.19 Cell Cycle Synchronization by Thymidine Block

Cells were seeded on 12-well plates with $1.2x10^5$ cells per well. On the following day, cells were treated twice with 2mM Thymidine (Sigma, #T9250) for 16 hours each time with an 8-hour interval between treatments by replacing with fresh RPM1 media containing 10%FBS. After the thymidine treatment, cells were harvested for Western blot analysis at 0 hours, 4 hours, 8 hours, and 12 hours time points counted from the second thymidine release.

3.20 Differential gene expression analysis of melanoma tumor samples in cancer genome atlas database

The RNA-seq data of 480 skin Cutaneous Melanoma samples in the TCGA database were used for further analysis of the roles of PRDM7 in melanoma. The tumors were sorted based on PRDM7 expression, and the 30 melanoma tumor samples with the highest and 30 with the lowest PRDM7 mRNA expression were classified into the $PRDM7^{high}$ or $PRDM7^{low}$ groups, respectively. The different expression analyses between the two groups were performed using TCGAbiolinks in the R-Bioconductor package.

RNA samples were isolated from PRDM7-KO cells and their corresponding controls using Quick-RNA MiniPrep Kit (Zymo research, #R1055). The isolated RNA then sent to Decode Genetics for paired-end sequencing with 50 million reads per sample. The sequencing reads were quality-controlled using FastQC (Simons, 2010) before alignment to the human genome (build GRCh38) using Kallisto (Bray et al., 2016). Various downstream analysis was then conducted, including differential expression analysis performed by Sleuth (Pimentel et al., 2017) and enrichment analysis using GSEA software (Subramanian et al., 2005).

3.21 Cleavage Under Targets and Release Using Nuclease (CUT&RUN)

The protocol used for the Cut&Run analysis was described by (Dilshat et al., 2021a). To determine which changes are mediated in H3K4me3, H3K4me9, and H3K4me27 histone modifications upon PRDM7 and MITF depletion, Anti-H3K4me3, anti-H3K9me3 and anti-H3K27me3, and anti-IgG Cut&Run were performed in PRDM7-KO, MITF-KO cells, and their corresponding controlz. $10x10^6$ cells at log-phased in culture were harvested by cell scraping. The cells

were then washed twice in washing buffer (20 mM HEPES, pH7.5, 150 mM NaCl, 0.5 mM spermidine and the protease-inhibitor cocktail, Roche cOmplete Mini, EDTA-free). The cells were then suspended in a washing buffer and added into the pre-activated Concanavalin A-coated magnetic beads (Bangs Laboratories, Inc) in binding buffer (20mM HEPES pH 7.5, 10mM KCl, 1mM CaCl2, 1mM MnCl2) in the ratio 1:1 V/V. The tube was incubated at RT for 10min for the cells to adhere to the beads. The ConA beads conjugated with cells were then suspended in antibody buffer (wash buffer with 2 mM EDTA and 0.03% digitonin) and appropriate antibody before incubating at 4°C on a rotating wheel overnight.

In the next stage, the wash buffer containing 0.03% digitonin (dig-wash buffer) was used to wash the cells before performing chromatin digestion by the pAG-MNase. The digesting step was terminated by 2X Stop buffer (340 mM NaCl, 20 mM EDTA, 4 mM EGTA, 0.02% Digitonin, 100 µg/mL RNAse A, 50 µg/mL Glycogen, and 1ng/mL E. coli Spike-in DNA control EpiCypher). The released DNA fragments were treated with 0.1% SDS at final concentration and 1.2ul Proteinase K (ThermoFisher, #EO0491) for 1 hour at 50°C and purified by Phenol:chloroform:IsoamylAlcohol ethanol-precipitated. All CUT&RUN experiments were performed in duplicate.

3.22 Cut&Run library preparation and data analysis

CUT& RUN libraries were prepared using NEBNext Ultra II DNA Library Prep Kit for Illumina (Neb, #E7645L) according to the manufacturer's instructions. The quality of library amplification was determined by using 2100 Bioanalyzer for fragment analysis. Libraries were then paired-end sequenced with a sequence depth of approximately 7 million reads per sample and a read length of 2x150 on Illumina Novaseq. Bowtie2 version 2.1.0 (Langmead and Salzberg, 2012) was used to map the reads against the hg38 genome assembly. The peak call and downstream analyses were performed using the R-package.

3.23 Statistical analysis

Experimental data were analyzed with GraphPad Prism 9.0 software (San Diego, CA). All experiments were performed in at least three biological replicates. An unpaired t-test was conducted to compare the two groups. A significant difference was established with *$p<0.05$. All the data were expressed as mean ± SEM. For RNA-seq data, we selected differentially expressed genes with the cut-off of $|\log2 (\text{foldchange})| \geq 1$ and qval <0.05 for downstream analysis.

4 Results

4.1 Characterisation of the molecular properties of the Mitf$^{mi\text{-}sl}$ suppressor mutation (Paper II -manuscript in preparation)

4.1.1 MITF$^{mi\text{-}sl}$ protein accumulates in the nucleus

The MITF$^{mi\text{-}sl}$ mutation affects a domain of MITF that has been implicated in protein stability, localization, and transcription activation. This domain has all the characteristics of an internally disordered region (IDR), lacking 3D structure, although Alphafold predicts a couple of helices and a short β-sheet structure; the confidence of the prediction is low. To determine how this mutation mediates the genetic suppression observed, we investigated the effects of the mutation on various protein properties.

To investigate the effects of the MITF$^{mi\text{-}sl}$ mutation on nuclear localization, Flag-tagged (at C-terminus) MITF-WT, MITF$^{mi\text{-}sp}$, and MITF$^{mi\text{-}sl}$ proteins were expressed in a dox-inducible vector and transfected into A375P melanoma cells, which express little endogenous MITF. To equalize expression at a steady state, the A375P cell lines were treated with varying concentrations of doxycycline for 24 hours. The nuclear and cytoplasmic fractions were separated as described (Ramsby and Makowski, 1999; Senichkin et al., 2021), and the MITF proteins were characterized by Western blot. The MITF protein is observed as two bands where the upper band is phosphorylated at S73 (hereafter referred to as pS73-MITF), and the lower band is not phosphorylated at S73 (hereafter referred to as unpS73-MITF) (Fock et al., 2019; Ngeow et al., 2018). For the MITF-WT and MITF$^{mi\text{-}sp}$ proteins, both bands were observed at similar ratios in the nuclear and cytoplasmic fractions. However, for MITF$^{mi\text{-}sl}$, both bands were predominantly located in the nucleus, although a portion was still found in the cytoplasm (Figures 8A and 8B). A similar result was observed when the MITF-WT, MITF$^{mi\text{-}sp}$, and MITF$^{mi\text{-}sl}$ proteins were overexpressed in 501Mel and SKmel28 melanoma cell lines, expressing a high endogenous level of MITF (Figures 8C-F). Flag-tagging the MITF protein at the N-end or replacing the C-terminus Flag with GFP also resulted in the significantly increased nuclear presence of the MITF$^{mi\text{-}sl}$ protein (Figures 8G and 8H).

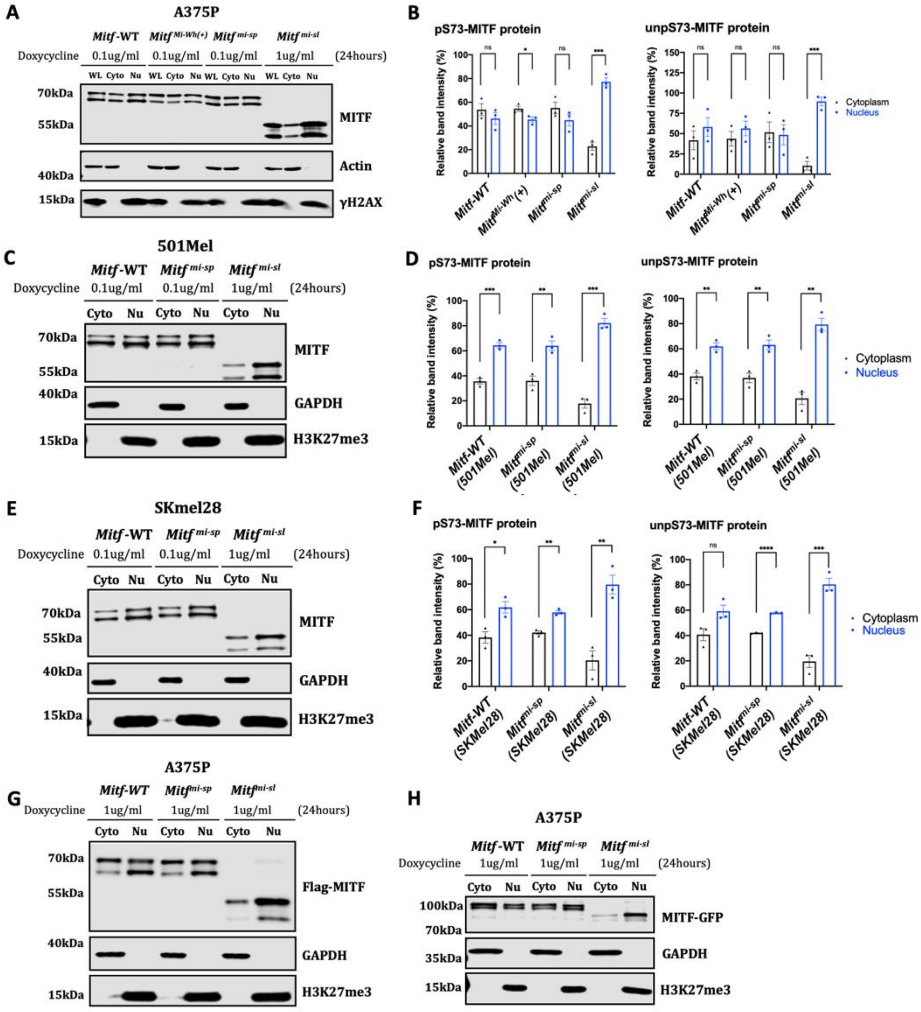

Figure 8. The 316-419 domain affects MITF localization (A), (C), (E), (G), (H) Western blot analysis of subcellular fractions isolated from A375P (A, G, H) or 501Mel (C) or SKmel28 melanoma cells induced for 24 hours overexpressing indicated MITF mutant proteins with either Flag-tag at C-terminus (A, C, E) or Flag-tag at N-terminus (G) or GFP-tag at C-terminus (H) were visualized using either Flag or GFP antibody. MITF mutant proteins in whole cell lysate (WL), cytoplasmic (Cyto) and nuclear fractions (Nu) were visualized using Flag or GFP antibody depending on the fusion tag. Actin/GAPDH and γH2AX/H3K27me3 were loading controls for cytoplasmic and nuclear fractions, respectively. (B), (D), (F) The indicated pS73- and unpS73-MITF protein band intensities from the Western blot analysis (A),(C), and (E) respectively, were quantified separately with ImageJ software and are depicted as percentages of the total amount of protein present in the two fractions. Error bars represent SEM of three independent experiments. Statistically significant differences (Student's t-test) are indicated by *, $p < 0.05$.

To determine whether the six amino acids encoded by exon 6A are involved in mediating nuclear localization, the MITF$^{Mi\text{-}Wh(-)}$ (lacking the 6aa domain) and MITF$^{Mi\text{-}Wh(+)}$ (containing the 6aa domain) proteins were transiently expressed in A375P cells. No difference was observed in the distribution of MITF between the nuclear and cytoplasmic fractions of the two constructs (Figure 9A). We also generated a version of *Mitf*$^{mi\text{-}sl}$ which contains exon 6A (*Mitf*$^{mi\text{-}sl(+)}$) (Figure 9B), and studied its effects on nuclear localization in A375P cells. The results showed that the MITF$^{mi\text{-}sl(+)}$ protein was also primarily nuclear (Figure 9A). Taken together, we have demonstrated that the 316-419 domain of MITF, but not exon 6A or the tags, mediate MITF nuclear localization.

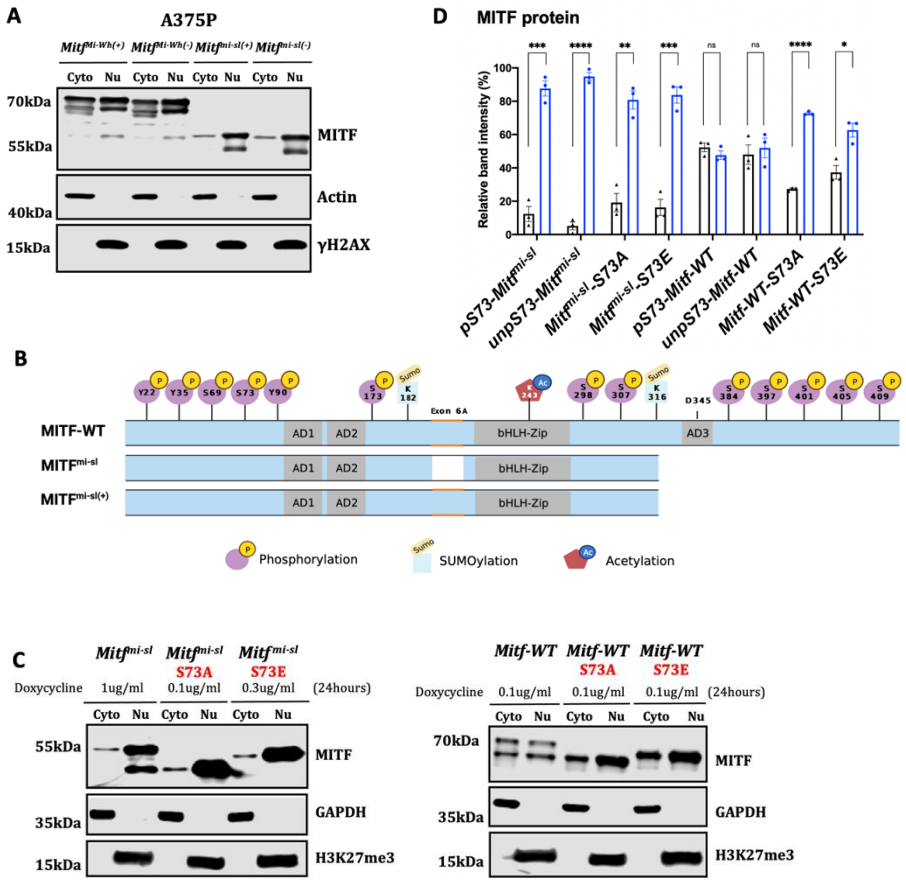

Figure 9. The C-terminus is essential for MITF$^{mi\text{-}sl}$ nuclear accumulation, regardless of S73 phosphorylation status. (A) Western blotanalysis of subcellular fractions isolated from A375P cells transiently overexpressed the indicated MITF mutant protein. MITF proteins in cytoplasmic (Cyto) and nuclear fractions (Nu) were visualized using Flag antibody. Actin and γH2AX were loading controls for cytoplasmic and nuclear fractions,

respectively. (B) Schematic of MITF$^{mi\text{-}sl(+)}$ mutant construct which was generated by deletion exon 6A. (C) Western blot analysis of subcellular fractions isolated from A375P melanoma cells induced for 24 hours overexpressing different MITF mutant proteins. MITF proteins in cytoplasm fraction (Cyto) and nuclear fractions (Nu) were visualized using Flag antibody. GAPDH and H3K27me3 were loading controls for cytoplasmic and nuclear fractions, respectively. (D The indicated pS73- and unpS73-MITF band intensities in the cytoplasmic and nuclear fractions from Western blot analysis (C) were quantified separately with ImageJ software and are depicted as percentages of the total amount of protein present in the two fractions. Error bars represent SEM of three independent experiments. Statistically significant differences (Student's t-test) are indicated by *, $p< 0.05$.

Previous work has shown that the phosphorylation of S73 leads to the nuclear export of MITF (Ngeow et al., 2018). To determine whether the effects of the 316-419 domains on subcellular localization of MITF depend on S73 phosphorylation, we replaced S73 with either the non-phosphorylated alanine residue or the phosphorylation mimic glutamic acid in the *Mitf-WT* and *Mitf$^{mi\text{-}sl}$* constructs. Cellular fractionation was then performed. Like the MITF$^{mi\text{-}sl}$ protein, MITF$^{mi\text{-}sl}$-S73A and MITF$^{mi\text{-}sl}$-S73E showed significant accumulation in the nucleus (Figures 9C and 9D). Although, a higher enrichment was observed for MITF-WT-S73A and MITF-WT-S73E in the nuclear compartment than MITF-WT (Figures 9C and 9D), the most pronounced effect was observed for the MITF$^{mi\text{-}sl}$, MITF$^{mi\text{-}sl}$ -S73A, and MITF$^{mi\text{-}sl}$ -S73E proteins. Our findings suggest that lacking the C-terminus is essential for MITF$^{mi\text{-}sl}$ nuclear accumulation, regardless of S73 phosphorylation status.

4.1.2 The 316-326 and 378-419 domains of MITF affect its localization

To determine which domains within the carboxyl end of MITF determine the nuclear retention properties, we generated truncated versions of MITF$^{mi\text{-}sp}$ with Flag-tag fusion at the carboxyl end in our inducible vector system (schematic diagram in Figure 10A). The results showed that the unpS73-MITF$^{mi\text{-}sp}$-del326-377 protein behaves like unpS73-MITF-WT in that the protein is distributed equally between the cytoplasmic and nuclear fractions; the pS73-MITF$^{mi\text{-}sp}$-del326-377 was slightly more cytoplasmic (Figures 10B and 10C). In contrast, a significant portion of the MITF$^{mi\text{-}sp}$-326X and MITF$^{mi\text{-}sp}$-378X proteins was present in the nuclear fraction, suggesting that the 378-419 domain, including the phosphorylation sites (indicated in Figure 10A), plays an essential role in the nuclear accumulation of MITF. However, since the MITF$^{mi\text{-}sl}$ protein was more nuclear than the MITF$^{mi\text{-}sp}$-326X and MITF$^{mi\text{-}sp}$-378X proteins (Figures 10B and 6C),

the absence of the 378-419 domain is not the only reason for the nuclear enrichment of MITF$^{mi\text{-}sl}$. The MITF$^{mi\text{-}sp}$-del316-326 construct, which lacks the SUMO-site and adjacent residues, did not alter the cytoplasmic-nuclear distribution of MITF (Figures 10B and 10C). Taken together, our results suggest that the 378-419 domain plays a major role in the nuclear retention of MITF.

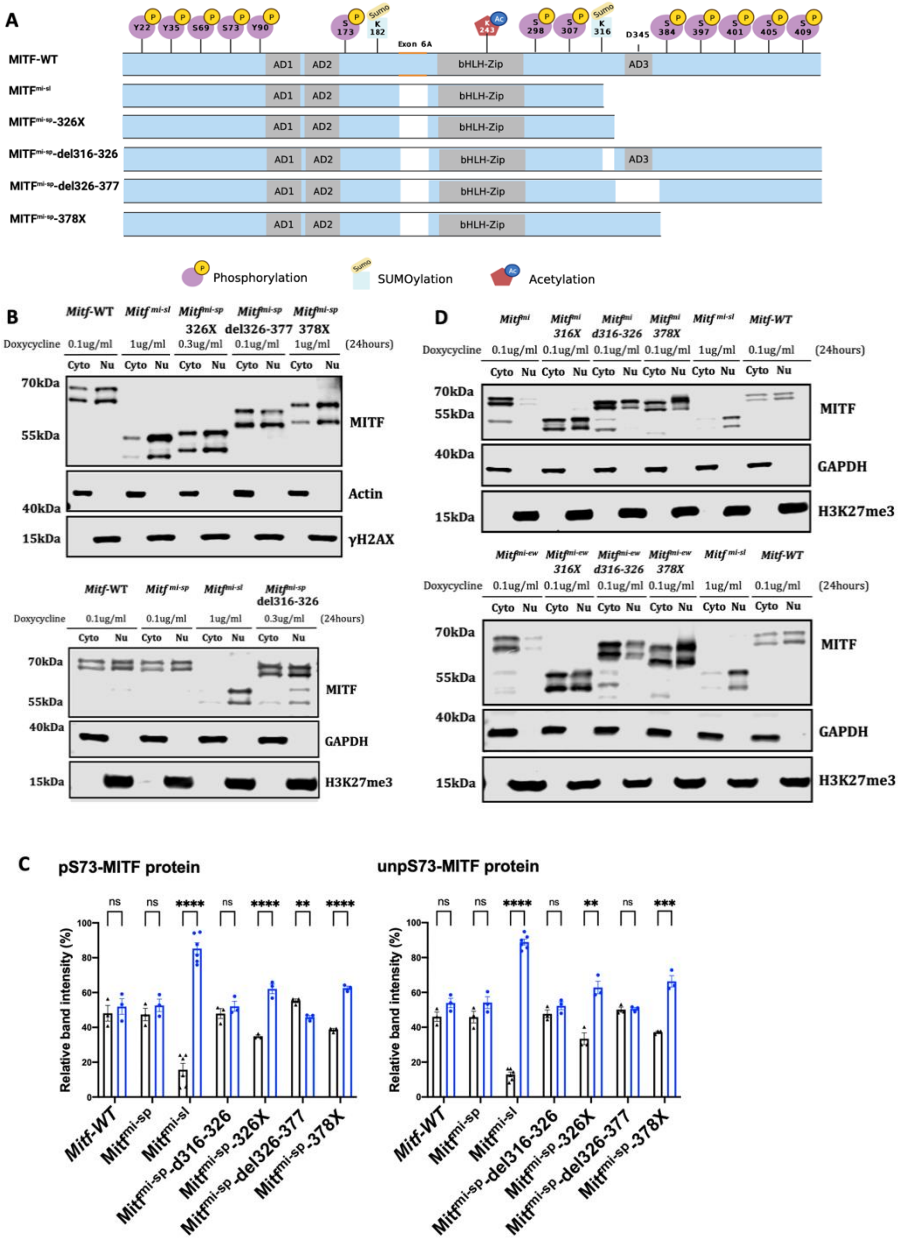

Figure 10. The 316-326 and 378-419 play important roles in regulating MITF localization. (A) Schematic of C-terminus MITF$^{mi\text{-}sp}$ truncation constructs. C-term truncations were generated by introducing stop codons at position Q326 or L378 or deletion fragments 326-377 or 316-326. MITF$^{mi\text{-}sp}$-326X introduces a stop-codon at residue 326, which contains the SUMO-site at 316; MITF$^{mi\text{-}sp}$-del326-377 lacks the tentative activation domain AD3; MITF$^{mi\text{-}sp}$-del316-326 lacks SUMO-site and adjacent amino acid; MITF$^{mi\text{-}sp}$-378X lacks the series of phosphorylation sites at the carboxyl-end of the protein. (B) and (D) Western blot analysis of subcellular fractions isolated from A375P melanoma cells induced for 24 hours overexpressing different MITF mutant proteins. Using the FLAG antibody, the indicated MITF mutants were visualized in the cytoplasmic and nuclear fractions. Actin or GAPDH and γH2AX or H3K27me3 were loading controls for cytoplasmic and nuclear fractions, respectively. (C) The indicated pS73 MITF and unpS73 MITF protein band intensities in the cytoplasmic and nuclear fractions from Western blot analysis (B) were quantified separately with ImageJ software and are depicted as percentages of the total amount of protein present in the two fractions. Error bars represent SEM of three independent experiments. Statistically significant differences (Student's t-test) are indicated by *, $p < 0.05$.

To further investigate the effects of the 316-326 and 378-419 domains in regulating MITF localization, versions of MITF^{mi} and MITF$^{mi\text{-}ew}$ lacking the C-terminus were generated in our inducible vector system, expressed in A375P melanoma cells, and characterized as before. Intriguingly, the results showed that MITF^{mi} and MITF$^{mi\text{-}ew}$ proteins that also contained the 316X, 378X, and del316-326 mutations were more nuclear than the MITF^{mi} and MITF$^{mi\text{-}ew}$ proteins (Figure 10D). This suggests that the 316-326 and 378-419 domains can mediate the nuclear localization of MITF and that they override the karyophilic effects of the bHLHZip domain.

Previous work has shown that treatment with 12-*O*-tetradecanoylphorbol-13-acetate (TPA) leads to phosphorylation of S73 of MITF and shifts the protein to the cytoplasm (Ngeow et al., 2018). Therefore, we treated A375P cells expressing various constructs with TPA and determined their effects on localization. Consistent with the previous literature, TPA treatment promoted S73 phosphorylation (as seen by the almost exclusive presence of the upper MITF-band) and shifted the protein out of the nucleus (Figures 11) (Ngeow et al., 2018). Similar to MITF-WT, the MITF$^{mi\text{-}sp}$-del326-377 and MITF$^{mi\text{-}sp}$-378X proteins were predominantly phosphorylated at S73 and located in the cytoplasm after the treatment. In contrast, although the MITF$^{mi\text{-}sl}$, MITF$^{mi\text{-}sp}$-326X, and MITF$^{mi\text{-}sp}$-del316-326 proteins were phosphorylated at S73 after 1 hour of TPA treatment, the proteins were present in both cytoplasmic and nuclear fractions; a significant proportion of the MITF$^{mi\text{-}sl}$ protein was nuclear, whereas MITF$^{mi\text{-}sp}$-326X protein was equally distributed between the two compartments and one-third of MITF$^{mi\text{-}sp}$-del316-326 protein was located in the nuclear fraction (Figures 11). These data suggest that the 316-326 domain of MITF can override the effects of TPA on nuclear export. Taken together, the results suggest that the 316-326 and the 378-419 domains play a crucial role in the nucleo-cytoplasmic shuttling of MITF.

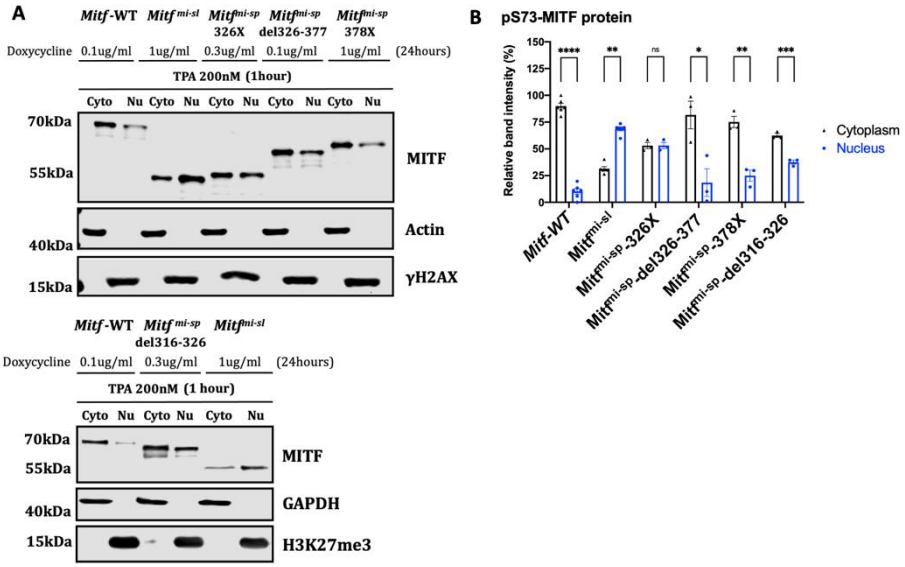

Figure 11. The 316-326 domain overrides the effect of TPA to export phosphorylated S73 MITF out of the nucleus. (A) Western blot analysis of subcellular fractions isolated from 24-hours-inducible A375P melanoma cells overexpressing different MITF mutant proteins before treatment with TPA at 200nM for 1 hour. MITF-WT, MITF$^{mi\text{-}sl}$, MITF$^{mi\text{-}sp}$-326X, MITF$^{mi\text{-}sp}$-del326-377, MITF$^{mi\text{-}sp}$-d316-326, and MITF$^{mi\text{-}sp}$-378X protein in cytoplasmic fraction (Cyto) and nuclear fractions (Nu) were visualized using Flag antibody. Actin or GAPDH and γH2AX or H3K27me3 were loading controls for cytoplasmic and nuclear fractions, respectively. (B) The indicated pS73-MITF proteins band intensities from Western blot analysis (A) in the cytoplasmic and nuclear fractions from the cell treated with TPA were quantified separately with ImageJ software and are depicted as percentages of the total amount of protein present in the two fractions. Error bars represent SEM of three independent experiments. Statistically significant differences (Student's t-test) are indicated by *, $p< 0.05$.

Previous work has shown that MITF phosphorylated at S173 interacts with the 14-3-3 protein, leading to the retention of MITF in the cytosol in the osteoclasts (Bronisz et al., 2006). To determine whether the difference in nuclear localization between the MITF-WT, MITF$^{mi\text{-}sp,}$ and MITF$^{mi\text{-}sl}$ proteins was due to interactions with 14-3-3, we co-expressed ε-14-3-3 and **ζ**-14-3-3 fused with Flag together with either MITF-WT-GFP, MITF$^{mi\text{-}sl}$-GFP or MITF$^{mi\text{-}sp}$-GFP proteins in A375 cells and performed co-immunoprecipitation (co-IP) of the whole cell lysis using the Flag-antibodies. Our results showed that MITF-WT, MITF$^{mi\text{-}sp,}$ and MITF$^{mi\text{-}sl}$ proteins interacted with the ε-14-3-3 and **ζ**-14-3-3 isoforms, and no difference was observed in signal intensity between the two mutants (Figure 12). This suggests that the nuclear accumulation of MITF$^{mi\text{-}sl}$ protein is not due to effects on interactions with 14-3-3.

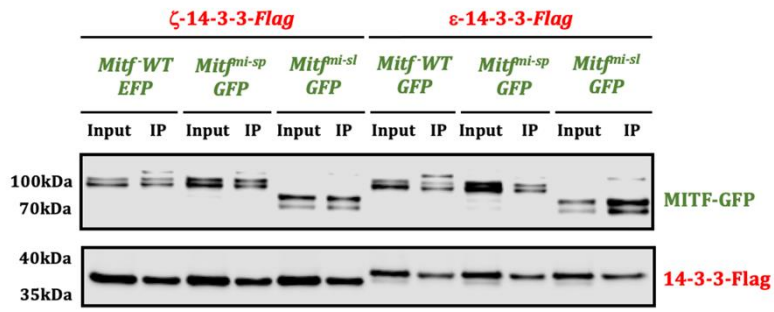

Figure 12. MITF$^{mi\text{-}sl}$ protein can be complex with 14-3-3 proteins at a similar level as MITF$^{mi\text{-}sp}$ and MITF-WT. Western blot analysis showing the results of a co-immunoprecipitation experiment. MITF$^{mi\text{-}sp}$-GFP, MITF$^{mi\text{-}sl}$-GFP, or MITF-WT-GFP construct was cotransfected with either ε-14-3-3-Flag or ζ-14-3-3-Flag in A375P melanoma cells. Co-immunoprecipitation (co-IP) of the whole cell lysate using Flag-antibodies was performed and visualized using Flag antibody. Input fraction (Input), unbound fraction (Unb), and an immunoprecipitated fraction (IP) were indicated in the Western blot.

4.1.3 The SUMOylation site at K316 and the S409 phosphorylation site interact to regulate MITF subcellular localization

To determine the role of the different phosphorylation sites at the carboxyl end of MITF in mediating nuclear localization, we substituted S384, S397, S401, S405, and S409 phosphorylation sites with the non-phosphorylatable alanine, separately or together in the MITF$^{mi\text{-}sp}$ construct. Our results showed that the S384A, S397A, S401A, and S405A in MITF$^{mi\text{-}sp}$ were equally distributed between the nucleus and cytoplasm (Figures 13A) whereas MITF$^{mi\text{-}sp}$-S409A was slightly more nuclear (Figures 13B and 13C). As S409 serves as a priming site for phosphorylation at S405, S401, and S397 (Ploper et al., 2015), the effect of the quadruple S397/401/405/409A mutation in MITF$^{mi\text{-}sp}$ (MITF$^{mi\text{-}sp}$-4A) and MITF-WT (MITF-WT-4A) on localization was determined. It showed that both pS73 and unpS73 forms of MITF$^{mi\text{-}sp}$-4A and MITF-WT-4A were more nuclear (Figures 13B and 13C). This suggests that phosphorylation at S409 affects MITF localization and that the phosphorylation cascade at the carboxyl end may be involved in the cytoplasmic retention of MITF.

To determine whether the SUMOylation site at K316 was involved in regulating MITF subcellular localization, we replaced the K316 residue with arginine in the MITF-WT and MITF$^{mi\text{-}sp}$ constructs. We also determined the effects of the E318K mutation. Neither the K316R nor the E318K mutation altered the localization of the MITF-WT and MITF$^{mi\text{-}sp}$ proteins (Figures 13B and 13C). Although the single SUMOylation site at K316 does not contribute to MITF localization and S409 only

moderately enriched nuclear localization, the K316 residue may cooperate with the phosphorylation sites to mediate the effects on MITF localization. To further investigate this, we generated the K316R or E318K mutations in MITF$^{mi\text{-}sp}$-S384A, MITF$^{mi\text{-}sp}$ -S397A, MITF$^{mi\text{-}sp}$ -S401A, MITF$^{mi\text{-}sp}$ -S405A, and MITF$^{mi\text{-}sp}$-S409A constructs and determined effects on nuclear localization. When together with the S384A, S397A, S401A, and S405A mutations, the K316R and E318K mutations did not alter nuclear localization of MITF (Figure 13D). Intriguingly, however, the MITF$^{mi\text{-}sp}$ K316R-S409A and E318K-S409A proteins were more nuclear, regardless of S73-phosphorylation (Figures 13B and 13C). The effect on nuclear enrichment was slightly more pronounced than observed in the single S409A mutation. This suggests that a specific interplay between the SUMOylation site at K316 and the phosphorylation site at S409 affects MITF subcellular localization. Interestingly, none of the double point mutations or the combinations of the K316R and E318K mutations with the C-terminus deletions exhibited a similar impact on nuclear enrichment as observed for MITF$^{mi\text{-}sl}$ (Figures 13E and 13F). Together, our findings suggest that the individual SUMOylation and phosphorylation sites located at the MITF carboxyl end are important but insufficient for the nuclear localization of MITF. Instead, nuclear localization depends on both the region around SUMOylation site at K316 and the carboxyl end.

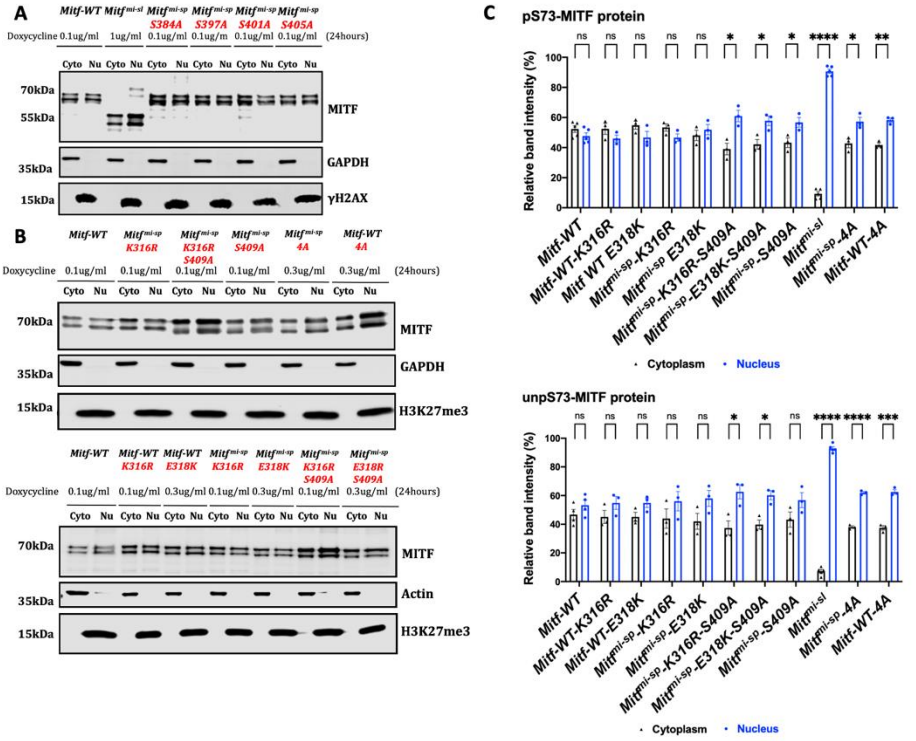

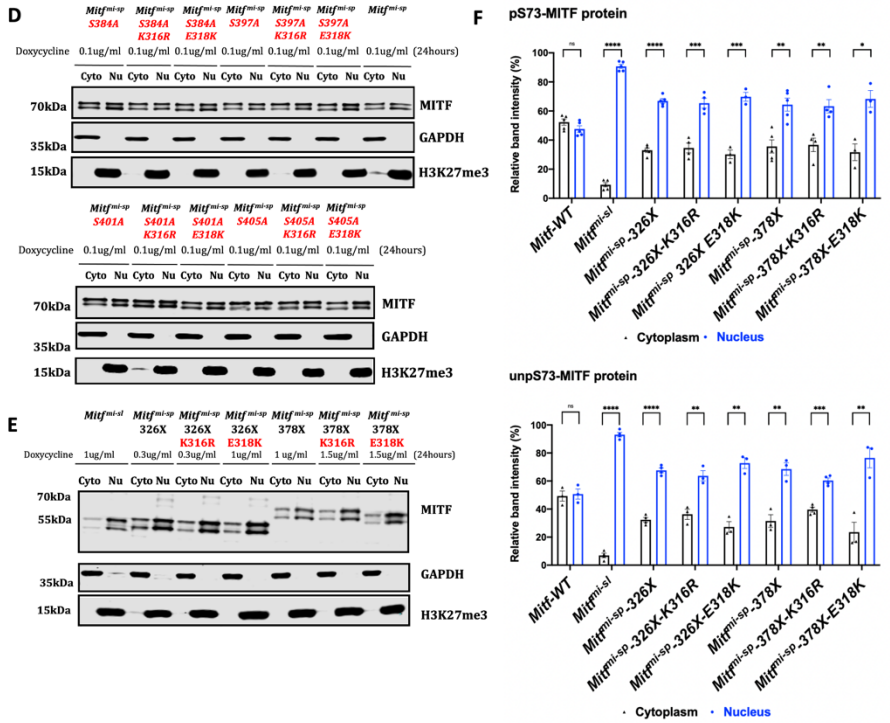

Figure 13. SUMOylation at K316 and phosphorylation at S409 interplay to mediate MITF localization. (A), (B), (D), (E) Western blot analysis of subcellular fractions isolated from 24-hours-inducible A375P melanoma cells overexpressing different MITF mutant proteins. Indicated MITF protein in cytoplasmic fraction (Cyto) and nuclar fractions (Nu) were visualized using Flag antibody. GAPDH and H3K27me3 were loading controls for cytoplasmic and nuclear fractions, respectively. (C) and (F) The indicated pS73 MITF and unpS73 MITF protein band intensities in the cytoplasmic and nuclear fraction from Western blot analysis (A and B) or (D and E) were quantified separately with ImageJ software and are depicted as percentages of the total amount of protein present in the two fractions. Error bars represent SEM of three independent experiments. Statistically significant differences (Student's t-test) are indicated by *, p< 0.05.

To confirm the cooperation between K316 and the carboxyl terminus of MITF in regulating MITF localization, we inducibly expressed the MITF$^{mi\text{-}sp}$-326X-K316R, MITF$^{mi\text{-}sp}$-378X-K316R, MITF$^{mi\text{-}sp}$-326X-E318K, and MITF$^{mi\text{-}sp}$-378X-E318K proteins in A375P cells for 24 hours. The cells were then treated with TPA at 200nM for 1 hour before harvesting for fractionation. While the pS73-MITF$^{mi\text{-}sp}$-326X protein was approximately equally distributed between the two compartments, the pS73-MITF$^{mi\text{-}sp}$-326X-K316R and MITF$^{mi\text{-}sp}$-326X-E318K showed a marginally higher proportion in the nucleus (Figures 14A and 14B). Similarly, TPA treatment of the MITF$^{mi\text{-}sp}$-378X construct also carrying the K316R or E318K mutations reduced the percentage of pS73-MITF protein in the cytoplasmic fraction (Figures 14A and 14B).

Critically, the double mutation K316R-S409A in the MITF$^{mi\text{-}sp}$ construct overrides the effects of TPA on nuclear export, resulting in equal distribution between the nucleus and cytoplasm (Figures 14C and 14D). A similar effect was observed for the MITF$^{mi\text{-}sp}$-E318K-S409A mutant protein (Figures 14C and 14D). TPA treatment of A375P cells expressing MITF$^{mi\text{-}sp}$-4A, MITF$^{mi\text{-}sp}$-4A-K316R, and MITF$^{mi\text{-}sp}$-4A-E318K also increased the nuclear localization of MITF (Figures 14C and 14D). However, MITF$^{mi\text{-}sp}$-S384A, MITF$^{mi\text{-}sp}$-S397A, MITF$^{mi\text{-}sp}$-S401A, MITF$^{mi\text{-}sp}$-S405A carrying either the K316R or E318K mutations, as well as the MITF$^{mi\text{-}sp}$-K316R, MITF$^{mi\text{-}sp}$-E318K, MITF-WT-K316R, MITF-WT-E318K proteins were primarily located in the cytoplasmic compartment after the treatment, similar to MITF-WT (Figure 14E). The data suggest that there is cooperation between the domain around K316 and the S409 site at the MITF C-terminus, which regulates the nuclear export/retention dynamic of pS73-MITF. Taken together, we conclude that both the 316-326 and 378-419 domains of MITF are essential for nuclear retention.

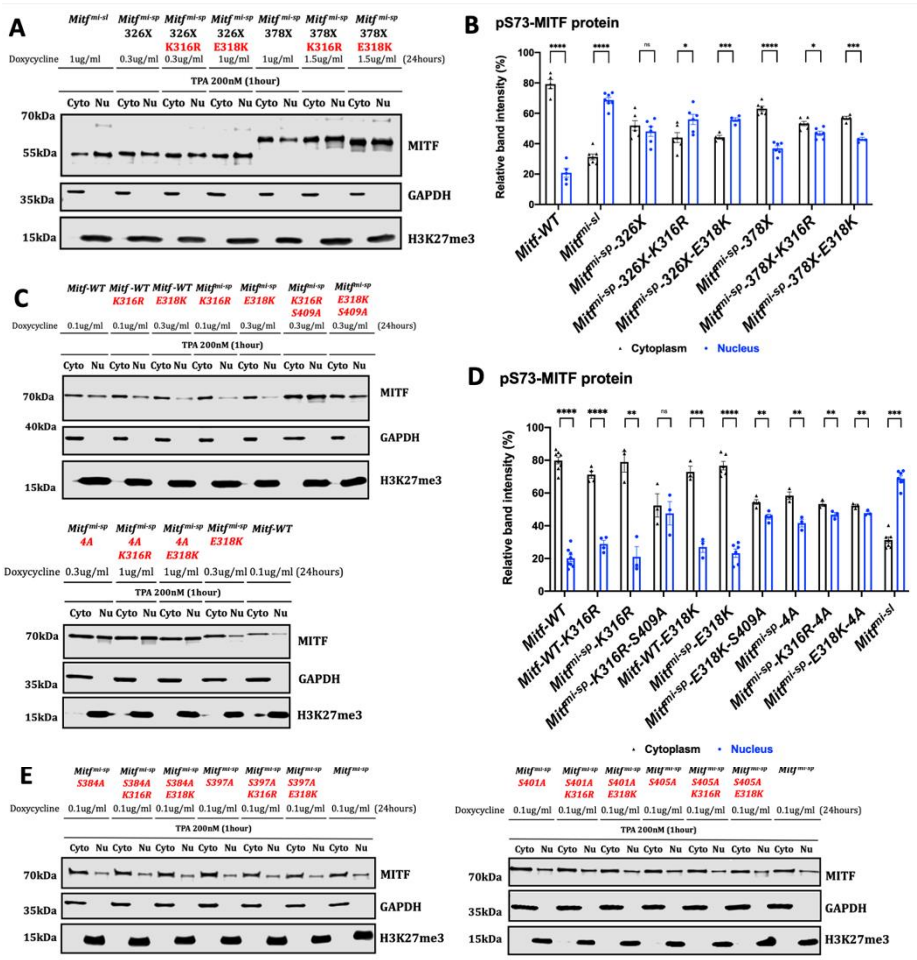

Figure 14. Lack of SUMOylation at K316 and phosphorylation at S409 impairs the MITF nucleus export upon TPA treatment. (A), (C), (E) Western blot analysis of subcellular fractions isolated from A375P melanoma cells induced for 24 hours overexpressing different MITF mutant proteins before treatment with TPA at 200nM for 1 hour. Indicated MITF mutant protein in cytoplasmic (Cyto) and nuclear fractions (Nu) were visualized using Flag antibody. GAPDH and H3K27me3 were loading controls for cytoplasmic and nuclear fractions, respectively. (B) and (D) The indicated pS73-MITF proteins band intensities from Western blot analysis (A) and (C), respectively, in the cytoplasmic and nuclear fraction from the cell treated with TPA were quantified separately with ImageJ software and are depicted as percentages of the total amount of protein present in the two fractions. Error bars represent SEM of three independent experiments. Statistically significant differences (Student's t-test) are indicated by *, $p < 0.05$.

4.1.4 The carboxyl-end is important for MITF protein stability

The effects of the suppressor mutation on protein stability were also determined using the dox-inducible A375P melanoma cells overexpressing our MITF-Flag fusion proteins. After inducing the expression of MITF for 24 hours, the cells were treated with the translation inhibitor cycloheximide (CHX) for different periods and harvested to visualize the MITF protein by Western blot. The bands on the Western blot were quantitated, and the changes in protein concentration were plotted over time. This data was used to calculate protein half-life, defined as the time required to reduce the initial protein abundance to 50%. The MITF-WT and MITF$^{mi\text{-}sp}$ proteins had comparable half-lives, which were approximately 3.2 hours for pS73-MITF and 1.2 hours for unpS73-MITF (Figures 15A and 15B). The stability of the pS73 and unpS73 versions of the MITF$^{Mi\text{-}Wh}$ protein, regardless of exon 6A, was not significantly different from that of MITF-WT (Figures 15C and 15D). This suggests that exon 6A does not contribute substantially to MITF stability. However, the MITF$^{mi\text{-}sl}$ protein was considerably less stable than the MITF-WT and MITF$^{mi\text{-}sp}$ proteins; the half-life of the pS73 and unpS73 forms of MITF$^{mi\text{-}sl}$ were 1.2 and 0.4 hours, respectively (Figures 15A and 15B). The MITF-WT and MITF$^{mi\text{-}sp}$ proteins were also more stable than the MITF$^{mi\text{-}sl}$ protein, regardless of S73 phosphorylation status, when overexpressed in the 501Mel and SKmel28 melanoma cell lines (Figures 15E-H). We also tested the stability of proteins carrying the Flag tag at the N-end (Flag-MITF-WT, Flag-MITF$^{mi\text{-}sp}$, and Flag-MITF$^{mi\text{-}sl}$) or GFP tag at the C-terminus (MITF-WT-GFP, MITF$^{mi\text{-}sp}$-GFP, MITF$^{mi\text{-}sp}$-GFP).

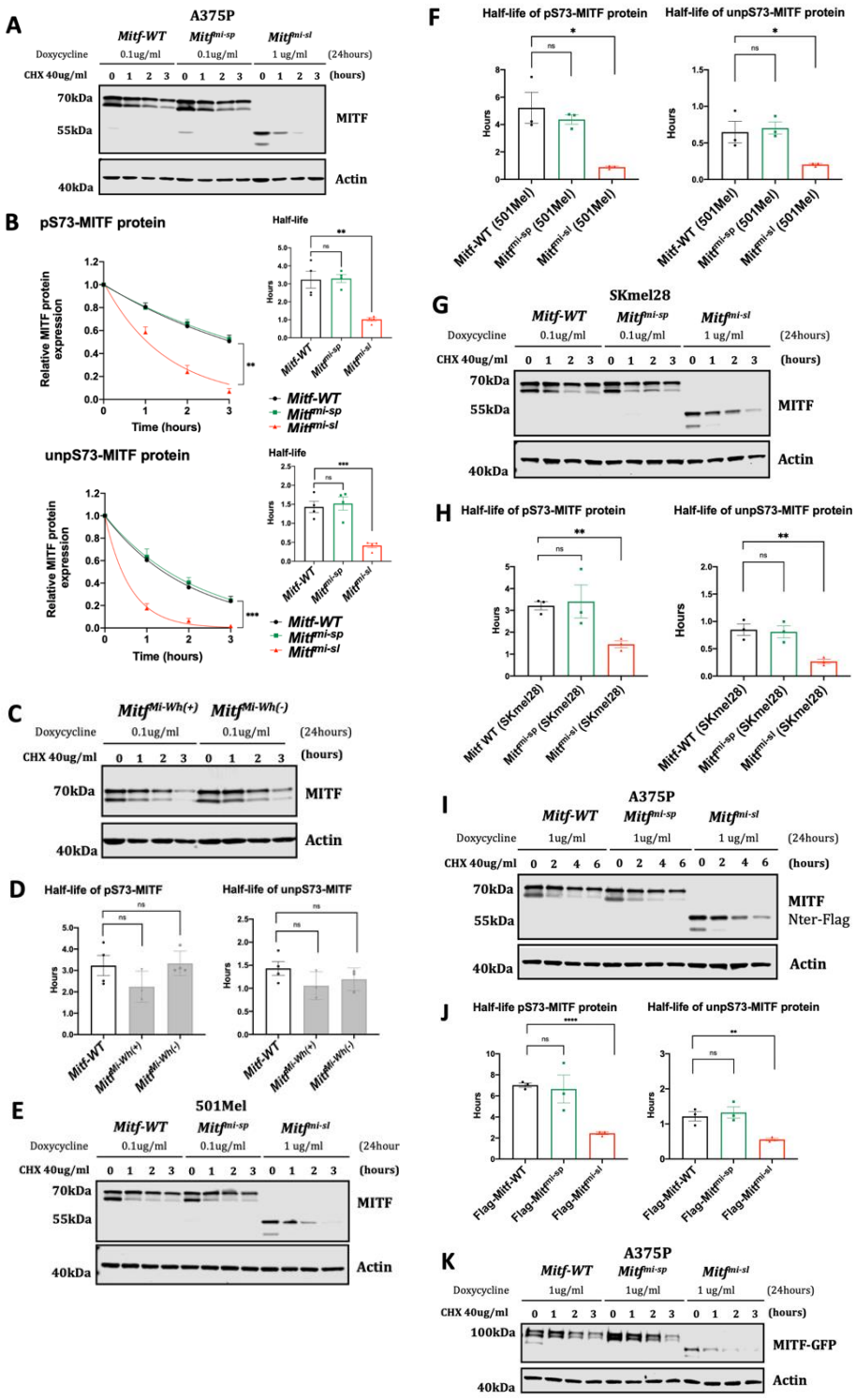
A
A375P
Mitf-WT
Mitfmi-sp
Mitfmi-sl
Doxycycline
0.1ug/ml
0.1ug/ml
1 ug/ml
(24hours)
CHX 40ug/ml
0 1 2 3 0 1 2 3 0 1 2 3
(hours)
70kDa
55kDa
40kDa
MITF
Actin
B
pS73-MITF protein
Half-life
Relative MITF protein expression
Time (hours)
Hours
Mitf-WT
Mitfmi-sp
Mitfmi-sl
unpS73-MITF protein
C
Mitfmi-Wh(+)
Mitfmi-Wh(-)
D
Half-life of pS73-MITF
Half-life of unpS73-MITF
E
501Mel
F
Half-life of pS73-MITF protein
Half-life of unpS73-MITF protein
Mitf-WT (501Mel)
Mitfmi-sp (501Mel)
Mitfmi-sl (501Mel)
G
SKmel28
H
Mitf WT (SKmel28)
Mitfmi-sp (SKmel28)
Mitfmi-sl (SKmel28)
I
1ug/ml
MITF
Nter-Flag
J
Flag-Mitf-WT
Flag-Mitfmi-sp
Flag-Mitfmi-sl
K
100kDa
MITF-GFP

Figure 15. The 316-419 domain affects MITF stability. (A), (C), (E), (G), (I), (K) Western blot analysis of the stability of the MITF proteins with different tags at either N-terminus or C-terminus. The inducible A375P (A, C, I, K) or 501Mel (C) or SKMel28 (G) cells were treated with doxycycline for 24h to express the indicated mutant MITF proteins before treating them with cycloheximide (CHX) 40ug/ml for 0, 1, 2, and 3 hours. MITF proteins quantity was then compared by Western blot using Flag antibody. Actin was used as a loading control. The band intensities were quantified using ImageJ software. (B), (D), (F), (H) and (J) Non-linear regression (one-phase decay) and half-life analysis of indicated pS73- and unpS73-MITF proteins degradation over time after CHX treatment. The MITF protein level relative to T0 were calculated, and non-linear regression analysis was performed. Error bars represent SEM of at least three independent experiments. Statistically significant differences (Student's t-test) are indicated by *, $p < 0.05$.

Although the pS73 form of Flag-MITF, regardless of mutation, showed more stability than the corresponding protein with a Flag tag at the C-terminus, Flag-MITF$^{mi\text{-}sl}$ was less stable than Flag-MITF-WT and Flag-MITF$^{mi\text{-}sp}$ (Figures 15I and 15J). Similarly, the MITF$^{mi\text{-}sl}$-GFP protein was less stable than MITF-WT-GFP and MITF$^{mi\text{-}sp}$-GFP (Figure 15K). Our finding suggests that the lack of the 316-419 domain significantly reduces the stability of MITF. Furthermore, regardless of mutation, in all cases, the unpS73 MITF (the lower band) was degraded faster than the pS73 form (upper band).

4.1.5 The domains at the carboxyl end of MITF are involved in regulating its stability

To determine which domains within the carboxyl end of MITF are essential for mediating effects on stability, a protein stability assay was performed in dox-inducible A375P melanoma cells expressing the truncated carboxyl-end MITF constructs in the presence of CHX. The half-life of these mutant proteins was then calculated. The results showed that, again, the pS73 form of MITF-WT, MITF$^{mi\text{-}sl}$, MITF$^{mi\text{-}sp}$-326X, and MITF$^{mi\text{-}sp}$-378X proteins was considerably more stable than the corresponding unpS73 proteins (Figure 16A and 16B). It also shows that MITF$^{mi\text{-}sp}$-326X, MITF$^{mi\text{-}sp}$-378X, and MITF$^{mi\text{-}sp}$-del316-326 proteins were less stable than the MITF-WT protein. However, the MITF$^{mi\text{-}sl}$ protein still showed the most rapid degradation upon CHX treatment compared to all the different proteins tested (Figures 16A and 16B). The results suggest that the carboxyl end is important for nuclear localization and MITF stability.

To further investigate the role of the 316-419 domain in mediating MITF protein stability, we determined the stability of the non-DNA binding MITF^{mi}-316X and MITF$^{mi\text{-}ew}$-316X proteins. Interestingly, these mutant proteins have similar stability to MITF-WT (Figure S16A and S16B). This suggests that the ability to bind to DNA in concert with carboxyl-end is important for mediating MITF stability.

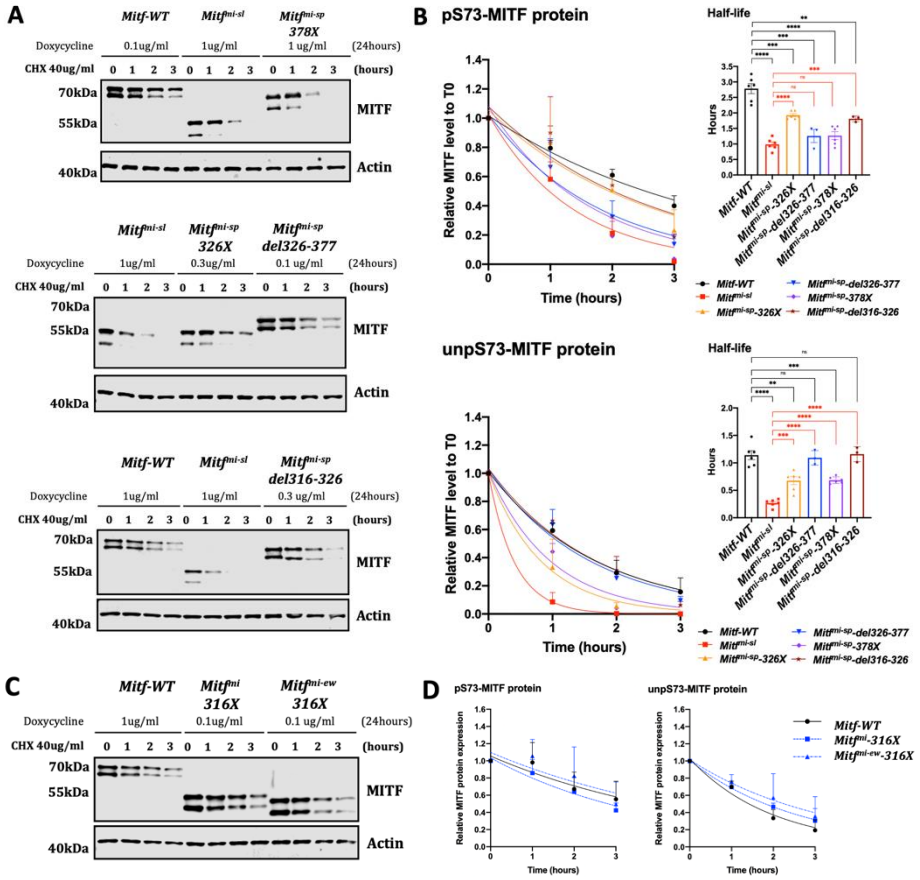

Figure 16. Different domains at the carboxyl terminus play different roles in maintaining MITF stability. (A) and (C) Western blot analysis of the stability of the MITF proteins. The inducible A375P cells were treated with doxycycline for 24h to express the indicated mutant MITF proteins before treating them with cycloheximide (CHX) 40ug/ml for 0, 1, 2, and 3 hours. The MITF proteins were then compared by Western blot using Flag antibody. Actin was used as a loading control. The band intensities were quantified using ImageJ software. (B) and (D) Non-linear regression (one-phase decay) and half-life analysis of the indicated pS73- and unpS73-MITF proteins over time after CHX treatment. The MITF protein levels relative to T0 were calculated, and non-linear regression analysis was performed. Error bars represent SEM of at least three independent experiments. Statistically significant differences (Student's t-test) are indicated by *, $p < 0.05$.

To clarify the role of the SUMOylation site at K316 in MITF protein stability, we tested the stability of the MITF-WT, MITF$^{mi\text{-}sp}$, MITF$^{mi\text{-}sp}$-378X, and MITF$^{mi\text{-}sp}$-326X proteins in the presence of the K316R mutation. The pS73-MITF-WT-K316R and pS73-MITF$^{mi\text{-}sp}$-K316R proteins were significantly more stable than pS73-MITF-WT; the stability of the unpS73-MITF-WT-K316R and unpS73-MITF$^{mi\text{-}sp}$-K316R proteins was slightly but not significantly increased (Figures 17A and 17B).

Interestingly, the pS73-MITF$^{mi\text{-}sl}$ protein was significantly less stable than the pS73-MITF$^{mi\text{-}sp}$-326X protein (Figures 17A and 17B), whereas the stability of the pS73-MITF$^{mi\text{-}sp}$-326X-K316R proteins was comparable to pS73-MITF$^{mi\text{-}sl}$ (Figures 17A and 17B). The unpS73-MITF$^{mi\text{-}sp}$-378X-K316R protein was not different from unpS73-MITF$^{mi\text{-}sl}$ (Figures 17A and 17B), whereas unpS73-MITF$^{mi\text{-}sp}$-378X was more stable than unpS73 MITF$^{mi\text{-}sl}$ (Figures 17A and 17B). This suggests that in the presence of the carboxyl end, the SUMO-site at K316 leads to reduced stability of S73-phosphorylated MITF. However, in the absence of the carboxyl end, the SUMO-site at K316 positively influences the stability of the S73-phosphorylated MITF protein. We hypothesize that the carboxyl domain (aa 378-419) of MITF interacts with the SUMO-site at K316, determining the stability of MITF and that phosphorylation at S73 further affects MITF stability.

The stability of MITF$^{mi\text{-}sp}$ proteins carrying the S384A, S397A, S401A, S405A, S409A, and 4A mutations was not affected (Figures 17C and 17D). Although the stability of the pS73 MITF$^{mi\text{-}sp}$-S397A protein was marginally increased compared to pS73-MITF-WT, the stability of unpS73 MITF$^{mi\text{-}sp}$-S397A was not changed (Figures 17C and 17D). Interestingly, replacing the S384, S397, and S401 residues with alanine did not change the ratio between pS73 and unpS73 proteins. In contrast, the S405A, S409A, and 4A mutations changed this ratio (Figure 17C), resulting in a higher proportion of pS73 than unpS73 MITF. This suggests that phosphorylation of either S405 or S409 might affect the pS73/unpS73 ratio by priming phosphorylation at S73 or by affecting its dephosphorylation.

To characterize the role of S73 phosphorylation in stability, we mutated S73 to either alanine or phosphomimetic glutamate and then determined the effects on MITF$^{mi\text{-}sl}$ stability. Interestingly, the MITF$^{mi\text{-}sl}$-S73A protein was more stable than the unpS73-MITF$^{mi\text{-}sl}$ protein and had similar stability as pS73-MITF$^{mi\text{-}sl}$ and unpS73-MITF-WT (Figures 18A and S18B). The MITF-WT-S73A protein was also more stable than unpS73-MITF-WT (Figures 18C and 18D). However, the S73E mutation did not alter the stability of MITF$^{mi\text{-}sl}$ and MITF-WT as compared to their corresponding pS73 forms (Figures 18C-F). Cells expressing MITF-WT, MITF$^{mi\text{-}sp}$, and MITF$^{mi\text{-}sl}$ were also treated with TPA to promote the formation of pS73-MITF, and stability was determined. The results showed that the pS73-MITF-WT and pS73-MITF$^{mi\text{-}sp}$ were more stable than pS73-MITF$^{mi\text{-}sl}$ (Figures 18G and S18H). Our findings suggest that pS73 is not required for MITF degradation but may affect the rate of the degradation process.

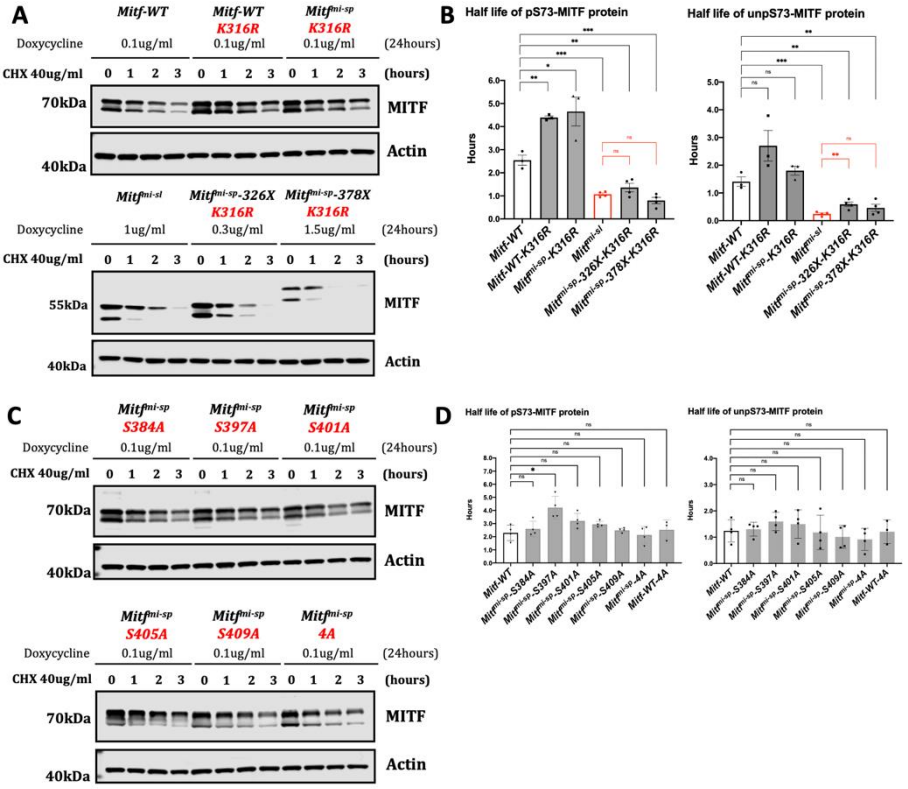

Figure 17. SUMOylation site at K316 regulated MITF stability differently in the presence or absence of a carboxyl terminus, and the four individual phosphorylation sites at C-terminus (S384, S397, S401, and S405) did not affect the MITF stability. (A) and (C) Western blot analysis of the stability of indicated MITF mutant proteins. The dox-inducible A375P cells were treated with doxycycline for 24h to express the indicated MITF proteins before treating them with cycloheximide (CHX) 40ug/ml for 0, 1, 2, and 3 hours. MITF proteins were then compared by Western blot using Flag antibody. Actin was used as a loading control. The band intensities were quantified using ImageJ software. (B) and (D) Half-life analysis of the indicated pS73- and unpS73-MITF proteins over time after CHX treatment. The MITF protein levels relative to T0 were calculated, and non-linear regression analysis was performed. Error bars represent SEM of at least three independent experiments. Statistically significant differences (Student's t-test) are indicated by *, $p < 0.05$.

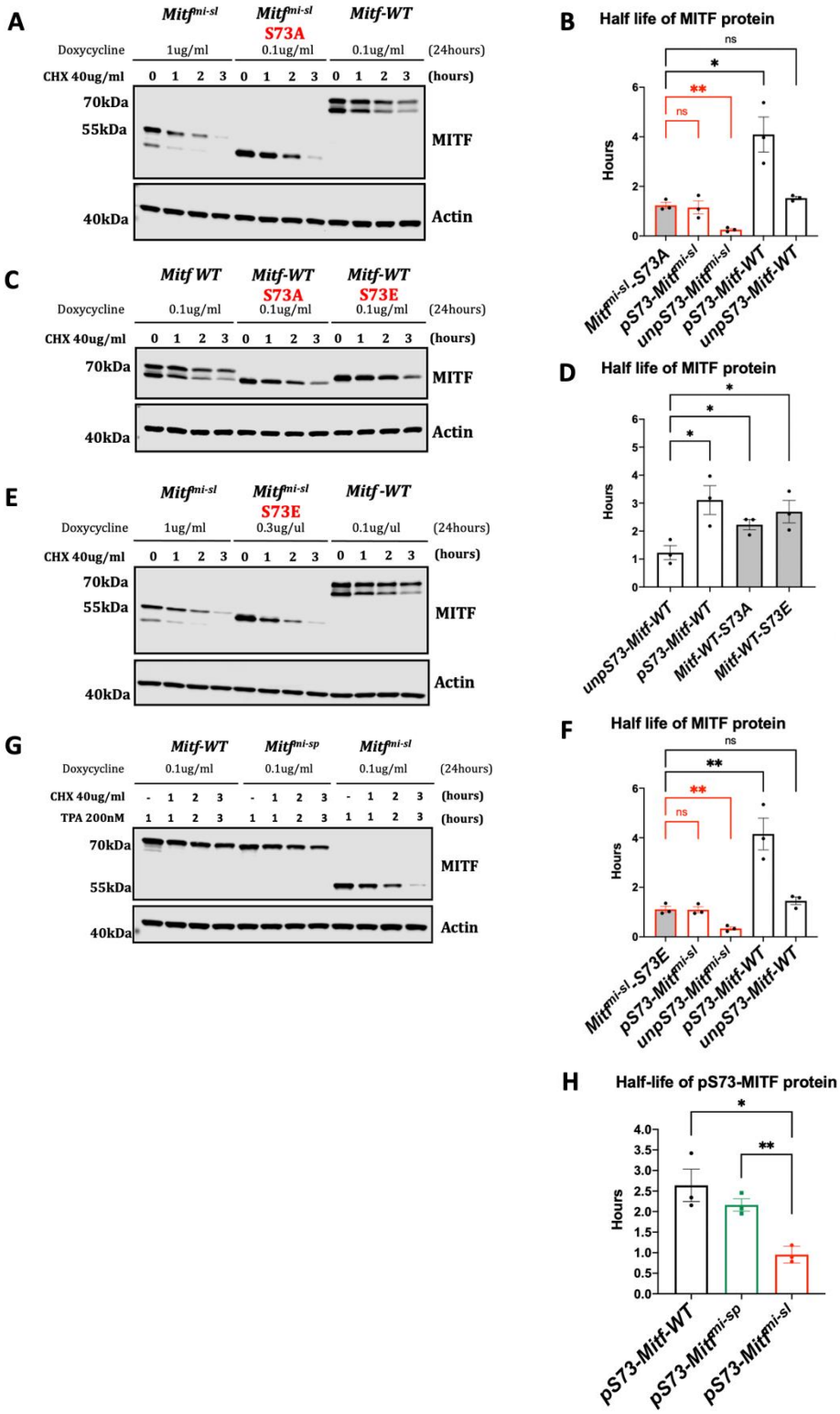
A
Mitf mi-sl
Mitf mi-sl S73A
Mitf-WT
Doxycycline
1ug/ml
0.1ug/ml
0.1ug/ml
(24hours)
CHX 40ug/ml
0 1 2 3 0 1 2 3 0 1 2 3
(hours)
70kDa
55kDa
MITF
40kDa
Actin
B
Half life of MITF protein
Hours
ns
*
**
ns
Mitf mi-sl S73A
pS73-Mitf mi-sl
unpS73-Mitf mi-sl
pS73-Mitf-WT
unpS73-Mitf-WT
C
Mitf WT
Mitf-WT S73A
Mitf-WT S73E
0.1ug/ml
0.1ug/ml
0.1ug/ml
D
Half life of MITF protein
unpS73-Mitf-WT
pS73-Mitf-WT
Mitf-WT-S73A
Mitf-WT-S73E
E
Mitf mi-sl
Mitf mi-sl S73E
Mitf -WT
1ug/ml
0.3ug/ul
0.1ug/ul
F
Half life of MITF protein
Mitf mi-sl S73E
G
Mitf-WT
Mitf mi-sp
Mitf mi-sl
0.1ug/ml
0.1ug/ml
0.1ug/ml
TPA 200nM
H
Half-life of pS73-MITF protein
pS73-Mitf-WT
pS73-Mitf mi-sp
pS73-Mitf mi-sl

Figure 18. The unpS73/pS73 dynamic could increase the stability of MITF protein
(A), (C), (E), and (G) Western blot analysis of the stability of the indicated MITF mutant proteins. The dox-inducible A375P melanoma cells were treated with doxycycline for 24h to express the indicated MITF proteins before treating them with cycloheximide (CHX) 40ug/ml for 0, 1, 2, and 3 hours with (G) or without (A, C, E) presenting of TPA 200nM. The MITF protein was then compared by Western blot using Flag antibody. Actin was used as a loading control. The band intensities were quantified using ImageJ software. (B), (D), (F), and (H) Half-life analysis of the indicated pS73- and unpS73- MITF proteins over time after CHX treatment, respectively. The MITF protein levels relative to T0 were calculated, and non-linear regression analysis was performed. Error bars represent SEM of at least three independent experiments. Statistically significant differences (Student's t-test) are indicated by *, p< 0.05.

The absence of the SUMOylation site at K316 in MITF$^{mi\text{-}sl}$ may accelerate SUMOylation at K182, reducing MITF$^{mi\text{-}sl}$ stability. To investigate this hypothesis, we measured the stability of the MITF-WT-K182R-K316R, MITF$^{mi\text{-}sp}$-K182R-K316R, and MITF$^{mi\text{-}sl}$-K182R proteins. The K182R mutation did not affect the stability of MITF$^{mi\text{-}sl}$ (Figures 19A and 19B). Interestingly, while the single MITF-WT-K316R and MITF$^{mi\text{-}sp}$-K316R mutations were more stable than MITF-WT (Figures 19A and 19B), the double mutation K182R-K316R in the MITF-WT and MITF$^{mi\text{-}sp}$ constructs did not alter their stability compared to that of the MITF-WT protein (Figures 19C and 19D). We, therefore, conclude that the SUMOylation site at K182 is not a major contributor to MITF$^{mi\text{-}sl}$ protein stability. How the K182R mutation reduces the effects of the K316R mutation on stability remains to be investigated.

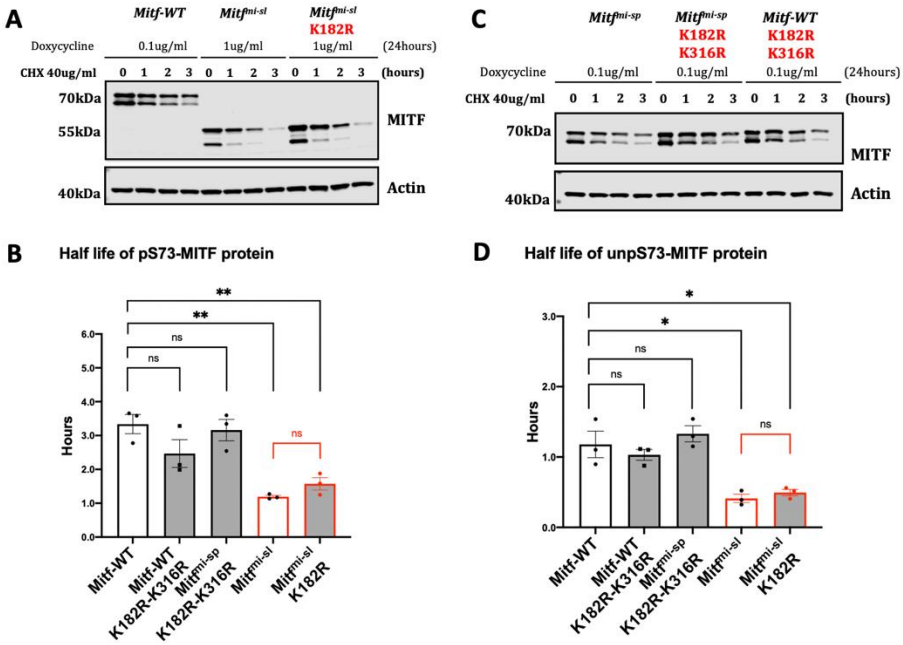

Figure 19. The arginine mutation at the K182 SUMOylation site could not rescue the stability of MITF$^{mi\text{-}sl}$. (A) and (C) Western blot analysis of the stability of the indicated MITF mutant proteins. The dox-inducible A375P melanoma cells were treated with doxycycline for 24h to express the indicated MITF proteins before treating them with cycloheximide (CHX) 40ug/ml for 0, 1, 2, and 3 hours. The MITF proteins were then compared by Western blot using Flag antibody. Actin was used as a loading control. The band intensities were quantified using ImageJ software. (B) and (D) Half-life analysis of the indicated pS73- and unpS73-MITF proteins over time after CHX treatment. The MITF protein levels relative to T0 were calculated, and non-linear regression analysis performed. Error bars represent SEM of at least three independent experiments. Statistically significant differences (Student's t-test) are indicated by *, $p< 0.05$.

4.1.6 MITF is mainly degraded through a ubiquitin-mediated proteasome pathway in the nucleus

To investigate which degradation pathway is responsible for MITF degradation, we treated the cells with either the ubiquitin-proteasomal inhibitor MG132 or the lysosomal inhibitor Baf-A1 together with CHX for 3 hours. Treatment with MG132 and CHX increased the intensities of both the upper and lower bands of the MITF-WT, MITF$^{mi\text{-}sp}$, and MITF$^{mi\text{-}sl}$ proteins (Figures 20A and 20B), although the change for unpS73-MITF$^{mi\text{-}sp}$ was not statistically significant. Upon Baf-A1 and CHX treatment, the pS73 band was unchanged for the MITF-WT and MITF$^{mi\text{-}sp}$ proteins, whereas the pS73-MITF$^{mi\text{-}sl}$ protein was severely reduced (Figures 20A and 20B); the lower unpS73 band was considerably decreased for all three proteins after the Baf-A1 and CHX treatment (Figures 20A and 20B). The dox-inducible A735P cells expressing MITF-WT, MITF$^{mi\text{-}sp,}$ and MITF$^{mi\text{-}sl}$ were treated with either MG132 or Baf-A1 for 3 hours without CHX before harvesting and Western blot. A significant increase was observed in the intensity of the pS73 band of the MITF$^{mi\text{-}sp}$ and MITF$^{mi\text{-}sl}$ proteins after MG132 and Baf-A1 treatment (Figures 20C and 20D). Interestingly, the unpS73-MITF-WT, unpS73-MITF$^{mi\text{-}sp,}$ and unpS73-MITF$^{mi\text{-}sl}$ bands showed a considerable increase after MG132 treatment (approximately 2.4-, 2.7- 6.7-fold increase respectively) (Figure 20D). No such increase was observed upon Baf-A1 treatment (Figure 20D). Taken together, our data suggest that the ubiquitin-proteasome pathway is the primary degradation machinery for MITF and that the unpS73 form of MITF, rather than the pS73 form, is the cleavage substrate of the ubiquitin-proteasomal pathway.

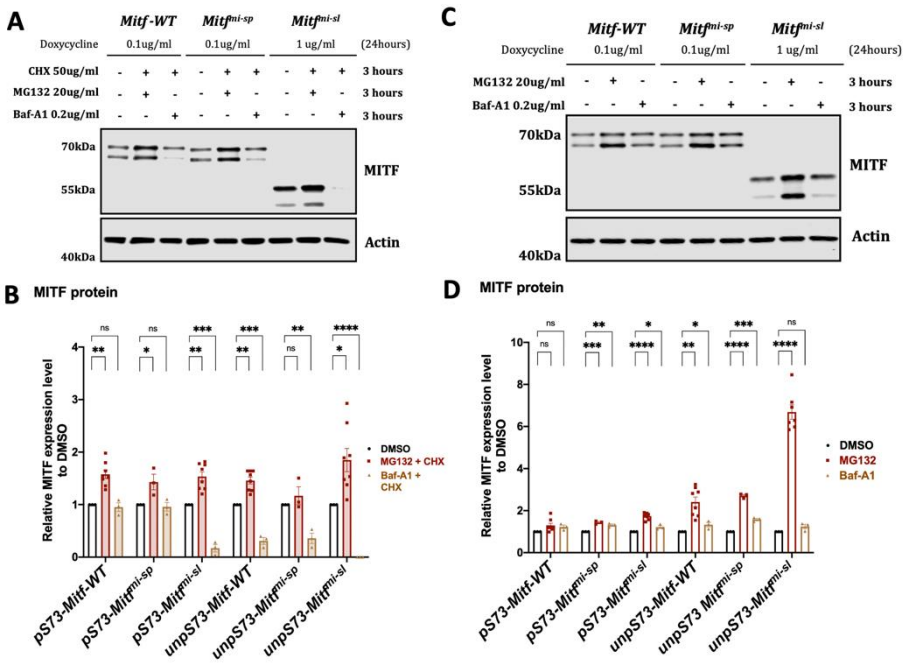

Figure 20. MITF is mainly degraded through the proteasome pathway. (A) Western blot analysis of the degradation of the MITF-WT, MITF$^{mi\text{-}sp}$, and MITF$^{mi\text{-}sl}$ proteins. The 24-hour-inducible A375P cells were treated with CHX 50ug/ml in the presence of either DMSO or MG132 40ug/ml or Baf-A1 0.1ug/ml for 3 hours. The MITF protein was then compared by Western blot using Flag antibody. Actin was used as a loading control. The band intensities were quantified using ImageJ software. (C) Western blot analysis of the degradation of the MITF-WT, MITF$^{mi\text{-}sp}$, and MITF$^{mi\text{-}sl}$ proteins. The 24-hour-inducible A375P cells were treated with either DMSO or MG132 40ug/ml or Baf-A1 0.1ug/ml for 3 hours. The MITF protein was then compared by Western blot using Flag antibody. Actin was used as a loading control. The band intensities were quantified using ImageJ software. (B) and (D) The indicated pS73- and unpS73-MITF protein band intensities from Western blot analysis (A) and (C), respectively, were quantified separately with ImageJ software and are depicted as relative protein expression to DMSO. Error bars represent SEM of at least three independent experiments. Statistically significant differences (Student's t-test) are indicated by *, $p< 0.05$.

To confirm that the unpS73 form of MITF is the cleavage substrate of the proteasome pathway, the MITF-WT-S73A, MITF$^{mi\text{-}sl}$-S73A, MITF-WT-S73E, and MITF$^{mi\text{-}sl}$-S73E proteins were expressed in the A375P melanoma cells for 24 hours before MG132-treatment in the presence or absence of CHX for 3 hours. The MG132 treatment led to an increase in MITF-WT-S73A protein level (about 1.7-fold compared to vehicle control) which was less of an increase than observed for unpS73-MITF-WT (approximately 2.4-fold compared to vehicle control)

(Figures 21A-C). Although the expression of MITF$^{mi\text{-}sl}$-S73A protein was increased 3.7-fold after treatment with MG132 compared to vehicle control, the unpS73-MITF$^{mi\text{-}sl}$ protein was observed to have a more robust accumulation in the presence of MG132 with an approximately 6.7-fold increase (Figures 21A-C). Consistent with the previous report proposing that S73 phosphorylation status is not the only mechanism regulating MITF degradation (Wellbrock and Marais, 2005), the data showed that the MITF-WT-S73E and MITF$^{mi\text{-}sl}$-S73E proteins were slightly increased upon MG132 treatment (Figures 21B-C), Furthermore, the significant increase of unpS73-MITF after MG132 treatment suggests that MITF needs to be dephosphorylated before cleaving by the proteasomal machinery. Our findings also hypothesized that the transformation between unpS73 and pS73 stages might accelerate the MITF degradation process.

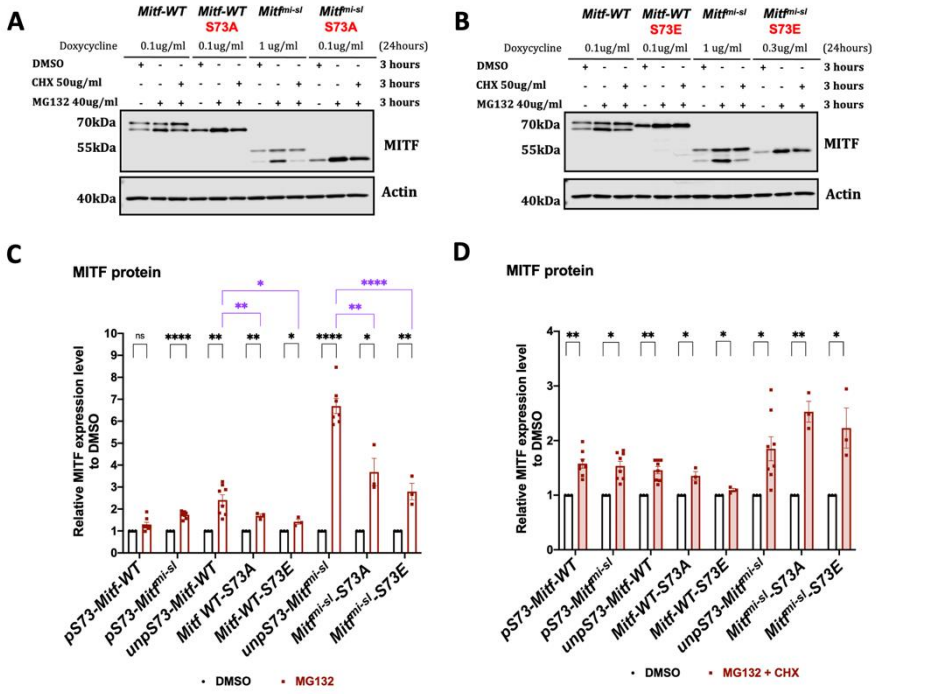

Figure 21. Both unpS73- and pS73-MITF proteins are substrates of the ubiquitin-proteasomal pathway. (A) and (B) Western blot analysis of the degradation of the indicated MITF mutant proteins. The 24-hour-inducible A375P cells were treated with either DMSO or MG132 40ug/ml or MG132 40ug/ml and CHX 40ug/ml for 3 hours. The MITF protein was then compared by Western blot using Flag antibody. Actin was used as a loading control. The band intensities were quantified using ImageJ software. (C) and (D) The indicated pS73- and unpS73- MITF protein band intensities were quantified separately with ImageJ software and are depicted as relative protein expression to DMSO. Error bars represent SEM of at least three independent experiments. Statistically significant differences (Student's t-test) are indicated by *, $p < 0.05$.

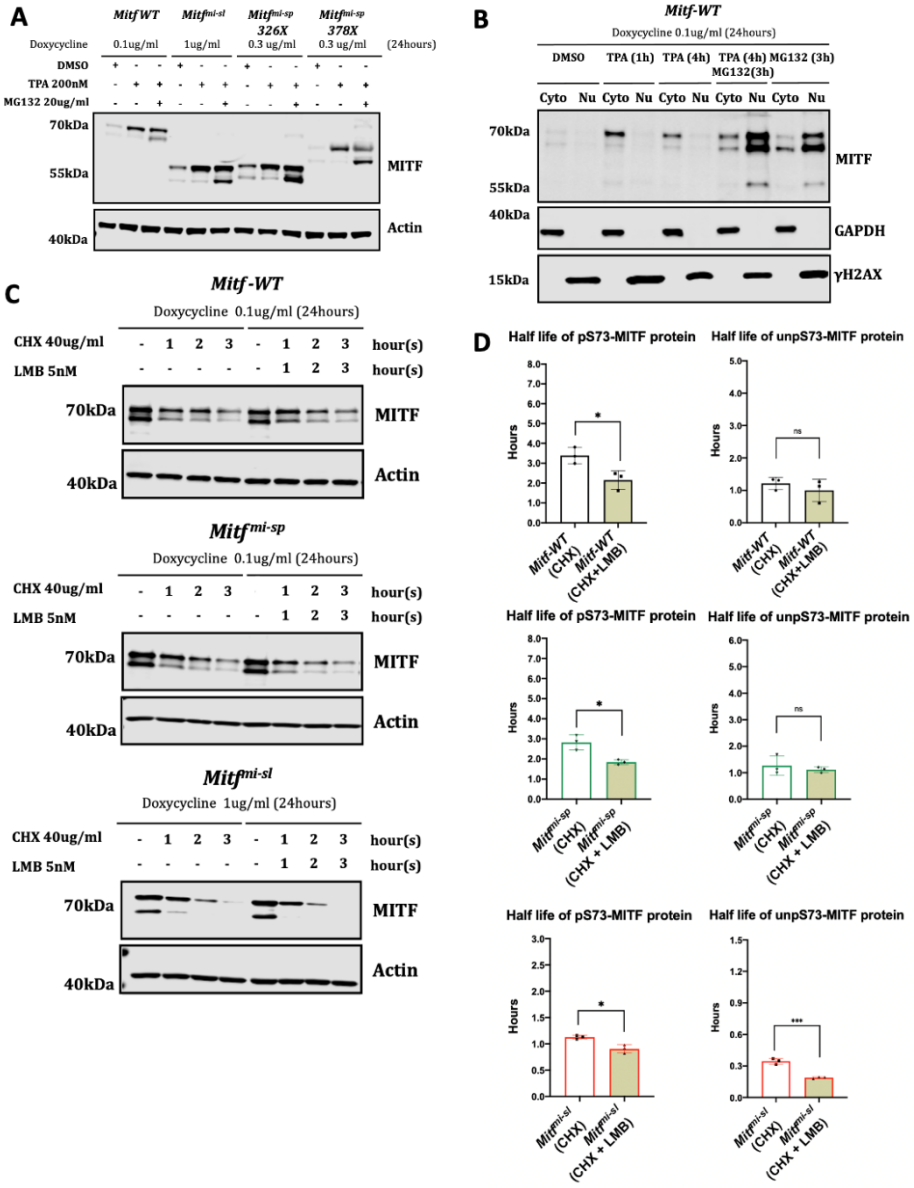
A
Mitf WT
Mitfmi-sl
Mitfmi-sp 326X
Mitfmi-sp 378X
Doxycycline
0.1ug/ml
1ug/ml
0.3 ug/ml
0.3 ug/ml
(24hours)
DMSO
TPA 200nM
MG132 20ug/ml
70kDa
55kDa
40kDa
MITF
Actin
B
Mitf-WT
Doxycycline 0.1ug/ml (24hours)
DMSO
TPA (1h)
TPA (4h)
TPA (4h) MG132 (3h)
MG132(3h)
Cyto
Nu
70kDa
55kDa
40kDa
15kDa
MITF
GAPDH
γH2AX
C
Mitf-WT
Doxycycline 0.1ug/ml (24hours)
CHX 40ug/ml
LMB 5nM
hour(s)
70kDa
40kDa
MITF
Actin
Mitfmi-sp
Doxycycline 0.1ug/ml (24hours)
Mitfmi-sl
Doxycycline 1ug/ml (24hours)
D
Half life of pS73-MITF protein
Half life of unpS73-MITF protein
Hours
ns
Mitf-WT (CHX)
Mitf-WT (CHX+LMB)
Mitfmi-sp (CHX)
Mitfmi-sp (CHX + LMB)
Mitfmi-sl (CHX)
Mitfmi-sl (CHX + LMB)

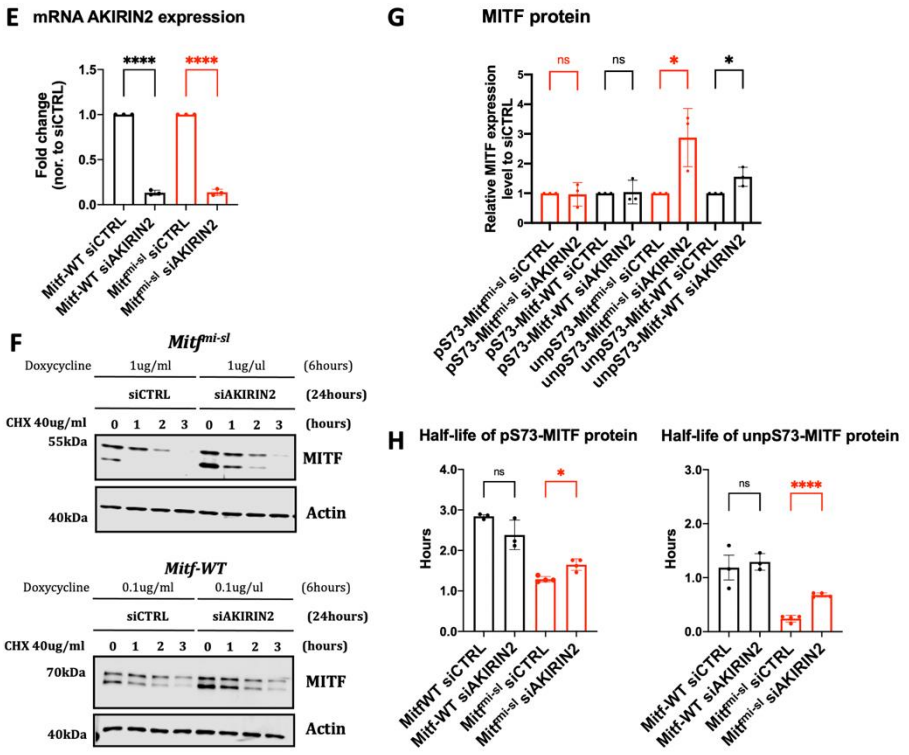

Figure 22. MITF is mainly degraded in the nucleus (A) Western blot analysis of whole cell lysate isolated from 24-hours-inducible A375P melanoma cells overexpressing MITF-WT protein before treating with either DMSO or TPA 200nM for 1 hour or TPA 200nM for 1 hour and then adding MG132 40ug/ml for the next 3 hours. MITF proteins were visualized using Flag antibody. Actin was used as a loading control. (B) Western blot analysis of subcellular fractions isolated from 24-hour-inducible A375P melanoma cells overexpressing MITF-WT protein before treating with either TPA 200nM for 1 hour or TPA 200nM for 4 hours or TPA 200nM for 1 hour and then adding MG132 40ug/ml for the next 3 hours, or MG132 40ug/ml for 3 hours. MITF-WT protein in cytoplasmic (Cyto) and nuclear fractions (Nu) were visualized using Flag antibody. GAPDH and γH2AX were loading controls for cytoplasmic and nuclear fractions, respectively. (C) Western blot analysis of the degradation of the indicated MITF mutant proteins. The 24-hour-inducible A375P cells were treated with CHX 40ug/ml in the presence of LMB 5nM for 0, 1, 2, and 3 hours. The MITF proteins were then compared by Western blot using Flag antibody. Actin was used as a loading control. The band intensities were quantified using ImageJ software. (D) Half-life analysis of the indicated pS73- and unpS73-MITF proteins over time after CHX plus LMB. The MITF protein levels relative to T0 were calculated, and non-linear regression analysis was performed. Error bars represent SEM of at least three independent experiments. Statistically significant differences (Student's t-test) are indicated by *, $p < 0.05$. (E) qPCR analysis of Akirin2 gene expression in A375P cells

treated with siAKIRIN2 for 24hour and dox-inducible A375P overexpressing MITF for 6 hours. The expression was normalized to siCTRL-treated cells. Error bars represent SEM of at least three independent experiments. Statistically significant differences (Student's t-test) are indicated by *, p< 0.05. (F) Western blot analysis of the stability of the MITF-WT and $MITF^{mi\text{-}sl}$ mutant proteins after Akirin2 knockdown for 24 hours and then dox-inducing MITF expression for 6 hours. The inducible A375P cells were treated with CHX 40ug/ml for 0, 1, 2, and 3 hours. The MITF proteins were then compared by Western blot using Flag antibody. Actin was used as a loading control. The band intensities were quantified using ImageJ software. (G) The indicated pS73- and unpS73-MITF protein band intensities from Western blot analysis (F) were quantified separately with ImageJ software and are depicted as relative protein expression to DMSO. Error bars represent SEM of three independent experiments. Statistically significant differences (Student's t-test) are indicated by *, p< 0.05. (H) Half-life analysis of the indicated pS73- and unpS73-MITF proteins in the 24-hour-siAKIRIN2-treated and then 6-hour-inducible overexpression MITF A375P cells over time after CHX treatment. The MITF protein levels relative to T0 were calculated, and non-linear regression analysis was performed. Error bars represent SEM of at least three independent experiments. Statistically significant differences (Student's t-test) are indicated by *, p< 0.05.

We also treated cells expressing MITF-WT, $MITF^{mi\text{-}sp}$, and the previously described C-terminus truncated $MITF^{mi\text{-}sp}$ proteins with TPA and MG132. After one hour of TPA treatment, the MITF-WT and mutant MITF proteins were mostly in pS73 form (Figure 22A). TPA treatment significantly increased the total MITF protein compared to vehicle controls (Figure 22A). Treating the cells for 3 hours with MG132 in the presence of TPA resulted in a significant increase in the lower unpS73 band in all cases (Figure 22A). Separating the nuclear and cytoplasmic fractions after the TPA and MG132 treatment revealed that the lower band primarily accumulated in nucleus (Figure 22B), suggesting that the proteasomal degradation of MITF takes place in the nucleus.

To further confirm that MITF degradation takes place in the nucleus, the dox-inducible A375P melanoma cells expressing MITF-WT, $MITF^{mi\text{-}sp}$, and $MITF^{mi\text{-}sl}$ were exposed to CHX and the nuclear export inhibitor leptomycin B (LMB) (Sun et al., 2013) for different time points before harvesting for Western blot. The results showed that the stability of pS73-MITF-WT and pS73-$MITF^{mi\text{-}sp}$ was slightly but significantly reduced, whereas unpS73 was not changed and that the stability of both unpS73- and pS73-$MITF^{mi\text{-}sl}$ decreased upon LMB treatment (Figures 22C and 22D). Akirin2 is essential for proteasomal degradation in the nucleus (de Almeida et al., 2021). Akirin2 was knocked down in dox-inducible A375P cells expressing MITF-WT and $MITF^{mi\text{-}sl}$ before CHX treatment and harvesting at different time points to measure protein stability. After treating the cells for 24 hours with siAKIRIN2, the expression of the Akirin2 mRNA was significantly

decreased, whereas the expression of both unpS73-MITF-WT and unpS73-MITF^{mi-sl} was significantly increased (Figures 22E-G). Although MITF-WT did not show an increase in stability, the stability of MITF^{mi-sl} was improved considerably upon Akirin2 knockdown (Figures 22F-H). Taken together, our results show that MITF is degraded in the nucleus through the proteasomal pathway. The increased nuclear presence of the MITF^{mi-sl} protein may explain its reduced stability.

4.1.7 MITF^{mi-sl} stability improves in the presence of other MITF mutants upon dragging its dimer partner into the nucleus

We further assessed the stability of MITF^{mi-sl} protein in cells also expressing either MITF^{mi-ew}, MITF^{mi}, or MITF^{Mi-Wh}. The results showed that the stability of both pS73 and unpS73 MITF^{mi-sl} was considerably increased in the presence of the MITF^{mi-ew}, MITF^{mi}, and MITF$^{Mi-Wh(+)}$ proteins, with the most pronounced effect observed in the cells also expressing MITF^{mi-ew} and MITF^{mi} (around 2.5-fold increase for pS73 and 3.5-fold increase for unpS73) (Figures 23A-E). The stability of pS73 and unpS73 versions of MITF^{mi-sl} was also significantly improved when co-expressed with MITF-WT (Figures 23F and 23G). To eliminate the possibility that we saturated the degradation machinery in the cells, we co-transfected the cells with Mitf^{mi-sl}-EGFP and MITF^{mi-sl}-Flag and measured the stability of MITF^{mi-sl}-Flag protein. The results showed that the stability of MITF^{mi-sl}-Flag was not rescued in the presence of Mitf^{mi-sl}-EGFP (Figure 23H).

To understand how MITF^{mi-sl} stability improves in the presence of other MITF mutants, we studied the dimerization between MITF^{mi-sl} or MITF^{mi-sp} proteins and non-DNA binding mutants of MITF. We co-expressed MITF$^{Mi-Wh(+)}$-Flag, MITF^{mi}-Flag, and MITF^{mi-ew}-Flag with either the MITF-WT-GFP, MITF^{mi-sl}-GFP, or MITF^{mi-sp}-GFP proteins in A375 cells and performed co-immunoprecipitation (co-IP) using Flag-antibodies. This showed that the MITF-WT-GFP, MITF^{mi-sl}-GFP, and MITF^{mi-sp}-GFP proteins were immunoprecipitated with the MITF$^{Mi-Wh(+)}$-Flag, MITF^{mi}-Flag, and MITF^{mi-ew}-Flag proteins indicating a similar ability of MITF-WT, MITF$^{mi-sp,}$ and MITF^{mi-sl} proteins to interact with the non-DNA binding MITF mutant proteins (Figure 24A). These interactions might result from a tetramer or oligomer forming between MITF^{mi-sl} and MITF mutant proteins.

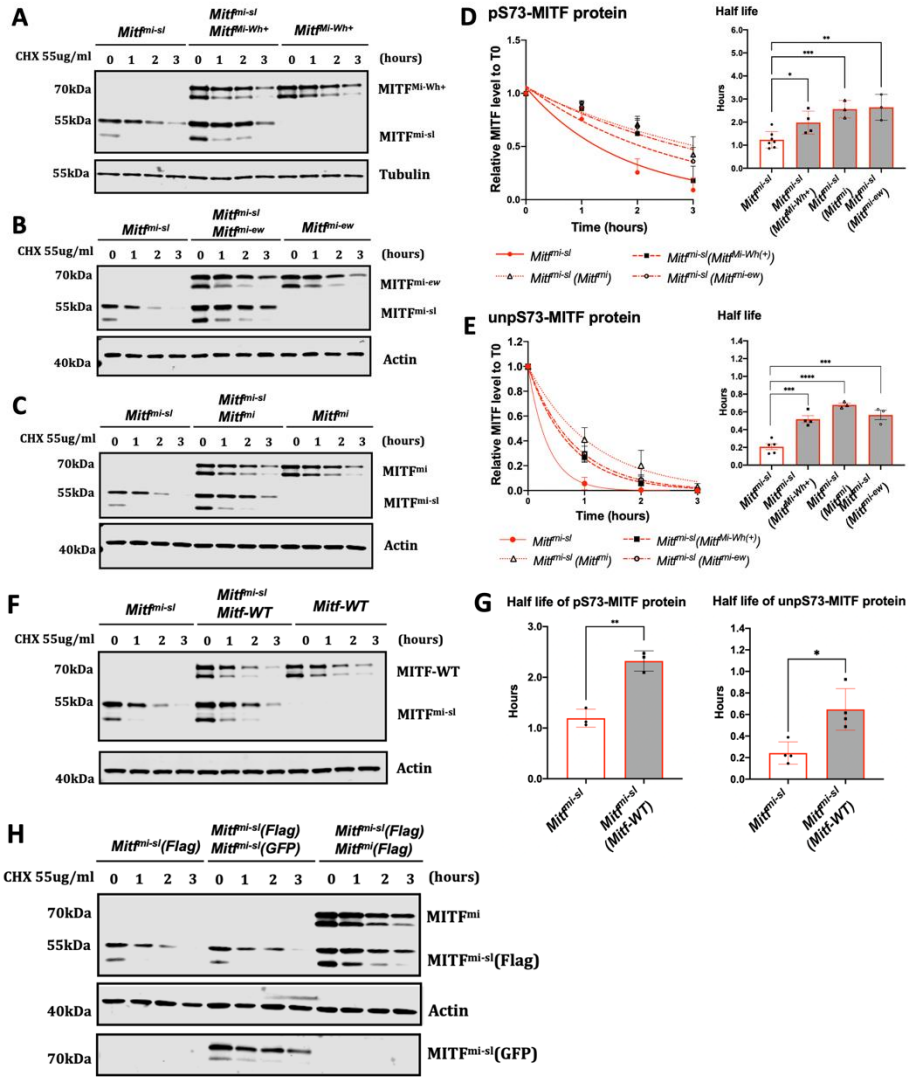

Figure 23. The stability of MITF$^{mi\text{-}sl}$ is significantly improved in presenting defective DNA binding MITF mutations. (A), (B), (C), and (F) Western blot analysis of the degradation of the MITF$^{mi\text{-}sl}$ protein in the presence of non-DNA binding MITF mutations or MITF-WT. The A375P cells were transiently co-transfected with MITF$^{mi\text{-}sl}$ and either MITF^{mi}, MITF$^{mi\text{-}ew}$, MITF$^{Mi\text{-}Wh}$, or MITF-WT for 24 hours before being treated with CHX 55ug/ml. The MITF protein was then compared by Western blot using Flag antibody. Actin was used as a loading control. The band intensities were quantified using ImageJ software. (D), (E), and (G) Non-linear regression (one-phase decay) and half-life analysis of indicated pS73- and unpS73-MITF proteins over time after CHX treatment. The MITF protein levels relative to T0 were calculated, and non-linear regression analysis was performed. Error bars represent SEM of at least three independent experiments. Statistically significant differences (Student's t-test) are indicated by *, p< 0.05. (H)

Western blot analysis of the degradation of the MITF$^{mi\text{-}sl}$ protein fusion with Flag-tag at C-terminus in the presence of either MITF$^{mi\text{-}sl}$ protein fusion with GFP tag at C-terminus or MITF^{mi} protein fusion with Flag at C-terminus. The A375P cells were transiently co-transfected with MITF$^{mi\text{-}sl}$-Flag and indicated MITF mutant protein for 24 hours before being treated with CHX 55ug/ml. The MITF protein was then compared by Western blot using Flag antibody. Actin was used as a loading control. The band intensities were quantified using ImageJ software.

To further clarify the interactions between MITF$^{mi\text{-}sl}$ and the non-DNA binding MITF mutants, we co-expressed the MITF^{mi}-Flag protein together with either MITF-WT-GFP, MITF$^{mi\text{-}sp}$-GFP, or MITF$^{mi\text{-}sl}$-GFP proteins in A375 cells. We then performed Blue native PAGE (Wittig et al., 2006) followed by a second dimension of SDS-PAGE. The results suggest that dimers indeed form between MITF^{mi} and the MITF$^{mi\text{-}sl}$ or MITF$^{mi\text{-}sp}$ proteins (Figures 24B and 24C). Interestingly, cells expressing MITF$^{mi\text{-}sl}$ showed that the MITF$^{mi\text{-}sl}$ protein was mostly in the form of a dimer (Figure 24C). Interestingly, on the Blue-PAGE, MITF-WT/MITF-WT, MITF^{mi}/MITF^{mi} homodimers, and MITF-WT/MITF^{mi} heterodimers were observed in cells co-expressing MITF^{mi} and MITF-WT. A similar pattern was also seen in cells co-expressing MITF^{mi} and MITF$^{mi\text{-}sp}$. However, only the heterodimer MITF$^{mi\text{-}sl}$-MITF^{mi} was seen in cells co-expressing MITF^{mi} and MITF$^{mi\text{-}sl}$. Our finding suggested that MITF$^{mi\text{-}sl}$ prefers to form dimers with MITF$^{mi\text{-}ew}$, MITF^{mi}, and MITF$^{Mi\text{-}Wh}$.

To determine if the MITF$^{mi\text{-}sl}$ protein affects the subcellular localization of the above non-DNA binding MITF mutations, MITF$^{mi\text{-}sl}$ protein was transiently overexpressed together with the other MITF mutant proteins, and their subcellular distribution was determined. As before, a significant portion of the pS73- and unpS73-MITF$^{mi\text{-}sl}$ proteins were observed in the nucleus (Figures 25A and 25B).

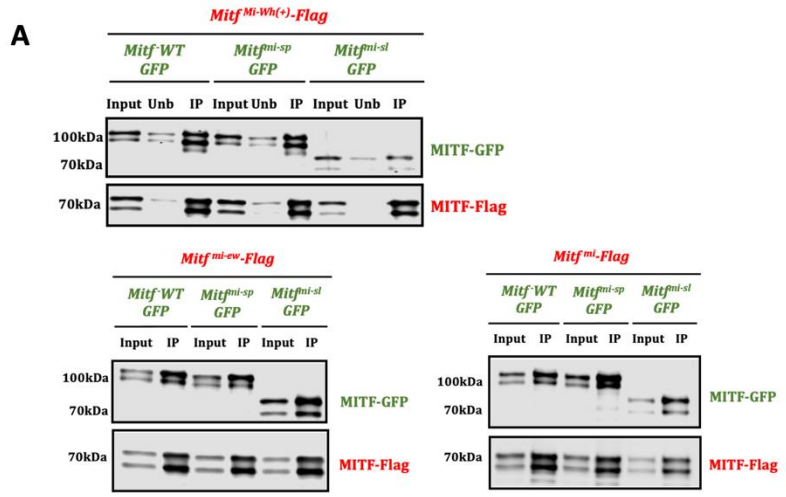

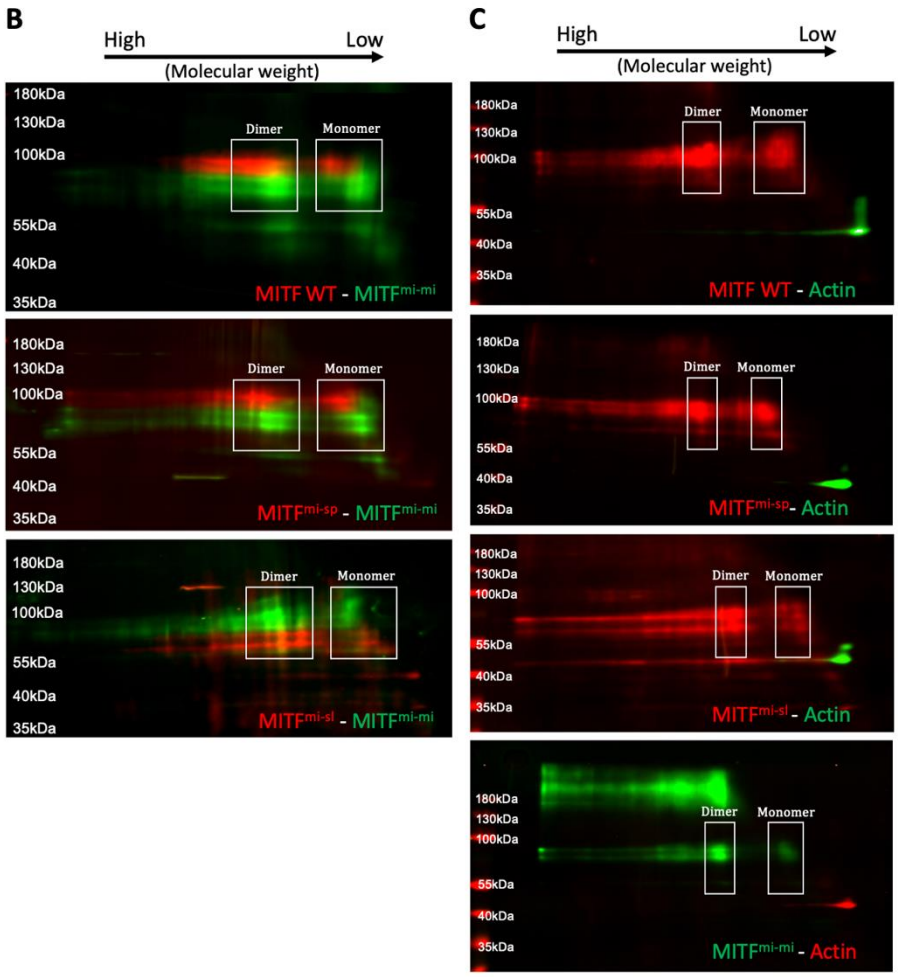

Figure 24. MITF$^{mi\text{-}sl}$ enables dimer formation with other MITF mutant protein (A) Western blot analysis showing the results of a co-immunoprecipitation experiment. MITF^{mi}-Flag MITF$^{Mi\text{-}Wh(+)}$-Flag, MITF$^{mi\text{-}ew}$-Flag construct was cotransfected with either MITF-WT-GFP, MITF$^{mi\text{-}sp}$-GFP or MITF$^{mi\text{-}sl}$-GFP in A375P melanoma cells. Co-immunoprecipitation (co-IP) of the whole cell lysate using Flag-antibodies was performed and visualized using Flag antibodies. Input fraction (Input), Unbound fraction (Unb), and Immunoprecipitated fraction (IP) were indicated in the Western blots. (B) and (C) Western blot analysis showing the results of a Blue native PAGE followed by the second dimension of SDS-PAGE. The A375P melanoma cells transiently (B) co-expressed the MITF^{mi}-Flag protein with either MITF WT-EGFP, MITF$^{mi\text{-}sp}$-EGFP, or MITF$^{mi\text{-}sl}$-EGFP proteins or (C) expressed MITF-WT-Flag, MITF$^{mi\text{-}sp}$-Flag, MITF$^{mi\text{-}sl}$-Flag, MITF^{mi}-Flag or in A375 cells. We then performed Blue native PAGE (Wittig et al., 2006) followed by a second dimension of SDS-PAGE.

The cells transiently expressing either MITF^{mi}, MITF$^{mi\text{-}ew}$, or MITF$^{Mi\text{-}Wh(+)}$ proteins showed equal distribution between cytoplasm and nucleus, whereas, in the presence of the MITF$^{mi\text{-}sl}$ protein, they were significantly translocated into the nucleus (Figures 25A and 25B). Similar results were observed in cells co-expressing MITF$^{mi\text{-}sl}$ and MITF-WT (Figures 25C and 25D). Taken together, the data strongly suggest that the MITF$^{mi\text{-}sl}$ protein drags its dimeric partners into the nucleus. This is consistent with the observed preference of MITF$^{mi\text{-}sl}$ for forming dimers with MITF$^{mi\text{-}ew}$, MITF^{mi}, and MITF$^{Mi\text{-}Wh}$ and the enhancement of MITF$^{mi\text{-}sl}$ stability in their presence.

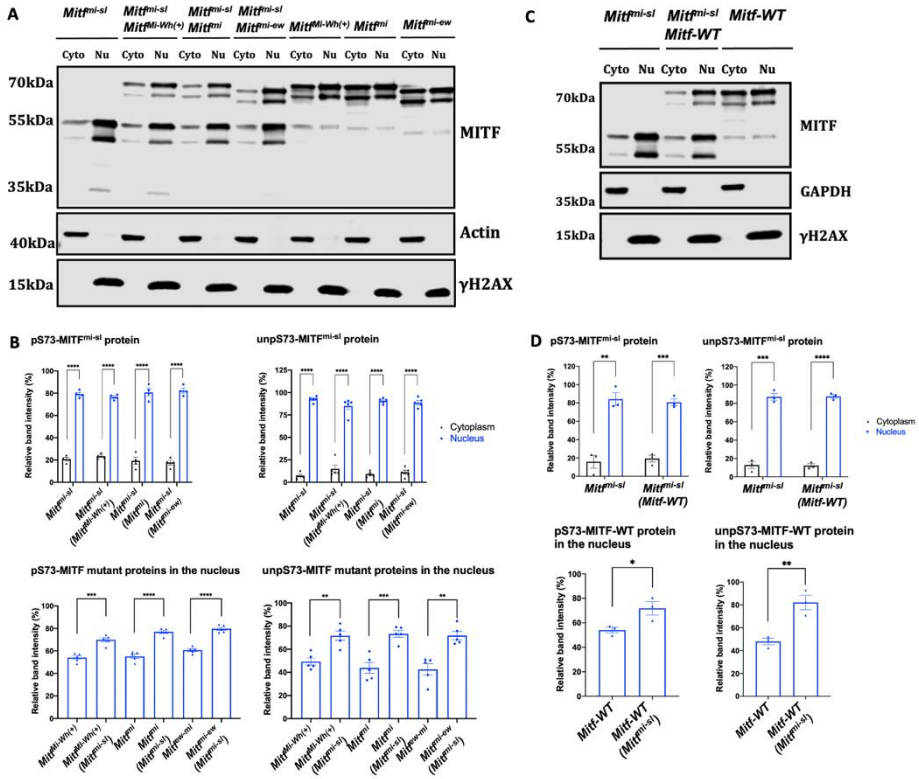

Figure 25. MITF$^{mi\text{-}sl}$ enables the localization of its dimer partner into the nucleus
(A) and (B) Western blot analysis of subcellular fractions isolated from A375P cells transiently co-overexpressed the MITF$^{mi\text{-}sl}$ protein with MITF mutant or wild type MITF. MITF proteins in cytoplasmic (Cyto) and nuclear fractions (Nu) were visualized using Flag antibody. GAPDH and γH2AX were loading controls for cytoplasmic and nuclear fractions, respectively. (C) and (D) pS73- and unpS73-MITF$^{mi\text{-}sl}$ protein band intensities in the cytoplasmic and nuclear fraction of A375P cells transiently co-overexpressing the MITF$^{mi\text{-}sl}$ protein with MITF mutant or wild type MITF were quantified separately with ImageJ software and are depicted as percentages of the total amount of protein present in the two fractions. Error bars represent SEM of three independent experiments. Statistically significant differences (Student's t-test) are indicated by *, $p < 0.05$.

4.1.8 The melanoma-associated E318K mutation reduces MITF stability

Individuals carrying the E318K mutation in MITF are predisposed to melanoma (Bertolotto et al., 2011; Yokoyama et al., 2011). The mutation abolishes SUMOylation at K316. Therefore, the stablity of MITF$^{mi\text{-}sp}$, MITF$^{mi\text{-}sp}$-326X, and MITF$^{mi\text{-}sp}$-378X constructs also carrying the E318K mutation was determined. The stability of these proteins was significantly reduced in the presence of the E318K mutation (Figures 26A-C). Interestingly, the MITF$^{mi\text{-}sp}$-378X-E318K protein showed similar stability as MITF$^{mi\text{-}sl}$ whereas the MITF$^{mi\text{-}sp}$-326X-E318K and MITF$^{mi\text{-}sp}$-326X proteins were equally stable and both more stable than MITF$^{mi\text{-}sl}$, regardless of phosphorylation at S73 (Figures 26A-C).

Interestingly, the E318K mutation in the MITF$^{mi\text{-}sp}$-378X and MITF$^{mi\text{-}sp}$ constructs resulted in a mobility shift on the SDS-gels, whereas the MITF$^{mi\text{-}sp}$-326X and MITF$^{mi\text{-}sp}$-326X-E318K did not (Figure 26A). This observation suggested that the E318K mutation might affect phosphorylation in the 316-326 domain, leading to a migration shift. The S325 residue is a potential phosphorylation site, so we investigated the effects of the S325A mutation on MITF stability. Although the MITF$^{mi\text{-}sp}$-326X-S325A also resulted in a slight mobility shift compared to MITF-WT, it did not alter MITF$^{mi\text{-}sp}$ protein stability (Figure 26D). Furthermore, the MITF$^{mi\text{-}sp}$-E318K-S325A double mutation shifted further and was less stable than K316R-S325A (Figure 26E). These results suggest that the reduction in stablity and mobility shift on SDS-gels of E318K mutation is not due to phosphorylation at S325.

4.1.9 The MITF$^{mi\text{-}sl}$ mutation affects transcription regulation

The lack of a carboxyl-end might affect the transcriptional activation potential of MITF$^{mi\text{-}sl}$. Hence, we determined the transcriptional activation potential of the MITF$^{mi\text{-}sl}$, MITF WT, and C-truncated MITF proteins. The human A375P cells were induced to express the indicated mouse MITF proteins at the same protein level, and RNA was harvested at different time points for qPCR analysis. The log2(fold change) of MITF target genes was first normalized to EV and then to the proportion of MITF proteins retained in the nucleus. Consistent with previous work (Ballesteros-Álvarez et al., 2020), the results showed that MITF-WT, MITF$^{mi\text{-}sl}$, and the C-terminally truncated MITF proteins significantly decreased expression of the endogenous human *MITF* mRNA starting at 6 hours post-transfection (Figure 27A). Expression of the endogenous Mitf protein was considerably reduced over the 36 hours sample period in all cases except for MITF$^{mi\text{-}sp}$-del326-377, which was similar to empty vector control starting at 12 hours. The expression of the *CDH2* and *NRP1* genes, which were shown to be repressed by MITF (Dilshat et al., 2021a) was significantly reduced in all cases, starting from the 6 hours time point (Figure 27B and 27C). The MITF$^{mi\text{-}sp}$-326X, MITF$^{mi\text{-}sp}$-378X, MITF$^{mi\text{-}sp}$-del326-377, and MITF-WT constructs were all able to activate the expression of the known MITF target genes PMEL and TRIM63 to similar levels. In contrast, the MITF$^{mi\text{-}sl}$ construct exhibited about half the ability of the other

constructs to activate the expression of these genes (Figures 27D and 27E). Interestingly, MITF$^{mi\text{-}sp}$-326X and MITF$^{mi\text{-}sl}$ did not activate the expression of the TYRP1 and MLANA genes (Figures 27F and 27G). Our results suggest that the 316-419 domain is critical for the selective transcriptional activation and repression activity of MITF.

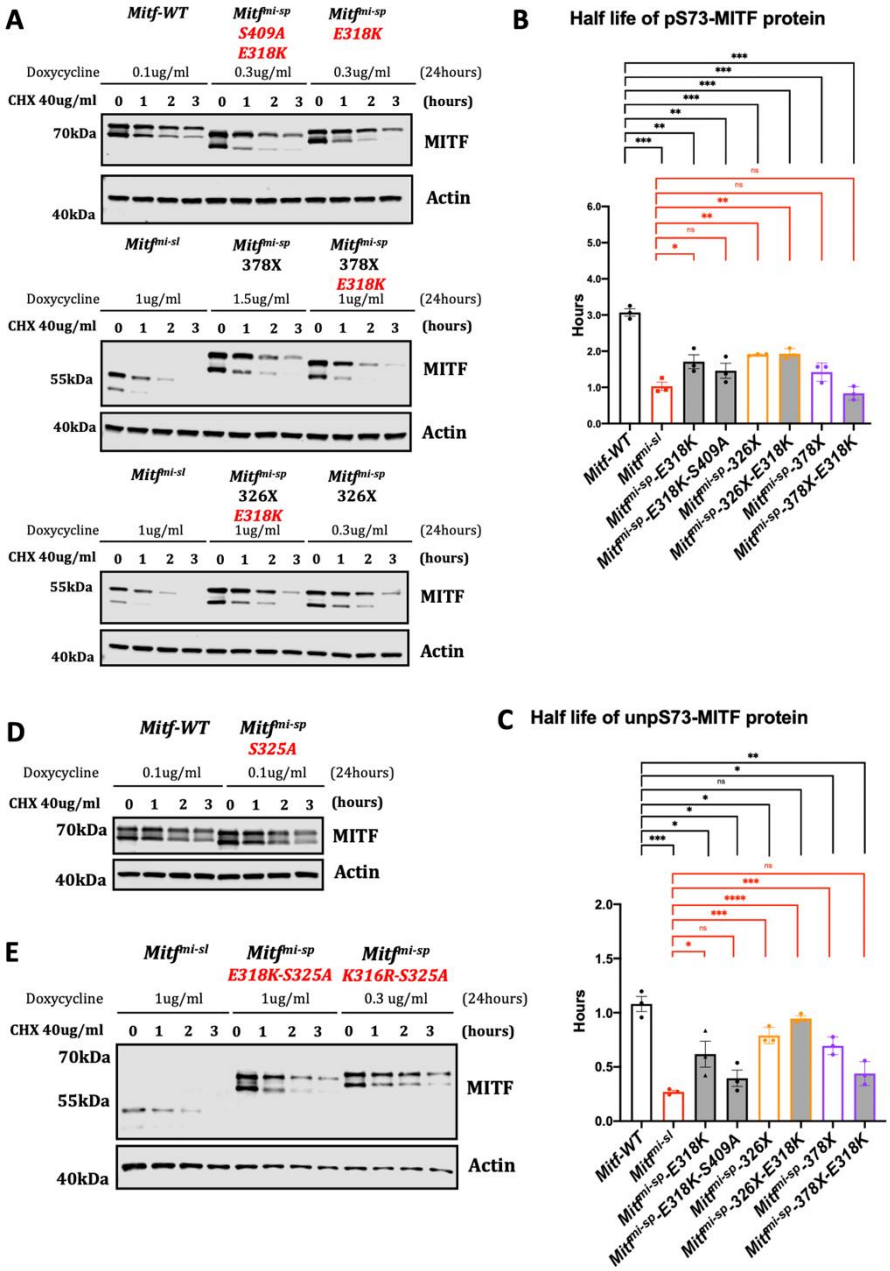

Figure 26. E318K mutation reduces the stability of MITF protein (A), (D), and (E) Western blot analysis of the stability of the MITF mutant proteins. The inducible A375P cells were treated with doxycycline for 24 hours to express the MITF proteins before treating them with cycloheximide (CHX) 40ug/ml for 0, 1, 2, and 3 hours. The MITF proteins were then compared by Western blot using Flag antibody. Actin was used as a loading control. The band intensities were quantified using ImageJ software. (B) and (C) Half-life analysis of indicated pS73- and unpS73- MITF proteins degradation over time after CHX treatment, respectively. The MITF protein levels relative to T0 were calculated, and non-linear regression analysis was performed. Error bars represent SEM of at least three independent experiments. Statistically significant differences (Student's t-test) are indicated by *, p< 0.05.

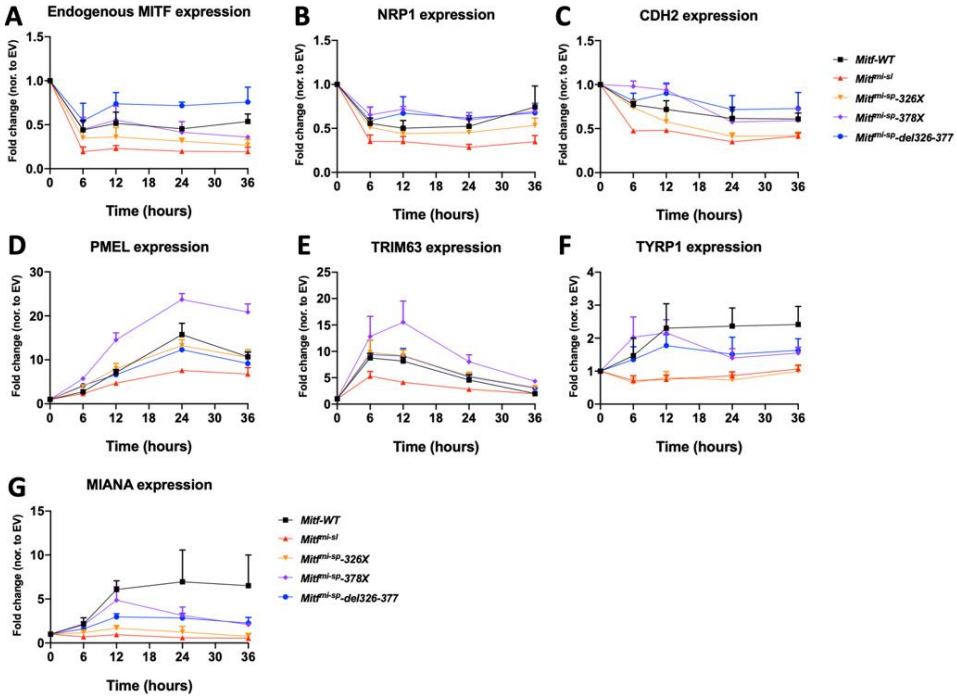

Figure 27. MITF$^{mi\text{-}sl}$ protein is a less potent activator than MITF$^{mi\text{-}sp}$ qPCR analysis of (A) endogenous MITF and MITF target genes: (B) NRP1, (C) CDH2, (D) PMEL, (E) TRIM63, (F) TYRP1, and (G) MLANA in the dox-inducible A375P overexpressing cells. The cells were treated with different doxycycline for 6, 12, 24, and 36 hours to induce MITF expression at the same level before harvesting. Expression was normalized to EV-FLAG-HA cell lines and then to the proportion of MITF proteins retained in the nucleus. Error bars represent SEM of at least three independent experiments. Statistically significant differences (Student's t-test) are indicated by *, p< 0.05.

4.2 Functional roles of PRDM7

4.2.1 PRDM7 expression is correlated with MITF

As proposed by the MITF rheostat model, the expression or activity of MITF determines the phenotypic outcome in melanoma cells. This is a reversible and dynamic process where cells can change their phenotype from proliferative to non-proliferative migrating cells (Goding and Arnheiter, 2019; Rambow et al., 2019). The dynamic changes might suggest that MITF might do this by regulating the expression of epigenetic modifiers to reshape the melanoma chromatin state. By searching for epigenetic modifiers depending on MITF expression, the histone methyltransferase *PRDM7* was observed to be significantly reduced upon MITF knockout in SKmel28 melanoma cell line (Dilixiati, 2019). The expression of *PRDM7* also showed a considerable increase upon transient overexpressing MITF-WT and $MITF^{mi\text{-}sp}$ isoforms. Consistent with that, the DNA-binding mutant $MITF^{Mi\text{-}Wh(+)}$ was not able to elevate *PRDM7* expression (Figure 28A). The positive correlation between *MITF* and *PRDM7* expression is also shown in 480 cutaneous melanoma tumor samples from the Cancer Genome Atlas (TCGA database) (Figure 28B) as well as in microarray data of 24 melanoma cell lines generated by Lionel Larue's group and made available to us (Figure 28C). Interestingly, *PRDM7* is a primate-specific gene (Fumasoni et al., 2007) and is uniquely expressed in melanoma among among all cancers type (Figure 28D). Among 53 melanoma cell lines grouped by phenotype (Tsoi et al., 2018), *PRDM7* is most highly expressed in melanocytic cells where *MITF* and *SOX10* are also highly expressed (Figure 28E). Although Chip-Seq data do not show direct binding of MITF at *PRDM7* promoter nor gene body (Laurette et al., 2015), there are more than 16 MITF Chip-peaks of high confidence and containing MITF binding sites in a TAD domain near *PRDM7*. Surprisingly, apart from PRDM7, none of the other genes located in that TAD showed changes in expression upon MITF depletion. Hi-C data from SKMel5 melanoma cells suggests long-range interactions between the areas containing MITF-Chip-peaks and the PRDM7 promoter region (http://3dgenome.fsm.northwestern.edu/view.php) (Appendix 3). This suggests the direct regulation of PRDM7 by MITF through long-range effects. Taken together, the data strongly suggests that PRDM7 is a direct MITF target gene.

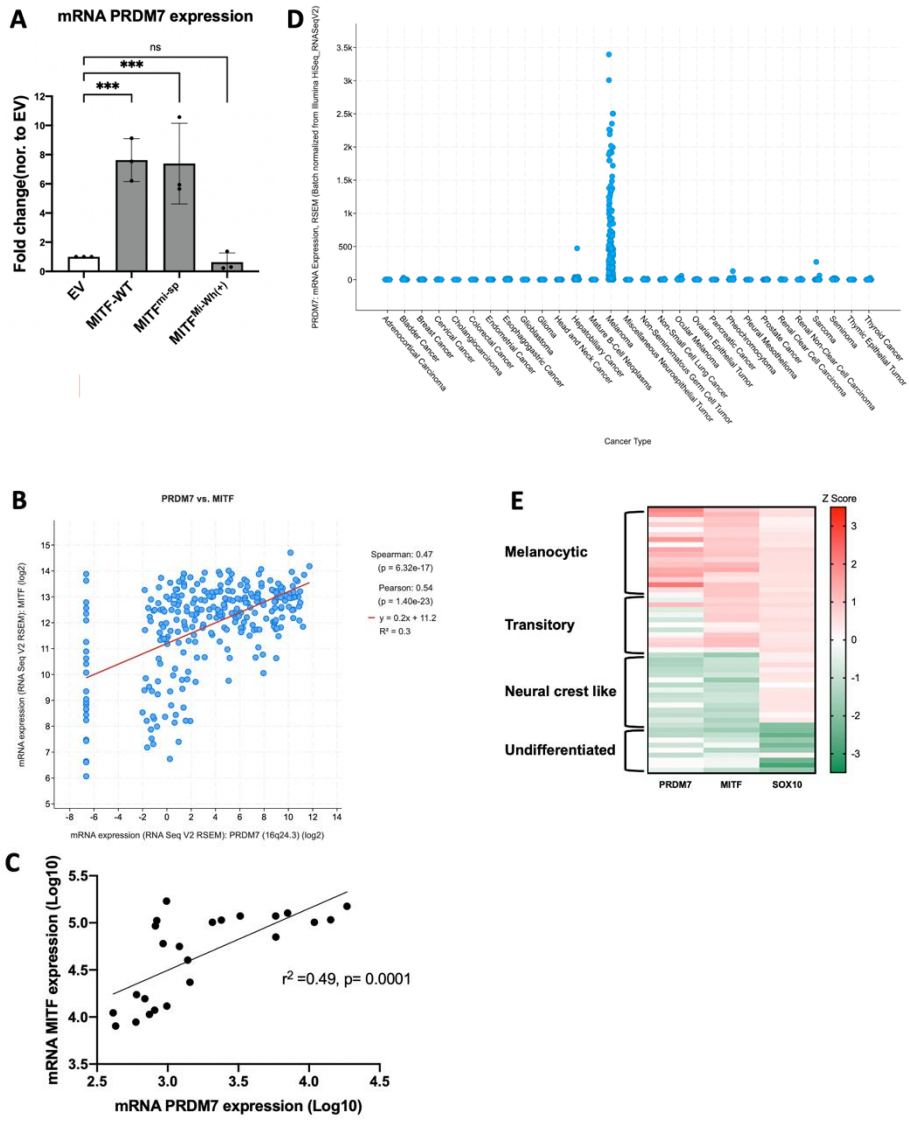

Figure 28. Positive correlation between PRDM7 and MITF expression (A) RNA-expression of PRDM7 in inducible A375P cells overexpression MITF-WT, MITF$^{mi\text{-}sp}$, MITF$^{Mi\text{-}Wh(+)}$ was measured by qPCR. Error bars represent SEM of at least three independent experiments. Statistically significant differences (Student's t-test) are indicated by *, p< 0.05. (B) and (C) Correlation of PRDM7 and MITF across 480 cutaneous melanoma tumor samples from the Cancer Genome Atlas (TCGA database) (B) or 24 melanoma cell lines generated by Lionel Larue's group (C). (D) PRDM7 mRNA expression across 30 cancer types in the TCGA database. (E) PRDM7, MITF, and SOX10 mRNA expression among 53 melanoma cell lines grouped by phenotype (Tsoi et al., 2018).

4.2.2 Alternative splicing and novel *PRDM7* isoforms in melanoma

To investigate the functional roles of *PRDM7* in melanoma cells, it was important to know which *PRDM7* isoforms are expressed in melanoma cells. Previous work has reported the existence of two *PRDM7* isoforms (Figure 7), of which isoform B containing KRAB and PR/SET domains, was shown to be abundant in melanocytes and melanoma cell lines (Fumasoni et al., 2007). However, alternative *PRDM7* isoforms were also predicted by computational analysis, with three other transcripts being proposed in the ENSEMBLE database (PRDM7-203 to PRDM7-205) (Figure 29A). To characterize which PRDM7 isoforms are expressed in melanoma, the StringTie *de novo* assembly analysis was performed on RNASeq data from 501Mel and Skmel28 cells to assemble possible transcripts. Interestingly, this analysis revealed that several potential novel transcripts are possible, none of which match the previously suggested transcripts (Figure 29A). Among the proposed PRDM7 transcripts, the nine with the highest predicted score started from the first exon of ENSEMBLE_PRDM7_205 (exon m3) and extended to the last exon of the ENSEMBLE_PRDM7_202 (exon 10) transcript and skipped some exons in between compared to isoform A. To verify the results obtained using the RNA-seq data, we conducted PCR using cDNA isolated from Skmel28 cells with the aim of amplifying the suggested PRDM7 isoforms. All possible PCR fragments were then Gibson cloned into the pUC19 vector for generating novel transcripts. Interestingly, seven new PRDM7 transcripts, which contain incomplete KRAB and SET domains, were identified; these transcripts are consistent with the results from the StringTie analysis (Figures 29B and 29C and Appendix 4). However, we did not find two of the StringTie-proposed (SKC3_3_2525.5 and SKC3_3_2525.3) PRDM7 transcripts by PCR analysis, possibly because of their low expression compared to other isoforms.

A

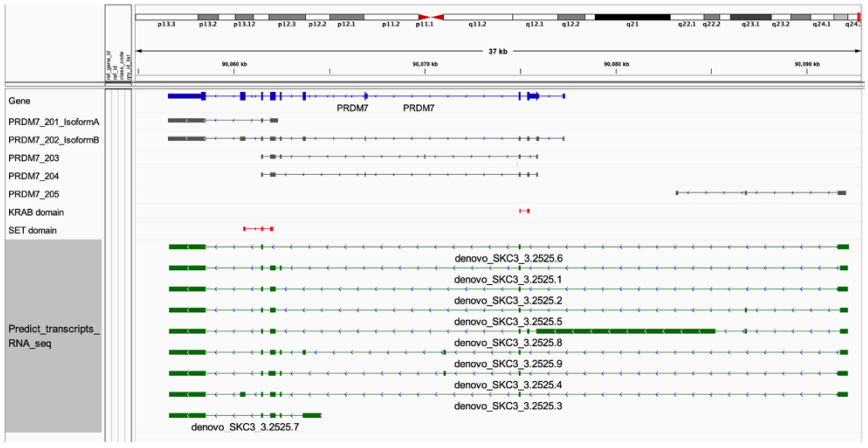

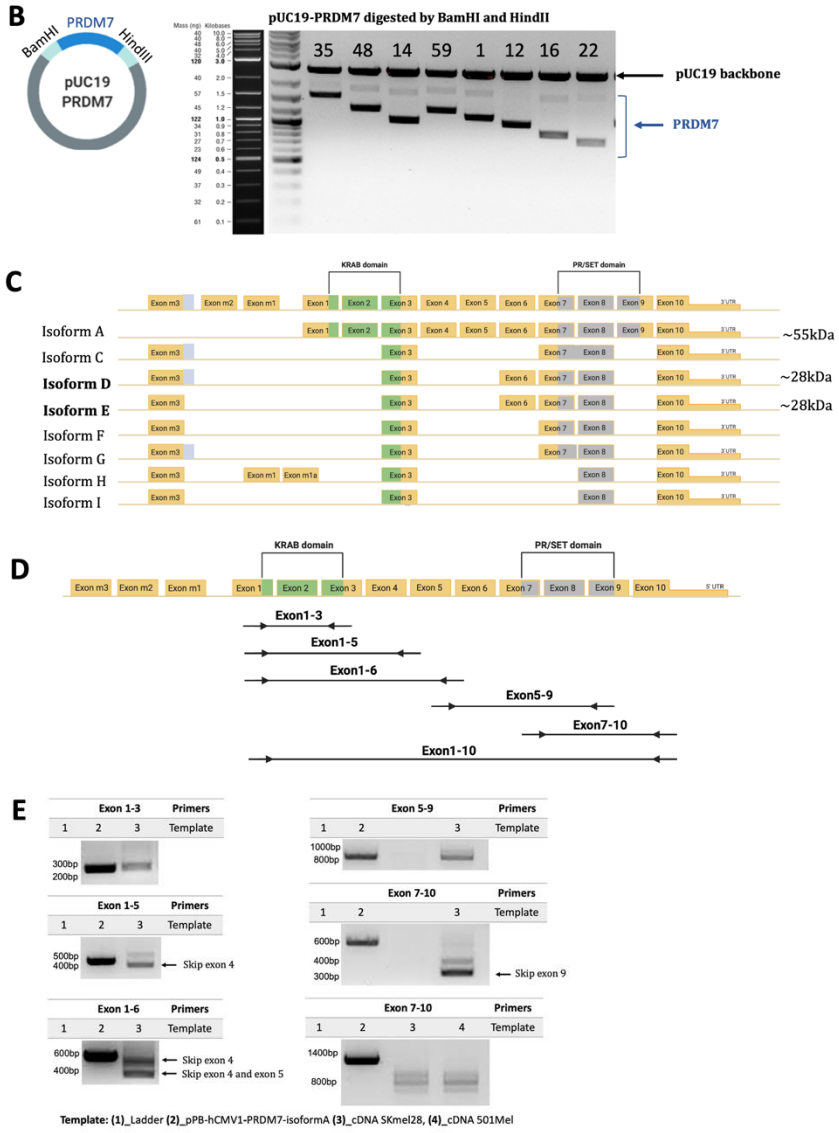

Figure 29. Alternative splicing and novel *PRDM7* isoforms in melanoma (A) Alternative *PRDM7* isoforms were predicted by Stringte analysis based on RNAseq data of SKMel28 (B) Seven PRDM7 isoforms were identified from the cDNA of Skmel28. (C) Schematic representation of the PRDM7 isoforms showing the distinct alternative splicing events. (D) Schematic representation of the location of designed primers to identify splicing events. (E) PCR amplification of cDNA isolated from Skmel28 cells to identify alternative splicing between adjacent exons

To further investigate and confirm the alternative splicing events, we also performed PCR using multiple sets of PCR primers to amplify cDNA isolated from Skmel28 cells to identify alternative splicing between adjacent exons (Table

6 and Figure 29D). The pPB-hCMV1_PRDM7_isoformA containing protein-coding regions of PRDM7 isoform A (equivalent to PRDM7_202 transcript following the ENSEMBLE database) was utilized as a control for the PCR product size. Consistent with the prediction based on RNA seq, our results show that exons 4, 5, and 9 are alternatively spliced (Figure 29E). Taken together, our data showed that although many of the proposed isoforms need to be further classified, at least seven PRDM7 transcripts are found (named isoforms C-I) in melanoma cells. Among the seven novel PRDM7 transcripts, only isoforms D and E potentially result in a 28kDa protein. Surprisingly, both isoforms D and E lack a major part of the KRAB and PR/SET domains compared to isoform A, proposing a significant difference in function between the different PRDM7 isoforms. Due to the lack of useful anti-PRDM7 antibodies, we have not yet been able to determine which of the proposed proteins are expressed in melanoma cells.

4.2.3 Generation of melanoma cells lacking PRDM7

To study the long-term effect of PRDM7 depletion in melanoma, PRDM7 was permanently knocked out in 501Mel and Skmel28 melanoma cell lines using the clustered regularly interspaced short palindromic repeats (CRISPR/Cas9) technique. The resulting knock-out PRDM7 (PRDM7-KO) melanoma cell lines would be an efficient model to study the PRDM7-low cell state in melanoma progression.

It is not practical to target the PR/SET or KRAB domain of *PRDM7* without the risk of affecting *PRDM9* because only 9 basepairs in the PR/SET and 2 basepairs in the KRAB coding sequence of PRDM7 are different from that of PRDM9 (Blazer et al., 2016) (Appendix 5). Besides, our analysis identified multiple *PRDM7* transcripts with different alternative splicing in melanoma cells. Therefore, exon 3 of *PRDM7*, located right after the KRAB domain and present in all detected isoforms, was targeted to be mutated by CRISPR/Cas9. The sequence-specific crRNA targeting exon 3 of *PRDM7* in 501Mel and SKmel28 melanoma cell lines were designed and ordered from Integrated DNA Technologies (USA) (Figure 30A). The Skmel28 and 501Mel cells were incubated for 48 hours post-transfection with a Cas9:crRNA:trRNA RPN-complex and then serially diluted to form single colonies. Following five weeks in stepwise expansion culture, single-cell colonies were screened for mutant alleles by using the T7 Endonuclease I assay and Sanger sequencing. We obtained 24 501Mel and 19 SKmel28 positive colonies, of which all were shown to carry the mutation. The PRDM7 knock-out cell lines targeting exon 3 are referred to as 501Mel-PRDM7-KO and Skmel28-PRDM7-KO to indicate the cell line of origin. The control cell lines, termed Skmel28-Control and 501Mel-Control, were generated by transfecting the

cells without a crRNA:trRNA duplex. The expression of the *PRDM7* mRNA in control and knock-out cell lines was compared using qPCR.

501Mel-PRDM7-KO and SKmel28-PRDM7-KO clones were screened for deletion mutations. The sequence analysis showed that all of the positive PRDM7-KO clones had a different mutation, whereas no mutation was detected in the PRDM7 sequence in any of the Skmel28-Control and 501Mel-Control clones. The PRDM9 genome sequence was also confirmed to be unaltered in all the PRDM7-KO clones and in the single-cell control clones (Appendix 6). For further studies, we selected two PRDM7-KO single-cell clones for each cell line (501Mel-PRDM7-KO13, 501Mel-PRDM7-KO24, SKMel28-PRDM7-KO13, and SKmel28-PRDM7-KO17); all showed a marked reduction in the expression of PRDM7 mRNA compared to the wild type controls (501Mel-C1 and SKmel28-C3) (Figure 30B). Three mutations were detected in the genome sequence of 501Mel-PRDM7-KO13: (i) deletion of two base pairs (AC) resulting in a premature stop codon at residues R98 of WT-PRDM7; (ii and iii) deletion of six base pairs resulting in the replacement of two T96-P97 residues by either a serine or a proline (Figure 30C). Sequence analysis of the 501Mel-PRDM7-KO24 clone discovered two mutations: (i) deletion of one base pair leading to a frameshift and premature stop codon at L130 amino acid position of WT-PRDM7; (ii) insertion of 1 base pair which resulted in a stop codon at R98 position (PRDM7 isoform B numbering) (Figure 30C). Only one mutation was discovered in each PRDM7 genome sequence of SKMel28-PRDM7-KO single-cell clones. The SKMel28-PRDM7-KO13 cells contain a deletion of one base pair, which gives rise to a premature stop codon at the L130 of WT-PRDM7, whereas the SKMel28-PRDM7-KO17 cells have one base pair insertion at the P97, resulting in a stop codon immediately at R98 of WT-PRDM7 (Figure 30D). The mutations were confirmed by analysis of the RNA-sequencing data of 501Mel-PRDM7-KO13, 501Mel-PRDM7-KO24, SKMel28-PRDM7-KO13, and SKmel28-PRDM7-KO17 cell lines (Appendix 6). The three frameshift mutations are likely to result in nonsense-mediated decay and a significant decrease in PRDM7 mRNA, whereas the two in-frame mutations might not severely alter the function of the PRDM7 protein.

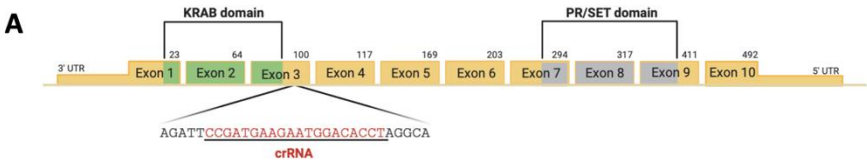

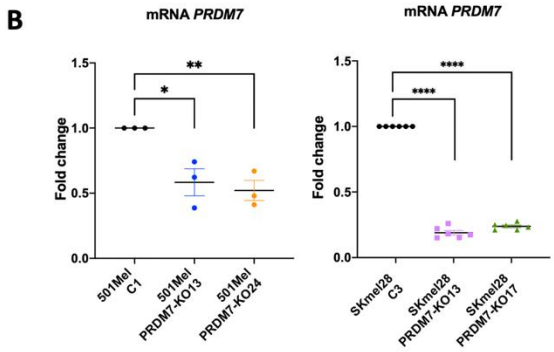

C

	89	90	91	92	93	94	95	96	97	98	99	100	101	102	103	104	105	106
PRDM7-WT	E	D	S	D	E	E	W	T	P	R	Q	Q	V	K	P	P	W	M
	GAA	GAT	TCC	GAT	GAA	GAA	TGG	ACA	CCT	AGG	CAG	CAA	GTC	AAA	CCT	CCT	TGG	ATG
501Mel-PRDM7-KO13	E	D	S	D	E	E	W	T		*	A	A	S	Q	T	S	L	D
	GAA	GAT	TCC	GAT	GAA	GAA	TGG	A--CC		TAG	GCA	GCA	AGT	CAA	ACC	TCC	TTG	GAT
501Mel-PRDM7-KO13	E	D	S	D	E	E	S			R	Q	Q	V	K	P	P	W	M
	GAA	GAT	TCC	GAT	GAA	GAA	T------CT			AGG	CAG	CAA	GTC	AAA	CCT	CCT	TGG	ATG
501Mel-PRDM7-KO13	E	D	S	D	E	E	P			R	Q	Q	V	K	P	P	W	M
	GAA	GAT	TCC	GAT	GAA	GAA	------CCT			AGG	CAG	CAA	GTC	AAA	CCT	CCT	TGG	ATG

	89	90	91	92	93	94	95	96	97	98	99	100	101	.....	128	129	130	131
PRDM7-WT	E	D	S	D	E	E	W	T	P	R	Q	Q	V	.....	S	S	L	R
	GAA	GAT	TCC	GAT	GAA	GAA	TGG	ACA	CCT	AGG	CAG	CAA	GTC	.....	TCT	AGT	TTG	AGA
501Mel-PRDM7-KO24	E	D	S	D	E	E	W	T		L	G	S	K	.....	V	L	*	E
	GAA	GAT	TCC	GAT	GAA	GAA	TGG	AC-C		CTA	GGC	AGC	AAG	.....	CTA	GTT	TGA	GAG
501Mel-PRDM7-KO24	E	D	S	D	E	E	W	T	?	*	A	A	S	.....	I	*	F	E
	GAA	GAT	TCC	GAT	GAA	GAA	TGG	ACA	NCC	TAG	GCA	GCA	AGT	.....	ATC	TAG	TTT	GAG

D

	89	90	91	92	93	94	95	96	97	98	99	100	101	.....	128	129	130	131
PRDM7-WT	E	D	S	D	E	E	W	T	P	R	Q	Q	V	.....	S	S	L	R
	GAA	GAT	TCC	GAT	GAA	GAA	TGG	ACA	CCT	AGG	CAG	CAA	GTC	.....	TCT	AGT	TTG	AGA
SKmel28-PRDM7-KO13	E	D	S	D	E	E	W	T		L	G	S	K	.....	V	L	*	E
	GAA	GAT	TCC	GAT	GAA	GAA	TGG	AC-C		CTA	GGC	AGC	AAG	.....	CTA	GTT	TGA	GAG
SKmel28-PRDM7-KO17	E	D	S	D	E	E	W	T	?	*	A	A	S	.....	I	*	F	E
	GAA	GAT	TCC	GAT	GAA	GAA	TGG	ACA	NCC	TAG	GCA	GCA	AGT	.....	ATC	TAG	TTT	GAG

Figure 30. Generated PRDM7 knock-out melanoma cells (A) Schematic illustration of the guide RNA targeting exon 3 of PRDM7. (B) RNA expression of PRDM7 in PRDM7-KO and its corresponding control was measured by qPCR. Error bars represent the SEM of at least three independent experiments. Statistically significant differences (Student's t-test) are indicated by *, p< 0.05. (C) and (D) Mutations detected in the PRDM7-KO cell lines.

Although the PRDM7 mRNA was detected to be expressed in 501mel and SKMel28 by qPCR, SKmel28 cells showed a higher expression than 501Mel cells. However, endogenous PRDM7 protein was not detected in either cell line by either Western blot or Immunostaining using commercial PRDM7-specific antibodies, including PRDM7 antibodies from Sigma #HPA059944, DSHB #3F10S, and Abcam #ab177033. It is possible that endogenous PRDM7 expression is very low in SKmel28 and 501Mel melanoma cells, which qPCR data have suggested. However, it is also possible that the epitopes located in exon 9 are absent in the major PRDM7 transcripts.

4.2.4 PRDM7-KO alters gene expression of SKmel28 and 501Mel melanoma cells

To identify the main functional roles of PRDM7, mRNA sequencing of 501Mel and SKmel28 PRDM7-KO cells and their corresponding control cells was performed. First, total RNA was isolated from control and PRDM7 knockout cell lines (501Mel-C1, 501Mel-PRDM7-KO13, 501Mel-PRDM7-KO24, SKmel28-C3, SKmel28-PRDM7-KO13, SKmel28-PRDM7-KO17). Paired-end sequencing was performed on an Illumina Hiseq instrument at deCODE genetics. The reads were aligned to the human transcriptome version GRCh38 using Kallisto (Bray et al., 2016). After that, differential expression analysis was performed by quantifying transcripts by Sleuth in R through Bioconductor (Pimentel et al., 2017). While the Wald test was used as a model to estimate differentially expressed genes (DEGs), the LRT test was applied to estimate differentially expressed genes (DEGs). There were 5.021 and 3.851 differentially expressed genes (DEGs) between the 501Mel-C1 controls on the one hand and either 501Mel-PRDM7-KO24 or 501Mel-PRDM7-KO13 on the other hand, with a cut-off FDR of <0.05 and >1-fold change in expression (Figures 31A and 31B). The number of DEGs between SKmel28-C3 and the SKmel28-PRDM7-KO clones KO17 or KO13 were 1.351 or 3.598, respectively. A total of 219 DEGs were shared between SKmel28 and 501Mel cells after knocking out PRDM7. The limited number of shared genes and the difference in the total number of genes affected in SKmel28 versus 501Mel cells might be explained by either the cell line characteristics or distinct roles of PRDM7 in these different cell lines.

In order to further characterize the relationship between MITF and PRDM7, we also performed DEGs analysis on PRDM7^{high} (30 tumor samples with the highest PRDM7 expression) and PRDM7^{low} (30 tumor samples with the highest PRDM7 expression) tumors from the Cancer Genome Atlas using RNA-seq data from 480 cutaneous melanoma samples (TCGA) (Cancer Genome Atlas, 2015). This analysis showed that 1.561 genes were induced in expression in PRDM7^{high} tumors while 585 genes were reduced in expression in PRDM7^{high} tumors (Figure 31C).

The DEGs between PRDM7-KO and their corresponding control as well as between PRDM7^{high} and PRDM7^{low} tumors in TCGA database were next classified into functional gene ontology (GO) groups (e.g., biological pathways (BP) and KEGG pathways). This showed that the DEGs upregulated in the PRDM7-KO cells were enriched for biological pathways such as synapse organization, extracellular matrix organization, extracellular structure organization, cell junction assembly, and cell-substrate adhesion (Figure 31D). KEGG pathway analysis of DEGs between PRDM7-KO and its corresponding controls revealed that the upregulated genes are associated with EMC-receptor interaction, PI3K-AKT signaling pathway, and cytokine-cytokine receptor interaction (Figure 31D). Similarly, the same pathways were also enriched in PRDM7^{low} tumors in the TCGA data sets, suggesting that PRDM7-KO cells exhibit cellular alterations similar to those observed in melanoma tumors.

Previous work has established that when MITF is knocked out, this leads to reduced proliferation and increased numbers of focal adhesions ((Dilshat et al., 2021a; Goding and Arnheiter, 2019). Therefore, we compared the expression profile of PRDM7-KO cells to that of MITF-KO cells. The functional gene ontology groups showed similar GO terms to be upregulated in both MITF-KO and PRDM7-KO cells, including extracellular matrix and structure organization and cell-to-cell adhesion via plasma adhesion (Figure 31D). Furthermore, previous work reported that MITF could bind to the c-Jun enhancer region and repress c-Jun expression; therefore, reducing MITF expression amplifies TNFα-stimulated cytokine signatures through inhibiting c-Jun expression (Riesenberg et al., 2015). Therefore, in the next step, GSEA analysis was performed to determine the correlation between transcriptomic profiles of SKmel28-PRDM7-KO, SKmel28-MITF-KO cells and MITF^{low}/JUN^{high} stage. Interestingly, a positive correlation between the transcriptomic profiles of PRDM7-KO cells and MITF^{low}/JUN^{high} stage was clearly observed (Figure 31E).

4.2.5 PRDM7 affects the morphology of SKmel28 and 501Mel melanoma cells

In the next step, the morphology of the cells has been characterized. The phase contrast microscopy and vimentin immunostaining showing altered morphologies and cytoskeletal structure of PRDM7-KO cells. While 501Mel-C1 cells consist mostly of multipolar stellate shape, the 501Mel-PRDM7-KO13 and PRDM7-KO24 cells are more rounded and spread out (Figures 32A and 32B). In contrast, knocking out PRDM7 in SKmel28 cells resulted in an increased number of cells showing elongated neuron-like morphology compared with SKmel28-C3 cells, which showed a round shape as a main feature (Figures 32A and 32B). Critically, the morphological changes in 501mel and SKmel28 cells upon PRDM7 depletion are not due to changes in quantitative of vimentin expression (Figure 32C). Interestingly, DAPI staining also suggested that the size of the nucleus in SKmel28 PRDM7-KO13 and PRDM7-KO17 cells are larger than that of SKmel28-C3 cells. However, no significant differences were observed in nuclear size between 501Mel-PRDM7-KO and 501Mel-C1 cells (Figure 32D).

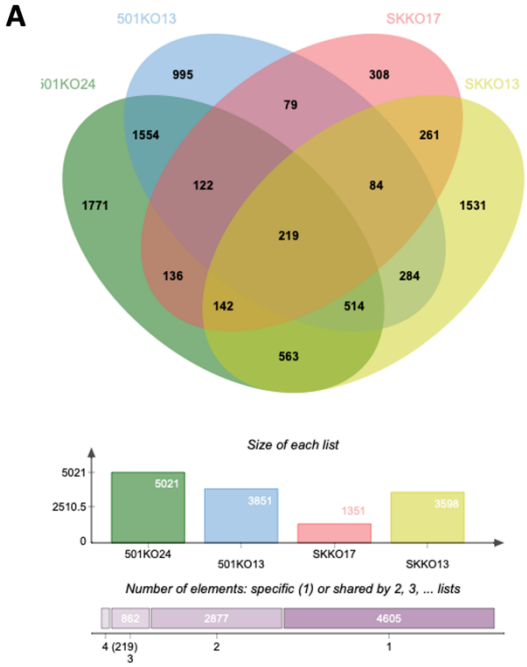

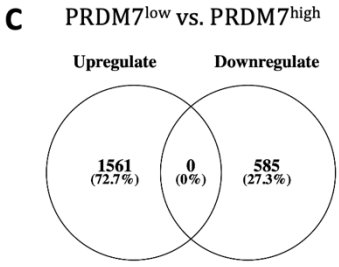

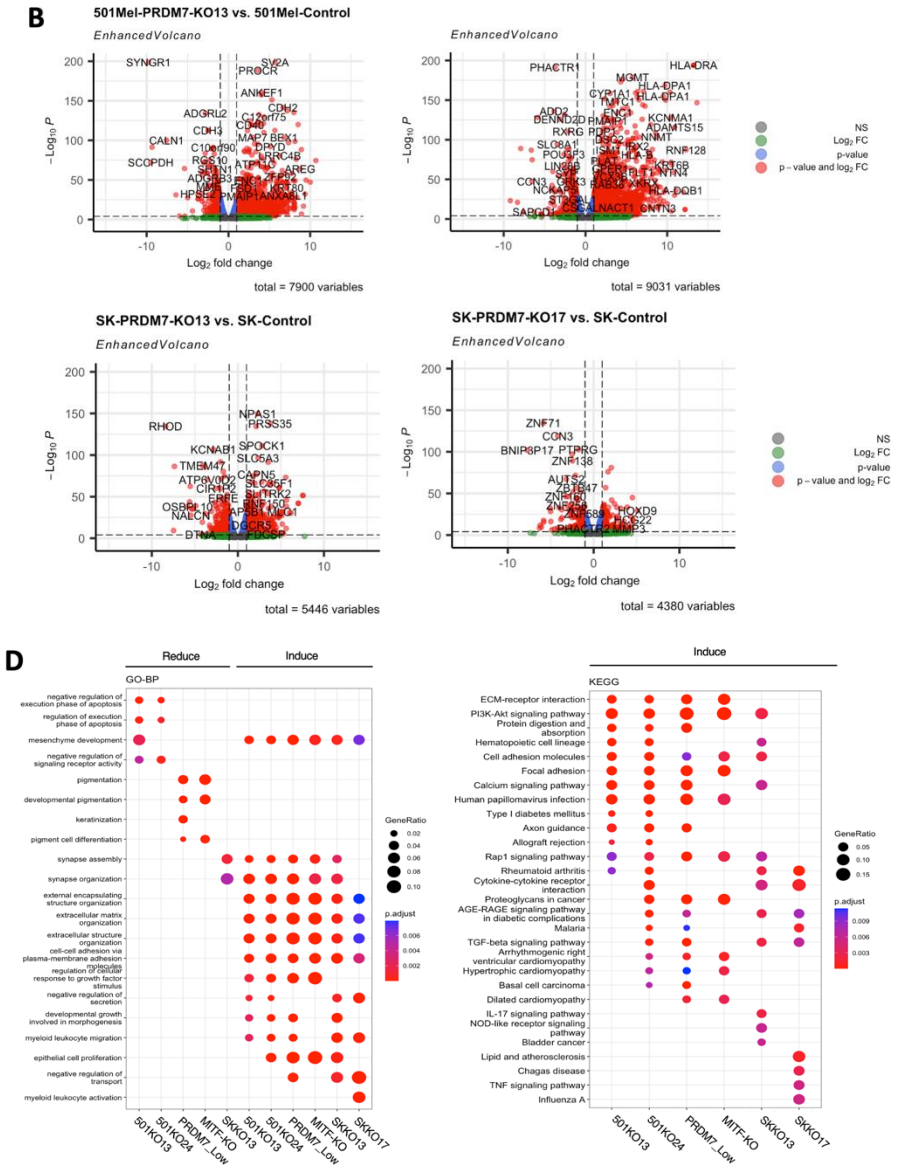

Figure 31. Gene expression profile of PRDM7-KO cell lines (A) Venn diagram showing the number of overlapping differentially expressed genes (DEGs) in PRDM7-KO SKmel28 and 501Mel cells. (B) Volcano plot showing differentially expressed genes (DEGs) in PRDM7-KO cells compared to its corresponding control with log2 2-fold change and FDR<0.05 represented in red dots. (C) Venn diagram showing the number of DEGs that are increased and reduced in TCGA SKCM PRDM7^{low} vs PRDM7^{high} tumors. (D) Gene ontology of biological pathway and KEGG pathway analysis on induced and repressed genes in PRDM7-KO, MITF-KO, PRDM7^{high} vs PRDM7^{low}. The color indicates the p-value, and the size of the circles indicates the gene ratio. (E) GSEA analysis on PRDM7-KO and MITF-KO DEGs for MITF^{low}/Jun^{high} gene signatures.

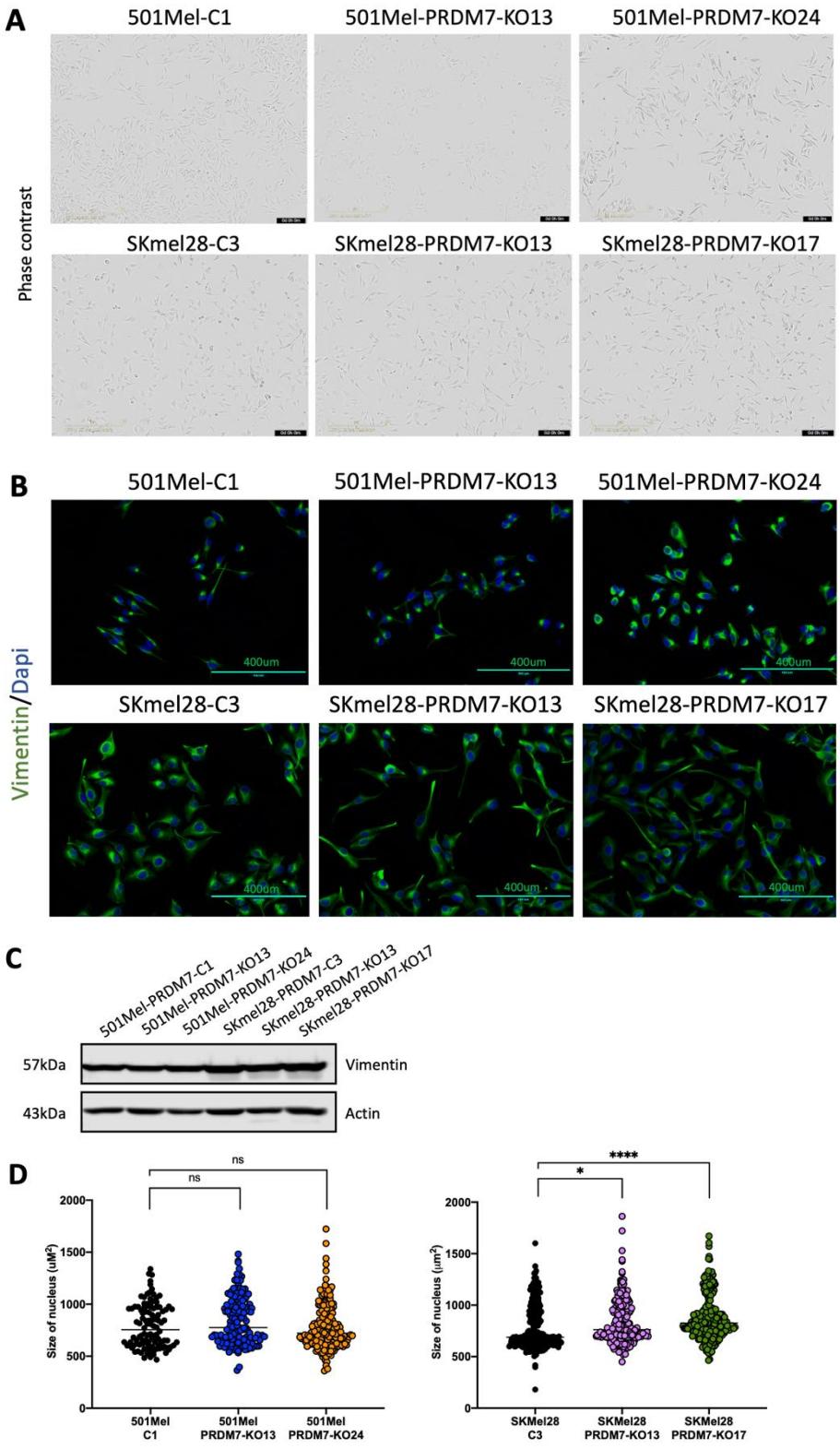
A
501Mel-C1
501Mel-PRDM7-KO13
501Mel-PRDM7-KO24
Phase contrast
SKmel28-C3
SKmel28-PRDM7-KO13
SKmel28-PRDM7-KO17
B
501Mel-C1
501Mel-PRDM7-KO13
501Mel-PRDM7-KO24
Vimentin/Dapi
SKmel28-C3
SKmel28-PRDM7-KO13
SKmel28-PRDM7-KO17
400um
C
501Mel-PRDM7-C1
501Mel-PRDM7-KO13
501Mel-PRDM7-KO24
SKmel28-PRDM7-C3
SKmel28-PRDM7-KO13
SKmel28-PRDM7-KO17
57kDa
Vimentin
43kDa
Actin
D
ns
ns
Size of nucleus (uM²)
2000
1500
1000
500
0
501Mel C1
501Mel PRDM7-KO13
501Mel PRDM7-KO24
****
*
Size of nucleus (um²)
SKMel28 C3
SKMel28 PRDM7-KO13
SKMel28 PRDM7-KO17

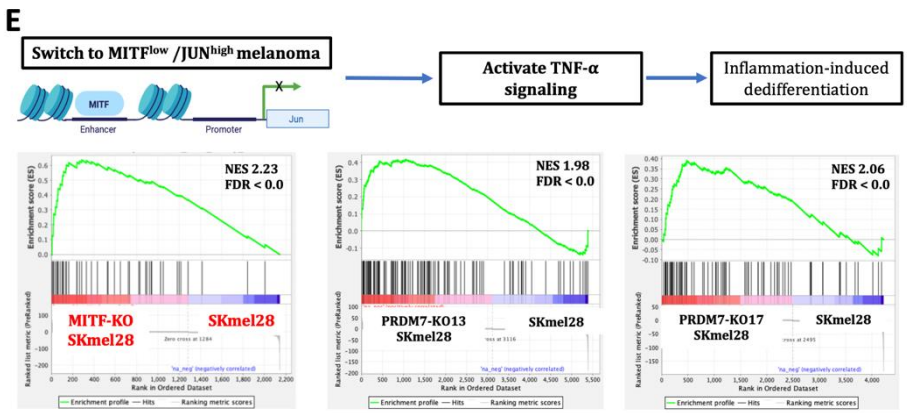

Figure 32. PRDM7-KO affects cell morphology (A) Phase contrast images of PRDM7-KO and its corresponding control showed different morphology in cell culture. (B) Vimentin and dapi staining displayed the cytoskeleton in PRDM7-KO and its corresponding control. (C) Western blot analysis of PRDM7-KO and its corresponding control. The vimentin was shown by vimentin staining. Actin was used as a loading control. (D) The size of nuclei in PRDM7-KO cells was measured based on dapi immunostaining (B) by using imageJ software.

4.2.6 Depletion of PRDM7 affects the proliferation rate and ability to form colonies

Distinct gene signatures in melanoma, characterized by unique gene expression patterns, are linked to various stages of melanoma development and progression. Therefore, using our RNA-Seq data, we performed a gene set enrichment analysis (Subramanian et al., 2005) to determine the correlation between our data set and several previously characterized datasets, including the Verfaillie proliferative and invasive signatures (Verfaillie et al., 2015) as well as the GSEA EMT hallmark (Mootha et al., 2003; Subramanian et al., 2005). Our analysis showed that PRDM7-KO cells were negatively correlated with Verfaillie proliferative signature and positively enriched for the Verfaillie invasive signature (Verfaillie et al., 2015) and EMT hallmark (Mootha et al., 2003; Subramanian et al., 2005) (Figure 33A). In line with that, the depletion of PRDM7 led to a considerable increase in the expression of cell cycle inhibitors, including CDKN2A, CDKN2B, CDKN2C, CDK2, and CDKN1B (Figures 33B and 33C).

Therefore, we further investigated the growth rate of PRDM7-KO cells. The cells were incubated in the Incucyte S3 live cell imaging system, images were acquired every two hours for four days, and cell proliferation was analyzed. The doubling time was calculated based on the quantification of cell confluency over time. This shows that the doubling times of 501Mel PRDM7-KO13 and PRDM7-KO24 cell lines are significantly increased compared to the 501Mel-C1 control

cell line (Figure 33D). The doubling time of 501Mel control cells was 18.91 hours. However, the doubling time of the 501Mel PRDM7-KO13 and PRDM7-KO24 cells was 23.51 hours and 27.91 hours, respectively. The IncuCyte live cell imaging showed that SKmel28 control and PRDM7-KO cells have similar growth rates (Figure 33D). The proliferation rate of the inducible PRDM7 knockdown in melanoma cells was also measured. The microRNA (miR) construct was knockdown of the PRDM7 mRNA in PRDM7-KD cells (Figure 33E), and the proliferation rate of 501Mel cells upon either miR1-PRDM7 or miR2-PRDM7 induction was significantly reduced compared to miR-CTRL (Figure 33E). Similar to the SKmel28 PRDM7-KO cells, short-term inactivation of PRDM7 in the SKmel28 PRDM7-KD cells had similar cell proliferation as the SKmel28 miR-CTRL cells (Figure 33E).

A colony formation assay was performed to better assess the roles of PRDM7 in maintaining cell growth and forming colonies from single cells. Both control and PRDM7-KO 501Mel and SKmel28 cells were able to form colonies. However, the number, size, and shape of the PRDM7-KO colonies are altered compared to the control cell lines (Figures 33F and 33G). 12 days after seeding, the 501Mel-C1 cells formed different types of colonies: small, intermediate, and large colonies with both loosely and tightly packed cells. In contrast, the 501Mel-PRDM7-KO13 cells dominantly resulted in small and intermediate-sized colonies, and 501Mel-PRDM7-KO24 formed mainly small and loosely adherent colonies (Figures 33F). The number of colonies in 501Mel-PRDM7-KO24 cell lines was reduced by 80% as compared to 501MelC1 cells (Figure 33F). Although there was no significant reduction in the number of colonies between SKmel28 control and PRDM7-KO cells, SKmel28 PRDM7-KO13 and PRDM7-KO17 formed mainly smaller and densely packed colonies, which were lighter stained by crystal violet (Figures 33F and 33G). Together, these data indicate that although the effects of PRDM7-KO were not the same in 501Mel and SKmel28 cell lines, the absence of functional PRDM7 in the two melanoma cell lines contributes to a significant defect in proliferation in both the short-term and long-term and reduces colony formation capabilities.

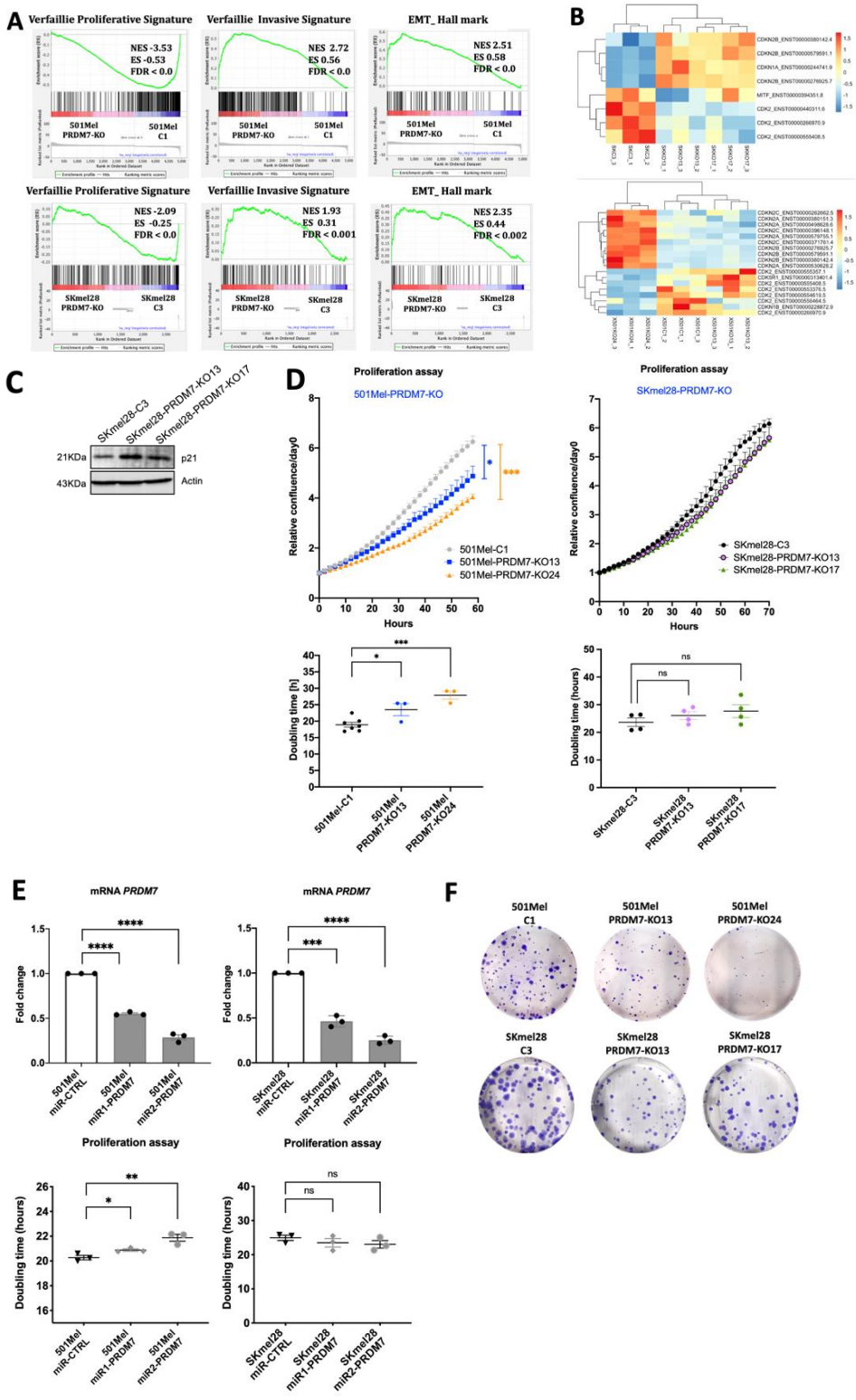
A
Verfaillie Proliferative Signature
NES -3.53
ES -0.53
FDR < 0.0
501Mel PRDM7-KO
501Mel C1
Verfaillie Invasive Signature
NES 2.72
ES 0.56
FDR < 0.0
EMT_ Hall mark
NES 2.51
ES 0.58
FDR < 0.0
Verfaillie Proliferative Signature
NES -2.09
ES -0.25
FDR < 0.0
SKmel28 PRDM7-KO
SKmel28 C3
Verfaillie Invasive Signature
NES 1.93
ES 0.31
FDR < 0.001
EMT_ Hall mark
NES 2.35
ES 0.44
FDR < 0.002
B
C
SKmel28-C3
SKmel28-PRDM7-KO13
SKmel28-PRDM7-KO17
21KDa
p21
43KDa
Actin
D
Proliferation assay
501Mel-PRDM7-KO
Relative confluence/day0
Hours
501Mel-C1
501Mel-PRDM7-KO13
501Mel-PRDM7-KO24
Doubling time [h]
501Mel-C1
501Mel PRDM7-KO13
501Mel PRDM7-KO24
Proliferation assay
SKmel28-PRDM7-KO
SKmel28-C3
SKmel28-PRDM7-KO13
SKmel28-PRDM7-KO17
Doubling time (hours)
ns
SKmel28-C3
SKmel28 PRDM7-KO13
SKmel28 PRDM7-KO17
E
mRNA PRDM7
Fold change
501Mel miR-CTRL
501Mel miR1-PRDM7
501Mel miR2-PRDM7
Proliferation assay
Doubling time (hours)
mRNA PRDM7
Fold change
SKmel28 miR-CTRL
SKmel28 miR1-PRDM7
SKmel28 miR2-PRDM7
Proliferation assay
Doubling time (hours)
F
501Mel C1
501Mel PRDM7-KO13
501Mel PRDM7-KO24
SKmel28 C3
SKmel28 PRDM7-KO13
SKmel28 PRDM7-KO17

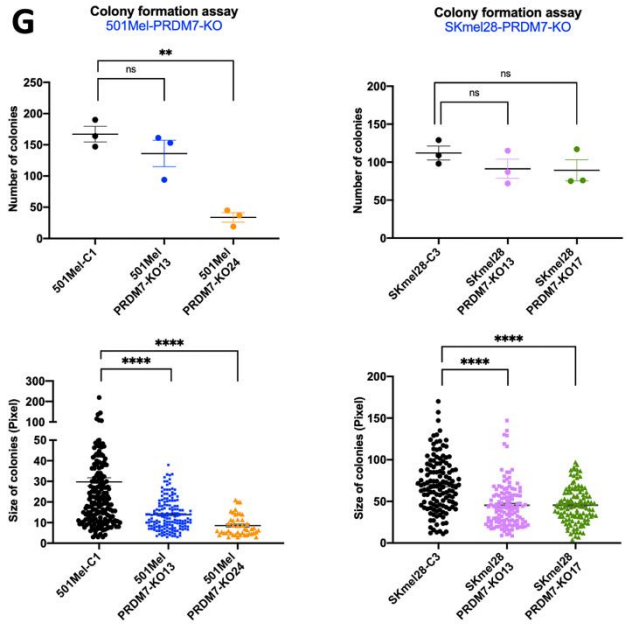

Figure 33. Depletion of PRDM7 affects the proliferation rate and ability to form colonies (A) GSEA analysis on PRDM7-KO and MITF-KO DEGs for Verfaillie proliferative/invasive and EMT gene signatures. (B) Expression of a subset of cycle inhibitor genes plotted in a heatmap. Log2 2-fold change of PRDM7-KO DEGs was used for plotting. (C) Western blot analysis of p21 in PRDM7-KO and its corresponding control. Actin was used as a loading control. (D) Doubling time in hours calculated from quantification of cell confluency over 70 hours for the PRDM7-KO and its corresponding control. Statistically significant differences (Student's t-test) are indicated by *, $p < 0.05$. (E) The upper panel showed PRDM7 mRNA expression in PRDM7-KD and its corresponding control was measured by qPCR. The lower panel indicated doubling time in hours calculated from the quantification of cell confluency over 70 hours for the PRDM7-KD and its corresponding control. Statistically significant differences (Student's t-test) are indicated by *, $p < 0.05$. (F) Colony-formation assays were performed using PRDM7-KO cells. (G) The number and size of colony-forming ability of PRDM7-KO cells were measured by ImageJ software. Statistically significant differences (Student's t-test) are indicated by *, $p < 0.05$.

4.2.7 Overexpressing PRDM7 isoform A did not affect proliferation

To further determine the effects of different PRDM7 expression levels in melanoma cell lines, PRDM7 was overexpressed in 501Mel and SKmel28 cell lines utilizing a piggy-bac transposon vector system. The PRDM7 coding sequence for isoform A, which contains KRAB and SET domain (Figure 7) was cloned into the pPB-hCMV vector (Table 2). Similar to the system in PRDM7-KD

cells, the inducible promoter, which is a Tetracycline-On system, regulates PRDM7 expression by adding doxycycline. The overexpressed PRDM7 isoform A and control cells are termed PRDM7-OE and EV, respectively. The success of PRDM7 overexpression was confirmed by western blot analysis (Figure 34A). However, overexpressing PRDM7 in 501Mel and SKmel28 cells did not show any effect on proliferation using the IncuCyte proliferation and colony formation assays (Figures 34A and 34B).

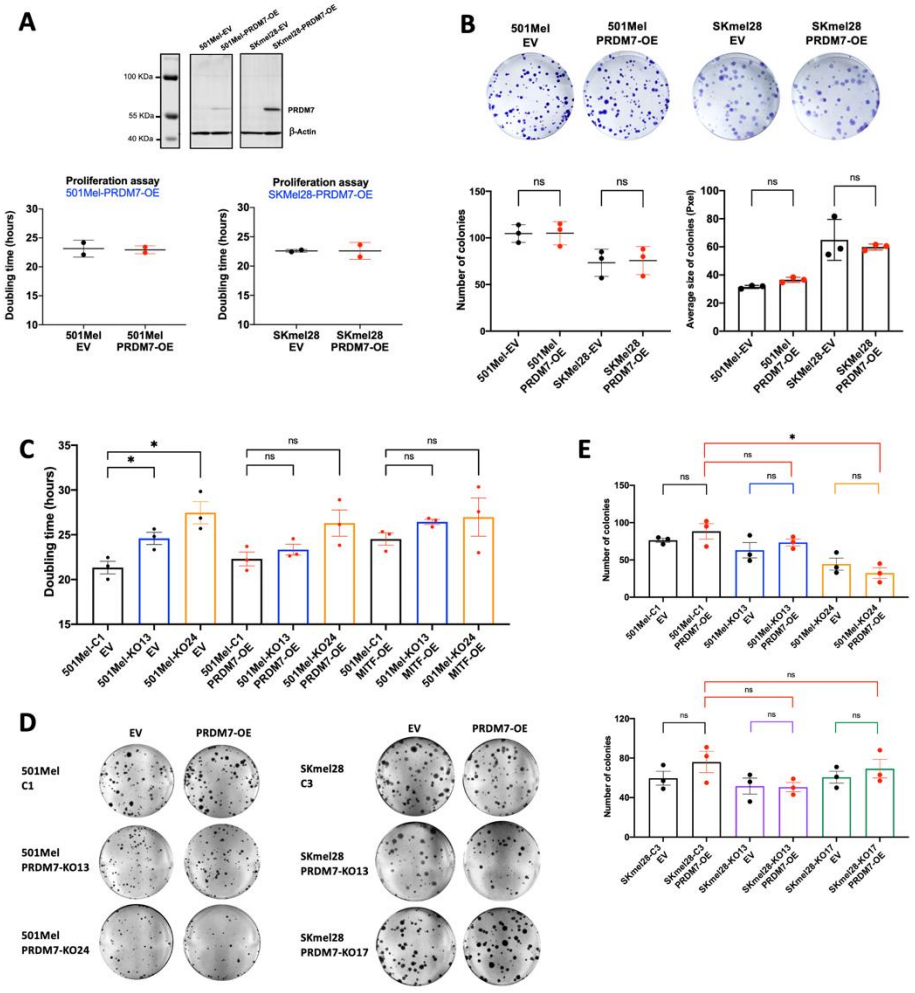

Figure 34. Overexpressing PRDM7 isoform A did not affect proliferation (A) The upper panel shows the representative western blot analysis of PRDM7 isoform A protein in PRDM7-OE 501Mel and SKmel28 cell lines. PRDM7 protein was detected using Flag antibody, and Actin was used as a loading control. The lower panel indicates doubling time in hours calculated from the quantification of cell confluency over 70 hours for the

PRDM7-OE and its corresponding control. Statistically significant differences (Student's t-test) are indicated by *, p< 0.05 . (B) Colony-formation assays were performed using PRDM7-OE in both SKmel28 and 501Mel melanoma cells. ImageJ software measured the number and size of PRDM7-OE cells' colony-forming. Statistically significant differences (Student's t-test) are indicated by *, p< 0.05. (C) Doubling time in hours was calculated from the quantification of cell confluency over 70 hours for the PRDM7-KO cells followed by overexpressing PRDM7 isoform A. Statistically significant differences (Student's t-test) are indicated by *, p< 0.05. (D) and (E) Rescue of the colony-forming ability of PRDM7-KO by overexpressing PRDM7 isoform A. ImageJ software measured the number and size of PRDM7-OE cells' colony-forming. Statistically significant differences (Student's t-test) are indicated by *, p< 0.05.

Overexpressing PRDM7 or MITF in PRDM7-KO cells was also performed to rescue the phenotypic effects upon depletion of PRDM7. Again, the effects on proliferation were determined using Incucyte proliferation and colony formation assays. However, overexpressing PRDM7 isoform A did not alter the proliferation rate of 501Mel-PRDM7-KO cells, nor did it affect the colony formation ability of 501Mel-PRDM7-KO and SKmel28-PRDM7-KO cells (Figures 34C-E). In contrast, overexpression of MITF reduced the difference in proliferation between PRDM7-KO and its corresponding control (Figure 34C). One caveat is that in our overexpression experiments, we overexpressed the A isoform of PRDM7, which is not the predominant isoform in melanoma cells. These experiments, therefore, need to be repeated using the more common isoforms detected by RNA-seq and qPCR analysis.

4.2.8 Increased apoptosis observed in 501Mel-PRDM7-KO cells

The defect in proliferation observed in the 501Mel-PRDM7-KO cells may be due to increased cell death. To investigate this hypothesis, apoptosis was determined in the 501Mel PRDM7-KO and control cells using the IncuCyte Caspase-3/7 Green Reagent in the Incucyte S3 system. In this assay, caspase-3/7 dyes are added to the cell culture. The caspase-3/7 dye couples with a DNA intercalating dye to an activated caspase-3/7 recognition motif (DEVD) and thus allows the quantification of cells undergoing apoptosis. An apoptotic index was determined by the percentage of fluorescent cells over total cell confluency (%) (Figure 35A). Upon depletion of PRDM7, more apoptotic cell death was detected in 501Mel PRDM7-KO cells than in control cell lines. Notably, the apoptosis index of 501Mel PRDM7-KO24 cells after seeding for 12, 24, 36, and 48 hours was significantly higher than that of 501Mel control cells (Figures 35A and 35B). However, knocking out PRDM7 in SKmel28 did not alter the apoptosis index (Figures 35A and 35B). This observation, again, raises the question whether PRDM7 plays cell-specific roles in the different melanoma cell lines.

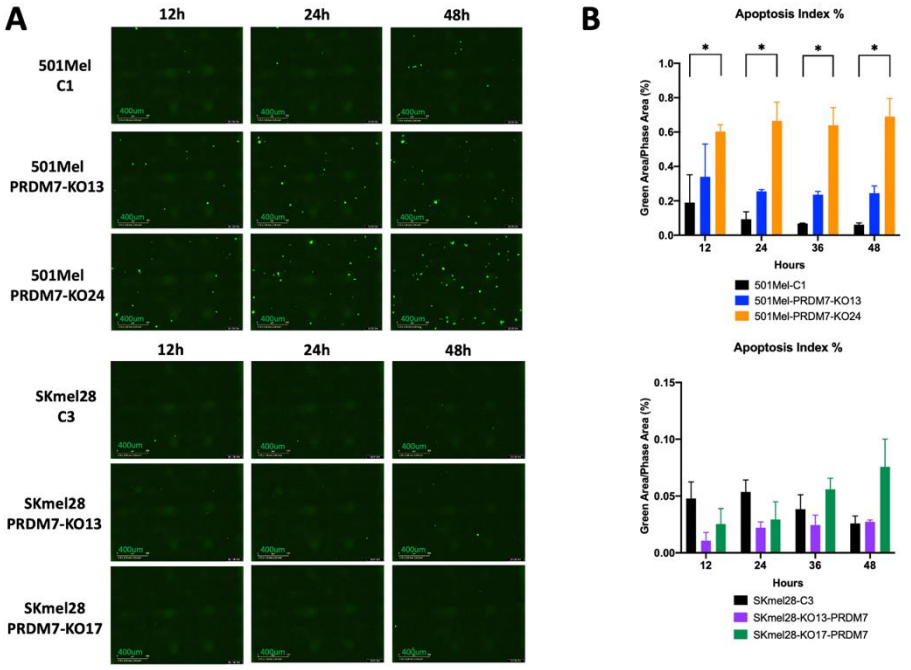

Figure 35. Increased apoptosis observed in 501Mel-PRDM7-KO cells (A) Representative images showing the apoptosis of PRDM7-KO and its corresponding control (Scale bars = 400 μm). The green fluorescence indicated cell death. (B) The graph showed the apoptosis index of PRDM7-KO by 12h, 24h, and 36h following exposure to caspase 3/7.

4.2.9 PRDM7 knock-out and knock-down cells affect migration.

Gene enrichment analysis suggested that RNA expression of PRDM7-KO cells correlated with the Verfaillie invasive signature. In order to determine if PRDM7 plays a role in melanoma immigration, the wound-scratch assay and single cell movement assay were performed. After 501Mel and SKMel28 PRDM7-KO and KD cells reached 100% confluency, scratches were made on a confluent layer of cells using the Woundmaker96 instrument (Essen Bioscience). The cell migration rate was calculated based on gap closure quantification. The migration rate of the 501Mel PRDM7-KO24 cells was only 2.25 μm/hour, which is three times slower than that of 501Mel control cells (6.11 μm/hour) (Figure 36A). In contrast, SKmel28 PRDM7-KO, SKmel28 PRDM7-KD, and 501Mel PRDM7-KD cells showed no difference in the ability of the cells to close the wound compared to their corresponding control cells (Figures 36A and 36B). The cell migration rate, as measured by wound-scratch assay, is affected by at least three main factors,

including invasion ability, proliferation, and expansion of the cells. The 501Mel PRDM7-KO24 cells significantly reduced the growth rate compared to their parental counterpart. Hence, we used time-lapse videos to analyze the movement of single cells to investigate further the role of PRDM7 in regulating melanoma invasion. Although the average speed of movement of 501Mel and SKmel28 cells did not change due to the lack of PRDM7, interestingly, the maximal distance traveled between movements showed a significant increase in PRDM7-KO cells (Figure 36C). Together, our results suggest that the absence of functional PRDM7 may affect certain pathways involved in the invasion ability of melanoma cells.

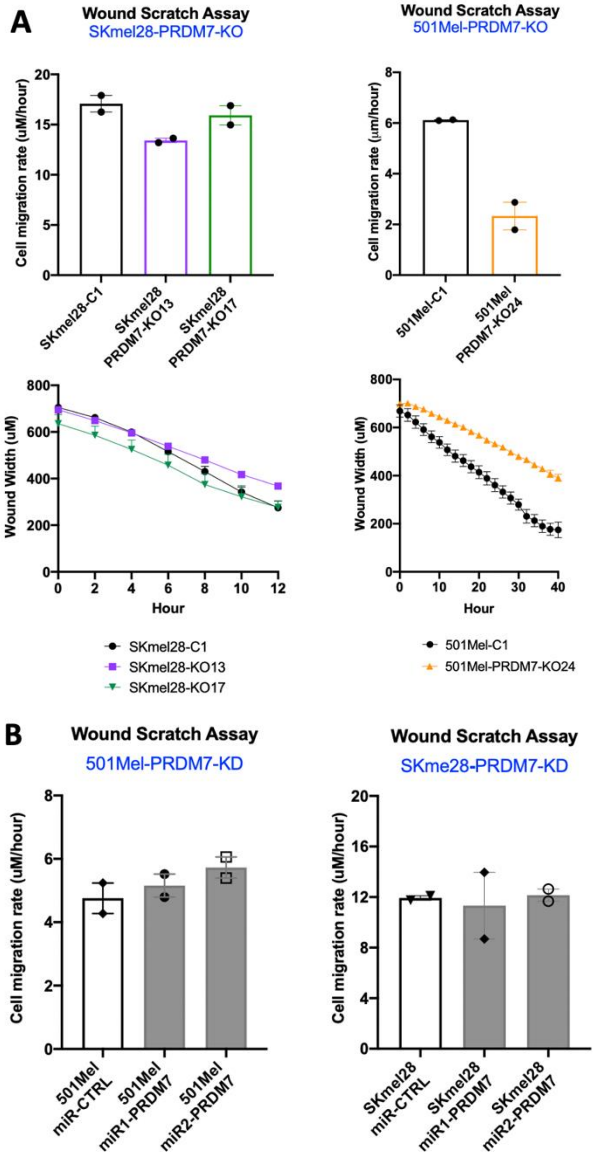

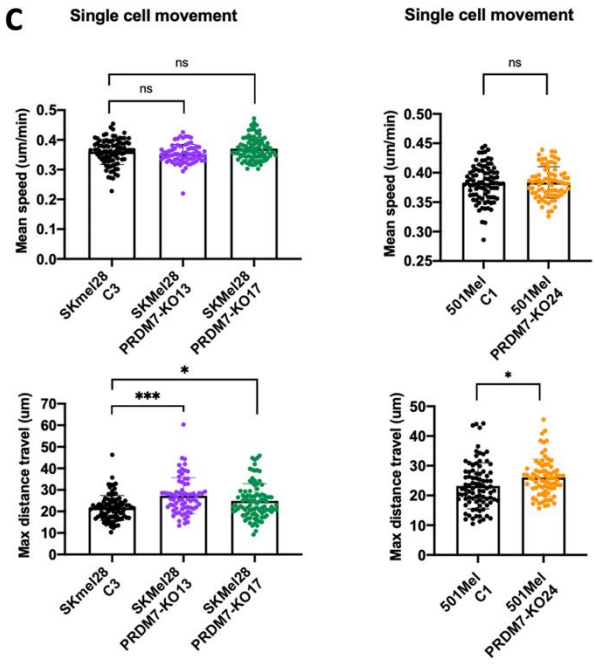

Figure 36. PRDM7 knock-out and knock-down cells affect invasion (A) Scratch assay was performed in PRDM7-KO cells and its corresponding control. Quantified gap closure was quantified over 12 hours for PRDM7-KO SKmel28 or 40 hours for PRDM7-KO 501Mel, and the cell migration rate was determined. (B) Scratch assay was performed in PRDM7-KD cells and their corresponding controls. (C) Mean speed and maximal moving distance were measured by using a single-cell movement assay. Error bars represent the SEM. Statistically significant differences (Student's t-test) are indicated by *, $p < 0.05$.

4.2.10 Focal adhesions are increased in SKmel28-PRDM7-KO cells

The RNA-seq data suggested that focal adhesion genes are also markedly increased in PRDM7-KO cells (Figure 37A). Therefore, we investigated whether PRDM7 knockout leads to changes in focal adhesions. Immunostaining for Paxillin (pTyr111), which is required for focal points (Panetti, 2002), was conducted on PRDM7-KO cells and the respective controls (Figure 37A). The images were analyzed using ImageJ for both the number of focal adhesions and their size (by counting pixel numbers per focal adhesion point). While SKmel28-PRDM7-KO cells had increased numbers of focal points, 501Mel-PRDM7-KO cells showed a significant reduction in focal point numbers, especially of focal points that are greater than 10 pixels in size (Figure 37B). Overexpression of PRDM7 isoform A in SKmel28 cell lines slightly reduced the number of focal points, but the difference was not statistically significant (Figures 37C and 37D).

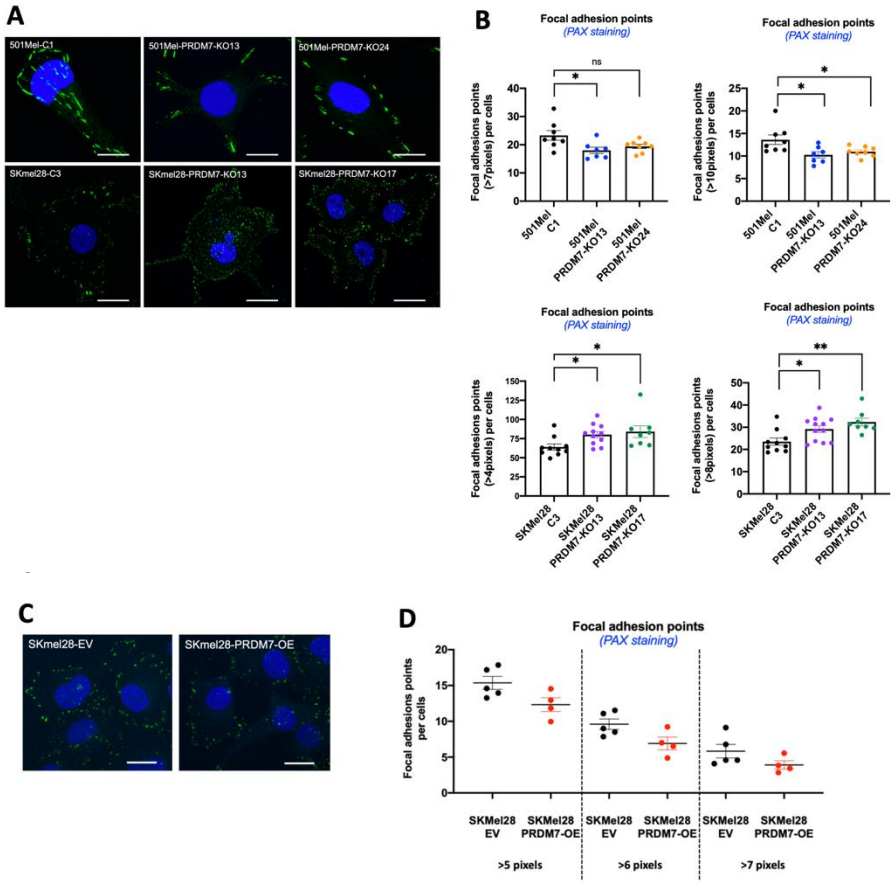

Figure 37. Focal adhesions are increased in SKmel28-PRDM7-KO cells (A) and (C) Immunostaining for Paxillin(Tyr111) in PRDM7-KO (A) and PRDM7-OE (C) cell lines. Scale bars: 10μM (B) and (D) Focal adhesion points quantified by using Cellprofiler software. Error bars represent the SEM. Statistically significant differences (Student's t-test) are indicated by *, p< 0.05.

4.2.11 PRDM7 depletion leads to reduced MITF expression

A positive correlation between the transcriptomic profiles of PRDM7-KO cells and $MITF^{low}/JUN^{high}$ stage was observed. No changes were observed in the expression of the *MITF* mRNA in PRDM7-KO cells (Figure 38A). Surprisingly, however, MITF protein expression was significantly reduced in SKmel28-PRDM7-KO cells as well as when PRDM7 was knocked down in SKMel28 and 50Mel-PRDM7-KD cells using siPRDM7(Figures 38B and 38C).

To further investigate the changes of MITF protein expression upon PRDM7-KO through the cell cycle, the SKmel28-PRDM7-KO and 501Mel-PRDM7-KO cells,

and their corresponding control were synchronized using a double thymidine block. By treating the cell with thymidine, which is a DNA synthesis inhibitor, the cells are arrested at the G1/S boundary. After the thymidine treatment, cells were harvested at 0 hours, 4 hours, 8 hours, and 12 hours time points for MITF protein analysis using Western blot. This showed that MITF expression changes through the cell cycle, gradually increasing from the S phase and peaking at the G1 phase (Figures 38D and 38E), suggesting that the expression of MITF is regulated during the cell cycle. Although the lack of PRDM7 did not completely abolish the expression of the MITF protein, the expression of MITF in the G1 phase of SKmel28 and 501Mel cells was not increased in PRDM7-KO cells (Figures 38D and 38E).

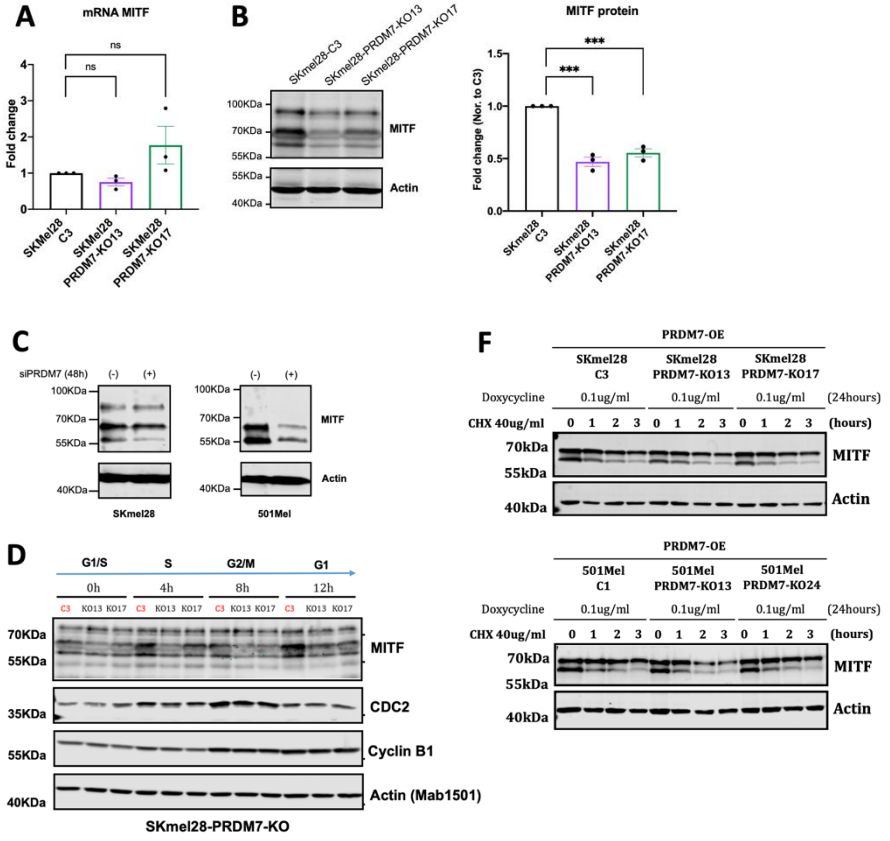

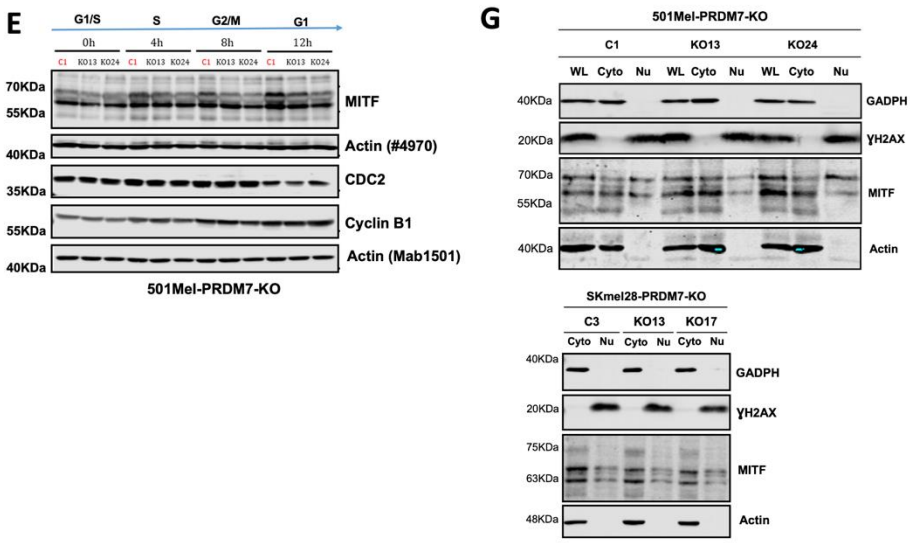

Figure 38. PRDM7 depletion leads to reduced MITF expression (A) MITF mRNA expression in SKmel28-PRDM7-KO and its corresponding control was measured by qPCR. (B) Western blot analysis and quantification of MITF protein expression in SKmel28-PRDM7-KO and its corresponding control. Actin was used as a loading control. (C) MITF mRNA expression in PRDM7-KD and its corresponding control was measured by qPCR. (D) and (E) Western blot analysis of MITF protein changes through the cell cycle in SKmel28-PRDM7-KO and its corresponding control. Actin was used as a loading control. CDC2 and Cyclin B1 were used as cell cycle indicators. (F) Western blot analysis of the stability of the MITF proteins in PRDM7-KO cells. The inducible PRDM7-KO cells were treated with doxycycline for 24h to express the MITF-WT proteins before treating them with cycloheximide (CHX) 40ug/ml for 0, 1, 2, and 3 hours. The MITF proteins were then compared by Western blot using Flag antibody. Actin was used as a loading control. (G) Western blot analysis of subcellular fractions isolated from PRDM7-KO cells. MITF protein in cytoplasmic (Cyto) and nuclear fractions (Nu) were visualized using MITF antibody. GAPDH and γH2AX were loading controls for cytoplasmic and nuclear fractions, respectively. . Error bars represent the SEM. Statistically significant differences (Student's t-test) are indicated by *, $p < 0.05$.

A reduction in MITF protein expression might explain the overlapping phenotype observed in the PRDM7-KO and PRDM7-KD cells. However, the molecular mechanism of how PRDM7 regulates MITF protein expression remains unknown. It may act by reducing the stability of MITF protein or altering MITF localization. Therefore, we overexpressed a MITF-Flag fusion protein in PRDM7-KO cells and performed a stability assay. The MITF-Flag protein expressed in PRDM7-KO and control cell lines exhibited the same degradation rate (Figure 38F), suggesting that protein degradation is not important for stability. The subcellular localization

of the endogenous MITF protein in 501Mel and SKmel28 was not altered upon PRDM7 knockout (Figure 38G). In line with that, overexpressing MITF in PRDM7 cells was partially able to rescue the expression of MITF^{low}/Jun^{high} TNFa signature genes, including IL8, IL1B, and NRP1 (Figure 39). Taken together, our data confirmed the role of PRDM7 in affecting MITF protein expression, possibly through mediating the MITF translation process or post-transcriptional processing of mRNA. However, this needs to be further investigated.

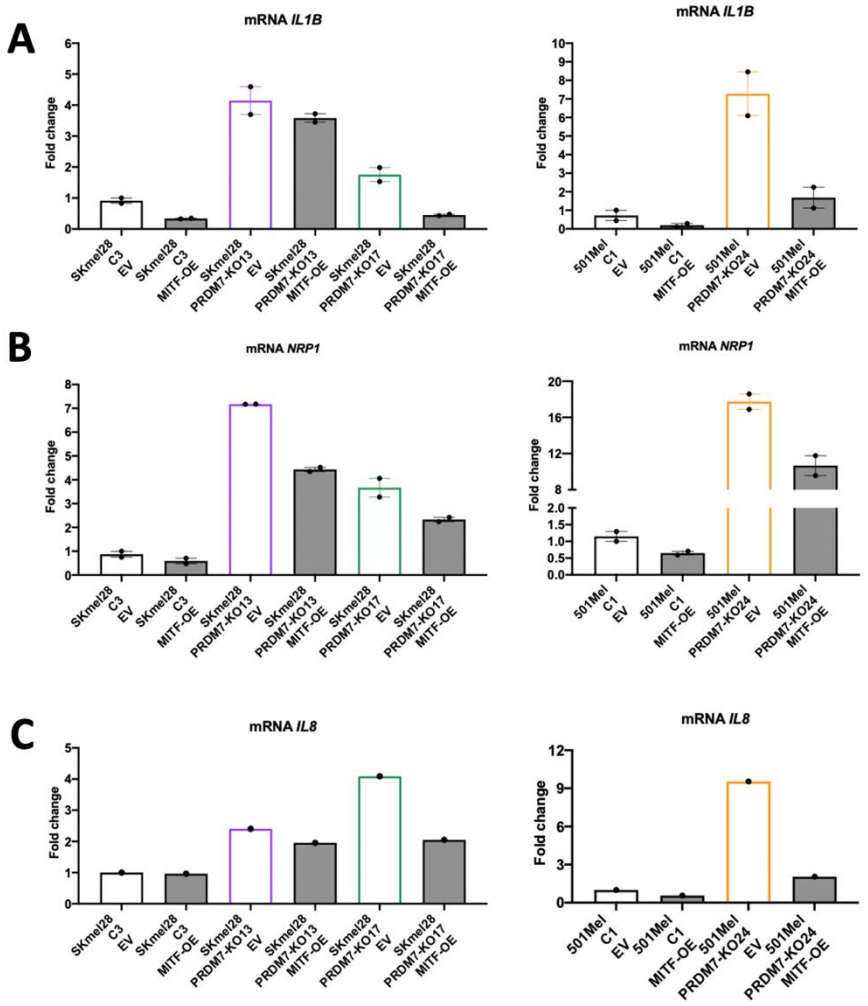

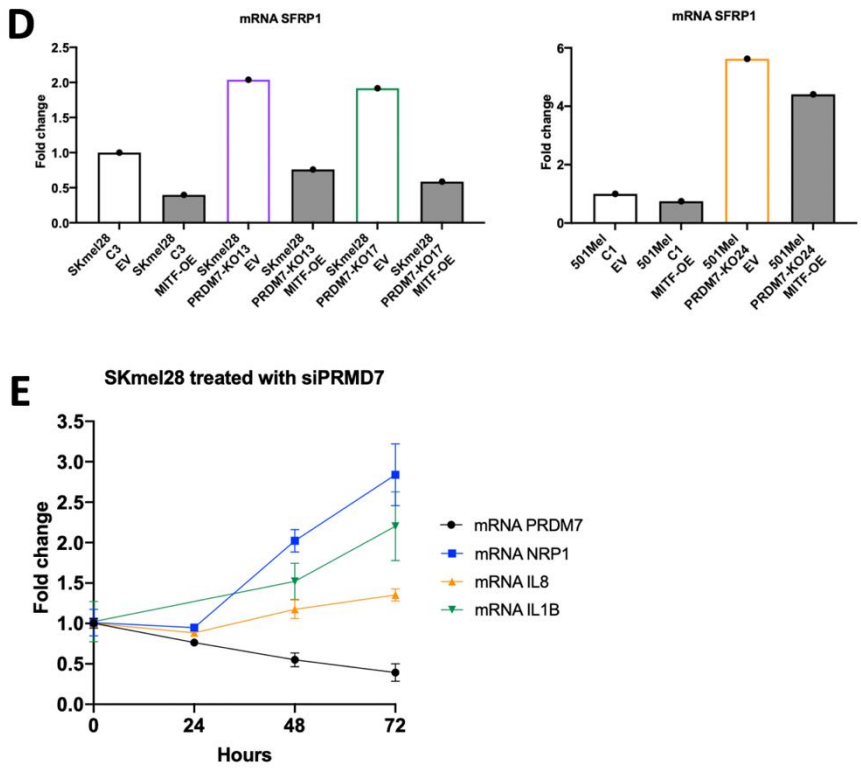

Figure 39. Overexpression of MITF partially rescued PRDM7-KO cells (A) IL1B, (B) NRP1, (C) IL8, (D) SFRP1 mRNA expression in PRDM7-KO cells overexpressing MITF was measured by qPCR. (E) IL1B, NRP1, and IL8 mRNA expression in PRDM7-KD was measured by qPCR.

4.2.12 PRDM7 does not affect sensitivity to PLX treatment

The clear link between PRDM7 and MITF and the suggested role of MITF in response to PLX treatment raised the question if PRDM7 was involved in developing resistance to BRAF inhibitors in melanoma cells. In order to test this, the response of SKMel28 and 501Mel cells to PLX treatment was first determined. The growth curve of these cells upon treatment with different PLX concentrations was determined using IncuCyte live imaging (Figure 40A). SKmel28 and 501mel cells showed comparable sensitivity to PLX treatment, with IC50 of 0.5uM in both cases. Upon treatment with 0.5uM PLX, the colony formation ability of PRDM7-KO cells was significantly impaired (Figures 40B and 40C). However, different PRDM7-KO clones responded in distinct ways, suggesting variation between cell lines. While the 501Mel-PRDM7-KO13 cells are less sensitive to PLX treatment than 501-C1 cells both in terms of number and

size of colonies, the 501Mel-PRDM7-KO24 cells did not show any significant difference compared to the control. Upon PLX treatment, the number of SKmel28-PRDM7-KO13 colonies was significantly reduced compared to SKMel28-C3. Although the SKmel28-PRDM7-KO17 colonies were loosely adherent, their size was considerably greater than observed in the corresponding control. Overexpressing PRDM7 isoform A in either 501Mel or Skmel28 did not affect sensitivity to PLX (Figures 40D and 40E). Our data showed that both MITF and PRDM7 mRNA expression significantly increased in 501Mel PLX-treated cells. However, MITF and PRDM7 mRNA expression was significantly reduced upon longer PLX treatment (Figure 40F). Taken together, our findings suggest that PRDM7 responds differently to PLX treatment depending on different melanoma cell lines, suggesting that it does not play a major role in PLX sensitivity response.

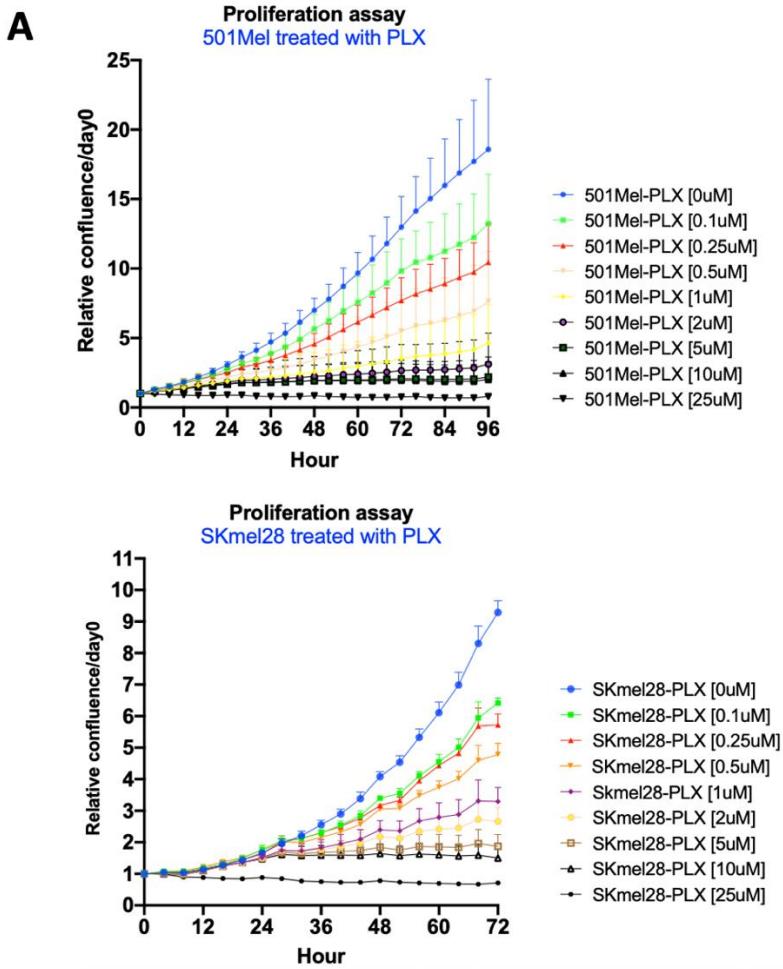

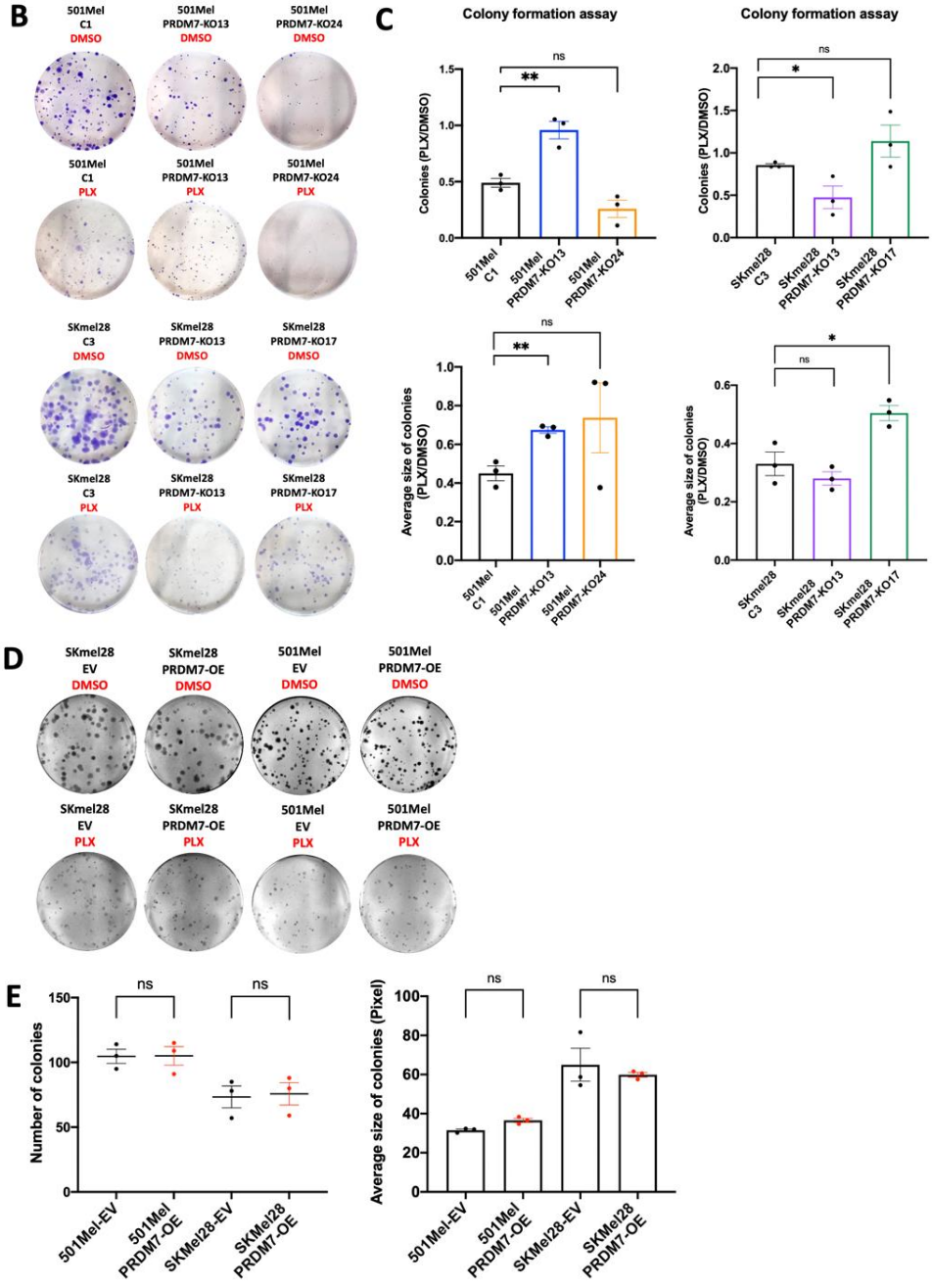
B
501Mel C1 DMSO
501Mel PRDM7-KO13 DMSO
501Mel PRDM7-KO24 DMSO
501Mel C1 PLX
501Mel PRDM7-KO13 PLX
501Mel PRDM7-KO24 PLX
SKmel28 C3 DMSO
SKmel28 PRDM7-KO13 DMSO
SKmel28 PRDM7-KO17 DMSO
SKmel28 C3 PLX
SKmel28 PRDM7-KO13 PLX
SKmel28 PRDM7-KO17 PLX
C
Colony formation assay
Colonies (PLX/DMSO)
Average size of colonies (PLX/DMSO)
ns
**
*
501Mel C1
501Mel PRDM7-KO13
501Mel PRDM7-KO24
SKmel28 C3
SKmel28 PRDM7-KO13
SKmel28 PRDM7-KO17
D
SKmel28 EV DMSO
SKmel28 PRDM7-OE DMSO
501Mel EV DMSO
501Mel PRDM7-OE DMSO
SKmel28 EV PLX
SKmel28 PRDM7-OE PLX
501Mel EV PLX
501Mel PRDM7-OE PLX
E
Number of colonies
Average size of colonies (Pixel)
501Mel-EV
501Mel PRDM7-OE
SKMel28-EV
SKMel28 PRDM7-OE

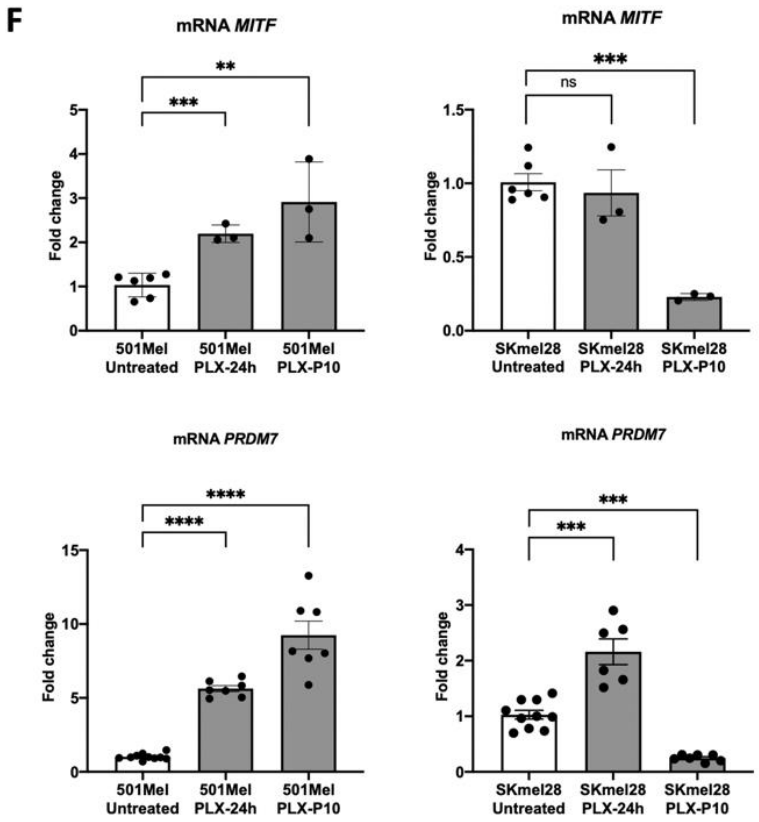

Figure 40. PRDM7 does not affect sensitivity to PLX treatment (A) The growth curve of 501Mel and SKmel28 cells upon treatment with different PLX concentrations were determined using IncuCyte live imaging. (B) Colony-formation assays were performed by treating PRDM7-KO cells with PLX at 0.5uM for SKmel28 and 0.25uM for 501Mel. (C) ImageJ software measured the number and size of PRDM7-KO cells upon PLX treatment. Statistically significant differences (Student's t-test) are indicated by *, p< 0.05. (D) Colony-formation assays were performed using PRDM7-OE upon treatment with PLX at 0.5uM for SKmel28 and 0.25uM for 501Mel. (E) ImageJ software measured the number and size of PRDM7-OE cells upon PLX treatment. Statistically significant differences (Student's t-test) are indicated by *, p< 0.05. (F) MITF and PRDM7 mRNA expression in SKmel28 and 501Mel after PLX treatment was measured by qPCR.

4.2.13 MITF-KO and PRDM7-KO alter histone modifications in melanoma cell lines

As PRDM7 is known as an H3K4me3 histone methyltransferase, its depletion might influence the histone modification pattern in melanoma cells. In order to determine if such changes occur, we performed Cut&Run to map the H3K4me3,

H3K9me3, and H3K27me3 histone modifications in MITF-KO SKMel28-MITF-X6 and SKmel28-MITF-X2) and PRDM7-KO cells and their corresponding controls. Surprisingly, although the overall number of H3K27me3 histone marks did not change, the distribution of active (H3K4me3) and repressive marks (H3K9me3 and H3K27me3) was significantly altered in PRDM7-KO and MITF-KO cells compared to the corresponding control (Figures 41A-E). Functional gene ontology group analysis between PRDM7-KO and their corresponding controls indicated that the deletion of PRDM7 in SKMel28 and 501Mel cells introduced a unique H3K4me3 mark in genes associated with RNA localization and regulation of RNA stability. Although PRDM7-KO cells and its corresponding controls showed overlapping H3K4me3 marks in a subset of genes, the H3K4me3 signals were located in genes responsible for DNA conformation changes and DNA geometric changes were significantly reduced in PRDM7-KO cells compared to control cell lines (Figures 41F-J).

Meanwhile, the mapping of H3K4me3 histone marks in MITF-KO and its corresponding control showed that the unique H3K4me3 marks, which were found only in MITF-KO cells compared to its control, are enriched in genes involved in the regulation of actin cytoskeleton organization, regulation of cell growth, and positively activated JUN kinase pathway (Figures 41H-I). Deletion of MITF also resulted in a loss of the H3K4me3 signal in genes involved in the regulation of translation, positive regulation of cellular catabolic processes, and vesicle organization categories (Figures 41H-I). The active histone modification H3K4me3 signal also changed in genes associated with chromatin segregation, RNA splicing, and regulation of chromatin organization (Figure 41) upon knocking out PRDM7 and MITF. Our data suggested that the depletion of either MITF or PRDM7 leads to a massive change in melanoma cells' repressive and active histone marks. Possibly, MITF and PRDM7 regulate each other's expression and are involved in reshaping the chromatin state in melanoma.

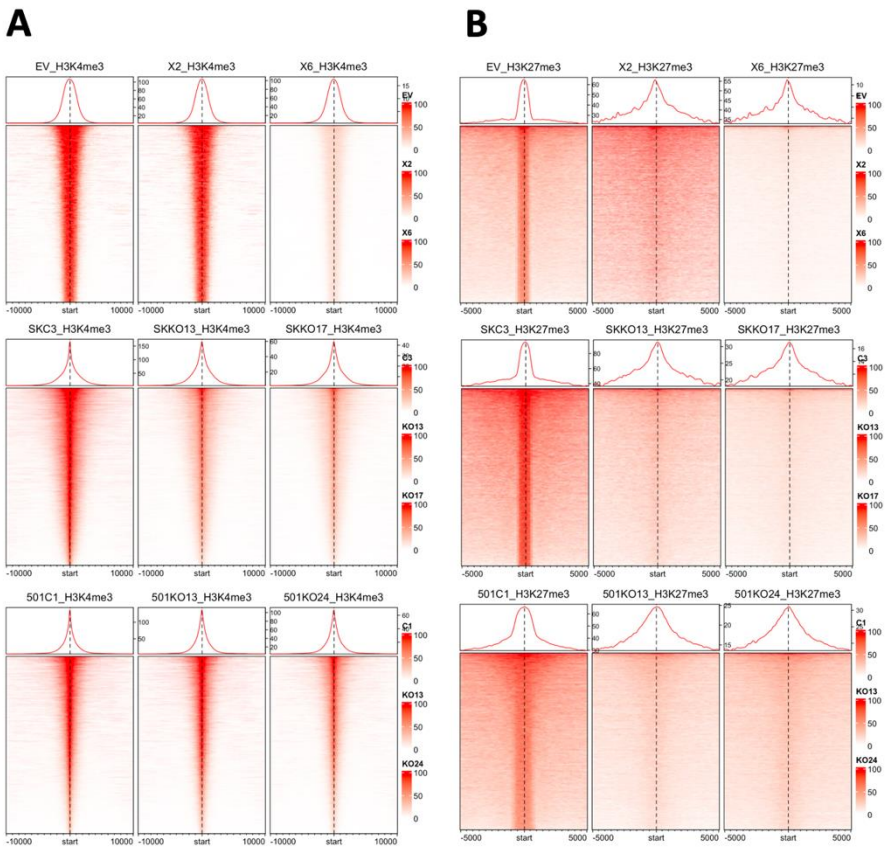
A
B
EV_H3K4me3
X2_H3K4me3
X6_H3K4me3
EV_H3K27me3
X2_H3K27me3
X6_H3K27me3
SKC3_H3K4me3
SKKO13_H3K4me3
SKKO17_H3K4me3
SKC3_H3K27me3
SKKO13_H3K27me3
SKKO17_H3K27me3
501C1_H3K4me3
501KO13_H3K4me3
501KO24_H3K4me3
501C1_H3K27me3
501KO13_H3K27me3
501KO24_H3K27me3
start

Top 1% peak

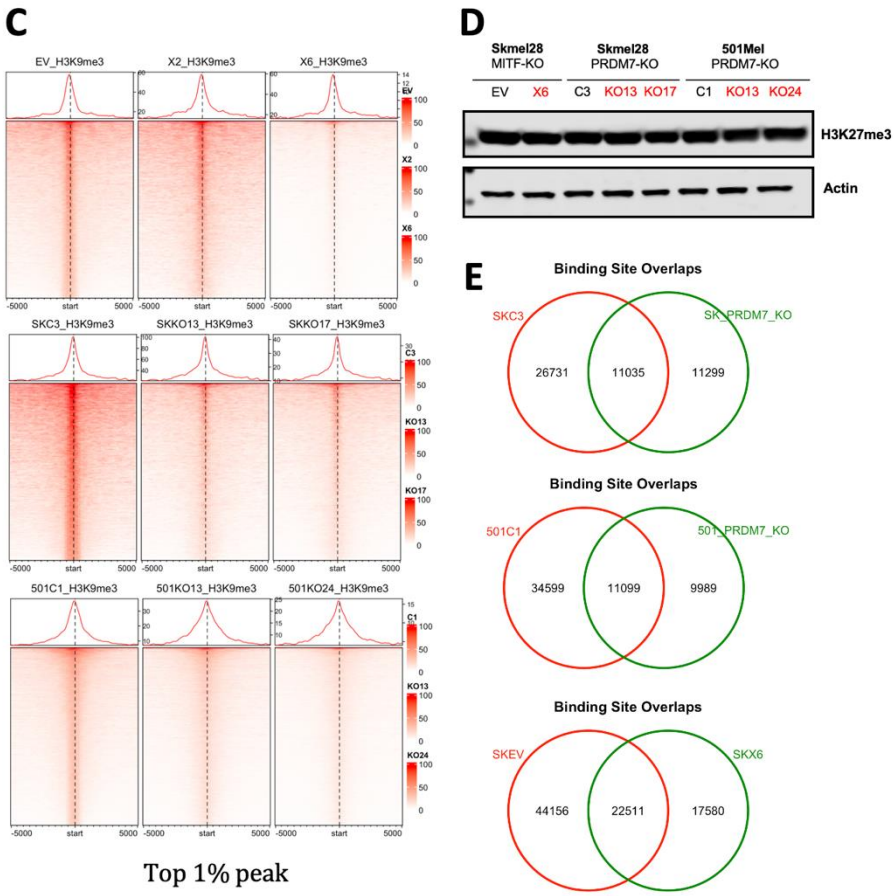
C
EV_H3K9me3
X2_H3K9me3
X6_H3K9me3
SKC3_H3K9me3
SKKO13_H3K9me3
SKKO17_H3K9me3
501C1_H3K9me3
501KO13_H3K9me3
501KO24_H3K9me3
-5000
start
5000
Top 1% peak
D
Skmel28
MITF-KO
Skmel28
PRDM7-KO
501Mel
PRDM7-KO
EV
X6
C3
KO13
KO17
C1
KO13
KO24
H3K27me3
Actin
E
Binding Site Overlaps
SKC3
SK_PRDM7_KO
26731
11035
11299
Binding Site Overlaps
501C1
501_PRDM7_KO
34599
11099
9989
Binding Site Overlaps
SKEV
SKX6
44156
22511
17580

F
BP_H3K4me3_Unique_Prdm7_SK
establishment of protein localization to organelle
histone modification
protein polyubiquitination
macroautophagy
peptidyl-lysine modification
regulation of cell morphogenesis
proteasome-mediated ubiquitin-dependent protein catabolic process
positive regulation of cellular catabolic process
ribonucleoprotein complex biogenesis
ribosome biogenesis
protein localization to nucleus
nucleocytoplasmic transport
nuclear transport
rRNA metabolic process
rRNA processing
histone H4 acetylation
chromatin remodeling
RNA splicing
regulation of cell cycle phase transition
Unique_SKmel28_CTRL
Unique_SKmel28_PRDM7-KO
GeneRatio
0.02
0.03
0.04
p.adjust
0.0075
0.0050
0.0025
BP_H3K4me3_Unique_Prdm7_501
nuclear export
ribonucleoprotein complex biogenesis
regulation of mRNA stability
regulation of mRNA catabolic process
stem cell population maintenance
regulation of RNA stability
RNA localization
protein-containing complex assembly
viral process
DNA duplex unwinding
DNA conformation change
maintenance of cell number
Unique_501Mel_PRDM7-KO
GeneRatio
0.02
0.03
p.adjust
0.0021
0.0020
0.0019
0.0018
0.0017
BP_H3K4me3_Unique_MITF
cell growth
macroautophagy
forebrain development
establishment of protein localization to organelle
regulation of actin cytoskeleton organization
regulation of neurogenesis
regulation of cell growth
regulation of actin filament-based process
actin filament organization
positive regulation of JUN kinase activity
axon development
axonogenesis
positive regulation of cellular component biogenesis
regulation of neuron projection development
ERBB signaling pathway
Golgi vesicle transport
substrate adhesion-dependent cell spreading
positive regulation of protein-containing complex assembly
establishment or maintenance of cell polarity
negative regulation of cell projection organization
epidermal growth factor receptor signaling pathway
Unique_SKmel28_MITF-KO
Unique_SKmel28_CTRL
GeneRatio
0.01
0.02
0.03
0.04
p.adjust
0.0075
0.0050
0.0025

G
CC_H3K4me3_Overlap_Diff_MITF
ribonucleoprotein complex biogenesis
chromosome segregation
mitotic sister chromatid segregation
mitotic nuclear division
ncRNA processing
sister chromatid segregation
RNA splicing
ribosome biogenesis
nuclear chromosome segregation
chromatin remodeling
rRNA metabolic process
regulation of chromosome organization
proteasome-mediated ubiquitin-dependent protein catabolic process
nuclear division
double-strand break repair
RNA splicing, via transesterification reactions
RNA splicing, via transesterification reactions with bulged adenosine as nucleophile
mRNA splicing, via spliceosome
mitotic cell cycle phase transition
establishment of protein localization to organelle
histone modification
regulation of translation
positive regulation of cellular catabolic process
macroautophagy
vesicle organization
Overlap_Up
SkMel28-MITF-KO
Overlap_Down
SkMel28-MITF-KO
p.adjust
6e-04
4e-04
2e-04
GeneRatio
0.02
0.03
0.04
CC_H3K4me3_Overlap_Diff_PRDM7_SK
ribonucleoprotein complex biogenesis
sister chromatid segregation
mitotic sister chromatid segregation
regulation of chromosome organization
ribosome biogenesis
mitotic nuclear division
positive regulation of chromosome organization
chromosome segregation
nuclear chromosome segregation
RNA splicing
establishment of protein localization to organelle
mitotic cell cycle phase transition
peptidyl-lysine modification
endosomal transport
double-strand break repair
ncRNA processing
nuclear division
proteasome-mediated ubiquitin-dependent protein catabolic process
regulation of DNA repair
anaphase-promoting complex-dependent catabolic process
DNA conformation change
DNA geometric change
Overlap_Up
SkMel28-PRDM7-KO
Overlap_Down
SkMel28-PRDM7-KO
p.adjust
0.00075
0.00050
0.00025
GeneRatio
0.01
0.02
0.03
0.04

Figure 41. MITF-KO and PRDM7-KO alter histone modifications in melanoma cell lines. (A), (B), and (C) Heatmap showing the distribution of histone mark H3K4me3 (A), H3K27me3 (B), and H3K9me3 (C) in MITF-KO and PRDM7-KO cells around 10kb +/- corresponding histone marks in control cell lines. (D) Western blot analysis of H3K27me3 in SKMel28-PRDM7-KO and SKmel28-C3. Actin was used as a loading control. (E) Venn diagram showing the number of overlapping H3K4me3, H3K27me3, and H3K9me3 histone marks between PRDM7-KO or MITF-KO and their corresponding control. (F), (G), and (H) Gene ontology analysis of unique H3K4me3 histone marks in PRDM7-KO and MITF-KO cells. (I) and (J) Gene ontology analysis of the H3K4me3 histone marks of the overlapping H3K4me3 mark in PRDM7-KO or MITF-KO compared to their corresponding control.

5 Discussions and Conclusions

5.1 Characterization of the molecular mechanism behind the Mitf$^{mi\text{-}sl}$ suppressor mutation

5.1.1 Molecular effects of the Mitf$^{mi\text{-}sl}$ mutation

Suppressor mutation screening is an important approach to providing valuable information about gene function, molecular pathways, and protein-protein interactions (Bautista et al., 2021; Sujatha and Chatterji, 2000). Suppressor screens are commonly performed in yeast, Drosophila, and C. elegans but rarely in mice. A novel intragenic suppressor mutation at the *Mitf* locus in the mouse was generated and shown that it is a re-mutation at the *Mitf* locus, which results in a truncation of the already mutated *Mitf$^{mi\text{-}sp}$* protein.

In homozygous conditions, the *Mitf$^{mi\text{-}sl}$* mutation leads to brownish coat color compared to the normal black coat of *Mitf$^{mi\text{-}sp}$* homozygotes. In compound heterozygous conditions with other *Mitf* mutations, including severe dominant-negative or loss-of-function mutations, the *Mitf$^{mi\text{-}sl}$* mutation improves the phenotype as compared to combinations of the same alleles with the original *Mitf$^{mi\text{-}sp}$* mutation. At the molecular level, we show that this suppressor mutation increases the nuclear localization of the MITF protein and reduces its stability. Importantly, in the presence of defective DNA-binding mutations such as MITF$^{mi\text{-}ew}$, MITF^{mi}, and MITF$^{Mi\text{-}Wh}$, the *Mitf$^{mi\text{-}sl}$* protein will dimerize with these partners and drag them into the nucleus, thus increasing the stability of the *Mitf$^{mi\text{-}sl}$* protein itself. This can explain the dichotomous phenotypic effects of the *Mitf$^{mi\text{-}sl}$* mutation. The "brownish" phenotype of *Mitf$^{mi\text{-}sl}$* homozygotes is likely to be due to the reduced stability of *Mitf$^{mi\text{-}sl}$* protein. Although there is more of it in the nucleus, its stability is reduced, thus resulting in reduced expression of target genes involved in pigmentation, e.g. Pmel, Tyrp1, and Mlana. Here, the total concentration of active MITF$^{mi\text{-}sl}$ protein in the nucleus at any given time will depend on the relationship between effects on nuclear import on the one hand and stability on the other hand. Expression of the MITF-partner proteins TFEB and TFE3 is limited in melanocytes so that they will have negligible effects on MITF activity in the homozygous situation. However, when the *Mitf$^{mi\text{-}sl}$* mutation is combined with the various other *Mitf* mutations, MITF$^{mi\text{-}sl}$ preference to form

dimerize and drag its partner proteins (MITF-WT or mutant MITF) into the nucleus, in turn, protecting MITF$^{mi\text{-}sl}$ from degradation. Eventually, however, the dimers will release MITF$^{mi\text{-}sl}$ monomers from their non-DNA-binding dimeric partner, thus forming MITF$^{mi\text{-}sl}$ homodimers, which can bind DNA and activate the expression of target genes. This helps explain the suppressive effects. Here the combined effects of nuclear import, rate of nuclear degradation, DNA binding, and dimerization properties are likely to determine the final outcome; the steady-state levels of nuclear MITF$^{mi\text{-}sl}$ are likely to be determined by the rate of heterodimer dissociation and rate of degradation. The near-normal coat color phenotype of *Mitf*$^{mi\text{-}sl}$*/Mitf*^{mi} compound heterozygotes suggests that together these effects result in almost full MITF activity during critical stages of melanocyte development and function. This is a novel mechanism of genetic suppression.

5.1.2 Factors affecting MITF localization and stability

In addition to providing an explanation for the phenotypic outcome of the suppressor mutation, the mutation provides novel insights into how both stability and nuclear import of the MITF protein are regulated. Nuclear localization of MITF has been shown to involve a balance between import and export that depends on a number of domains, including the DNA-binding domain of MITF and the S69 and S73 phosphorylation sites (Fock et al., 2019; Ngeow et al., 2018). In wild-type cells, MITF is approximately equally distributed between the nucleus and cytoplasm, although, due to differences in nuclear and cytoplasmic volumes, it is more concentrated in the nucleus than in the cytoplasm, as evidenced by immunocytochemistry (Fock et al., 2019). Unexpectedly, our observations show that the C-end of MITF has major effects on nuclear localization and that residues 316-326 and 378-419 are critical factors in mediating nuclear localization. While lacking the 378-419 domain results in nuclear accumulation, the depletion of the 316-326 domain impairs the nuclear export dynamic of pS73-MITF. Interestingly, simultaneously mutating the SUMO-site at K316 and the phosphorylation site at S409 increased the nuclear localization of MITF compared to the single S409A mutation. However, other residues must also be involved since this double mutant protein did not fully replicate the effects observed with the *Mitf*$^{mi\text{-}sl}$ mutation alone. It is likely that other residues within the 378-419 region are important for mediating these effects.

The nuclear localization of MITF is not affected by the alternative six amino acids. Additionally, the interaction of MITF with the 14-3-3 family of proteins was not affected by the 104 aa deletions associated with the MITF$^{mi\text{-}sl}$ mutation. Previous work has shown that the interaction between MITF and 14-3-3 proteins depend on phosphorylation at S173 (Bronisz et al., 2006), a residue that is still present in

the MITF$^{mi\text{-}sl}$ protein. Consistent with our data, the MITF-S409A and TFEB-S467A (equivalent to S409 of MITF-WT) proteins retained their ability to form complexes with 14-3-3 proteins but significantly increased their nuclear retention compared to their WT counterparts (Bronisz et al., 2006; Palmieri et al., 2017; Wang et al., 2016). This is also consistent with the observation that reduced MAPK activity, as seen in *Kit^{tm1Alf}/Kit^{+}* mice, does not alter the *Mitf$^{mi\text{-}sl}$* phenotype and with previous results showing that transgenic Mitf BACs with an S409A mutation can fully rescue the phenotype of Mitf$^{mi\text{-}vga9}$/Mitf$^{mi\text{-}vga9}$ mice (Bauer et al., 2009). Furthermore, it has been reported that the localization of MITF is regulated by the BRAF/MAPK-regulated nuclear export signal (NES), which contains the phosphorylation at S69 and S73 residue (Ngeow et al., 2018). Interestingly, the nuclear localization of MITF is also modulated by three karyophilic signals in the bHLH-Zip domain spanning residues 197-206, 214-217, and 255-265 (Fock et al., 2019). In addition, a couple of NES signals located in the C-terminus of MITF (350-366 and 374-388 residue) are predicted by the LocNES algorithm and need further studies to verify their roles in regulating MITF localization.

This work shows that MITF is mainly degraded through ubiquitin-proteasomal degradation located in the nucleus. Again, the effects on stability are mediated by the domains encoded by residues 316-326 and 378-419. The fact that the effects on nuclear localization and stability are encoded in the same domains suggests that these events are related. The effects on nuclear localization are likely dominant since the nuclear proteasome machinery will degrade the protein as soon as the protein is in the nucleus. Notably, DNA binding ability of MITF$^{mi\text{-}sl}$ is essential for the degradation process. However, how DNA binding contributes to MITF stability is not clear. It is possible that the interaction of the two carboxyl domains can only take place when bound to DNA. Alternatively, DNA binding may be essential for either SUMOylation of K316 or phosphorylation of S409. It is also possible that the increase in cytoplasmic proportion of MITF^{mi}-316X and MITF$^{mi\text{-}ew}$-316X compared to that of MITF$^{mi\text{-}sl}$ could potentially explain the increase in their stability. Importantly our work shows that the interaction between the SUMOylation site at K316 and the phosphorylation site at S409 are important for regulating MITF localization and stability. smFRET results obtained by the Masters student Matthías Már Valdimarsson show that these two residues are near each other in space, suggesting that direct interactions are involved.

Previous work using HEK293 cells has shown that an S409A mutant protein has similar stability to that of MITF-WT, whereas the S73A-S409A double mutant is more stable (Wu et al., 2000). Consistent with that, in our A375 model, the S409A mutation alone did not affect stability. Critically, we show for the first time

that the SUMO-site at K316 is involved in mediating MITF stability and surprisingly cooperates with the S409 phosphorylation site in mediating this. Consistent with previous work (Murakami and Arnheiter, 2005), we also showed that the double K182/316R MITF mutant did not alter stability. SUMOylation at K182 and K316 may play specific roles and complement each other in MITF stability and subsequent effects on transcription regulation.

Surprisingly, our results show that the unpS73 form of MITF-WT is much less stable than the pS73 form. In our model, there is an almost 3-fold difference in the stability of the two forms. Interestingly, the *Mitf*$^{mi\text{-}sl}$ mutation reduced the stability of both the pS73 and unpS73 forms of MITF about 3-fold in each case, suggesting that the effects of the C-end on stability are independent of the effects of pS73. Additionally, the observation that pS73-MITF is exported from the nucleus (Ngeow et al., 2018) suggests that the kinetics of S73 phosphorylation and dephosphorylation may determine the subcellular location and thus mediate protein stability. Currently, there is limited information on the kinetics or pathways involved.

5.1.3 Model for the molecular effects of E318K mutation in melanoma

Independent reports have shown that the E318K variant in human MITF predisposes to melanoma (Bertolotto et al., 2011; Yokoyama et al., 2011). This variant alters an essential residue in the SUMOylation motif ΨKXD/E, including K316, the actual SUMOylation site. We show that the E318K mutant protein, which cannot be SUMOylated at this site, exhibits normal nuclear localization. However, when the S409A mutation is also present, the protein is more nuclear, regardless of S73 phosphorylation status. The E318K mutation resulted in reduced MITF stability both in the presence and absence of the S409A mutation. It has been reported that MITF-E318K occupied a larger number of binding sites (Bertolotto et al., 2011). In line with that, DNA binding ability might increase the degradation rate, suggesting a reason for the reduced stability in the MITF-E318K mutation.

Interestingly, MITF-E318K has been reported to induce invasion and suppress the senescence promoted by the BRAF^{V600E} mutation (Bonet 2017). Since BRAF-signalling has been proposed to mediate the effects of the E318K mutation, our work suggests a cooperation of the K316 SUMOylation site with phosphorylation at S409 in mediating effects on MITF localization and stability. This may suggest that signaling enhances the effects of the E318K mutation. S409 has been suggested to be phosphorylated by the MAPkinase p90Rsk (Wu et al., 2000) or

by AKT (Wang et al., 2016). The gain-of-function $BRAF^{V600E}$ mutation and loss-of-function PTEN might accelerate the p90Rsk or AKT kinase activity, respectively, and promote S409 phosphorylation. Eventually, this ability of $BRAF^{V600E}$ to phosphorylate S409 might promote cytoplasmic retention of MITF-E318K, which subsequently could increase the stability of MITF and maintain the level of MITF at steady-state levels. Thus, the medium-risk allele E318K (Bertolotto et al., 2011; Yokoyama et al., 2011) may depend on particular environmental signals (e.g., sun exposure) in mediating disease predisposition.

Based on our data, we propose a model (Figure 42) where the two regions of the C-end of MITF contribute to nuclear localization and stability. MITF needs to bind DNA upon which the protein is SUMOylated at K316 and phosphorylated at S409, thus leading to interactions between the two domains. Lacking phosphorylation at S409 and SUMOylation at K316 results in the impairment of nuclear export, suggesting that SUMOylation at K316 and phosphorylation at S409 might be important for the interaction of MITF and export proteins (e.g., CRM1, NPM1). Consequently, the interaction between MITF and nuclear export protein is suggested to affect protein degradation and stability. Perhaps this is a feedback loop to limit the activity of MITF based on environmental signals. We, therefore, conclude that generating suppressor mutations in the mouse is an exciting and feasible option for studying gene function and may reveal unexpected aspects of protein function and regulation, leading to novel insights into protein activities in the living organism.

5.1.4 Future perspectives regarding MITF carboxyl terminus

In this study, the 316-419 domain has been shown to play important roles in regulating both stability and localization. Importantly, we showed that phosphorylation at S409 and SUMOylation at K316 has been shown to play a critical role in modulating both localization and stability. However, which signaling pathway is involved in accelerating the degradation rate of MITF due to lack of carboxyl end remains to be further investigated. It is possible that lack of carboxyl end results in the exposure of degron signal and subsequently reduces stability in $MITF^{mi\text{-}sl}$. However, the degron signal's location at the carboxyl end and how it recruits the proteasomal degradation machinery to degraded MITF still need to be further investigated.

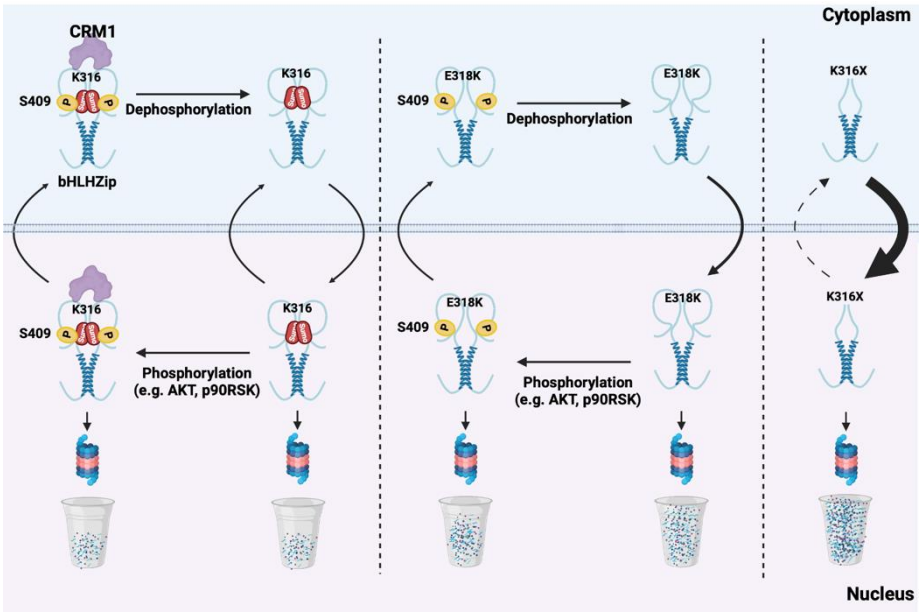

Figure 42. Propose model mechanism of 316-419 domain regulate MITF stability and localization.

Furthermore, the nuclear accumulation of MITF$^{mi\text{-}sl}$ has been shown due to the impairment of both nuclear import and export. However, the exact sequence of NES and NIS signals located at the carboxyl end remains to be verified and further studied. Additionally, it would be further interesting to understand the interactome of MITF carboxyl-end. The comparison of MITF-WT and MITF$^{mi\text{-}sl}$ interactome could propose carboxyl-end MITF interaction partner proteins that might regulate MITF localization. Performing a CRISPR screen could also be a powerful screening technique for the specific kinases and SUMOylation enzymes, which regulates the phosphorylation at S409 and SUMOylation at K316, respectively. As a result, the signaling pathways involved in regulating MITF localization and stability would be clarified.

Additionally, besides the cycloheximide decay kinetics, radioactive pulse-chase assays also offer a complementary approach to measuring protein stability and turnover rate. While cycloheximide decay kinetics assays provide valuable insights into the global turnover rates of proteins, they do not discriminate between newly synthesized and pre-existing proteins. In contrast, radioactive pulse-chase assays enable the specific measurement of protein stability by incorporating a radioactive amino acid during synthesis and subsequently tracking its fate over time. This technique, therefore, might provide precise information about the synthesis and turnover kinetics of MITF proteins, allowing

us to distinguish between newly synthesized and pre-existing protein pools and possibly distinguish between upS73- and pS73-MITF. Additionally, radioactive pulse-chase assays offer the opportunity to study MITF trafficking and localization, providing further insights into upS73- and pS73-MITF dynamics within cells.

5.2 Functional roles of PRDM7

The link between MITF activity and melanoma phenotype suggests that MITF might be involved in reshaping chromatin states in melanoma by mediating the expression of epigenetic modifiers. In this study, we reported that MITF positively regulates the methyltransferase PRDM7, a primate-specific gene that is exclusively expressed in melanoma. To investigate the functional roles of PRDM7, we generated PRDM7-KO melanoma cell lines using CRISPR-Cas9 and used them to profile the transcriptome and phenotypic effects of PRDM7. The RNA-seq data of PRDM7-KO melanoma cells resembles $PRDM7^{low}$ tumor samples. In both datasets, we observed a significant increase in the expression of genes associated with extracellular matrix organization, extracellular structure organization, cell junction assembly, and cell-substrate adhesion. This is consistence with the changes in morphologies upon depletion of PRDM7 using miRNAs. Additionally, the transcriptomic profile of PRDM7-KO was positively correlated with the Verfaillie proliferative and invasive signatures (Verfaillie et al., 2015) and the EMT hallmark. Notably, the EMT hallmark, which was default set by GSEA, included genes defining epithelial-mesenchymal transition (e.g., wound healing, fibrosis, and metastasis) (Subramanian et al., 2005). The Verfaillie proliferative or invasive signatures were based on transcriptome data of tumor biopsies and defined by signature genes in either proliferative or invasive clusters (Verfaillie et al., 2015). Cell lines with high MITF expression exhibited the proliferative phenotype, and cells with low MITF expression exhibited the signature of an invasive phenotype (Hoek, Eichhoff, et al., 2008; Widmer et al., 2012).

Depletion of PRDM7 in both 501Mel and SKmel28 cells resulted in increased expression of cell cycle inhibitors genes. In line with that, 501Mel and SKmel28 PRDM7-KO cells significantly reduced their proliferation rate and colony formation abilities compared to their corresponding controls. The 501Mel-PRDM7-KD cells also showed a slower proliferation rate using the Incucyte system. Knockdown of PRDM7 showed less of an effect than knockout cells. The duration of the knockdown and incomplete depletion of PRDM7 might explain the difference observed between the 501Mel PRDM7-KO and PRDM7-KD cells. The slower proliferation of 501Mel-PRDM7-KO might be explained by increased apoptosis.

Although the RNA-seq data suggested that PRDM7 might play a role in migration and invasion, the scratch assay did not support that. Single-cell movement assays did not suggest a difference in the mean migration speeds upon PRDM7 deletion; however, PRDM7-KO cells showed a notable increase in the maximal distance traveled, suggesting the role of PRDM7 in regulating cell stretching and morphology during migration. PRDM7 also influenced the number of focal points, although the SKmel28-PRDM7-KO and 501Mel-PRDM7-KO showed opposite effects.

Previous work has shown changes in cell morphology, focal adhesion, proliferation, and invasion upon MITF depletion (Dilshat et al., 2021a). The RNA-seq data of PRDM7-KO cells resembles MITF-KO cells in that the deletion of either PRDM7 or MITF leads to induced expression of genes associated with extracellular matrix and structural organization as well as with EMT genes. Consistent with that, a reduction in MITF protein expression was observed in PRDM7-KO cells, whereas no changes were observed at the mRNA level. Reduced MITF protein expression might explain the phenotypic similarity seen between PRDM7-KO and MITF-KO cells.

Interestingly, our observation shows that MITF protein expression changes through the cell cycle. If MITF expression increases over a specific threshold, it might activate or repress the genes that are responsible for cell cycle regulation. However, depletion of PRDM7 reduced the expression of MITF protein, making the cells non-proliferative and unable to switch between stages. Interestingly, consistent with the reduction of MITF protein in PRDM7-KO cells, overexpressing MITF partially rescued the PRDM7-KO cells. However, the reduction of MITF protein in PRDM7-KO cells was not due to the alteration of MITF stability or changes in MITF localization. It is possible that PRDM7, known as a methyltransferase, regulates the MITF translation process through methylating mRNA. However, it is not known if this is the case or how this is mediated.

Although the PRDM7-KO knockouts altered the cellular phenotypes, overexpression of the PRDM7 isoform A did not significantly influence proliferation, invasion, focal adhesion, or sensitivity to PLX treatment. Importantly, overexpression of PRDM7 isoform A could not rescue the phenotype of the PRDM7-KO cells. It is possible that the PRDM7 isoform A used in these experiments is not functional in melanoma cells. We have discovered seven novel PRDM7 isoforms to be expressed in melanoma cells that did not contain complete KRAB and SET domains. Possibly, different isoforms play different functional roles. Thus, it is possible that the isoform A used to rescue PRDM7-KO simply does not replicate the similar function of other PRDM7 isoforms, which

might be dominant presenting in melanoma cells. Therefore, these experiments need to be repeated using the novel isoforms.

Furthermore, in this study, two melanoma cell lines, 501Mel and SKmel28, were used to study the function of PRDM7. Although PRDM7 depletion in 501Mel and SKmel28 affected cell proliferation, morphologies, and focal adhesion, PRDM7-KO in these two cell lines did not show the same results. It might be explained by specific cell line characteristics, including the difference in endogenous PRDM7 and MITF expression level, which eventually leads to different responses due to reduced MITF protein expression. However, many questions are still open regarding PRDM7 and remain to be further investigated. First of all, the dominant PRDM7 isoforms and their specific functional roles in melanoma need to be studied through the rescue of PRDM7-KO melanoma. Secondly, the effect of PRDM7 on the expression of MITF protein needs to be further investigated. Although PRDM7 has not been shown to affect MITF protein localization and stability, PRDM7 might play roles in regulating the MITF translation process, possibly through methylation of MIT mRN and recruiting translation machinery for MITF protein synthesis. Further, it is critical and important to understand how the histone modification changes upon deletion of PRDM7. Although the PRDM7 protein has not been detected by using commercial antibodies, CRISPR-knockin could be used to tag PRDM7 and mass spectrometry could be performed to investigate the PRDM7 interactome. The question of whether PRDM7 interacts with chromatin modifiers or polycomb to direct the histone modification could then be answered.

References

Abel, E.V., Basile, K.J., Kugel, C.H., *et al.* (2013). Melanoma adapts to RAF/MEK inhibitors through FOXD3-mediated upregulation of ERBB3. The Journal of clinical investigation *123*, 2155-2168.

Akbani, R., Akdemir, K.C., Aksoy, B.A., *et al.* (2015). Genomic classification of cutaneous melanoma. Cell *161*, 1681-1696.

Alaskhar Alhamwe, B., Khalaila, R., Wolf, J., *et al.* (2018). Histone modifications and their role in epigenetics of atopy and allergic diseases. Allergy, Asthma & Clinical Immunology *14*, 1-16.

Alexaki, V.-I., Javelaud, D., Van Kempen, L.C., *et al.* (2010). GLI2-mediated melanoma invasion and metastasis. Journal of the National Cancer Institute *102*, 1148-1159.

Ali, Z., Yousaf, N., and Larkin, J. (2013). Melanoma epidemiology, biology and prognosis. EJC supplements *11*, 81.

Amiel, J., Watkin, P.M., Tassabehji, M., *et al.* (1998). Mutation of the MITF gene in albinism-deafness syndrome (Tietz syndrome). Clin Dysmorphol *7*, 17-20.

Ancelin, K., Lange, U.C., Hajkova, P., *et al.* (2006). Blimp1 associates with Prmt5 and directs histone arginine methylation in mouse germ cells. Nat Cell Biol *8*, 623-630.

Anelli, V., Santoriello, C., Distel, M., *et al.* (2009). Global repression of cancer gene expression in a zebrafish model of melanoma is linked to epigenetic regulation. Zebrafish *6*, 417-424.

Anna, B., Blazej, Z., Jacqueline, G., *et al.* (2007). Mechanism of UV-related carcinogenesis and its contribution to nevi/melanoma. Expert Rev Dermatol *2*, 451-469.

Aoude, L.G., Pritchard, A.L., Robles-Espinoza, C.D., *et al.* (2015). Nonsense mutations in the shelterin complex genes ACD and TERF2IP in familial melanoma. Journal of the National Cancer Institute *107*, dju408.

Arnheiter, H. (2010). The discovery of the microphthalmia locus and its gene, Mitf. Pigment Cell Melanoma Res *23*, 729-735.

Ballesteros-Álvarez, J., Dilshat, R., Fock, V., *et al.* (2020). MITF and TFEB cross-regulation in melanoma cells. PloS one *15*, e0238546.

Bannister, A.J., and Kouzarides, T. (2011). Regulation of chromatin by histone modifications. Cell Research *21*, 381-395.

Bartkova, J., Lukas, J., Guldberg, P., *et al.* (1996). The p16-cyclin D/Cdk4-pRb pathway as a functional unit frequently altered in melanoma pathogenesis. Cancer Research *56*, 5475-5483.

Bastian, B.C., and Pinkel, D. (2008). Expanding the genetic spectrum of pigmentation (Wiley Online Library).

Baudat, F., Buard, J., Grey, C., *et al.* (2010). PRDM9 is a major determinant of meiotic recombination hotspots in humans and mice. Science (New York, NY) *327*, 836-840.

Bauer, G.L., Praetorius, C., Bergsteinsdottir, K., *et al.* (2009). The role of MITF phosphorylation sites during coat color and eye development in mice analyzed by bacterial artificial chromosome transgene rescue. Genetics *183*, 581-594.

Bauer, J., Büttner, P., Murali, R., *et al.* (2011). BRAF mutations in cutaneous melanoma are independently associated with age, anatomic site of the primary tumor, and the degree of solar elastosis at the primary tumor site. Pigment Cell Melanoma Res *24*, 345-351.

Bautista, D.E., Carr, J.F., and Mitchell, A.M. (2021). Suppressor Mutants: History and Today's Applications. EcoSal Plus *9*, eESP-0037-2020.

Beaumont, K.A., Shekar, S.L., Newton, R.A., *et al.* (2007). Receptor function, dominant negative activity and phenotype correlations for MC1R variant alleles. Human molecular genetics *16*, 2249-2260.

Bennett, D.C. (2003). Human melanocyte senescence and melanoma susceptibility genes. Oncogene *22*, 3063-3069.

— (2008). How to make a melanoma: what do we know of the primary clonal events? Pigment cell & melanoma research *21*, 27-38.

Berlin, I., Denat, L., Steunou, A.L., *et al.* (2012). Phosphorylation of BRN2 modulates its interaction with the Pax3 promoter to control melanocyte migration and proliferation. Mol Cell Biol *32*, 1237-1247.

Bertolotto, C., Lesueur, F., Giuliano, S., *et al.* (2011). A SUMOylation-defective MITF germline mutation predisposes to melanoma and renal carcinoma. Nature *480*, 94-98.

Bertrand, J.U., Steingrimsson, E., Jouenne, F., *et al.* (2020). Melanoma risk and melanocyte biology. Acta Dermato-Venereologica *100*, 272-283.

Berwick, M., MacArthur, J., Orlow, I., *et al.* (2014). MITF E318K's effect on melanoma risk independent of, but modified by, other risk factors. Pigment cell & melanoma research *27*, 485-488.

Berwick, M., Orlow, I., Hummer, A.J., *et al.* (2006). The prevalence of CDKN2A germ-line mutations and relative risk for cutaneous malignant melanoma: an international population-based study. Cancer Epidemiology Biomarkers & Prevention *15*, 1520-1525.

Bianchi-Smiraglia, A., Bagati, A., Fink, E.E., *et al.* (2017). Microphthalmia-associated transcription factor suppresses invasion by reducing intracellular GTP pools. Oncogene *36*, 84-96.

Birck, A., Ahrenkiel, V., Zeuthen, J., *et al.* (2000). Mutation and allelic loss of the PTEN/MMAC1 gene in primary and metastatic melanoma biopsies. Journal of Investigative Dermatology *114*, 277-280.

Blazer, L.L., Lima-Fernandes, E., Gibson, E., *et al.* (2016). PR Domain-containing Protein 7 (PRDM7) Is a Histone 3 Lysine 4 Trimethyltransferase. J Biol Chem *291*, 13509-13519.

Boissy, R.E., and Lamoreux, M.L. (1995). In vivo and in vitro morphological analysis of melanocytes homozygous for the misp allele at the murine microphthalmia locus. Pigment Cell Res *8*, 294-301.

Bondurand, N., Pingault, V., Goerich, D.E., *et al.* (2000). Interaction among SOX10, PAX3 and MITF, three genes altered in Waardenburg syndrome. Hum Mol Genet *9*, 1907-1917.

Bonet, C., Luciani, F., Ottavi, J.-F., *et al.* (2017). Deciphering the role of oncogenic MITFE318K in senescence delay and melanoma progression. JNCI: Journal of the National Cancer Institute *109*.

Bonvin, E., Falletta, P., Shaw, H., *et al.* (2012). A phosphatidylinositol 3-kinase-Pax3 axis regulates Brn-2 expression in melanoma. Mol Cell Biol *32*, 4674-4683.

Borg, A.k., Sandberg, T., Nilsson, K., *et al.* (2000). High frequency of multiple melanomas and breast and pancreas carcinomas in CDKN2A mutation-positive melanoma families. Journal of the National Cancer Institute *92*, 1260-1266.

Borun, T.W., Pearson, D., and Paik, W.K. (1972). Studies of histone methylation during the HeLa S-3 cell cycle. Journal of Biological Chemistry *247*, 4288-4298.

Bossi, D., Cicalese, A., Dellino, G.I., *et al.* (2016). In Vivo Genetic Screens of Patient-Derived Tumors Revealed Unexpected Frailty of the Transformed PhenotypeIdentification of Novel Epigenetic Essential Genes. Cancer discovery *6*, 650-663.

Bowman, G.D., and Poirier, M.G. (2015). Post-Translational Modifications of Histones That Influence Nucleosome Dynamics. Chemical Reviews *115*, 2274-2295.

Box, N.F., Duffy, D.L., Chen, W., *et al.* (2001). MC1R genotype modifies risk of melanoma in families segregating CDKN2A mutations. The American Journal of Human Genetics *69*, 765-773.

Bray, N.L., Pimentel, H., Melsted, P., *et al.* (2016). Near-optimal probabilistic RNA-seq quantification. Nature biotechnology *34*, 525-527.

Brayer, K.J., and Segal, D.J. (2008). Keep your fingers off my DNA: protein-protein interactions mediated by C2H2 zinc finger domains. Cell biochemistry and biophysics *50*, 111-131.

Briknarová, K., Atwater, D.Z., Glicken, J.M., *et al.* (2011). The PR/SET domain in PRDM4 is preceded by a zinc knuckle. Proteins: Structure, Function, and Bioinformatics *79*, 2341-2345.

Brito, F.C., and Kos, L. (2008). Timeline and distribution of melanocyte precursors in the mouse heart. Pigment cell & melanoma research *21*, 464-470.

Bronisz, A., Sharma, S.M., Hu, R., *et al.* (2006). Microphthalmia-associated transcription factor interactions with 14-3-3 modulate differentiation of committed myeloid precursors. Molecular biology of the cell *17*, 3897-3906.

Bürkle, A. (2001). Posttranslational Modification. In, S. Brenner, and J.H.B.T.E.o.G. Miller, eds. (New York: Academic Press), pp. 1533-1533.

Bush, W.D., and Simon, J.D. (2007). Quantification of Ca2+ binding to melanin supports the hypothesis that melanosomes serve a functional role in regulating calcium homeostasis. Pigment cell research *20*, 134-139.

Buyse, I.M., Shao, G., and Huang, S. (1995). The retinoblastoma protein binds to RIZ, a zinc-finger protein that shares an epitope with the adenovirus E1A protein. Proceedings of the National Academy of Sciences of the United States of America *92*, 4467-4471.

Cancer Genome Atlas, N. (2015). Genomic Classification of Cutaneous Melanoma. Cell *161*, 1681-1696.

Carreira, S., Goodall, J., Aksan, I., *et al.* (2005). Mitf cooperates with Rb1 and activates p21Cip1 expression to regulate cell cycle progression. Nature *433*, 764-769.

Carreira, S., Goodall, J., Denat, L., *et al.* (2006). Mitf regulation of Dia1 controls melanoma proliferation and invasiveness. Genes & development *20*, 3426-3439.

Ceol, C.J., Houvras, Y., Jane-Valbuena, J., *et al.* (2011). The histone methyltransferase SETDB1 is recurrently amplified in melanoma and accelerates its onset. Nature *471*, 513-517.

Chappell, W.H., Steelman, L.S., Long, J.M., *et al.* (2011). Ras/Raf/MEK/ERK and PI3K/PTEN/Akt/mTOR inhibitors: rationale and importance to inhibiting these pathways in human health. Oncotarget *2*, 135.

Cheli, Y., Guiliano, S., Botton, T., *et al.* (2011). Mitf is the key molecular switch between mouse or human melanoma initiating cells and their differentiated progeny. Oncogene *30*, 2307-2318.

Chen, X., Chen, H., Cai, W., *et al.* (2017). The melanoma-linked "redhead" MC1R influences dopaminergic neuron survival. Ann Neurol *81*, 395-406.

Cheng, L., Lopez-Beltran, A., Massari, F., *et al.* (2018). Molecular testing for BRAF mutations to inform melanoma treatment decisions: a move toward precision medicine. Mod Pathol *31*, 24-38.

Chia, N.Y., Chan, Y.S., Feng, B., *et al.* (2010). A genome-wide RNAi screen reveals determinants of human embryonic stem cell identity. Nature *468*, 316-320.

Chien, A.J., Moore, E.C., Lonsdorf, A.S., *et al.* (2009). Activated Wnt/ß-catenin signaling in melanoma is associated with decreased proliferation in patient tumors and a murine melanoma model. Proceedings of the National Academy of Sciences *106*, 1193-1198.

Choi, S., Yamashita, E., Yasuhara, N., *et al.* (2014). Structural basis for the selective nuclear import of the C2H2 zinc-finger protein Snail by importin beta. Acta Crystallogr D Biol Crystallogr *70*, 1050-1060.

Cichorek, M., Wachulska, M., Stasiewicz, A., *et al.* (2013). Skin melanocytes: biology and development. Advances in Dermatology and Allergology/Postępy Dermatologii i Alergologii *30*, 30-41.

Clifton, M.K., Westman, B.J., Thong, S.Y., *et al.* (2014). The identification and structure of an N-terminal PR domain show that FOG1 is a member of the PRDM family of proteins. PloS one *9*, e106011-e106011.

Costin, G.-E., and Hearing, V.J. (2007). Human skin pigmentation: melanocytes modulate skin color in response to stress. The FASEB journal *21*, 976-994.

Cronin, J.C., Watkins-Chow, D.E., Incao, A., *et al.* (2013). SOX10 ablation arrests cell cycle, induces senescence, and suppresses melanomagenesis. Cancer Res *73*, 5709-5718.

Cronin, J.C., Wunderlich, J., Loftus, S.K., *et al.* (2009). Frequent mutations in the MITF pathway in melanoma. Pigment cell & melanoma research *22*, 435-444.

Cully, M., You, H., Levine, A.J., *et al.* (2006). Beyond PTEN mutations: the PI3K pathway as an integrator of multiple inputs during tumorigenesis. Nature Reviews Cancer *6*, 184-192.

Curtin, J.A., Busam, K., Pinkel, D., *et al.* (2006). Somatic activation of KIT in distinct subtypes of melanoma. Journal of clinical oncology *24*, 4340-4346.

Dahl, C., and Guldberg, P. (2007). The genome and epigenome of malignant melanoma. Apmis *115*, 1161-1176.

Damsky, W., and Bosenberg, M. (2017). Melanocytic nevi and melanoma: unraveling a complex relationship. Oncogene *36*, 5771-5792.

Davies, H., Bignell, G.R., Cox, C., *et al.* (2002). Mutations of the BRAF gene in human cancer. Nature *417*, 949-954.

Davis, C.A., Haberland, M., Arnold, M.A., *et al.* (2006). PRISM/PRDM6, a transcriptional repressor that promotes the proliferative gene program in smooth muscle cells. Mol Cell Biol *26*, 2626-2636.

de Almeida, M., Hinterndorfer, M., Brunner, H., *et al.* (2021). AKIRIN2 controls the nuclear import of proteasomes in vertebrates. Nature *599*, 491-496.

de Snoo, F.A., and Hayward, N.K. (2005). Cutaneous melanoma susceptibility and progression genes. Cancer Letters *230*, 153-186.

Denecker, G., Vandamme, N., Akay, Ö., *et al.* (2014). Identification of a ZEB2-MITF-ZEB1 transcriptional network that controls melanogenesis and melanoma progression. Cell Death & Differentiation *21*, 1250-1261.

Deng, Q., and Huang, S. (2004). PRDM5 is silenced in human cancers and has growth suppressive activities. Oncogene *23*, 4903-4910.

Dhomen, N., and Marais, R. (2007). New insight into BRAF mutations in cancer. Current opinion in genetics & development *17*, 31-39.

Dilixiati, R. (2019). The role of MITF in regulating transcriptional cell states in melanoma (University of Iceland).

Dilshat, R., Fock, V., Kenny, C., *et al.* (2021a). MITF reprograms the extracellular matrix and focal adhesion in melanoma. Elife *10*, e63093.

Dilshat, R., Vu, H.N., and Steingrímsson, E. (2021b). Epigenetic regulation during melanocyte development and homeostasis. Experimental Dermatology *30*, 1033-1050.

Du, J., Widlund, H.R., Horstmann, M.A., *et al.* (2004). Critical role of CDK2 for melanoma growth linked to its melanocyte-specific transcriptional regulation by MITF. Cancer cell *6*, 565-576.

Duan, Z., Person, R.E., Lee, H.-H., *et al.* (2007). Epigenetic regulation of protein-coding and microRNA genes by the Gfi1-interacting tumor suppressor PRDM5. Molecular and cellular biology *27*, 6889-6902.

Duarte, L.F., Young, A.R., Wang, Z., *et al.* (2014). Histone H3. 3 and its proteolytically processed form drive a cellular senescence programme. Nature communications *5*, 5210.

Eccles, M.R., He, S., Ahn, A., *et al.* (2013). MITF and PAX3 Play Distinct Roles in Melanoma Cell Migration; Outline of a "Genetic Switch" Theory Involving MITF and PAX3 in Proliferative and Invasive Phenotypes of Melanoma. Front Oncol *3*, 229.

Eichhoff, O.M., Weeraratna, A., Zipser, M.C., *et al.* (2011). Differential LEF1 and TCF4 expression is involved in melanoma cell phenotype switching. Pigment Cell Melanoma Res *24*, 631-642.

Elworthy, S., Lister, J.A., Carney, T.J., *et al.* (2003). Transcriptional regulation of mitfa accounts for the sox10 requirement in zebrafish melanophore development.

Emmons, M.F., Faião-Flores, F., Sharma, R., *et al.* (2019). HDAC8 Regulates a Stress Response Pathway in Melanoma to Mediate Escape from BRAF Inhibitor TherapyHDAC8 and Melanoma. Cancer research *79*, 2947-2961.

Eom, G.H., Kim, K., Kim, S.-M., *et al.* (2009). Histone methyltransferase PRDM8 regulates mouse testis steroidogenesis. Biochemical and Biophysical Research Communications *388*, 131-136.

Eram, M.S., Bustos, S.P., Lima-Fernandes, E., *et al.* (2014). Trimethylation of histone H3 lysine 36 by human methyltransferase PRDM9 protein. J Biol Chem *289*, 12177-12188.

Faiao-Flores, F., Alves-Fernandes, D., Pennacchi, P.C., *et al.* (2017). Targeting the hedgehog transcription factors GLI1 and GLI2 restores sensitivity to vemurafenib-resistant human melanoma cells. Oncogene *36*, 1849-1861.

Falletta, P., Sanchez-del-Campo, L., Chauhan, J., *et al.* (2017). Translation reprogramming is an evolutionarily conserved driver of phenotypic plasticity and therapeutic resistance in melanoma. Genes & development *31*, 18-33.

Falzone, L., Marconi, A., Loreto, C., *et al.* (2016). Occupational exposure to carcinogens: Benzene, pesticides and fibers. Molecular medicine reports *14*, 4467-4474.

Fan, J., Eastham, L., Varney, M.E., *et al.* (2010). Silencing and re-expression of retinoic acid receptor beta2 in human melanoma. Pigment cell & melanoma research *23*, 419-429.

Fan, J., Krautkramer, K.A., Feldman, J.L., *et al.* (2015). Metabolic Regulation of Histone Post-Translational Modifications. ACS Chemical Biology *10*, 95-108.

Fan, T., Jiang, S., Chung, N., *et al.* (2011). EZH2-Dependent Suppression of a Cellular Senescence Phenotype in Melanoma Cells by Inhibition of p21/CDKN1A ExpressionEZH2 Suppression of Melanoma Senescence. Molecular cancer research *9*, 418-429.

Fedorenko, I.V., Gibney, G.T., and Smalley, K.S. (2013). NRAS mutant melanoma: biological behavior and future strategies for therapeutic management. Oncogene *32*, 3009-3018.

Ferguson, J., Smith, M., Zudaire, I., *et al.* (2017). Glucose availability controls ATF4-mediated MITF suppression to drive melanoma cell growth. Oncotarget *8*, 32946.

Fiziev, P., Akdemir, K.C., Miller, J.P., *et al.* (2017). Systematic epigenomic analysis reveals chromatin states associated with melanoma progression. Cell reports *19*, 875-889.

Flørenes, V.A., Skrede, M., Jørgensen, K., *et al.* (2004). Deacetylase inhibition in malignant melanomas: impact on cell cycle regulation and survival. Melanoma research *14*, 173-181.

Flotho, A., and Melchior, F. (2013). Sumoylation: a regulatory protein modification in health and disease. Annual review of biochemistry *82*, 357-385.

Fock, V., Gudmundsson, S.R., Gunnlaugsson, H.O., *et al.* (2019). Subcellular localization and stability of MITF are modulated by the bHLH-Zip domain. Pigment Cell Melanoma Res *32*, 41-54.

Fog, C.K., Galli, G.G., and Lund, A.H. (2012). PRDM proteins: important players in differentiation and disease. BioEssays : news and reviews in molecular, cellular and developmental biology *34*, 50-60.

Fournier, M., and Tora, L. (2017). KAT2-mediated PLK4 acetylation contributes to genomic stability by preserving centrosome number. Molecular & Cellular Oncology *4*, e1270391-e1270391.

Fumasoni, I., Meani, N., Rambaldi, D., *et al.* (2007). Family expansion and gene rearrangements contributed to the functional specialization of PRDM genes in vertebrates. BMC evolutionary biology *7*, 1-11.

Gallagher, S.J., Mijatov, B., Gunatilake, D., *et al.* (2014a). Control of NF-kB activity in human melanoma by bromodomain and extra-terminal protein inhibitor I-BET 151. Pigment cell & melanoma research *27*, 1126-1137.

Gallagher, S.J., Mijatov, B., Gunatilake, D., *et al.* (2014b). The epigenetic regulator I-BET151 induces BIM-dependent apoptosis and cell cycle arrest of human melanoma cells. Journal of Investigative Dermatology *134*, 2795-2805.

Gallagher, S.J., Tiffen, J.C., and Hersey, P. (2015). Histone modifications, modifiers and readers in melanoma resistance to targeted and immune therapy. Cancers *7*, 1959-1982.

Gambichler, T., Sand, M., and Skrygan, M. (2013). Loss of 5-hydroxymethylcytosine and ten-eleven translocation 2 protein expression in malignant melanoma. Melanoma research *23*, 218-220.

Garraway, L.A., Weir, B.A., Zhao, X., *et al.* (2005). "Lineage addiction" in human cancer: lessons from integrated genomics. Cold Spring Harb Symp Quant Biol *70*, 25-34.

George, A., Zand, D.J., Hufnagel, R.B., *et al.* (2016). Biallelic Mutations in MITF Cause Coloboma, Osteopetrosis, Microphthalmia, Macrocephaly, Albinism, and Deafness. Am J Hum Genet *99*, 1388-1394.

Gershey, E., Haslett, G., Vidali, G., *et al.* (1969). Chemical studies of histone methylation: evidence for the occurrence of 3-methylhistidine in avian

erythrocyte histone fractions. Journal of Biological Chemistry *244*, 4871-4877.

Ghiorzo, P., Pastorino, L., Queirolo, P., *et al.* (2013). Prevalence of the E 318 K MITF germline mutation in Italian melanoma patients: associations with histological subtypes and family cancer history. Pigment cell & melanoma research *26*, 259-262.

Gibney, G.T., and Smalley, K.S. (2013). An unholy alliance: cooperation between BRAF and NF1 in melanoma development and BRAF inhibitor resistance. Cancer discovery *3*, 260-263.

Gilchrest, B.A., Eller, M.S., Geller, A.C., *et al.* (1999). The pathogenesis of melanoma induced by ultraviolet radiation. New England Journal of Medicine *340*, 1341-1348.

Giuliano, S., Cheli, Y., Ohanna, M., *et al.* (2010). Microphthalmia-associated transcription factor controls the DNA damage response and a lineage-specific senescence program in melanomas. Cancer research *70*, 3813-3822.

Giunta, E.F., Arrichiello, G., Curvietto, M., *et al.* (2021). Epigenetic Regulation in Melanoma: Facts and Hopes. Cells *10*, 2048.

Goding, C.R., and Arnheiter, H. (2019). MITF—the first 25 years. Genes & development *33*, 983-1007.

Goldstein, A.M., Chan, M., Harland, M., *et al.* (2007). Features associated with germline CDKN2A mutations: a GenoMEL study of melanoma-prone families from three continents. Journal of medical genetics *44*, 99-106.

Goodall, J., Carreira, S., Denat, L., *et al.* (2008). Brn-2 represses microphthalmia-associated transcription factor expression and marks a distinct subpopulation of microphthalmia-associated transcription factor–negative melanoma cells. Cancer research *68*, 7788-7794.

Goodall, J., Wellbrock, C., Dexter, T.J., *et al.* (2004). The Brn-2 transcription factor links activated BRAF to melanoma proliferation. Mol Cell Biol *24*, 2923-2931.

Greer, E.L., and Shi, Y. (2012). Histone methylation: a dynamic mark in health, disease and inheritance. Nature reviews Genetics *13*, 343-357.

Grill, C., Bergsteinsdóttir, K., Ögmundsdóttir, M.H., *et al.* (2013). MITF mutations associated with pigment deficiency syndromes and melanoma have different effects on protein function. Human Molecular Genetics *22*, 4357-4367.

Grob, J., Gouvernet, J., Aymar, D., *et al.* (1990). Count of benign melanocytic nevi as a major indicator of risk for nonfamilial nodular and superficial spreading melanoma. Cancer *66*, 387-395.

Guo, C., Chen, L.H., Huang, Y., *et al.* (2013). KMT2D maintains neoplastic cell proliferation and global histone H3 lysine 4 monomethylation. Oncotarget *4*, 2144.

Gyory, I., Wu, J., Fejer, G., *et al.* (2004). PRDI-BF1 recruits the histone H3 methyltransferase G9a in transcriptional silencing. Nat Immunol *5*, 299-308.

Halpern, A.C., Guerry, D., Elder, D.E., *et al.* (1991). Dysplastic nevi as risk markers of sporadic (nonfamilial) melanoma: a case-control study. Archives of dermatology *127*, 995-999.

Han, S., Ren, Y., He, W., *et al.* (2018). ERK-mediated phosphorylation regulates SOX10 sumoylation and targets expression in mutant BRAF melanoma. Nature Communications *9*, 28.

Handolias, D., Salemi, R., Murray, W., *et al.* (2010). Mutations in KIT occur at low frequency in melanomas arising from anatomical sites associated with chronic and intermittent sun exposure. Pigment cell & melanoma research *23*, 210-215.

Harland, M., Petljak, M., Robles-Espinoza, C.D., *et al.* (2016). Germline TERT promoter mutations are rare in familial melanoma. Familial cancer *15*, 139-144.

Hartman, M.L., Talar, B., Noman, M.Z., *et al.* (2014). Gene expression profiling identifies microphthalmia-associated transcription factor (MITF) and Dickkopf-1 (DKK1) as regulators of microenvironment-driven alterations in melanoma phenotype. PLoS One *9*, e95157.

Hayashi, K., Yoshida, K., and Matsui, Y. (2005). A histone H3 methyltransferase controls epigenetic events required for meiotic prophase. Nature *438*, 374-378.

He, L., Yu, J.X., Liu, L., *et al.* (1998). RIZ1, but not the alternative RIZ2 product of the same gene, is underexpressed in breast cancer, and forced RIZ1 expression causes G2-M cell cycle arrest and/or apoptosis. Cancer Res *58*, 4238-4244.

Heerschop, S., Fagrouch, Z., Verschoor, E.J., *et al.* (2021). Pinpointing the PRDM9-PRDM7 Gene Duplication Event During Primate Divergence. Front Genet *12*, 593725.

Heintzman, N.D., Stuart, R.K., Hon, G., *et al.* (2007). Distinct and predictive chromatin signatures of transcriptional promoters and enhancers in the human genome. Nature genetics *39*, 311-318.

Hemesath, T.J., Price, E.R., Takemoto, C., *et al.* (1998). MAP kinase links the transcription factor Microphthalmia to c-Kit signalling in melanocytes. Nature *391*, 298-301.

Hemesath, T.J., Steingrímsson, E., McGill, G., *et al.* (1994). Microphthalmia, a critical factor in melanocyte development, defines a discrete transcription factor family. Genes & development *8*, 2770-2780.

Hershey, C.L., and Fisher, D.E. (2005). Genomic analysis of the Microphthalmia locus and identification of the MITF-J/Mitf-J isoform. Gene *347*, 73-82.

Hodgkinson, C.A., Moore, K.J., Nakayama, A., *et al.* (1993). Mutations at the mouse microphthalmia locus are associated with defects in a gene encoding a novel basic-helix-loop-helix-zipper protein. Cell *74*, 395-404.

Hodis, E., Watson, I.R., Kryukov, G.V., *et al.* (2012). A landscape of driver mutations in melanoma. Cell *150*, 251-263.

Hoek, K.S., and Goding, C.R. (2010). Cancer stem cells versus phenotype-switching in melanoma. Pigment Cell Melanoma Res *23*, 746-759.

Hohenauer, T., and Moore, A.W. (2012). The Prdm family: expanding roles in stem cells and development. Development (Cambridge, England) *139*, 2267-2282.

Hoon, D.S., Spugnardi, M., Kuo, C., *et al.* (2004). Profiling epigenetic inactivation of tumor suppressor genes in tumors and plasma from cutaneous melanoma patients. Oncogene *23*, 4014-4022.

Horn, S., Figl, A., Rachakonda, P.S., *et al.* (2013). TERT promoter mutations in familial and sporadic melanoma. Science *339*, 959-961.

Hou, P., Liu, D., Dong, J., *et al.* (2012). The BRAFV600E causes widespread alterations in gene methylation in the genome of melanoma cells. Cell Cycle *11*, 286-295.

Huang, S. (2002). Histone methyltransferases, diet nutrients and tumour suppressors. Nature reviews Cancer *2*, 469-476.

Huang, S., Shao, G., and Liu, L. (1998). The PR domain of the Rb-binding zinc finger protein RIZ1 is a protein binding interface and is related to the SET domain functioning in chromatin-mediated gene expression. The Journal of biological chemistry *273*, 15933-15939.

Huber, W.E., Price, E.R., Widlund, H.R., *et al.* (2003). A tissue-restricted cAMP transcriptional response: SOX10 modulates α-melanocyte-stimulating hormone-triggered expression of microphthalmia-associated transcription factor in melanocytes. Journal of Biological Chemistry *278*, 45224-45230.

Ito, S., and Wakamatsu, K. (2003). Quantitative Analysis of Eumelanin and Pheomelanin in Humans, Mice, and Other Animals: a Comparative Review. Pigment Cell Research *16*, 523-531.

Jacquemin, P., Lannoy, V.J., O'Sullivan, J., *et al.* (2001). The transcription factor onecut-2 controls the microphthalmia-associated transcription factor gene. Biochemical and biophysical research communications *285*, 1200-1205.

Javelaud, D., Alexaki, V.I., Pierrat, M.J., *et al.* (2011). GLI2 and M-MITF transcription factors control exclusive gene expression programs and inversely regulate invasion in human melanoma cells. Pigment cell & melanoma research *24*, 932-943.

Jenuwein, T., Laible, G., Dorn, R., *et al.* (1998). SET domain proteins modulate chromatin domains in eu- and heterochromatin. Cellular and Molecular Life Sciences CMLS *54*, 80-93.

Kajimura, S., Seale, P., and Spiegelman, B.M. (2010). Transcriptional control of brown fat development. Cell Metab *11*, 257-262.

Kapoor, A., Goldberg, M.S., Cumberland, L.K., *et al.* (2010). The histone variant macroH2A suppresses melanoma progression through regulation of CDK8. Nature *468*, 1105-1109.

Karami Fath, M., Azargoonjahromi, A., Soofi, A., *et al.* (2022). Current understanding of epigenetics role in melanoma treatment and resistance. Cancer Cell International *22*, 1-23.

Kato, S., Weng, Q.Y., Insco, M.L., *et al.* (2020). Gain-of-Function Genetic Alterations of G9a Drive Oncogenesis. Cancer Discov *10*, 980-997.

Kawakami, A., and Fisher, D.E. (2017). The master role of microphthalmia-associated transcription factor in melanocyte and melanoma biology. Laboratory Investigation *97*, 649-656.

Kim, K.C., Geng, L., and Huang, S. (2003). Inactivation of a histone methyltransferase by mutations in human cancers. Cancer Res *63*, 7619-7623.

Konieczkowski, D.J., Johannessen, C.M., Abudayyeh, O., *et al.* (2014). A Melanoma Cell State Distinction Influences Sensitivity to MAPK Pathway InhibitorsMelanoma Cell State Affects Intrinsic MAPK Inhibitor Resistance. Cancer discovery *4*, 816-827.

Krauthammer, M., Kong, Y., Bacchiocchi, A., *et al.* (2015). Exome sequencing identifies recurrent mutations in NF1 and RASopathy genes in sun-exposed melanomas. Nature genetics *47*, 996-1002.

Lahtz, C., Stranzenbach, R., Fiedler, E., *et al.* (2010). Methylation of PTEN as a prognostic factor in malignant melanoma of the skin. The Journal of investigative dermatology *130*, 620-622.

Lang, D., Lu, M.M., Huang, L., *et al.* (2005). Pax3 functions at a nodal point in melanocyte stem cell differentiation. Nature *433*, 884-887.

Langmead, B., and Salzberg, S.L. (2012). Fast gapped-read alignment with Bowtie 2. Nature methods *9*, 357-359.

Larribere, L., Hilmi, C., Khaled, M., *et al.* (2005). The cleavage of microphthalmia-associated transcription factor, MITF, by caspases plays an

essential role in melanocyte and melanoma cell apoptosis. Genes & Development *19*, 1980-1985.

Laurette, P., Strub, T., Koludrovic, D., *et al.* (2015). Transcription factor MITF and remodeller BRG1 define chromatin organisation at regulatory elements in melanoma cells. Elife *4*, e06857.

Lawrence, M., Daujat, S., and Schneider, R. (2016). Lateral thinking: how histone modifications regulate gene expression. Trends in Genetics *32*, 42-56.

Le Douarin, N., LeDouarin, N.M., and Kalcheim, C. (1999). The neural crest (Cambridge university press).

Leclerc, J., Garandeau, D., Pandiani, C., *et al.* (2019). Lysosomal acid ceramidase ASAH1 controls the transition between invasive and proliferative phenotype in melanoma cells. Oncogene *38*, 1282-1295.

Lee, M., Goodall, J., Goding, C.R., *et al.* (2000). Direct regulation of the Microphthalmia promoter by Sox10 links Waardenburg-Shah syndrome (WS4)-associated hypopigmentation and deafness to WS2. Journal of Biological Chemistry *275*, 37978-37983.

Léger, S., Balguerie, X., Goldenberg, A., *et al.* (2012). Novel and recurrent non-truncating mutations of the MITF basic domain: genotypic and phenotypic variations in Waardenburg and Tietz syndromes. European Journal of Human Genetics *20*, 584-587.

Leonardi, G.C., Falzone, L., Salemi, R., *et al.* (2018). Cutaneous melanoma: From pathogenesis to therapy. International journal of oncology *52*, 1071-1080.

LeRoy, G., Rickards, B., and Flint, S. (2008). The double bromodomain proteins Brd2 and Brd3 couple histone acetylation to transcription. Molecular cell *30*, 51-60.

Levy, C., Khaled, M., and Fisher, D.E. (2006). MITF: master regulator of melanocyte development and melanoma oncogene. Trends Mol Med *12*, 406-414.

Lian, C.G., Xu, Y., Ceol, C., *et al.* (2012). Loss of 5-hydroxymethylcytosine is an epigenetic hallmark of melanoma. Cell *150*, 1135-1146.

Lister, J.A., Close, J., and Raible, D.W. (2001). Duplicate mitf genes in zebrafish: complementary expression and conservation of melanogenic potential. Developmental biology *237*, 333-344.

Livak, K.J., and Schmittgen, T.D. (2001). Analysis of relative gene expression data using real-time quantitative PCR and the 2− ΔΔCT method. methods *25*, 402-408.

Loercher, A.E., Tank, E.M., Delston, R.B., *et al.* (2005). MITF links differentiation with cell cycle arrest in melanocytes by transcriptional activation of INK4A. The Journal of cell biology *168*, 35-40.

Louphrasitthiphol, P., Siddaway, R., Loffreda, A., *et al.* (2020). Tuning transcription factor availability through acetylation-mediated genomic redistribution. Molecular cell *79*, 472-487. e410.

Ma, Z., Swigut, T., Valouev, A., *et al.* (2011). Sequence-specific regulator Prdm14 safeguards mouse ESCs from entering extraembryonic endoderm fates. Nat Struct Mol Biol *18*, 120-127.

Mallarino, R., Henegar, C., Mirasierra, M., *et al.* (2016). Developmental mechanisms of stripe patterns in rodents. Nature *539*, 518-523.

Mascolo, M., Vecchione, M.L., Ilardi, G., *et al.* (2010). Overexpression of Chromatin Assembly Factor-1/p60 helps to predict the prognosis of melanoma patients. BMC cancer *10*, 1-14.

McGill, G.l.G., Haq, R., Nishimura, E.K., *et al.* (2006). c-Met expression is regulated by Mitf in the melanocyte lineage. Journal of Biological Chemistry *281*, 10365-10373.

Medic, S., and Ziman, M. (2010). PAX3 expression in normal skin melanocytes and melanocytic lesions (naevi and melanomas). Plos one *5*, e9977.

Mehrotra, A., Mehta, G., Aras, S., *et al.* (2014). SWI/SNF chromatin remodeling enzymes in melanocyte differentiation and melanoma. Critical Reviews™ in Eukaryotic Gene Expression *24*.

Meyle, K.D., and Guldberg, P. (2009). Genetic risk factors for melanoma. Human genetics *126*, 499-510.

Micevic, G., Theodosakis, N., and Bosenberg, M. (2017). Aberrant DNA methylation in melanoma: biomarker and therapeutic opportunities. Clinical epigenetics *9*, 1-15.

Miller, A.J., Levy, C., Davis, I.J., *et al.* (2005). Sumoylation of MITF and its related family members TFE3 and TFEB. Journal of Biological Chemistry *280*, 146-155.

Mirmohammadsadegh, A., Marini, A., Nambiar, S., *et al.* (2006). Epigenetic silencing of the PTEN gene in melanoma. Cancer research *66*, 6546-6552.

Miyamoto, T., Koh, E., Sakugawa, N., *et al.* (2008). Two single nucleotide polymorphisms in PRDM9 (MEISETZ) gene may be a genetic risk factor for Japanese patients with azoospermia by meiotic arrest. Journal of assisted reproduction and genetics *25*, 553-557.

Möller, K., Sigurbjornsdottir, S., Arnthorsson, A.O., *et al.* (2019). MITF has a central role in regulating starvation-induced autophagy in melanoma. Scientific reports *9*, 1-12.

Mootha, V.K., Lindgren, C.M., Eriksson, K.-F., *et al.* (2003). PGC-1α-responsive genes involved in oxidative phosphorylation are coordinately downregulated in human diabetes. Nature Genetics *34*, 267-273.

Morera, L., Lübbert, M., and Jung, M. (2016). Targeting histone methyltransferases and demethylases in clinical trials for cancer therapy. Clinical Epigenetics *8*, 57-57.

Moro, N., Mauch, C., and Zigrino, P. (2014). Metalloproteinases in melanoma. European journal of cell biology *93*, 23-29.

Murakami, H., and Arnheiter, H. (2005). Sumoylation modulates transcriptional activity of MITF in a promoter-specific manner. Pigment cell research *18*, 265-277.

Ngeow, K.C., Friedrichsen, H.J., Li, L., *et al.* (2018). BRAF/MAPK and GSK3 signaling converges to control MITF nuclear export. Proc Natl Acad Sci U S A *115*, E8668-e8677.

Nguyen, N.T., and Fisher, D.E. (2019). MITF and UV responses in skin: From pigmentation to addiction. Pigment Cell Melanoma Res *32*, 224-236.

Nishimura, E.K. (2011). Melanocyte stem cells: a melanocyte reservoir in hair follicles for hair and skin pigmentation. Pigment Cell & Melanoma Research *24*, 401-410.

Ohanna, M., Cheli, Y., Bonet, C., *et al.* (2013). Secretome from senescent melanoma engages the STAT3 pathway to favor reprogramming of naive melanoma towards a tumor-initiating cell phenotype. Oncotarget *4*, 2212.

Ohanna, M., Giuliano, S., Bonet, C., *et al.* (2011). Senescent cells develop a PARP-1 and nuclear factor-κB-associated secretome (PNAS). Genes & development *25*, 1245-1261.

Orouji, E., Federico, A., Larribère, L., *et al.* (2019). Histone methyltransferase SETDB1 contributes to melanoma tumorigenesis and serves as a new potential therapeutic target. International journal of cancer *145*, 3462-3477.

Palmieri, M., Pal, R., Nelvagal, H.R., *et al.* (2017). mTORC1-independent TFEB activation via Akt inhibition promotes cellular clearance in neurodegenerative storage diseases. Nature communications *8*, 1-19.

Panetti, T.S. (2002). Tyrosine phosphorylation of paxillin, FAK, and p130CAS: effects on cell spreading and migration. Frontiers in Bioscience-Landmark *7*, 143-150.

Panni, S. (2019). Phospho-peptide binding domains in S. cerevisiae model organism. Biochimie *163*, 117-127.

Park, W.-Y., Hong, B.-J., Lee, J., *et al.* (2016). H3K27 demethylase JMJD3 employs the NF-κB and BMP signaling pathways to modulate the tumor microenvironment and promote melanoma progression and metastasis. Cancer research *76*, 161-170.

Parvanov, E.D., Petkov, P.M., and Paigen, K. (2010). Prdm9 controls activation of mammalian recombination hotspots. Science (New York, NY) *327*, 835-835.

Pennello, G., Devesa, S., and Gail, M. (2000). Association of surface ultraviolet B radiation levels with melanoma and nonmelanoma skin cancer in United States blacks. Cancer Epidemiology Biomarkers & Prevention *9*, 291-297.

Peterson, C.L., and Laniel, M.-A. (2004). Histones and histone modifications. Current biology : CB *14*, R546-551.

Phung, B., Kazi, J.U., Lundby, A.*, et al.* (2016). KIT/D816V induces SRC-mediated tyrosine phosphorylation of MITF and altered transcription program in melanoma. Cancer Research *76*, 1127-1127.

Pimentel, H., Bray, N.L., Puente, S.*, et al.* (2017). Differential analysis of RNA-seq incorporating quantification uncertainty. Nature Methods *14*, 687-690.

Pingault, V., Bondurand, N., Kuhlbrodt, K.*, et al.* (1998). SOX10 mutations in patients with Waardenburg-Hirschsprung disease. Nature Genetics *18*, 171-173.

Pinheiro, I., Margueron, R., Shukeir, N.*, et al.* (2012). Prdm3 and Prdm16 are H3K9me1 methyltransferases required for mammalian heterochromatin integrity. Cell *150*, 948-960.

Pinner, S., Jordan, P., Sharrock, K.*, et al.* (2009). Intravital imaging reveals transient changes in pigment production and Brn2 expression during metastatic melanoma dissemination. Cancer Res *69*, 7969-7977.

Platz, A., Egyhazi, S., Ringborg, U.*, et al.* (2008). Human cutaneous melanoma; a review of NRAS and BRAF mutation frequencies in relation to histogenetic subclass and body site. Molecular oncology *1*, 395-405.

Ploper, D., Taelman, V.F., Robert, L.*, et al.* (2015). MITF drives endolysosomal biogenesis and potentiates Wnt signaling in melanoma cells. Proceedings of the National Academy of Sciences *112*, E420-E429.

Pogenberg, V., Ballesteros-Álvarez, J., Schober, R.*, et al.* (2020). Mechanism of conditional partner selectivity in MITF/TFE family transcription factors with a conserved coiled coil stammer motif. Nucleic acids research *48*, 934-948.

Pogenberg, V., Ögmundsdóttir, M.H., Bergsteinsdóttir, K.*, et al.* (2012). Restricted leucine zipper dimerization and specificity of DNA recognition of the melanocyte master regulator MITF. Genes & development *26*, 2647-2658.

Qadeer, Z.A., Harcharik, S., Valle-Garcia, D.*, et al.* (2014). Decreased expression of the chromatin remodeler ATRX associates with melanoma progression. The Journal of investigative dermatology *134*, 1768.

Rabbani, P., Takeo, M., Chou, W., *et al.* (2011). Coordinated activation of Wnt in epithelial and melanocyte stem cells initiates pigmented hair regeneration. Cell *145*, 941-955.

Raimondi, S., Sera, F., Gandini, S., *et al.* (2008). MC1R variants, melanoma and red hair color phenotype: a meta-analysis. International journal of cancer *122*, 2753-2760.

Ramazi, S., and Zahiri, J. (2021). Post-translational modifications in proteins: resources, tools and prediction methods. Database *2021*.

Rambow, F., Marine, J.-C., and Goding, C.R. (2019). Melanoma plasticity and phenotypic diversity: therapeutic barriers and opportunities. Genes & development *33*, 1295-1318.

Ramsby, M.L., and Makowski, G.S. (1999). Differential detergent fractionation of eukaryotic cells. 2-D proteome analysis protocols, 53-66.

Randerson-Moor, J.A., Harland, M., Williams, S., *et al.* (2001). A germline deletion of p14ARF but not CDKN2A in a melanoma–neural system tumour syndrome family. Human molecular genetics *10*, 55-62.

Rastrelli, M., Tropea, S., Rossi, C.R., *et al.* (2014). Melanoma: epidemiology, risk factors, pathogenesis, diagnosis and classification. In vivo *28*, 1005-1011.

Raychaudhuri, S., Thomson, B.P., Remmers, E.F., *et al.* (2009). Genetic variants at CD28, PRDM1 and CD2/CD58 are associated with rheumatoid arthritis risk. Nature genetics *41*, 1313-1318.

Read, J., Wadt, K.A., and Hayward, N.K. (2016). Melanoma genetics. Journal of medical genetics *53*, 1-14.

Realini, N., Palese, F., Pizzirani, D., *et al.* (2016). Acid ceramidase in melanoma: expression, localization, and effects of pharmacological inhibition. Journal of Biological Chemistry *291*, 2422-2434.

Reisman, D., Glaros, S., and Thompson, E. (2009). The SWI/SNF complex and cancer. Oncogene *28*, 1653-1668.

Ren, B., Chee, K.J., Kim, T.H., *et al.* (1999). PRDI-BF1/Blimp-1 repression is mediated by corepressors of the Groucho family of proteins. Genes & development *13*, 125-137.

Riesenberg, S., Groetchen, A., Siddaway, R., *et al.* (2015). MITF and c-Jun antagonism interconnects melanoma dedifferentiation with pro-inflammatory cytokine responsiveness and myeloid cell recruitment. Nat Commun *6*, 8755.

Riley, P.A. (1997). Melanin. The international journal of biochemistry & cell biology *29*, 1235-1239.

Robles-Espinoza, C.D., Harland, M., Ramsay, A.J., *et al.* (2014). POT1 loss-of-function variants predispose to familial melanoma. Nature genetics *46*, 478-481.

Roesch, A., Fukunaga-Kalabis, M., Schmidt, E.C., *et al.* (2010). A temporarily distinct subpopulation of slow-cycling melanoma cells is required for continuous tumor growth. Cell *141*, 583-594.

Saginala, K., Barsouk, A., Aluru, J.S., *et al.* (2021). Epidemiology of melanoma. Medical sciences *9*, 63.

Saito, H., Yasumoto, K., Takeda, K., *et al.* (2002). Melanocyte-specific microphthalmia-associated transcription factor isoform activates its own gene promoter through physical interaction with lymphoid-enhancing factor 1. J Biol Chem *277*, 28787-28794.

Sarkar, D., Leung, E.Y., Baguley, B.C., *et al.* (2015). Epigenetic regulation in human melanoma: past and future. Epigenetics *10*, 103-121.

Sarraf, S.A., and Stancheva, I. (2004). RETRACTED: Methyl-CpG Binding Protein MBD1 Couples Histone H3 Methylation at Lysine 9 by SETDB1 to DNA Replication and Chromatin Assembly (Elsevier).

Schinke, C., Mo, Y., Yu, Y., *et al.* (2010). Aberrant DNA methylation in malignant melanoma. Melanoma research *20*, 253-265.

Schultz, D.C., Ayyanathan, K., Negorev, D., *et al.* (2002). SETDB1: a novel KAP-1-associated histone H3, lysine 9-specific methyltransferase that contributes to HP1-mediated silencing of euchromatic genes by KRAB zinc-finger proteins. Genes & development *16*, 919-932.

Sengupta, D., Byrum, S.D., Avaritt, N.L., *et al.* (2016). Quantitative histone mass spectrometry identifies elevated histone H3 lysine 27 (Lys27) trimethylation in melanoma. Molecular & Cellular Proteomics *15*, 765-775.

Senichkin, V.V., Prokhorova, E.A., Zhivotovsky, B., *et al.* (2021). Simple and efficient protocol for subcellular fractionation of normal and apoptotic cells. Cells *10*, 852.

Seo, E.Y., Jin, S.-P., Sohn, K.-C., *et al.* (2017). UCHL1 Regulates Melanogenesis through Controlling MITF Stability in Human Melanocytes. Journal of Investigative Dermatology *137*, 1757-1765.

Šestáková, B., Ondrušová, L., and Vachtenheim, J. (2010). Cell cycle inhibitor p21/WAF1/CIP1 as a cofactor of MITF expression in melanoma cells. Pigment cell & melanoma research *23*, 238-251.

Seto, E., and Yoshida, M. (2014). Erasers of histone acetylation: the histone deacetylase enzymes. Cold Spring Harbor perspectives in biology *6*, a018713.

Shakhova, O., Zingg, D., Schaefer, S.M., *et al.* (2012). Sox10 promotes the formation and maintenance of giant congenital naevi and melanoma. Nat Cell Biol *14*, 882-890.

Sigalotti, L., Covre, A., Fratta, E., *et al.* (2010). Epigenetics of human cutaneous melanoma: setting the stage for new therapeutic strategies. Journal of translational medicine *8*, 1-22.

Simons, A. (2010). A quality control tool for high throughput sequence data. A quality control tool for high throughput sequence data.

Skamnaki, V., Owen, D., Noble, M., *et al.* (1999). Catalytic mechanism of phosphorylase kinase probed by mutational studies. Biochemistry *38*, 14718-14730.

Smith, S.D., Kelley, P.M., Kenyon, J.B., *et al.* (2000). Tietz syndrome (hypopigmentation/deafness) caused by mutation of MITF. J Med Genet *37*, 446-448.

Soura, E., Eliades, P.J., Shannon, K., *et al.* (2016). Hereditary melanoma: Update on syndromes and management: Genetics of familial atypical multiple mole melanoma syndrome. Journal of the American Academy of Dermatology *74*, 395-407.

Souroullas, G.P., Jeck, W.R., Parker, J.S., *et al.* (2016). An oncogenic Ezh2 mutation induces tumors through global redistribution of histone 3 lysine 27 trimethylation. Nature medicine *22*, 632-640.

Steingrimsson, E. (2010). Interpretation of complex phenotypes: lessons from the Mitf gene. Pigment Cell Melanoma Res *23*, 736-740.

Steingrimsson, E., Copeland, N.G., and Jenkins, N.A. (2004). Melanocytes and the microphthalmia transcription factor network. Annu Rev Genet *38*, 365-411.

Steingrimsson, E., Moore, K.J., Lamoreux, M.L., *et al.* (1994). Molecular basis of mouse microphthalmia (mi) mutations helps explain their developmental and phenotypic consequences. Nat Genet *8*, 256-263.

Straume, O., Smeds, J., Kumar, R., *et al.* (2002). Significant impact of promoter hypermethylation and the 540 C> T polymorphism of CDKN2A in cutaneous melanoma of the vertical growth phase. The American journal of pathology *161*, 229-237.

Strub, T., Ballotti, R., and Bertolotto, C. (2020). The "ART" of epigenetics in melanoma: from histone "alterations, to resistance and therapies". Theranostics *10*, 1777.

Strub, T., Giuliano, S., Ye, T., *et al.* (2011). Essential role of microphthalmia transcription factor for DNA replication, mitosis and genomic stability in melanoma. Oncogene *30*, 2319-2332.

Sturm, R.A. (2009). Molecular genetics of human pigmentation diversity. Human molecular genetics *18*, R9-R17.

Sturm, R.A., Fox, C., McClenahan, P., *et al.* (2014). Phenotypic characterization of nevus and tumor patterns in MITF E318K mutation carrier melanoma patients. Journal of Investigative Dermatology *134*, 141-149.

Subramanian, A., Tamayo, P., Mootha, V.K., *et al.* (2005). Gene set enrichment analysis: a knowledge-based approach for interpreting genome-wide expression profiles. Proc Natl Acad Sci U S A *102*, 15545-15550.

Sujatha, S., and Chatterji, D. (2000). Understanding protein-protein interactions by genetic suppression. Journal of Genetics *79*, 125-129.

Sun, Q., Carrasco, Y.P., Hu, Y., *et al.* (2013). Nuclear export inhibition through covalent conjugation and hydrolysis of Leptomycin B by CRM1. Proceedings of the National Academy of Sciences *110*, 1303-1308.

Swygert, S.G., and Peterson, C.L. (2014). Chromatin dynamics: Interplay between remodeling enzymes and histone modifications. Biochimica et Biophysica Acta (BBA) - Gene Regulatory Mechanisms *1839*, 728-736.

Tachibana, M. (1999). Sound needs sound melanocytes to be heard. Pigment cell research *12*, 344-354.

Tachibana, M., Sugimoto, K., Nozaki, M., *et al.* (2002). G9a histone methyltransferase plays a dominant role in euchromatic histone H3 lysine 9 methylation and is essential for early embryogenesis. Genes Dev *16*, 1779-1791.

Takeda, K., Takemoto, C., Kobayashi, I., *et al.* (2000). Ser298 of MITF, a mutation site in Waardenburg syndrome type 2, is a phosphorylation site with functional significance. Human molecular genetics *9*, 125-132.

Tanemura, A., Terando, A.M., Sim, M.-S., *et al.* (2009). CpG island methylator phenotype predicts progression of malignant melanoma. Clinical Cancer Research *15*, 1801-1807.

Tassabehji, M., Newton, V.E., and Read, A.P. (1994). Waardenburg syndrome type 2 caused by mutations in the human microphthalmia (MITF) gene. Nature Genetics *8*, 251-255.

Terranova, C.J., Tang, M., Maitituoheti, M., *et al.* (2021). Reprogramming of bivalent chromatin states in NRAS mutant melanoma suggests PRC2 inhibition as a therapeutic strategy. Cell reports *36*, 109410.

Thomas, A.J., and Erickson, C.A. (2009). FOXD3 regulates the lineage switch between neural crest-derived glial cells and pigment cells by repressing MITF through a non-canonical mechanism.

Thomas, N.E., Berwick, M., and Cordeiro-Stone, M. (2006). Could BRAF Mutations in Melanocytic Lesions Arise from DNA Damage Induced by Ultraviolet Radiation? Journal of Investigative Dermatology *126*, 1693-1696.

Thurber, A.E., Douglas, G., Sturm, E.C., *et al.* (2011). Inverse expression states of the BRN2 and MITF transcription factors in melanoma spheres and tumour xenografts regulate the NOTCH pathway. Oncogene *30*, 3036-3048.

Tollefsbol, T.O. (2017). Handbook of Epigenetics: The New Molecular and Medical Genetics (Elsevier Science).

Truderung, O.A., Sagi, J.C., Semsei, A.F., *et al.* (2021). Melanoma susceptibility: An update on genetic and epigenetic findings. International Journal of Molecular Epidemiology and Genetics *12*, 71.

Tsoi, J., Robert, L., Paraiso, K., *et al.* (2018). Multi-stage differentiation defines melanoma subtypes with differential vulnerability to drug-induced iron-dependent oxidative stress. Cancer cell *33*, 890-904. e895.

Tsuneyoshi, N., Sumi, T., Onda, H., *et al.* (2008). PRDM14 suppresses expression of differentiation marker genes in human embryonic stem cells. Biochemical and Biophysical Research Communications *367*, 899-905.

Vachtenheim, J., and Borovanský, J. (2010). "Transcription physiology" of pigment formation in melanocytes: central role of MITF. Experimental dermatology *19*, 617-627.

van den Hurk, K., Niessen, H.E., Veeck, J., *et al.* (2012). Genetics and epigenetics of cutaneous malignant melanoma: a concert out of tune. Biochimica et Biophysica Acta (BBA)-Reviews on Cancer *1826*, 89-102.

Van Raamsdonk, C.D., Bezrookove, V., Green, G., *et al.* (2009). Frequent somatic mutations of GNAQ in uveal melanoma and blue naevi. Nature *457*, 599-602.

Vandewalle, C., Van Roy, F., and Berx, G. (2009). The role of the ZEB family of transcription factors in development and disease. Cellular and molecular life sciences *66*, 773-787.

Vardabasso, C., Gaspar-Maia, A., Hasson, D., *et al.* (2015). Histone variant H2A. Z. 2 mediates proliferation and drug sensitivity of malignant melanoma. Molecular cell *59*, 75-88.

Vardabasso, C., Hasson, D., Ratnakumar, K., *et al.* (2014). Histone variants: emerging players in cancer biology. Cellular and molecular life sciences *71*, 379-404.

Verastegui, C., Bille, K., Ortonne, J.-P., *et al.* (2000). Regulation of the microphthalmia-associated transcription factor gene by the Waardenburg syndrome type 4 gene, SOX10. Journal of Biological Chemistry *275*, 30757-30760.

Verfaillie, A., Imrichova, H., Atak, Z.K., *et al.* (2015). Decoding the regulatory landscape of melanoma reveals TEADS as regulators of the invasive cell state. Nature communications *6*, 1-16.

Vinod Saladi, S., Marathe, H., and de la Serna, I.L. (2010). SWItching on the transcriptional circuitry in melanoma. Epigenetics *5*, 469-475.

Vu, H.N., Dilshat, R., Fock, V., *et al.* (2021). User guide to MiT-TFE isoforms and post-translational modifications. Pigment Cell & Melanoma Research *34*, 13-27.

Walker, G.J., Flores, J.F., Glendening, J.M., *et al.* (1998). Virtually 100% of melanoma cell lines harbor alterations at the DNA level within CDKN2A, CDKN2B, or one of their downstream targets. Genes, Chromosomes and Cancer *22*, 157-163.

Wang, C., Zhao, L., Su, Q., *et al.* (2016). Phosphorylation of MITF by AKT affects its downstream targets and causes TP53-dependent cell senescence. The international journal of biochemistry & cell biology *80*, 132-142.

Watanabe, A., Takeda, K., Ploplis, B., *et al.* (1998). Epistatic relationship between Waardenburg Syndrome genes MITF and PAX3. Nature Genetics *18*, 283-286.

Watt, A.J., Kotsis, S.V., and Chung, K.C. (2004). Risk of melanoma arising in large congenital melanocytic nevi: a systematic review. Plastic and reconstructive surgery *113*, 1968-1974.

Wellbrock, C., and Marais, R. (2005). Elevated expression of MITF counteracts B-RAF—stimulated melanocyte and melanoma cell proliferation. The Journal of cell biology *170*, 703-708.

Wellbrock, C., Rana, S., Paterson, H., *et al.* (2008). Oncogenic BRAF regulates melanoma proliferation through the lineage specific factor MITF. PloS one *3*, e2734.

Wiesner, T., Obenauf, A.C., Murali, R., *et al.* (2011). Germline mutations in BAP1 predispose to melanocytic tumors. Nature genetics *43*, 1018-1021.

Wilmott, J.S., Colebatch, A.J., Kakavand, H., *et al.* (2015). Expression of the class 1 histone deacetylases HDAC8 and 3 are associated with improved survival of patients with metastatic melanoma. Modern Pathology *28*, 884-894.

Wittig, I., Braun, H.-P., and Schägger, H. (2006). Blue native PAGE. Nature protocols *1*, 418-428.

Wolfe, H.G., and Coleman, D.L. (1964). Mi-spotted:a mutation in the mouse. Genet Res Camb *5*, 432-440.

Wu, H., Goel, V., and Haluska, F.G. (2003). PTEN signaling pathways in melanoma. Oncogene *22*, 3113-3122.

Wu, M., Hemesath, T.J., Takemoto, C.M., *et al.* (2000). c-Kit triggers dual phosphorylations, which couple activation and degradation of the essential melanocyte factor Mi. Genes & development *14*, 301-312.

Wu, Y., Ferguson, J.E., 3rd, Wang, H., *et al.* (2008). PRDM6 is enriched in vascular precursors during development and inhibits endothelial cell proliferation, survival, and differentiation. J Mol Cell Cardiol *44*, 47-58.

Wu, Z., Zheng, S., Li, Z., *et al.* (2010). Polycomb protein EZH2 regulates E2F1-dependent apoptosis through epigenetically modulating Bim expression. Cell Death & Differentiation *17*, 801-810.

Xu, W., Gong, L., Haddad, M.M., *et al.* (2000). Regulation of microphthalmia-associated transcription factor MITF protein levels by association with the ubiquitin-conjugating enzyme hUBC9. Experimental cell research *255*, 135-143.

Yajima, I., and Larue, L. (2008). The location of heart melanocytes is specified and the level of pigmentation in the heart may correlate with coat color. Pigment cell & melanoma research *21*, 471-476.

Yang, G., Li, Y., Nishimura, E.K., *et al.* (2008). Inhibition of PAX3 by TGF-beta modulates melanocyte viability. Mol Cell *32*, 554-563.

Yasumoto, K., Amae, S., Udono, T., *et al.* (1998). A big gene linked to small eyes encodes multiple Mitf isoforms: many promoters make light work. Pigment Cell Res *11*, 329-336.

Ye, Y., Jin, L., Wilmott, J.S., *et al.* (2013). PI (4, 5) P2 5-phosphatase A regulates PI3K/Akt signalling and has a tumour suppressive role in human melanoma. Nature communications *4*, 1-15.

Yi, M., Yang, J., Chen, X., *et al.* (2011). RASSF1A suppresses melanoma development by modulating apoptosis and cell-cycle progression. Journal of Cellular Physiology *226*, 2360-2369.

Yokoyama, S., Woods, S.L., Boyle, G.M., *et al.* (2011). A novel recurrent mutation in MITF predisposes to familial and sporadic melanoma. Nature *480*, 99-103.

Yu, J., Angelin-Duclos, C., Greenwood, J., *et al.* (2000). Transcriptional Repression by Blimp-1 (PRDI-BF1) Involves Recruitment of Histone Deacetylase. Molecular and cellular biology *20*, 2592-2603.

Yu, Y., Schleich, K., Yue, B., *et al.* (2018). Targeting the senescence-overriding cooperative activity of structurally unrelated H3K9 demethylases in melanoma. Cancer cell *33*, 322-336. e328.

Zee, B.M., Levin, R.S., Xu, B., *et al.* (2010). In vivo residue-specific histone methylation dynamics. The Journal of biological chemistry *285*, 3341-3350.

Zentner, G.E., and Henikoff, S. (2013). Regulation of nucleosome dynamics by histone modifications. Nature structural & molecular biology *20*, 259-266.

Zhao, X., Fiske, B., Kawakami, A., *et al.* (2011). Regulation of MITF stability by the USP13 deubiquitinase. Nature Communications *2*, 414.

Original publications

Paper I

Received: 4 July 2020 | Revised: 31 July 2020 | Accepted: 13 August 2020

DOI: 10.1111/pcmr.12922

REVIEW

WILEY

User guide to MiT-TFE isoforms and post-translational modifications

Hong Nhung Vu | **Ramile Dilshat** | **Valerie Fock** | **Eiríkur Steingrímsson**

Department of Biochemistry and Molecular Biology, BioMedical Center, Faculty of Medicine, University of Iceland, Reykjavík, Iceland

Correspondence
Eiríkur Steingrímsson, Department of Biochemistry and Molecular Biology, BioMedical Center, Faculty of Medicine, University of Iceland, Sturlugata 8, 102 Reykjavík, Iceland.
Email: eirikurs@hi.is

Present address
Valerie Fock, Department of Dermatology, Medical University of Vienna, Vienna, Austria

Funding information
Grants from the Research Fund of Iceland, Grant/Award Number: 184861 and 207067; The University of Iceland Doctoral Grants Fund

Abstract

The microphthalmia-associated transcription factor (MITF) is at the core of melanocyte and melanoma fate specification. The related factors TFEB and TFE3 have been shown to be instrumental for transcriptional regulation of genes involved in lysosome biogenesis and autophagy, cellular processes important for mediating nutrition signals and recycling of cellular materials, in many cell types. The MITF, TFEB, TFE3, and TFEC proteins are highly related. They share many structural and functional features and are targeted by the same signaling pathways. However, the existence of several isoforms of each factor and the increasing number of residues shown to be post-translationally modified by various signaling pathways poses a difficulty in indexing amino acid residues in different isoforms across the different proteins. Here, we provide a resource manual to cross-reference amino acids and post-translational modifications in all isoforms of the MiT-TFE family in humans, mice, and zebrafish and summarize the protein accession numbers for each isoform of these factors in the different genomic databases. This will facilitate future studies on the signaling pathways that regulate different isoforms of the MiT-TFE transcription factor family.

KEYWORDS
isoform, MITF, post-translational modifications, TFE, transcription factor

1 | INTRODUCTION

The MiT-TFE family of transcription factors consists of the MITF, TFEB, TFE3, and TFEC proteins (Hemesath et al., 1994; Hodgkinson, et al., 1993). They all share the common basic helix-loop-helix leucine zipper (bHLH-Zip) motif required for dimerization and DNA binding as well as a couple of other functional domains including transactivation and nuclear translocation domains (reviewed in Goding & Arnheiter, 2019; Steingrímsson, Copeland, & Jenkins, 2004). These proteins can bind DNA as either homodimers or as heterodimers exclusively with each other but not with other members of the bHLH-Zip family of proteins (Hemesath et al., 1994; Pogenberg et al., 2012). In principle, four homodimers and six heterodimers can be generated between MiT-TFE family members. However, little is known about the relative affinities of the different monomers to each other in the different cells and tissues where they are expressed. The restriction of dimerization within the MiT-TFE family is due to the presence of a three-residue sequence EQQ[260–262] (based on MITF-M numbering) in the zipper domain of only the MiT-TFE subfamily of bHLH-Zip transcription factors (Pogenberg et al., 2012, 2020).

MITF has emerged as a key regulator of proliferation, differentiation, cell cycle, and survival of melanocytes and melanoma cells (reviewed in Goding & Arnheiter, 2019). It also affects mast cells, retinal pigment epithelium (RPE) and osteoclast development and in addition plays a role in olfaction as well as in circadian regulation of gene expression (Atacho et al., 2020; Malcov-Brog et al., 2018; Morii et al., 1996; Shibahara et al., 2000; Weilbaecher et al., 2001). In humans, MITF mutations have been linked to Tietz syndrome (Amiel, Watkin, Tassabehji, Read, & Winter, 1998; Smith, Kelley, Kenyon,

& Hoover, 2000), Waardenburg syndrome type 2A (Tassabehji, Newton, & Read, 1994) as well as the more serious COMMAD syndrome observed in individuals carrying MITF mutations on each of the two chromosomes (George et al., 2016). Importantly, it has been shown that MITF plays a role in melanoma where it regulates proliferation and invasiveness (Carreira et al., 2006) and has been suggested as a distinct class of lineage survival oncogene for both tissue-specific cancer development and tumor progression (Garraway et al., 2005). Notably, individuals carrying the Glu318Lys germline mutation, which affects a SUMO-site in MITF, have an increased chance of developing melanoma (Bertolotto et al., 2011; Yokoyama et al., 2011).

TFEB and TFE3 are known as master controllers of lysosomal biogenesis and autophagy in many cell types. They are important for nutrient sensing and regulation of energy metabolism (Martina et al., 2014; Roczniak-Ferguson et al., 2012; Sardiello et al., 2009; Settembre et al., 2011). Under normal physiological conditions, mTORC1 directly mediates the phosphorylation of TFEB and TFE3, which leads to cytoplasmic retention of these proteins due to interaction with 14-3-3 proteins (Martina, Chen, Gucek, & Puertollano, 2012; Martina et al., 2014; Roczniak-Ferguson et al., 2012). When mTOR is inactivated upon starvation, it leads to dephosphorylation of TFEB and TFE3 by calcineurin (Medina et al., 2015; Settembre et al., 2011), resulting in nuclear translocation and transcriptional activation of genes important for recycling of cellular components (Medina et al., 2015; Settembre & Ballabio, 2011; Zhang et al., 2016). MITF has also been implicated in regulating the expression of genes involved in endolysosomal biogenesis and the starvation-induced autophagy response (Möller et al., 2019; Ploper et al., 2015; Zhang et al., 2015).

Like MITF, TFEB and TFE3 have been linked to cancer. Translocations of *TFEB* or *TFE3* have been described in a distinct subset of renal cell carcinoma (RCC), with *TFE3* translocations more frequent than those of *TFEB* (Zhong et al., 2012; reviewed in Raben & Puertollano, 2016). At least fourteen different *TFE3* translocation partners have been identified consisting of *ASPL* (Argani et al., 2001), *PRCC* (Shipley et al., 1995), *PSF/SFPQ* (Clark et al., 1997), *NonO* (Clark et al., 1997), *CLTC* (Argani et al., 2003), *PARP14* (Huang et al., 2015), *GRIPAP1* (Classe et al., 2017), *MED15* (Ye et al., 2019), *LUC7L3* (Malouf et al., 2014), *KHSRP* (Malouf et al., 2014), *NEAT1* (Pei et al., 2019), *KAT6A* (Pei et al., 2019), *DVL2*, and *RBM10* (Cancer Genome Atlas Research Network et al., 2016). The multiple gene rearrangements lead to various fusion proteins but all chimeric TFE3 proteins contain the bHLH-Zip domain of TFE3 and are overexpressed under the regulation of the partner's promoter, resulting in abnormal *TFE3* expression (Kauffman et al., 2014). Approximately 40% of pediatric RCC involve *TFE3* translocations (Ross & Argani, 2010), whereas only around 1%–5% of adult RCC are associated with *TFE3* translocations (Komai et al., 2009; Zhong et al., 2012). Additionally, *TFE3* gene fusions have been found in alveolar soft part sarcomas (Argani et al., 2001; Ladanyi et al., 2001). Several fusion partners have also been found for *TFEB* in RCC, including *MALAT1* (Argani et al., 2005; Davis et al., 2003), *COL21A*, and *CADM2* (Cancer Genome Atlas Research Network et al., 2016). The *MALAT1-TFEB* fusion retains the full *TFEB* coding region but its expression is regulated from the highly activated *MALAT1* promoter, resulting in overexpression of TFEB (Kuiper et al., 2003; reviewed in Raben & Puertollano, 2016). Additionally, TFEB and TFE3 have been shown to play a role in pancreatic ductal adenocarcinoma (PDA; Perera et al., 2015). In PDA cells, TFEB and TFE3 are constitutively transported to the nucleus and as a result, the expression of genes responsible for PDA growth is considerably increased (Perera et al., 2015). In contrast, the functional role of TFEC remains largely uncharacterized.

2 | MiT-TFE ISOFORMS

2.1 | MITF isoforms

The human *MITF* gene spans approximately 230,000 bp and is located on chromosome 3 (GRCh38/hg38 chr3:69,739,435–69,968,336), whereas the mouse *Mitf* gene is on chromosome 6 and extends over 215,000 bp (GRCm38/mm10 chr6:97,807,058–98,021,349). Both human *MITF* and mouse *Mitf* genes are significantly conserved, and they share a similar gene organization with several promoters and tissue-specific first exons as well as the common exons 2–9 (reviewed in Goding & Arnheiter, 2019). Due to alternative promoter usage and splicing, the human *MITF* and mouse *Mitf* genes generate multiple mRNAs and protein isoforms which differ primarily at their 5′-ends and amino termini, respectively. The distinct first exons are termed exon 1A, 1B1a, 1C, 1D, 1E, 1J, 1H, 1Mc, and 1M (Figure 1; reviewed in Goding & Arnheiter, 2019). Each of these first exons is regulated by specific promoters. Thus, there are nine distinct promoters and nine major *MITF/Mitf* mRNAs which are generally named by their unique first exon, as summarized in Tables 1 and 2. The *MITF/Mitf-A*, *Mitf-D*, *Mitf-J*, *Mitf-H*, and *Mitf-M* isoforms have been identified in both human and mouse whereas the mouse homolog of the human *MITF-B* and *MITF-C* transcripts and the human homolog of the mouse *Mitf-E* and *Mitf-Mc* transcripts were later identified in genomic DNA and can be translated (Hershey & Fisher, 2005). It should be noted that the full-length protein sequences of several human and mouse MITF isoforms are currently not available in all databases or have been only predicted by automated computational analysis (Tables 1 and 2). Adding a level of confusion, the nomenclature system of mouse and human MITF differs between databases as well as between the two species. In the NCBI database, the human MITF isoforms are named as isoforms 1–5, 7, and 9 without direct reference to the genetic nomenclature (Table 1). Meanwhile, the mouse MITF isoforms are numbered in the order of identification, with the mouse MITF-A, MITF-M, and MITF-H isoforms termed MITF isoforms 1, 2, and 3, respectively (Table 2).

In both human and mouse, each of the isoform-specific exons 1A, 1B1a, 1C, 1D, 1E, 1J, 1Mc, and 1H is spliced to exon 1B1b; and then to the common exons 2–9. In addition, there is exon 1M which is directly joined to exons 2–9. Five of the first exons of human *MITF*, including exons 1A, 1B1a, 1C, 1H, and 1M, contain their own

FIGURE 1 Schematic representation of the human *MITF* isoforms showing the distinct N-termini. The alternative exon 6A has been described in human MITF-A, MITF-H, and MITF-M proteins. Translation start and stop codons are indicated by the (▾) symbol and (*) symbol, respectively. The (▽) symbol shows the alternative start codon of the MITF-B isoform. The numbers indicate amino acid residues. The cell lines exhibiting the major expression of the human MITF isoforms according to the FANTOM database are presented

translation initiation sites (reviewed in Goding & Arnheiter, 2019). As a result, the human 1A, 1B1a, 1C, 1H, and 1M exons encode 35, 10, 34, 19, and 11 amino acids, respectively (Figure 1). However, the first methionine residue located in exon 1B1b has also been proposed as a translation start site for the *MITF-B* mRNA, translating into either 468- or 474-residue proteins (reviewed in Goding & Arnheiter, 2019). In contrast, human exons 1J, 1Mc, 1E, and 1D do not contain a start codon. Therefore, the proposed translation start sites of the resulting transcripts are located in exon *1B1b* and are the same as the alternative start codon of the *MITF-B* transcript (Figure 1). Thus, the nine different splice forms of human *MITF* generate at least six distinct proteins with different amino termini. In the mouse *Mitf* gene, a start codon is present in exons 1A, 1B1a, 1C, 1H, 1Mc, and 1M, whereas exon 1J, 1E, and 1D do not include their own translation start sites. The mouse *Mitf-A*, *Mitf-B*, *Mitf-D*, *Mitf-E*, *Mitf-J*, *Mitf-H*, and *Mitf-M* transcripts are expected to be translated into proteins which are of the same length as the human counterparts; each of the mouse and human isoforms shares approximately 95% identity with their corresponding human MITF protein homologs. Conversely, the mouse *Mitf-C* and *Mitf-Mc* transcripts are translated into proteins containing 11- and 43-residue unique amino termini, respectively, which are different from those of the human MITF-C and MITF-Mc proteins.

In zebrafish, there are two *mitf* genes encoding two Mitf proteins, termed Mitfa and Mitfb (Table 3). The zebrafish *mitfa* gene spans approximately 6,600 bp and is located on chromosome 6 (GRCz11/danRer11 chr6:43,426,669–43,433,277), whereas the zebrafish *mitfb* gene extends over 53,000 bp and is found on chromosome 23 (GRCz11/danRer11 chr23:711,075–764,135). The zebrafish Mitfa and Mitfb proteins are homologs of human MITF-M and MITF-A, respectively (Lister, Close, & Raible, 2001). Two zebrafish *mitfb* isoforms translating into either 427- or 500-residue proteins have been identified and reported in both NCBI and UNIPROT databases (Table 3). Confusingly, while the zebrafish Mitfb 427-residue protein is called microphthalmia-associated transcription factor b, the zebrafish Mitfb 500-residue protein is called melanocyte-inducing transcription factor b in the UNIPROT database (Table 3).

The human and mouse MITF isoforms are further classified into MITF(+) or MITF(−) isoforms based on containing or lacking a six-amino acid fragment (ACIFPT) encoded by the 18 bp exon 6A (Figure 2). While this small insert region has been found in the *MITF-A*/*Mitf-A*, *MITF-H*/*Mitf-H*, *Mitf-E*, *Mitf-J*, *Mitf-Mc*, and *MITF-M*/*Mitf-M* transcripts (Amae et al., 1998; Hallsson et al., 2000; Murakami, Iwata, & Funaba, 2007; Primot et al., 2010), the other human and mouse isoforms also are expected to express it but have not been described in the literature. It has been shown that the ratio of the (+) and (−) isoforms is controlled by the MEK1-ERK2 pathway (Primot et al., 2010). Functional differences have been observed between the (+) and (−) isoforms of MITF. In melanocytes, MITF(+) affects cell cycle regulation by interfering with S-phase (Bismuth, Maric, & Arnheiter, 2005). Interestingly, the specific DNA binding ability of the MITF(−) isoform to its cognate binding sites (the E-box and the M-box) is reduced when compared to the MITF(+) isoform (Pogenberg et al., 2012). The expression of the MITF(−) isoform has been suggested to be increased in metastatic melanoma (Primot et al., 2010). In the zebrafish *mitfa* and *mitfb* genes, the region occupied by the six-amino acid fragment (ACIFPT) in mammalian MITF contains an unrelated 31-amino acid sequence. All zebrafish *mitfa*

TABLE 1 Summary of human MITF isoforms

				NCBI database		UNIPROT database		
	Isoform	Species	Length	Accession number of proteins	Description in NCBI database	Accession number of proteins	Description in UNIPROT database	Ref.
1	MITF-A−	*Homo sapiens*	520 aa	NP_937802.1	Microphthalmia-associated transcription factor isoform 1	O75030-2	Microphthalmia-associated transcription factor isoform A2	(Amae et al., 1998)
2	MITF-A+	*Homo sapiens*	526 aa	NP_001341533.1	Microphthalmia-associated transcription factor isoform 9	O75030-1	Microphthalmia-associated transcription factor isoform A1	
3	MITF-B−	*Homo sapiens*	495 aa	_	_	O75030-4	Microphthalmia-associated transcription factor isoform B2	(Udono et al., 2000)
4	MITF-B+	*Homo sapiens*	501 aa	_	_	O75030-3	Microphthalmia-associated transcription factor isoform B1	
5	MITF-D−/E−/J−/Mc−	*Homo sapiens*	468 aa	NP_001171896.1	Microphthalmia-associated transcription factor isoform 7	O75030-12	Microphthalmia-associated transcription factor isoform 12	(Hershey & Fisher, 2005; Oboki et al., 2002; Takeda et al., 2002; Takemoto et al., 2002)
6	MITF-D+/E+/J+/Mc+	*Homo sapiens*	474 aa	_	_	_	_	
7	MITF-C−	*Homo sapiens*	519 aa	NP_006713.1	Microphthalmia-associated transcription factor isoform 3	O75030-6	Microphthalmia-associated transcription factor isoform C2	(Fuse et al., 1999)
8	MITF-C+	*Homo sapiens*	525 aa	_	_	O75030-5	Microphthalmia-associated transcription factor isoform C1	
9	MITF-H−	*Homo sapiens*	504 aa	NP_937820.1	Microphthalmia-associated transcription factor isoform 2	O75030-8	Microphthalmia-associated transcription factor isoform H2	(Amae et al., 1998)
10	MITF-H+	*Homo sapiens*	510 aa	_	_	O75030-7	Microphthalmia-associated transcription factor isoform H1	
11	MITF-M−	*Homo sapiens*	413 aa	NP_937801.1	Microphthalmia-associated transcription factor isoform 5	O75030-10	Microphthalmia-associated transcription factor isoform M2	(Tassabehji et al., 1994; Yasumoto et al., 1998)
12	MITF-M+	*Homo sapiens*	419 aa	NP_000239.1	Microphthalmia-associated transcription factor isoform 4	O75030-9	Microphthalmia-associated transcription factor isoform M1	

Note: (_) The full-length protein sequence of the human MITF isoform is currently not available in the respective database.

TABLE 2 Summary of mouse MITF isoforms

				NCBI database		UNIPROT database		
	Isoform	Species	Length	Accession number of proteins	Description in NCBI database	Accession number of proteins	Description in UNIPROT database	Ref.
1	MITF-A+	*Mus musculus*	526aa	NP_001106669.1	Microphthalmia-associated transcription factor isoform 1	Q08874-1	Microphthalmia-associated transcription factor isoform A	(Amae et al., 1998)
2	MITF-A−	*Mus musculus*	520aa	*XP_006505748.1	Microphthalmia-associated transcription factor isoform X2	A0A5H1ZRM6-1	Microphthalmia-associated transcription factor	
3	MITF-B+	*Mus musculus*	501 aa	_	_	_	_	(Hershey & Fisher, 2005; Udono et al., 2000)
4	MITF-B−	*Mus musculus*	495 aa	_	_	_	_	
5	MITF-C+	*Mus musculus*	502 aa	_	_	_	_	(Fuse et al., 1999; Hershey & Fisher, 2005)
6	MITF-C−	*Mus musculus*	496 aa	_	_	_	_	
7	MITF-D+/E+/J+	*Mus musculus*	474 aa	*XP_006505757.1	Microphthalmia-associated transcription factor isoform X8	_	_	(Hershey & Fisher, 2005; Oboki et al., 2002; Takeda et al., 2002)
8	MITF-D−/E−/J−	*Mus musculus*	468 aa	*XP_030111074.1	Microphthalmia-associated transcription factor isoform X9	_	_	
9	MITF-H+	*Mus musculus*	510 aa	NP_001171520.1	Microphthalmia-associated transcription factor isoform 3	Q08874-4	Microphthalmia-associated transcription factor isoform H	(Steingrímsson et al., 1994)
10	MITF-H−	*Mus musculus*	504 aa	*XP_030111071.1	Microphthalmia-associated transcription factor isoform X5	_	_	
11	MITF-M+	*Mus musculus*	419 aa	NP_032627.1	Microphthalmia-associated transcription factor isoform 2	Q08874-8	Microphthalmia-associated transcription factor isoform M	(Hodgkinson, et al., 1993)
12	MITF-M−	*Mus musculus*	413 aa	*XP_006505758.1	Microphthalmia-associated transcription factor isoform X10	Q08874-9	Microphthalmia-associated transcription factor isoform M1	
13	MITF-Mc+	*Mus musculus*	534 aa	_	_	_	_	(Takemoto et al., 2002)
14	MITF-Mc−	*Mus musculus*	528 aa	_	_	_	_	

Note: (_) The full-length protein sequence of the mouse MITF isoform is currently not available in the respective database.

(*) The full-length protein sequence of the mouse MITF isoform is predicted by automated computational analysis.

TABLE 3 Summary of zebrafish Mitf isoforms

	Isoform	Species	Length	NCBI database		UNIPROT database		Ref.
				Accession number of proteins	Description in NCBI database	Accession number of proteins	Description in UNIPROT database	
1	Mitfa	*Danio rerio*	412 aa	NP_570998.1	Melanocyte-inducing transcription factor isoform 1	Q9PWC2-1	Melanocyte-inducing transcription factor a	(Lister, Robertson, Lepage, Johnson, & Raible, 1999)
2	Mitfb	*Danio rerio*	427 aa	AAK95588.1	Microphthalmia-associated transcription factor b	Q90XP4-1	Microphthalmia-associated transcription factor b	(Lister et al., 2001)
			500 aa	NP_571922.2	Melanocyte-inducing transcription factor b	F1Q885-1	Melanocyte-inducing transcription factor b	

and *mitfb* transcripts described to date contain the 31-amino acid sequence. Clearly, it would be interesting to investigate further the role of the six and 31-amino acid sequences in melanocytes and melanoma in the different species. In addition to the 18 bp alternative splice forms, several other alternatives splicing events have been described in MITF, for example, an isoform lacking a portion of exon 2 (Bauer et al., 2009; Debbache et al., 2012) and the M-Del isoform (Wang, Radfar, Liu, Riker, & Khong, 2010). The characterization of these isoforms is limited. Currently, it is not known if all theoretical combinations of splice forms are expressed (e.g., does the M-Del variant exist for all isoforms?) and therefore the total number of alternative MITF transcripts and proteins is currently not known.

The *MITF* isoforms are expressed in a tissue-specific manner (Figure 1). For example, *MITF-M* is expressed mainly in melanocytes and melanoma cells (Hershey & Fisher, 2005; Hodgkinson, et al., 1993; Yasumoto et al., 1998) and *MITF-Mc* is only detected in mastocytoma cell lines (Hershey & Fisher, 2005; Takemoto, Yoon, & Fisher, 2002). In addition, *MITF-E* is highly expressed in mast cells and *MITF-D* mainly accumulates in RPE, macrophages, mast cells, and osteoclasts (Bharti, Liu, Csermely, Bertuzzi, & Arnheiter, 2008; Hershey & Fisher, 2005; Oboki, Morii, Kataoka, Jippo, & Kitamura, 2002; Takeda et al., 2002). In contrast, *MITF-A*, *MITF-B*, *MITF-H*, and *MITF-J* are found in many cell types, with *MITF-H* being enriched in the heart and *MITF-A* and *-J* presenting through RPE development (Bharti et al., 2008; Hershey & Fisher, 2005; Steingrímsson et al., 1994; Tshori et al., 2007). Despite being detected in many cell lines, *MITF-C* is not found in cells of the melanocyte-lineage (Fuse et al., 1999). Consistent with the literature, the GTEx database shows that the *MITF-A* and *MITF-C* transcripts are widely expressed in many human tissues and have the highest expression level as compared to the other MITF isoforms, whereas the *MITF-M* transcript is found mainly in skin, adipose tissue, muscle and uterus (GTEx Consortium, 2013). Cell type-specific expression of the MITF isoforms can also be read in the FANTOM database based on the transcription start site (TSS) expression signal (Figure 1). This shows that *MITF-E* is mostly expressed in mast cells and *MITF-M* only in melanocytes and melanoma cell lines. According to FANTOM, the *MITF-Mc* transcript is detected in promyelocytes/myelocytes and mesenchymal stem cells (Noguchi et al., 2017).

The functional role of the different *MITF* isoforms has not been fully investigated. Isoform-specific knockouts showed that mice lacking *Mitf-M* do not have melanocytes in the epidermis, hair follicle, iris, and choroid, whereas there was no change of pigmentation in RPE and iris (Flesher et al., 2020). Surprisingly, both *Mitf-M* knockout mice and *Mitf-A* overexpressing mice showed enlarged kidneys (Flesher et al., 2020; Phelep et al., 2017). Knocking out the *Mitf-A* isoform only resulted in minor changes in melanin accumulation in the hair, reduced expression of Tyrosinase in the eye, and reduced number of nephrons (Flesher et al., 2020; Phelep et al., 2017). Clearly, the M-isoform is critical for pigmentation whereas the A isoform plays a limited role for this phenotype. Isoform-specific knockouts have not been generated for the other first exons but cell work suggests that the H-isoforms are involved in regulating

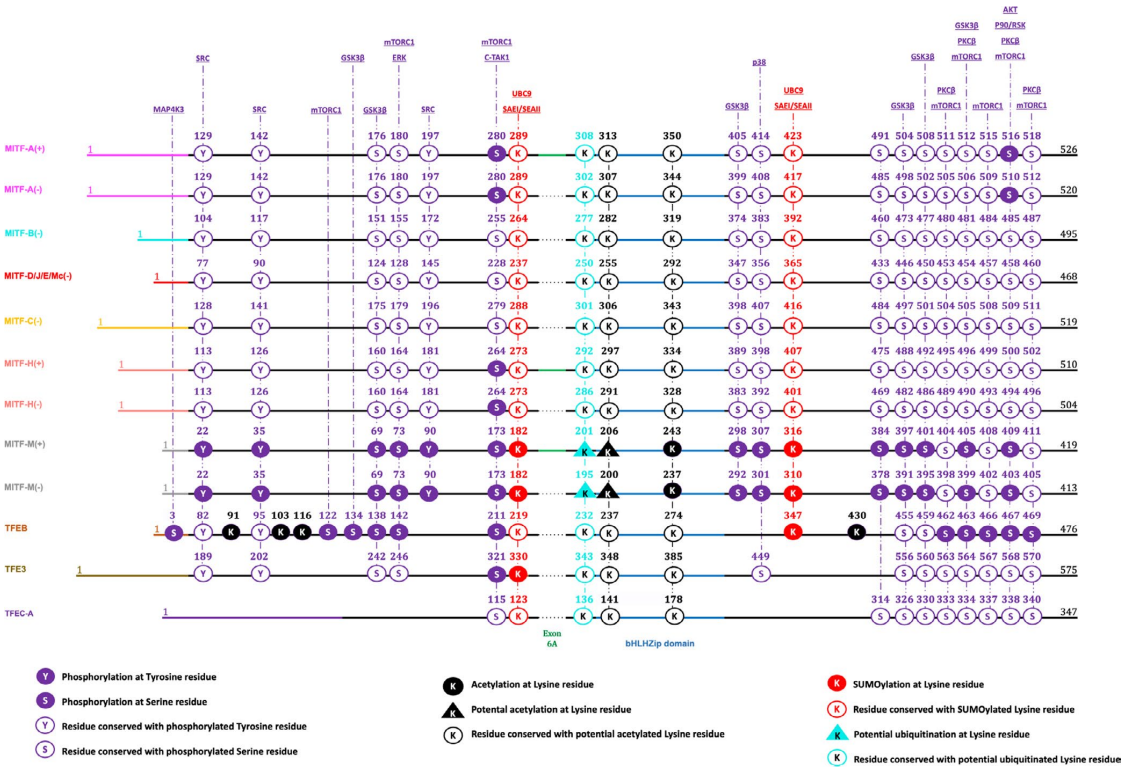

FIGURE 2 A schematic showing all post-translational modifications (PTMs) of human MITF, TFEB, and TFE3 isoforms. Phosphorylation (purple circles), SUMOylation (red circles), ubiquitination (turquoise circles), and acetylation (black circles) of specified residues are shown. The residues that have been shown to be modified are presented in filled circles. Residues that have been proposed as potentially modified sites are shown in filled triangles. Residues that are conserved with either modified or potential modified residues in the other MiT/TFE factors are indicated by unfilled circles. The responsible kinases for each PTM are indicated on top, and the numbers indicate amino acid residues. The bHLH-Zip domain is shown as a blue line, and the 6-amino acid insert region is shown as a green line

the expression of myosin light-chain 1a (MLC-1a) in cardiomyocytes (Tshori et al., 2007). The specific functions of the different MITF isoforms can now be addressed in cells or model organisms using CRISPR methods.

2.2 | TFEB, TFEC, and TFE3 isoforms

Similar to MITF, other MiT-TFE members are conserved between human, mouse, and zebrafish. The human *TFEB* gene has a similar gene organization as the *MITF* gene and is encoded by over 52,000 bp (GRCh38/hg38 chr6:41,683,978–41,736,259). It also has nine exons, with multiple non-coding first exons, each of which is spliced to the common coding exons 2–9 (Kuiper, Schepens, Thijssen, Schoenmakers, & van Kessel, 2004). At least seven transcripts, called *TFEB-A* through *G*, have been described and suggested to be regulated from different promoters (Kuiper et al., 2004). However, all seven identified *TFEB* transcripts have the same translational start site located in exon 2 (Kuiper et al., 2004) and are all translated into the same 476-residue protein (UNIPROT protein accession number: P19484-1). The alternative human *TFEB* transcripts are expressed in a tissue-specific manner such that *TFEB-E* and *TFEB-G* are expressed specifically in the brain and *TFEB-A* and *TFEB-F* are highly enriched in placenta and spleen, respectively. *TFEB-B* and *TFEB-C* are found in many tissues whereas the tissue-specific expression of the *TFEB-D* transcript has not been described due to its low expression level (Kuiper et al., 2004). There are at least two additional *TFEB* isoforms translating into either 490- or 391-residue proteins reported in both NCBI and UNIPROT databases. Unfortunately, the nomenclature of these isoforms is not uniform between databases. While the TFEB 391-residue protein is called transcription factor EB isoform 3 in the NCBI database (NCBI protein accession number NP_001258872.1), it is called transcription factor EB isoform 2 in the UNIPROT database (UNIPROT protein accession number: P19484-2). In the NCBI database, the TFEB 490-residue protein is called transcription factor EB isoform 2 (NP_001161299.2). According to the GTEx database, the transcript encoding the human TFEB 476-residue protein is expressed in many tissues and at a much higher level than that of the transcripts encoding the 490- and 391-residue proteins (GTEx Consortium, 2013). The mouse TFEB protein (UNIPROT protein

accession number: Q9R210-1) consists of 475 amino acids and shares 94% identity with the human TFEB 476-residue protein.

The human *TFEC* gene extends over 95,000 bp and is located on chromosome 7 (GRCh38/hg38 chr7:115,935,152–116,030,763). Similar to the *TFEB* and *MITF* genes, the human *TFEC* gene consists of 8 exons, with alternative 5′ exons and common exons 4–8 encoding the bHLH-Zip domain (Kuiper et al., 2004). There are at least three *TFEC* transcripts, namely *TFEC-A* (NCBI protein accession number NP_036384.1), *TFEC-B* (NCBI protein accession number NP_001018068.1), and *TFEC-C* (NCBI protein accession number NP_001231512.1), translating into 347-, 318-, and 280-residue proteins, respectively (Kuiper et al., 2004). The three *TFEC-A*, *B*, and *C* transcripts have been proposed to be regulated by different promoters and expressed in a tissue-specific manner (Kuiper et al., 2004). The *TFEC-B* transcript is expressed in various tissues, whereas *TFEC-C* is only expressed in kidney and small intestine and the highest expression of *TFEC-A* is in testis, trachea, and colon (Kuiper et al., 2004). In contrast to this, according to the GTEx database, *TFEC-A*, *B*, and *C* are expressed in many tissues and the percentage of *TFEC-B* transcript is lower than that of *TFEC-A* and *TFEC-C* (GTEx Consortium, 2013). *TFEC-A* is highly expressed in colon, esophagus, adrenal gland, adipose tissue, and lung, *TFEC-C* is enriched in small intestine, kidney, brain, and muscle, whereas *TFEC-B* is expressed most highly in uterus, vagina, brain, and muscle (GTEx Consortium, 2013). Consistent with a previous study (Rehli, Lichanska, Cassady, Ostrowski, & Hume, 1999), *TFEC* is found only in mononuclear phagocyte cell lines according to the FANTOM database (Noguchi et al., 2017) and is proposed to play a role in mononuclear phagocyte cell lines.

The human *TFE3* gene spans approximately 15,000 bp and contains 10 coding exons (GRCh38/hg38 chrX:49,028,726–49,043,357). Although the *TFE3* gene has the same structure of exon-intron borders as the other MiT-TFE family members (Rehli, Den Elzen, et al., 1999), it seems to have only one 5′ exon and to be regulated by a single promoter (Kuiper et al., 2004). The full-length human TFE3 protein consists of 575 amino acids (NCBI protein accession number: NP_006512.2 and UNIPROT protein accession number: P19532-1). It is 96% identical to the mouse TFE3 protein (NCBI protein accession number: NP_766060.2 and UNIPROT protein accession number: Q64092-1) and shares the conserved bHLH-Zip and transactivation domains with the other MiT-TFE family members (reviewed in Kauffman et al., 2014). In the NCBI database, an additional TFE3 isoform has been identified, termed transcription factor E3 isoform 2 (NP_001269071.1), translating into a 470-residue protein. According to the literature, the *TFE3* gene is expressed widely at low level in normal tissues but is expressed at a higher level in placenta, lung, and adrenal gland (Kuiper et al., 2004; reviewed in Folpe & Deyrup, 2006). The GTEx database shows that the transcript encoding the human TFE3 575-residue protein is expressed in many tissues including muscle, skin, lung, blood, and bone marrow (GTEx Consortium, 2013). The FANTOM database shows that the human full-length TFE3 transcript is found in fibroblasts, placental epithelial cells, mesenchymal stem cells, and mesothelioma cells (Noguchi et al., 2017).

3 | MiT-TFE POST-TRANSLATIONAL MODIFICATIONS

The activity of the MiT-TFE proteins has been shown to be mediated by various post-translational modifications (PTMs) including phosphorylation, SUMOylation, ubiquitination, and acetylation (Figures 2 and 3). Although little is known about PTMs of the zebrafish MiT-TFE factors, much more is known about PTMs of human and mouse MiT-TFE family members. In general, the human and mouse MiT-TFE proteins have been shown to be phosphorylated at multiple sites by an array of kinases. However, as the MiT-TFE family members and their isoforms are of different size, this has resulted in a confusion when cross-referencing residues between proteins. Therefore, we have aligned all the known isoforms of the MiT-TFE factors in human, mouse, and zebrafish, in order to allow cross-referencing of the PTMs (Figures 2 and 3).

3.1 | Phosphorylation

The phosphorylation status of MiT-TFE family members has been suggested to impact their transcriptional activity, stability, and subcellular localization (reviewed in Goding & Arnheiter, 2019; Hartman & Czyz, 2015; Puertollano, Ferguson, Brugarolas, & Ballabio, 2018). The ERK and p90/RSK kinases phosphorylate MITF-*M*(+) at the Ser73 and Ser409 residues, respectively (Hemesath, Price, Takemoto, Badalian, & Fisher, 1998; Wu et al., 2000). Phosphorylation of Ser73 leads to interactions between MITF and p300, resulting in effects on transcription activation. The stability of the MITF protein has also been suggested to be affected by phosphorylation of Ser73 and Ser409, possibly through ubiquitination of Lys201 by hUBC9 (Hemesath et al., 1998; Xu et al., 2000). Recently, it has been shown that phosphorylation of Ser409 serves as a priming site for phosphorylation by GSK3 at Ser405, Ser401, and Ser397 (Ploper et al., 2015) and that phosphorylation of Ser73 primes phosphorylation by GSK3 at Ser69 (Ngeow et al., 2018). All these phosphorylation sites (Ser69, Ser73, Ser397, Ser401, Ser405, and Ser409) are conserved in human and mouse MiT-TFE family members (Figure 2). Remarkably, in zebrafish mitfa, Ser69 which is equivalent to Ser69 in human MITF-M has been suggested to also be phosphorylated by GSK3 (Ngeow et al., 2018). Substituting Ser69 with alanine rescued melanophore development in the *mitfa*-null *nacre* zebrafish (Ngeow et al., 2018). In contrast, the zebrafish *mitfa* mutation Ser69Glu, which mimics constitutive phosphorylation, did not recover the development of melanophores in *mitfa*-null *nacre* zebrafish (Ngeow et al., 2018). GSK3β has also been shown to phosphorylate Ser298 of MITF-*M*(+) in vitro, leading to increased binding of MITF to the tyrosinase promoter (Takeda et al., 2000). It should be noted, however, that the typical GSK3-priming site is not found in the vicinity of Ser298. While phosphorylation of MITF-*M*(+) at Ser298, Ser397, Ser401, and Ser405 residues does not affect subcellular localization of MITF, the Ser69 and Ser73 phosphorylation sites regulate nuclear export of MITF-*M*(+) (Ngeow et al., 2018). The Ser298X and Ser73Ala

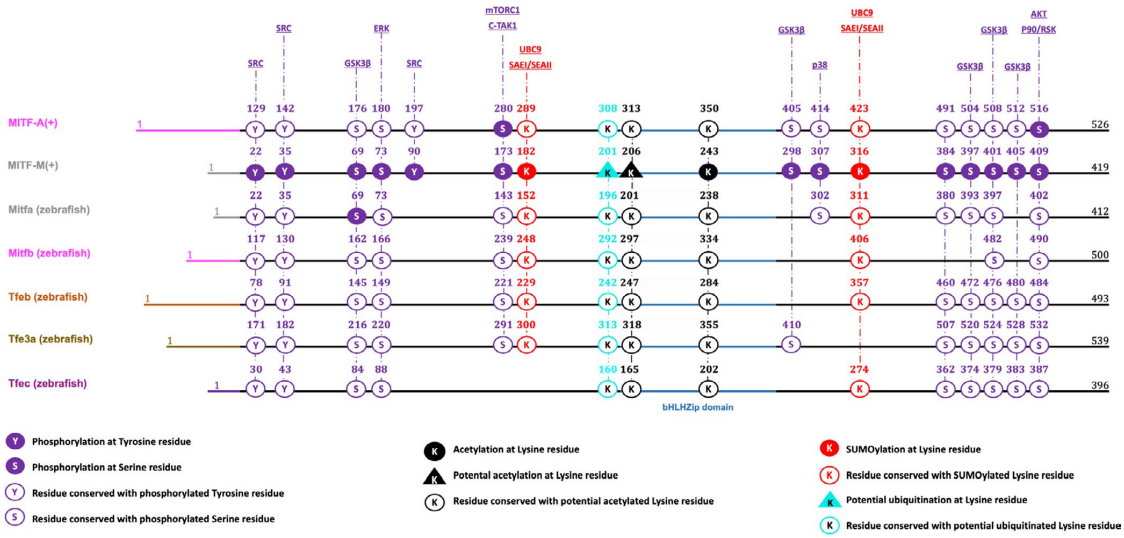

FIGURE 3 A schematic showing all known post-translational modifications (PTMs) of zebrafish *mitf*, *tfeb*, and *tfe3* isoforms. Human MITF-A(+) and MITF-*M*(+) are aligned with zebrafish Mitfa (NP_570998.1), Mitfb (NP_571922.2), Tfeb (NP_001244121.1), Tfe3a (NP_571923.2), and Tfec (NP_001025276.2) to map the conserved post-translationally modified residues in zebrafish MiT-TFE factors. PTMs including phosphorylation (purple circles), SUMOylation (red circles), ubiquitination (turquoise circles), and acetylation (black circles) of specified residues are shown. The residues that have been shown to be modified are presented in filled circles. Residues that have been proposed as potentially modified sites are presented in filled triangles. Residues conserved in the zebrafish MiT-TFE factors are shown as unfilled circles. The responsible kinases for each PTM are indicated on top, and the numbers indicate amino acid residues. The bHLH-Zip domain is shown as a blue line

mutations in MITF-*M*(+) do not affect MITF stability in 501MEL melanoma cells (Fock et al., 2019). Meanwhile, MITF-*M*(+) carrying the Ser397Ala, Ser401Ala, or Ser405Ala mutations has been demonstrated to be more stable by escaping from the proteasomal degradation process (Ploper et al., 2015).

The serine threonine kinase AKT has been shown to phosphorylate the MITF-A(−) isoform at Ser510 which is equivalent to the Ser409 residue of the MITF-*M*(+) isoform (Wang et al., 2016). MITF-A(−) phosphorylated at Ser510 enhanced binding to TP53, resulting in increased expression of CDKN1A, whereas the unphosphorylated MITF-A(−) protein elevated TYR expression (Wang et al., 2016). In addition to this, three tyrosine residues in MITF-*M*(+), Tyr22, Tyr35, and Tyr90, have been shown to be phosphorylated by any of 9 different SRC kinases upon a complex formation between the Asp816Val mutated KIT, SRC, and MITF proteins (Phung et al., 2017). MITF phosphorylated by SRC is retained in the cytoplasm, yet leading to an increase of the transcriptional activity of MITF target genes involved in melanoma proliferation, survival, cell cycle progression and invasion (Phung et al., 2017).

In osteoclasts, the Ser307 residue in MITF-*M*(+) has been shown to be a substrate of p38/MAPK in vitro (Mansky, Sankar, Han, & Ostrowski, 2002). Interestingly, the equivalent of Ser307 in MITF-*M*(+) is not conserved in TFEB. Therefore, phosphorylation of MITF-*M*(+) at Ser307 in osteoclasts may have unique effects on MITF activity (Mansky et al., 2002). Although the effects of MITF-Ser307 phosphorylation on activity in osteoclasts remain to be investigated further, it has been shown that the phosphorylated protein interacts with PU.1 in osteoclasts, integrating with the CSF-1/RANKL signals leading to activation of genes associated with osteoclast differentiation (Mansky et al., 2002; Sharma et al., 2007). In osteoclasts, the C-TAK1 kinase has been shown to phosphorylate Ser173 (based on MITF-*M*(+) numbering), leading to the formation of an MITF/14-3-3 complex and retention of MITF in the cytosol (Bronisz et al., 2006). Inversely, when CSF-1/RANKL signaling deactivates the C-TAK1 kinase, the interaction of MITF and 14-3-3 proteins is destabilized, resulting in MITF nuclear translocation, subsequently triggering the expression of genes involved in osteoclast differentiation (Bronisz et al., 2006). Notably, mutations of four phosphorylated residues, Ser73, Ser298, Ser307, and Ser409, did not impact the binding of MITF to 14-3-3 proteins (Bronisz et al., 2006). The phosphorylation of both MITF-A at Ser280 and MITF-H at Ser264, which are equivalent to Ser173 of MITF-*M*(+), by mTORC1 affects translocation of the MITF-A and MITF-H proteins into the nucleus (Martina & Puertollano, 2013). Many additional phosphorylation sites in MITF have been summarized in the PhosphoSitePlus web-based resource (Hornbeck et al., 2015). Based on proteomic discovery mass spectrometry, residues Thr54 and Ser55 (based on MITF-A(+) numbering), Ser50, Ser109, Ser250, Tyr253, Thr382, Ser395, Thr403, Ser404, and Ser408 (based on MITF-*M*(+) numbering) have all been suggested to be phosphorylated (Hornbeck et al., 2015). However, the responsible kinases and biological roles of many of these MITF phosphorylation sites remain to be investigated.

Similar to MITF, TFEB is phosphorylated at multiple sites but is mostly regulated by nutrition signaling. mTORC1 is an important player in mediating phosphorylation of TFEB (reviewed in Puertollano et al., 2018) and has been shown to phosphorylate three different residues of the TFEB protein, namely Ser122, Ser142 (equivalent to Ser73 of MITF-*M*(+) isoform), and Ser211 (equivalent to Ser173 of MITF-*M*(+); Figure 2; Martina et al., 2012; Roczniak-Ferguson et al., 2012; Vega-Rubin-de-Celis, Peña-Llopis, Konda, & Brugarolas, 2017). In TSC1/TSC2-deficient cells where mTORC1 is highly activated, mTORC1 additionally mediates phosphorylation at Ser462 (equivalent to Ser404 of the MITF-*M*(+) isoform), Ser463 (equivalent to Ser405 of the MITF-*M*(+) isoform), Ser466 (equivalent to Ser408 of the MITF-*M*(+) isoform), Ser467 (equivalent to Ser409 of MITF-*M*(+)), and Ser469 (equivalent to Ser411 of the MITF-*M*(+) isoform) of TFEB (Figure 2; reviewed in Puertollano et al., 2018). Phosphorylation of TFEB at Ser122, Ser142, and Ser211 is suggested to influence its subcellular localization as well as its stability. It has been shown that the chaperone protein HSP70 determines the interaction between the chaperone-dependent E3 ubiquitin ligase STUB1 and TFEB phosphorylated at Ser142 and Ser211. As a result, phosphorylated TFEB is triggered for ubiquitin-proteasomal degradation (Sha, Rao, Settembre, Ballabio, & Eissa, 2017). In terms of subcellular localization of TFEB, the phosphorylation of TFEB at Ser211 initiates the interaction of TFEB and 14-3-3 proteins. Similar to MITF-*M*(+) phosphorylated at Ser173, TFEB phosphorylated at Ser211 is retained in the cytosol through its binding to 14-3-3 proteins (Martina et al., 2012; Roczniak-Ferguson et al., 2012). Inversely, dephosphorylated TFEB is translocated to the nucleus for activating the expression of genes involved in autophagosome and lysosome biogenesis in response to nutrient deficiency (Roczniak-Ferguson et al., 2012; Settembre et al., 2012). Furthermore, it has been suggested that phosphorylation of TFEB at Ser142 is the priming site for TFEB phosphorylation at Ser138 (equivalent to Ser69 of MITF-*M*(+)—Figure 2) which in turn influences TFEB phosphorylation at Ser211 and TFEB nuclear translocation (Napolitano et al., 2018). Consistent with that, it has also been observed that mutating Ser142 of TFEB to alanine results in reduced Ser211 phosphorylation (Li et al., 2016). The Ser142 residue in TFEB can also be targeted by the extracellular signal-regulated kinase ERK2, a signaling pathway which phosphorylates Ser73 of MITF-*M*(+) (Settembre et al., 2011). However, how the ERK2 and mTORC1 signaling pathways interact to determine phosphorylation of TFEB at Ser142 is currently not understood. The Ser122 phosphorylation of TFEB also is vital to control its subcellular localization; however, the substitution of Ser122 with alanine did not affect TFEB cytoplasmic retention (Vega-Rubin-de-Celis et al., 2017). Meanwhile, the double mutation Ser122Ala and Ser211Ala resulted in nuclear translocation of TFEB (Vega-Rubin-de-Celis et al., 2017).

In osteoclasts, PKCβ phosphorylates the human TFEB protein at Ser462, Ser463, Ser467, and Ser469 (equivalent to Ser461, Ser462, Ser466, and Ser468 of mouse TFEB, respectively), affecting stability and transcription activity of the TFEB protein (Ferron et al., 2013). Residue Ser467 of TFEB can also be phosphorylated by AKT, resulting in the formation of a TFEB/14-3-3 complex and cytoplasmic sequestration of TFEB in an independent mTORC1-mediated TFEB phosphorylation mechanism (Palmieri et al., 2017). GSK3β specifically phosphorylates TFEB at Ser134 and Ser138. This affects the phosphorylation of TFEB at Ser211 and retains TFEB in the cytosol (Li et al., 2016; Napolitano et al., 2018). MAP4K3 has been shown to directly bind to and phosphorylate TFEB at Ser3. Interestingly, this phosphorylated site is required for the mTORC1-mediated phosphorylation of Ser211. In addition, phosphorylation at Ser3 also affects the subcellular localization of TFEB by preventing the travel of the phosphorylated TFEB protein to the nucleus (Hsu et al., 2018). Clearly, there are many different signaling pathways that mediate phosphorylation of different residues of TFEB but since most of these phosphorylation events affect Ser211 phosphorylation, this residue is likely to be the key switch determining localization of TFEB. In the PhosphoSitePlus web-based resource, an additional 17 TFEB phosphorylation sites have been reported based on proteomic discovery mass spectrometry (Hornbeck et al., 2015). These include Ser74, Tyr95, Ser97, Tyr100, Ser109, Ser114, Ser133, Thr183, Ser227, Thr330, Thr331, Ser332, Ser334, Ser423, Ser429, Ser441, and Ser455, all of which remain to be further characterized.

The only TFE3 phosphorylation site that has been verified to date using methods other than discovery mass spectrometry is Ser321 (equivalent to Ser211 of TFEB and Ser173 of MITF-*M*(+) isoform—Figure 2; Martina et al., 2014). Phosphorylation of this residue in TFE3 has been shown to lead to the binding of TFE3 to 14-3-3 proteins and to its cytoplasmic retention (Martina et al., 2014). According to PhosphoSitePlus, many phosphorylation sites in TFE3 have been identified using proteomic discovery mass spectrometry. Remarkably, among these reported phosphorylation residues, Ser202, S246, Ser556, Ser560, Ser563, Ser564, Ser567, Ser568, and Ser570 of TFE3 are conserved and also indicated to be phosphorylated in the other members of the MiT-TFE family (Figure 2; Hornbeck et al., 2015). According to the literature, no phosphorylation sites have been reported in TFEC to date; however, PhosphoSitePlus records three phosphorylated sites in TFEC, namely Thr2, Ser15, and Ser119 (Hornbeck et al., 2015). Obviously, future studies need to explore the regulatory pathways mediating PTMs in TFEC as well as their effects on dimers with other MiT-TFE family members.

3.2 | SUMOylation

The MiT-TFE proteins have been shown to be SUMOylated. MITF-*M*(+) was shown to be SUMOylated at Lys182 and Lys316 (Miller, Levy, Davis, Razin, & Fisher, 2005; Murakami & Arnheiter, 2005). The enzymes SAE I/SAE II and UBC9 have been suggested to be involved in the SUMOylation of MITF-*M*(+) at Lys182 and Lys316 (Murakami & Arnheiter, 2005). The germline mutation Glu318Lys in MITF-*M*(+) impairs its SUMOylation at Lys316 and increases the transcriptional activity of MITF (Bertolotto et al., 2011; Yokoyama et al., 2011), whereas it has no effects on MITF nuclear localization (Grill et al., 2013). TFE3 has been shown to be SUMOylated at Lys330, which is equivalent to

Lys182 in the MITF-*M*(+) isoform (Figure 2; Miller et al., 2005). In the PhosphoSitePlus web-based resource, Lys79 (based on MITF-A(+) numbering) and Lys33 (based on MITF-*M*(+) numbering) in MITF and Lys68 in TFE3 are also SUMOylated (Hornbeck et al., 2015). TFEB is subjected to SUMOylation at Lys347, which is equivalent to Lys316 of MITF-*M*(+) (Figure 2; Miller et al., 2005). However, the functional role of the SUMOylation of TFE3 and TFEB remains to be characterized.

3.3 | Ubiquitination and acetylation

While phosphorylation and SUMOylation of the MiT-TFE family members are well described, ubiquitination and acetylation are less well characterized. MITF has been shown to be deubiquitinated by the ubiquitin-specific protease 13 (USP13) which in turn affects the expression of genes involved in proliferation and growth of melanoma cell lines (Zhao, Fiske, Kawakami, Li, & Fisher, 2011). UCHL1 has been proposed to be a MITF ubiquitin ligase, which negatively affects MITF stability (Seo et al., 2017) and Lys201 of MITF-*M*(+) is a potential ubiquitination site (Xu et al., 2000). In the PhosphoSitePlus web-based resource, Lys21, Lys91, and Lys265 in MITF (based on MITF-*M*(+) numbering), Lys202 and Lys339 in TFE3, and Lys91 in TFEB are suggested to be ubiquitinated (Hornbeck et al., 2015). Furthermore, PhosphoSitePlus has reported that Lys21 in MITF (based on MITF-*M*(+) numbering) and Lys401 in TFE3 are acetylation sites (Hornbeck et al., 2015). Several lysine residues in MITF-*M*(+) have been shown to be acetylated, including Lys21, Lys33, Lys43, Lys243, and Lys248; acetylation of Lys243 was shown to affect binding to low-affinity binding sites (Louphrasitthiphol et al., 2020). Acetylation of TFEB has been suggested to affect its subcellular localization and transcriptional activity (Zhang et al., 2018). Four lysine residues in TFEB, namely Lys91, Lys103, Lys116, and Lys430, have been shown to be acetylated in cells treated with the histone deacetylase inhibitor SAHA, supporting the roles of TFEB acetylation in lysosomal activation, autophagy, and cell death induced by histone deacetylase inhibitors (Zhang et al., 2018). These four acetylated sites, which are not conserved in MITF and TFE3, might contribute to the unique activity of TFEB.

4 | CONCLUSIONS

To minimize discrepancies in nomenclature and to allow the cross-referencing of residues between MiT-TFE factors and isoforms, we have assembled this information in easy to use graphics (Figures 1-3). A comparison between MITF, TFEB, and TFE3 shows that these proteins are largely regulated by the same post-translational modifications at conserved amino acids and by the same signaling pathways, suggesting the involvement of similar molecular mechanisms in controlling transcriptional activity, stability, and nuclear localization of MiT-TFE factors. A few post-translational modifications are unique to the individual MiT-TFE factors and are not conserved in all members of the family, suggesting that they contribute to distinct biological functions. Important lessons about signaling to transcription factors and the consequent functional effects will be learned from comparing the MiT-TFE family of proteins.

ACKNOWLEDGEMENTS

The authors wish to thank Dr. Lionel Larue, Institut Curie, France and Dr. Margrét H. Ögmundsdóttir, University of Iceland, Iceland for critically reviewing the manuscript. This study was supported by Grants from the Research Fund of Iceland to ES (No.184861 and No.207067) and the University of Iceland Doctoral Grants Fund.

CONFLICT OF INTEREST

The authors have no conflict of interest to declare.

ORCID

Hong Nhung Vu https://orcid.org/0000-0002-8262-900X
Valerie Fock https://orcid.org/0000-0002-7812-4340
Eiríkur Steingrímsson https://orcid.org/0000-0001-5826-7486

REFERENCES

Amae, S., Fuse, N., Yasumoto, K.-I., Sato, S., Yajima, I., Yamamoto, H., … Shibahara, S. (1998). Identification of a novel isoform of microphthalmia-associated transcription factor that is enriched in retinal pigment epithelium. *Biochemical and Biophysical Research Communications*, *247*(3), 710–715. https://doi.org/10.1006/bbrc.1998.8838

Amiel, J., Watkin, P. M., Tassabehji, M., Read, A. P., & Winter, R. M. (1998). Mutation of the MITF gene in albinism-deafness syndrome (Tietz syndrome). *Clinical Dysmorphology*, *7*(1), 17–20. https://doi.org/10.1097/00019605-199801000-00003

Argani, P., Antonescu, C. R., Illei, P. B., Lui, M. Y., Timmons, C. F., Newbury, R., … Ladanyi, M. (2001). Primary renal neoplasms with the ASPL-TFE3 gene fusion of alveolar soft part sarcoma: A distinctive tumor entity previously included among renal cell carcinomas of children and adolescents. *American Journal of Pathology*, *159*(1), 179–192. https://doi.org/10.1016/s0002-9440(10)61684-7

Argani, P., Laé, M., Hutchinson, B., Reuter, V. E., Collins, M. H., Perentesis, J., … Ladanyi, M. (2005). Renal carcinomas with the t(6;11)(p21;q12): Clinicopathologic features and demonstration of the specific alpha-TFEB gene fusion by immunohistochemistry, RT-PCR, and DNA PCR. *The American Journal of Surgical Pathology*, *29*(2), 230–240. https://doi.org/10.1097/01.pas.0000146007.54092.37

Argani, P., Lui, M. Y., Couturier, J., Bouvier, R., Fournet, J. C., & Ladanyi, M. (2003). A novel CLTC-TFE3 gene fusion in pediatric renal adenocarcinoma with t(X;17)(p11.2;q23). *Oncogene*, *22*(34), 5374–5378. https://doi.org/10.1038/sj.onc.1206686

Atacho, D. A. M., Reynisson, H., Petursdottir, A. T., Eysteinsson, T., Steingrimsson, E., & Petersen, P. H. (2020). Mitf links neuronal activity and long-term homeostatic intrinsic plasticity. *eNeuro*, *7*(2), ENEURO.0412-19.2020. https://doi.org/10.1523/ENEURO.0412-19.2020

Bauer, G. L., Praetorius, C., Bergsteinsdóttir, K., Hallsson, J. H., Gísladóttir, B. K., Schepsky, A., … Steingrímsson, E. (2009). The role of MITF phosphorylation sites during coat color and eye development in mice analyzed by bacterial artificial chromosome transgene rescue. *Genetics*, *183*(2), 581–594. https://doi.org/10.1534/genetics.109.103945

Bertolotto, C., Lesueur, F., Giuliano, S., Strub, T., de Lichy, M., Bille, K., … Bressac-de Paillerets, B. (2011). A SUMOylation-defective MITF

germline mutation predisposes to melanoma and renal carcinoma. *Nature*, *480*(7375), 94–98. https://doi.org/10.1038/nature10539

Bharti, K., Liu, W., Csermely, T., Bertuzzi, S., & Arnheiter, H. (2008). Alternative promoter use in eye development: The complex role and regulation of the transcription factor MITF. *Development*, *135*(6), 1169–1178. https://doi.org/10.1242/dev.014142

Bismuth, K., Maric, D., & Arnheiter, H. (2005). MITF and cell proliferation: The role of alternative splice forms. *Pigment Cell Research*, *18*(5), 349–359. https://doi.org/10.1111/j.1600-0749.2005.00249.x

Bronisz, A., Sharma, S. M., Hu, R., Godlewski, J., Tzivion, G., Mansky, K. C., & Ostrowski, M. C. (2006). Microphthalmia-associated transcription factor interactions with 14–3-3 modulate differentiation of committed myeloid precursors. *Molecular Biology of the Cell*, *17*(9), 3897–3906. https://doi.org/10.1091/mbc.e06-05-0470

Cancer Genome Atlas Research Network, Linehan, W. M., Spellman, P. T., Ricketts, C. J., Creighton, C. J., & Fei, S. S., … Zuna, R. (2016). Comprehensive molecular characterization of papillary renal-cell carcinoma. *The New England Journal of Medicine*, *374*(2), 135–145. https://doi.org/10.1056/NEJMoa1505917

Carreira, S., Goodall, J., Denat, L., Rodriguez, M., Nuciforo, P., Hoek, K. S., … Goding, C. R. (2006). Mitf regulation of Dia1 controls melanoma proliferation and invasiveness. *Genes and Development*, *20*(24), 3426–3439. https://doi.org/10.1101/gad.406406

Clark, J., Lu, Y.-J., Sidhar, S. K., Parker, C., Gill, S., Smedley, D., … Cooper, C. S. (1997). Fusion of splicing factor genes PSF and NonO (p54nrb) to the TFE3 gene in papillary renal cell carcinoma. *Oncogene*, *15*(18), 2233–2239. https://doi.org/10.1038/sj.onc.1201394

Classe, M., Malouf, G. G., Su, X., Yao, H., Thompson, E. J., Doss, D. J., … Leroy, X. (2017). Incidence, clinicopathological features and fusion transcript landscape of translocation renal cell carcinomas. *Histopathology*, *70*(7), 1089–1097. https://doi.org/10.1111/his.13167

Davis, I. J., Hsi, B.-L., Arroyo, J. D., Vargas, S. O., Yeh, Y. A., Motyckova, G., … Fisher, D. E. (2003). Cloning of an Alpha-TFEB fusion in renal tumors harboring the t(6;11)(p21;q13) chromosome translocation. *Proceedings of the National Academy of Sciences of the United States of America*, *100*(10), 6051–6056. https://doi.org/10.1073/pnas.0931430100

Debbache, J., Zaidi, M. R., Davis, S., Guo, T., Bismuth, K., Wang, X., … Arnheiter, H. (2012). In vivo role of alternative splicing and serine phosphorylation of the microphthalmia-associated transcription factor. *Genetics*, *191*(1), 133–144. https://doi.org/10.1534/genetics.111.135996

Ferron, M., Settembre, C., Shimazu, J., Lacombe, J., Kato, S., Rawlings, D. J., … Karsenty, G. (2013). A RANKL-PKCβ-TFEB signaling cascade is necessary for lysosomal biogenesis in osteoclasts. *Genes and Development*, *27*(8), 955–969. https://doi.org/10.1101/gad.213827.113

Flesher, J. L., Paterson-Coleman, E. K., Vasudeva, P., Ruiz-Vega, R., Marshall, M., Pearlman, E., … Ganesan, A. K. (2020). Delineating the role of MITF isoforms in pigmentation and tissue homeostasis. *Pigment Cell and Melanoma Research*, *33*(2), 279–292. https://doi.org/10.1111/pcmr.12828

Fock, V., Gudmundsson, S. R., Gunnlaugsson, H. O., Stefansson, J. A., Ionasz, V., Schepsky, A., … Steingrimsson, E. (2019). Subcellular localization and stability of MITF are modulated by the bHLH-Zip domain. *Pigment Cell and Melanoma Research*, *32*(1), 41–54. https://doi.org/10.1111/pcmr.12721

Folpe, A. L., & Deyrup, A. T. (2006). Alveolar soft-part sarcoma: A review and update. *Journal of Clinical Pathology*, *59*(11), 1127–1132. https://doi.org/10.1136/jcp.2005.031120

Fuse, N., Yasumoto, K.-I., Takeda, K., Amae, S., Yoshizawa, M., Udono, T., … Shibahara, S. (1999). Molecular cloning of cDNA encoding a novel microphthalmia- associated transcription factor isoform with a distinct amino-terminus1. *The Journal of Biochemistry*, *126*(6), 1043–1051. https://doi.org/10.1093/oxfordjournals.jbchem.a022548

Garraway, L. A., Widlund, H. R., Rubin, M. A., Getz, G., Berger, A. J., Ramaswamy, S., … Sellers, W. R. (2005). Integrative genomic analyses identify MITF as a lineage survival oncogene amplified in malignant melanoma. *Nature*, *436*(7047), 117–122. https://doi.org/10.1038/nature03664

George, A., Zand, D. J., Hufnagel, R. B., Sharma, R., Sergeev, Y. V., Legare, J. M., … Brooks, B. P. (2016). Biallelic mutations in MITF cause coloboma, osteopetrosis, microphthalmia, macrocephaly, albinism, and deafness. *American Journal of Human Genetics*, *99*(6), 1388–1394. https://doi.org/10.1016/j.ajhg.2016.11.004

Goding, C. R., & Arnheiter, H. (2019). MITF-the first 25 years. *Genes and Development*, *33*(15–16), 983–1007. https://doi.org/10.1101/gad.324657.119

Grill, C., Bergsteinsdóttir, K., Ögmundsdóttir, M. H., Pogenberg, V., Schepsky, A., Wilmanns, M., … Steingrímsson, E. (2013). MITF mutations associated with pigment deficiency syndromes and melanoma have different effects on protein function. *Human Molecular Genetics*, *22*(21), 4357–4367. https://doi.org/10.1093/hmg/ddt285

GTEx Consortium. (2013). The genotype-tissue expression (GTEx) project. *Nature Genetics*, *45*(6), 580–585. https://doi.org/10.1038/ng.2653

Hallsson, J. H., Favor, J., Hodgkinson, C., Glaser, T., Lamoreux, M. L., Magnúsdóttir, R., … Steingrímsson, E. (2000). Genomic, transcriptional and mutational analysis of the mouse microphthalmia locus. *Genetics*, *155*(1), 291–300.

Hartman, M. L., & Czyz, M. (2015). MITF in melanoma: Mechanisms behind its expression and activity. *Cellular and Molecular Life Sciences*, *72*(7), 1249–1260. https://doi.org/10.1007/s00018-014-1791-0

Hemesath, T. J., Price, E. R., Takemoto, C., Badalian, T., & Fisher, D. E. (1998). MAP kinase links the transcription factor Microphthalmia to c-Kit signalling in melanocytes. *Nature*, *391*(6664), 298–301. https://doi.org/10.1038/34681

Hemesath, T. J., Steingrimsson, E., McGill, G., Hansen, M. J., Vaught, J., Hodgkinson, C. A., … Fisher, D. E. (1994). microphthalmia, a critical factor in melanocyte development, defines a discrete transcription factor family. *Genes and Development*, *8*(22), 2770–2780. https://doi.org/10.1101/gad.8.22.2770

Hershey, C. L., & Fisher, D. E. (2005). Genomic analysis of the Microphthalmia locus and identification of the MITF-J/Mitf-J isoform. *Gene*, *347*(1), 73–82. https://doi.org/10.1016/j.gene.2004.12.002

Hodgkinson, C. A., Moore, K. J., Nakayama, A., Steingrimsson, E., Copeland, N. G., Jenkins, N. A., & Arnheiter, H. (1993). Mutations at the mouse microphthalmia locus are associated with defects in a gene encoding a novel basic-helix-loop-helix-zipper protein. *Cell*, *74*(2), 395–404. https://doi.org/10.1016/0092-8674(93)90429-T

Hornbeck, P. V., Zhang, B., Murray, B., Kornhauser, J. M., Latham, V., & Skrzypek, E. (2015). PhosphoSitePlus, 2014: Mutations, PTMs and recalibrations. *Nucleic Acids Research*, *43*(D1), D512–D520. https://doi.org/10.1093/nar/gku1267

Hsu, C. L., Lee, E. X., Gordon, K. L., Paz, E. A., Shen, W.-C., Ohnishi, K., … La Spada, A. R. (2018). MAP4K3 mediates amino acid-dependent regulation of autophagy via phosphorylation of TFEB. *Nature Communications*, *9*(1), 942. https://doi.org/10.1038/s41467-018-03340-7

Huang, W., Goldfischer, M., Babayeva, S., Mao, Y., Volyanskyy, K., Dimitrova, N., … Zhong, M. (2015). Identification of a novel PARP14-TFE3 gene fusion from 10-year-old FFPE tissue by RNA-seq. *Genes, Chromosomes and Cancer*, *54*(8), 500–505. https://doi.org/10.1002/gcc.22261

Kauffman, E. C., Ricketts, C. J., Rais-Bahrami, S., Yang, Y., Merino, M. J., Bottaro, D. P., … Linehan, W. M. (2014). Molecular genetics and cellular features of TFE3 and TFEB fusion kidney cancers. *Nature Reviews Urology*, *11*(8), 465–475. https://doi.org/10.1038/nrurol.2014.162

Komai, Y., Fujiwara, M., Fujii, Y., Mukai, H., Yonese, J., Kawakami, S., … Fukui, I. (2009). Adult Xp11 translocation renal cell carcinoma

diagnosed by cytogenetics and immunohistochemistry. *Clinical Cancer Research*, *15*(4), 1170–1176. https://doi.org/10.1158/1078-0432.Ccr-08-1183

Kuiper, R. P., Schepens, M., Thijssen, J., Schoenmakers, E. F. P. M., & van Kessel, A. G. (2004). Regulation of the MiTF/TFE bHLH-LZ transcription factors through restricted spatial expression and alternative splicing of functional domains. *Nucleic Acids Research*, *32*(8), 2315–2322. https://doi.org/10.1093/nar/gkh571

Kuiper, R. P., Schepens, M., Thijssen, J., van Asseldonk, M., van den Berg, E., Bridge, J., … van Kessel, A. G. (2003). Upregulation of the transcription factor TFEB in t(6;11)(p21;q13)-positive renal cell carcinomas due to promoter substitution. *Human Molecular Genetics*, *12*(14), 1661–1669. https://doi.org/10.1093/hmg/ddg178

Ladanyi, M., Lui, M. Y., Antonescu, C. R., Krause-Boehm, A., Meindl, A., Argani, P., … Bridge, J. (2001). The der(17)t(X;17)(p11;q25) of human alveolar soft part sarcoma fuses the TFE3 transcription factor gene to ASPL, a novel gene at 17q25. *Oncogene*, *20*(1), 48–57. https://doi.org/10.1038/sj.onc.1204074

Li, Y., Xu, M., Ding, X., Yan, C., Song, Z., Chen, L., … Yang, C. (2016). Protein kinase C controls lysosome biogenesis independently of mTORC1. *Nature Cell Biology*, *18*(10), 1065–1077. https://doi.org/10.1038/ncb3407

Lister, J. A., Close, J., & Raible, D. W. (2001). Duplicate mitf genes in zebrafish: Complementary expression and conservation of melanogenic potential. *Developmental Biology*, *237*(2), 333–344. https://doi.org/10.1006/dbio.2001.0379

Lister, J. A., Robertson, C. P., Lepage, T., Johnson, S. L., & Raible, D. W. (1999). nacre encodes a zebrafish microphthalmia-related protein that regulates neural-crest-derived pigment cell fate. *Development*, *126*(17), 3757–3767.

Louphrasitthiphol, P., Siddaway, R., Loffreda, A., Pogenberg, V., Friedrichsen, H., Schepsky, A., … Goding, C. R. (2020). Tuning transcription factor availability through acetylation-mediated genomic redistribution. *Molecular Cell*, https://doi.org/10.1016/j.molcel.2020.05.025

Malcov-Brog, H., Alpert, A., Golan, T., Parikh, S., Nordlinger, A., Netti, F., … Levy, C. (2018). UV-protection timer controls linkage between stress and pigmentation skin protection systems. *Molecular Cell*, *72*(3), 444–456.e7. https://doi.org/10.1016/j.molcel.2018.09.022

Malouf, G. G., Su, X., Yao, H., Gao, J., Xiong, L., He, Q., … Tannir, N. M. (2014). Next-generation sequencing of translocation renal cell carcinoma reveals novel RNA splicing partners and frequent mutations of chromatin-remodeling genes. *Clinical Cancer Research: An Official Journal of the American Association for Cancer Research*, *20*(15), 4129–4140. https://doi.org/10.1158/1078-0432.CCR-13-3036

Mansky, K. C., Sankar, U., Han, J., & Ostrowski, M. C. (2002). Microphthalmia transcription factor is a target of the p38 MAPK pathway in response to receptor activator of NF-kappa B ligand signaling. *Journal of Biological Chemistry*, *277*(13), 11077–11083. https://doi.org/10.1074/jbc.M111696200

Martina, J. A., Chen, Y., Gucek, M., & Puertollano, R. (2012). MTORC1 functions as a transcriptional regulator of autophagy by preventing nuclear transport of TFEB. *Autophagy*, *8*(6), 903–914. https://doi.org/10.4161/auto.19653

Martina, J. A., Diab, H. I., Lishu, L., Jeong, A. L., Patange, S., Raben, N., & Puertollano, R. (2014). The nutrient-responsive transcription factor TFE3 promotes autophagy, lysosomal biogenesis, and clearance of cellular debris. *Science Signalling*, *7*(309), ra9. https://doi.org/10.1126/scisignal.2004754

Martina, J. A., & Puertollano, R. (2013). Rag GTPases mediate amino acid-dependent recruitment of TFEB and MITF to lysosomes. *The Journal of Cell Biology*, *200*(4), 475–491. https://doi.org/10.1083/jcb.201209135

Medina, D. L., Di Paola, S., Peluso, I., Armani, A., De Stefani, D., Venditti, R., … Ballabio, A. (2015). Lysosomal calcium signalling regulates autophagy through calcineurin and TFEB. *Nature Cell Biology*, *17*(3), 288–299. https://doi.org/10.1038/ncb3114

Miller, A. J., Levy, C., Davis, I. J., Razin, E., & Fisher, D. E. (2005). Sumoylation of MITF and its related family members TFE3 and TFEB. *Journal of Biological Chemistry*, *280*(1), 146–155. https://doi.org/10.1074/jbc.M411757200

Möller, K., Sigurbjornsdottir, S., Arnthorsson, A. O., Pogenberg, V., Dilshat, R., Fock, V., … Ogmundsdottir, M. H. (2019). MITF has a central role in regulating starvation-induced autophagy in melanoma. *Scientific Reports*, *9*(1), 1055. https://doi.org/10.1038/s41598-018-37522-6

Morii, E., Tsujimura, T., Jippo, T., Hashimoto, K., Takebayashi, K., Tsujino, K., … Kitamura, Y. (1996). Regulation of mouse mast cell protease 6 gene expression by transcription factor encoded by the mi locus. *Blood*, *88*(7), 2488–2494. https://doi.org/10.1182/blood.V88.7.2488.bloodjournal8872488

Murakami, H., & Arnheiter, H. (2005). Sumoylation modulates transcriptional activity of MITF in a promoter-specific manner. *Pigment Cell Research*, *18*(4), 265–277. https://doi.org/10.1111/j.1600-0749.2005.00234.x

Murakami, M., Iwata, Y., & Funaba, M. (2007). Expression and transcriptional activity of alternative splice variants of Mitf exon 6. *Molecular and Cellular Biochemistry*, *303*(1–2), 251–257. https://doi.org/10.1007/s11010-007-9474-x

Napolitano, G., Esposito, A., Choi, H., Matarese, M., Benedetti, V., Di Malta, C., … Ballabio, A. (2018). mTOR-dependent phosphorylation controls TFEB nuclear export. *Nature Communications*, *9*(1), 3312. https://doi.org/10.1038/s41467-018-05862-6

Ngeow, K. C., Friedrichsen, H. J., Li, L., Zeng, Z., Andrews, S., Volpon, L., … Goding, C. R. (2018). BRAF/MAPK and GSK3 signaling converges to control MITF nuclear export. *Proceedings of the National Academy of Sciences of the United States of America*, *115*(37), E8668–E8677. https://doi.org/10.1073/pnas.1810498115

Noguchi, S., Arakawa, T., Fukuda, S., Furuno, M., Hasegawa, A., Hori, F., … Hayashizaki, Y. (2017). FANTOM5 CAGE profiles of human and mouse samples. *Scientific Data*, *4*(1), 170112. https://doi.org/10.1038/sdata.2017.112

Oboki, K., Morii, E., Kataoka, T. R., Jippo, T., & Kitamura, Y. (2002). Isoforms of mi transcription factor preferentially expressed in cultured mast cells of mice. *Biochemical and Biophysical Research Communications*, *290*(4), 1250–1254. https://doi.org/10.1006/bbrc.2002.6332

Palmieri, M., Pal, R., Nelvagal, H. R., Lotfi, P., Stinnett, G. R., Seymour, M. L., … Sardiello, M. (2017). mTORC1-independent TFEB activation via Akt inhibition promotes cellular clearance in neurodegenerative storage diseases. *Nature Communications*, *8*(1), 14338. https://doi.org/10.1038/ncomms14338

Pei, J., Cooper, H., Flieder, D. B., Talarchek, J. N., Al-Saleem, T., Uzzo, R. G., … Wei, S. (2019). NEAT1-TFE3 and KAT6A-TFE3 renal cell carcinomas, new members of MiT family translocation renal cell carcinoma. *Modern Pathology*, *32*(5), 710–716. https://doi.org/10.1038/s41379-018-0191-7

Perera, R. M., Stoykova, S., Nicolay, B. N., Ross, K. N., Fitamant, J., Boukhali, M., … Bardeesy, N. (2015). Transcriptional control of autophagy-lysosome function drives pancreatic cancer metabolism. *Nature*, *524*(7565), 361–365. https://doi.org/10.1038/nature14587

Phelep, A., Laouari, D., Bharti, K., Burtin, M., Tammaccaro, S., Garbay, S., … Terzi, F. (2017). MITF - A controls branching morphogenesis and nephron endowment. *PLoS Genetics*, *13*(12), e1007093. https://doi.org/10.1371/journal.pgen.1007093

Phung, B., Kazi, J. U., Lundby, A., Bergsteinsdottir, K., Sun, J., Goding, C. R., … Ronnstrand, L. (2017). KIT(D816V) induces SRC-mediated tyrosine phosphorylation of MITF and altered transcription program in melanoma. *Molecular Cancer Research*, *15*(9), 1265–1274. https://doi.org/10.1158/1541-7786.Mcr-17-0149

Ploper, D., Taelman, V. F., Robert, L., Perez, B. S., Titz, B., Chen, H.-W., … De Robertis, E. M. (2015). MITF drives endolysosomal biogenesis and potentiates Wnt signaling in melanoma cells. *Proceedings of the National Academy of Sciences of the United States of America*, *112*(5), E420–E429. https://doi.org/10.1073/pnas.1424576112

Pogenberg, V., Ballesteros-Álvarez, J., Schober, R., Sigvaldadóttir, I., Obarska-Kosinska, A., Milewski, M., … Wilmanns, M. (2020). Mechanism of conditional partner selectivity in MITF/TFE family transcription factors with a conserved coiled coil stammer motif. *Nucleic Acids Research*, *48*(2), 934–948. https://doi.org/10.1093/nar/gkz1104

Pogenberg, V., Ogmundsdottir, M. H., Bergsteinsdottir, K., Schepsky, A., Phung, B., Deineko, V., … Wilmanns, M. (2012). Restricted leucine zipper dimerization and specificity of DNA recognition of the melanocyte master regulator MITF. *Genes and Development*, *26*(23), 2647–2658. https://doi.org/10.1101/gad.198192.112

Primot, A., Mogha, A., Corre, S., Roberts, K., Debbache, J., Adamski, H., … Galibert, M.-D. (2010). ERK-regulated differential expression of the Mitf 6a/b splicing isoforms in melanoma. *Pigment Cell and Melanoma Research*, *23*(1), 93–102. https://doi.org/10.1111/j.1755-148X.2009.00652.x

Puertollano, R., Ferguson, S. M., Brugarolas, J., & Ballabio, A. (2018). The complex relationship between TFEB transcription factor phosphorylation and subcellular localization. *The EMBO Journal*, *37*(11), e98804. https://doi.org/10.15252/embj.201798804

Raben, N., & Puertollano, R. (2016). TFEB and TFE3: Linking lysosomes to cellular adaptation to stress. *Annual Review of Cell and Developmental Biology*, *32*, 255–278. https://doi.org/10.1146/annurev-cellbio-111315-125407

Rehli, M., Den Elzen, N., Cassady, A. I., Ostrowski, M. C., & Hume, D. A. (1999). Cloning and characterization of the murine genes for bHLH-ZIP transcription factors TFEC and TFEB reveal a common gene organization for all MiT subfamily members. *Genomics*, *56*(1), 111–120. https://doi.org/10.1006/geno.1998.5588

Rehli, M., Lichanska, A., Cassady, A. I., Ostrowski, M. C., & Hume, D. A. (1999). TFEC is a macrophage-restricted member of the microphthalmia-TFE subfamily of basic helix-loop-helix leucine zipper transcription factors. *The Journal of Immunology*, *162*(3), 1559–1565.

Roczniak-Ferguson, A., Petit, C. S., Froehlich, F., Qian, S., Ky, J., Angarola, B., … Ferguson, S. M. (2012). The transcription factor TFEB links mTORC1 signaling to transcriptional control of lysosome homeostasis. *Science Signaling*, *5*(228), ra42. https://doi.org/10.1126/scisignal.2002790

Ross, H., & Argani, P. (2010). Xp11 translocation renal cell carcinoma. *Pathology*, *42*(4), 369–373. https://doi.org/10.3109/00313021003767348

Sardiello, M., Palmieri, M., di Ronza, A., Medina, D. L., Valenza, M., Gennarino, V. A., … Ballabio, A. (2009). A gene network regulating lysosomal biogenesis and function. *Science*, *325*(5939), 473–477. https://doi.org/10.1126/science.1174447

Seo, E. Y., Jin, S.-P., Sohn, K.-C., Park, C.-H., Lee, D. H., & Chung, J. H. (2017). UCHL1 regulates melanogenesis through controlling MITF stability in human melanocytes. *Journal of Investigative Dermatology*, *137*(8), 1757–1765. https://doi.org/10.1016/j.jid.2017.03.024

Settembre, C., & Ballabio, A. (2011). TFEB regulates autophagy: An integrated coordination of cellular degradation and recycling processes. *Autophagy*, *7*(11), 1379–1381. https://doi.org/10.4161/auto.7.11.17166

Settembre, C., Di Malta, C., Polito, V. A., Arencibia, M. G., Vetrini, F., Erdin, S., … Ballabio, A. (2011). TFEB links autophagy to lysosomal biogenesis. *Science*, *332*(6036), 1429–1433. https://doi.org/10.1126/science.1204592

Settembre, C., Zoncu, R., Medina, D. L., Vetrini, F., Erdin, S., Erdin, S. U., … Ballabio, A. (2012). A lysosome-to-nucleus signalling mechanism senses and regulates the lysosome via mTOR and TFEB. *The EMBO Journal*, *31*(5), 1095–1108. https://doi.org/10.1038/emboj.2012.32

Sha, Y., Rao, L., Settembre, C., Ballabio, A., & Eissa, N. T. (2017). STUB1 regulates TFEB-induced autophagy-lysosome pathway. *The EMBO Journal*, *36*(17), 2544–2552. https://doi.org/10.15252/embj.201796699

Sharma, S. M., Bronisz, A., Hu, R., Patel, K., Mansky, K. C., Sif, S., & Ostrowski, M. C. (2007). MITF and PU.1 recruit p38 MAPK and NFATc1 to target genes during osteoclast differentiation. *Journal of Biological Chemistry*, *282*(21), 15921–15929. https://doi.org/10.1074/jbc.M609723200

Shibahara, S., Yasumoto, K., Amae, S., Udono, T., Watanabe, K., Saito, H., & Takeda, K. (2000). Regulation of pigment cell-specific gene expression by MITF. *Pigment Cell Research*, *13*(Suppl 8), 98–102. https://doi.org/10.1034/j.1600-0749.13.s8.18.x

Shipley, J. M., Birdsall, S., Clark, J., Crew, J., Gill, S., Linehan, M., … Cooper, C. S. (1995). Mapping the X chromosome breakpoint in two papillary renal cell carcinoma cell lines with a t(X;1)(p11.2;q21.2) and the first report of a female case. *Cytogenetics and Cell Genetics*, *71*(3), 280–284. https://doi.org/10.1159/000134127

Smith, S. D., Kelley, P. M., Kenyon, J. B., & Hoover, D. (2000). Tietz syndrome (hypopigmentation/deafness) caused by mutation of MITF. *Journal of Medical Genetics*, *37*(6), 446–448. https://doi.org/10.1136/jmg.37.6.446

Steingrímsson, E., Copeland, N. G., & Jenkins, N. A. (2004). Melanocytes and the microphthalmia transcription factor network. *Annual Review of Genetics*, *38*(1), 365–411. https://doi.org/10.1146/annurev.genet.38.072902.092717

Steingrímsson, E., Moore, K. J., Lamoreux, M. L., Ferré-D'Amaré, A. R., Burley, S. K., Sanders Zimring, D. C., … Jenkins, N. A. (1994). Molecular basis of mouse microphthalmia (mi) mutations helps explain their developmental and phenotypic consequences. *Nature Genetics*, *8*(3), 256–263. https://doi.org/10.1038/ng1194-256

Takeda, K., Takemoto, C., Kobayashi, I., Watanabe, A., Nobukuni, Y., Fisher, D. E., & Tachibana, M. (2000). Ser298 of MITF, a mutation site in Waardenburg syndrome type 2, is a phosphorylation site with functional significance. *Human Molecular Genetics*, *9*(1), 125–132. https://doi.org/10.1093/hmg/9.1.125

Takeda, K., Yasumoto, K.-I., Kawaguchi, N., Udono, T., Watanabe, K.-I., Saito, H., … Shibahara, S. (2002). Mitf-D, a newly identified isoform, expressed in the retinal pigment epithelium and monocyte-lineage cells affected by Mitf mutations. *Biochimica et Biophysica Acta (BBA) - Gene Structure and Expression*, *1574*(1), 15–23. https://doi.org/10.1016/S0167-4781(01)00339-6

Takemoto, C. M., Yoon, Y.-J., & Fisher, D. E. (2002). The identification and functional characterization of a novel mast cell isoform of the microphthalmia-associated transcription factor. *The Journal of Biological Chemistry*, *277*(33), 30244–30252. https://doi.org/10.1074/jbc.m201441200

Tassabehji, M., Newton, V. E., & Read, A. P. (1994). Waardenburg syndrome type 2 caused by mutations in the human microphthalmia (MITF) gene. *Nature Genetics*, *8*(3), 251–255. https://doi.org/10.1038/ng1194-251

Tshori, S., Sonnenblick, A., Yannay-Cohen, N., Kay, G., Nechushtan, H., & Razin, E. (2007). Microphthalmia transcription factor isoforms in mast cells and the heart. *Molecular and Cellular Biology*, *27*(11), 3911–3919. https://doi.org/10.1128/MCB.01455-06

Udono, T., Yasumoto, K.-I., Takeda, K., Amae, S., Watanabe, K.-I., Saito, H., … Shibahara, S. (2000). Structural organization of the human microphthalmia-associated transcription factor gene containing four alternative promoters. *Biochimica et Biophysica Acta (BBA) - Gene Structure and Expression*, *1491*(1–3), 205–219. https://doi.org/10.1016/s0167-4781(00)00051-8

Vega-Rubin-de-Celis, S., Peña-Llopis, S., Konda, M., & Brugarolas, J. (2017). Multistep regulation of TFEB by MTORC1. *Autophagy*, *13*(3), 464–472. https://doi.org/10.1080/15548627.2016.1271514

Wang, C., Zhao, L. U., Su, Q., Fan, X., Wang, Y., Gao, S., … Liu, Z. (2016). Phosphorylation of MITF by AKT affects its downstream targets and causes TP53-dependent cell senescence. *International Journal of Biochemistry and Cell Biology*, *80*, 132–142. https://doi.org/10.1016/j.biocel.2016.09.029

Wang, Y., Radfar, S., Liu, S., Riker, A. I., & Khong, H. T. (2010). Mitf-Mdel, a novel melanocyte/melanoma-specific isoform of microphthalmia-associated transcription factor-M, as a candidate biomarker for melanoma. *BMC Medicine*, *8*(1), 14. https://doi.org/10.1186/1741-7015-8-14

Weilbaecher, K. N., Motyckova, G., Huber, W. E., Takemoto, C. M., Hemesath, T. J., Xu, Y., … Fisher, D. E. (2001). Linkage of M-CSF signaling to Mitf, TFE3, and the osteoclast defect in Mitf(mi/mi) mice. *Molecular Cell*, *8*(4), 749–758. https://doi.org/10.1016/s1097-2765(01)00360-4

Wu, M., Hemesath, T. J., Takemoto, C. M., Horstmann, M. A., Wells, A. G., Price, E. R., … Fisher, D. E. (2000). c-Kit triggers dual phosphorylations, which couple activation and degradation of the essential melanocyte factor Mi. *Genes and Development*, *14*(3), 301–312.

Xu, W., Gong, L., Haddad, M. M., Bischof, O., Campisi, J., Yeh, E. T., & Medrano, E. E. (2000). Regulation of microphthalmia-associated transcription factor MITF protein levels by association with the ubiquitin-conjugating enzyme hUBC9. *Experimental Cell Research*, *255*(2), 135–143. https://doi.org/10.1006/excr.2000.4803

Yasumoto, K., Amae, S., Udono, T., Fuse, N., Takeda, K., & Shibahara, S. (1998). A big gene linked to small eyes encodes multiple Mitf isoforms: Many promoters make light work. *Pigment Cell Research*, *11*(6), 329–336. https://doi.org/10.1111/j.1600-0749.1998.tb00491.x

Ye, H., Qin, S., Li, N., Lin, M., Xu, Y., & Li, X. (2019). A rare partner of TFE3 in the Xp11 translocation renal cell carcinoma: clinicopathological analyses and detection of MED15-TFE3 fusion. *BioMed Research International*, *2019*, 5974089. https://doi.org/10.1155/2019/5974089

Yokoyama, S., Woods, S. L., Boyle, G. M., Aoude, L. G., MacGregor, S., Zismann, V., … Brown, K. M. (2011). A novel recurrent mutation in MITF predisposes to familial and sporadic melanoma. *Nature*, *480*(7375), 99–103. https://doi.org/10.1038/nature10630

Zhang, J., Wang, J., Zhou, Z., Park, J.-E., Wang, L., Wu, S., … Shen, H.-M. (2018). Importance of TFEB acetylation in control of its transcriptional activity and lysosomal function in response to histone deacetylase inhibitors. *Autophagy*, *14*(6), 1043–1059. https://doi.org/10.1080/15548627.2018.1447290

Zhang, T., Zhou, Q., Ogmundsdottir, M. H., Moller, K., Siddaway, R., Larue, L., … Pignoni, F. (2015). Mitf is a master regulator of the v-ATPase, forming a control module for cellular homeostasis with v-ATPase and TORC1. *Journal of Cell Science*, *128*(15), 2938–2950. https://doi.org/10.1242/jcs.173807

Zhang, X., Cheng, X., Yu, L. U., Yang, J., Calvo, R., Patnaik, S., … Xu, H. (2016). MCOLN1 is a ROS sensor in lysosomes that regulates autophagy. *Nature Communications*, *7*, 12109. https://doi.org/10.1038/ncomms12109

Zhao, X., Fiske, B., Kawakami, A., Li, J., & Fisher, D. E. (2011). Regulation of MITF stability by the USP13 deubiquitinase. *Nature Communications*, *2*(1), 414. https://doi.org/10.1038/ncomms1421

Zhong, M., De Angelo, P., Osborne, L., Paniz-Mondolfi, A. E., Geller, M., Yang, Y., … Cai, D. (2012). Translocation renal cell carcinomas in adults: A single-institution experience. *The American Journal of Surgical Pathology*, *36*(5), 654–662. https://doi.org/10.1097/PAS.0b013e31824f24a6

How to cite this article: Vu HN, Dilshat R, Fock V, Steingrímsson E. User guide to MiT-TFE isoforms and post-translational modifications. *Pigment Cell Melanoma Res*. 2021;34:13–27. https://doi.org/10.1111/pcmr.12922

Appendix 1

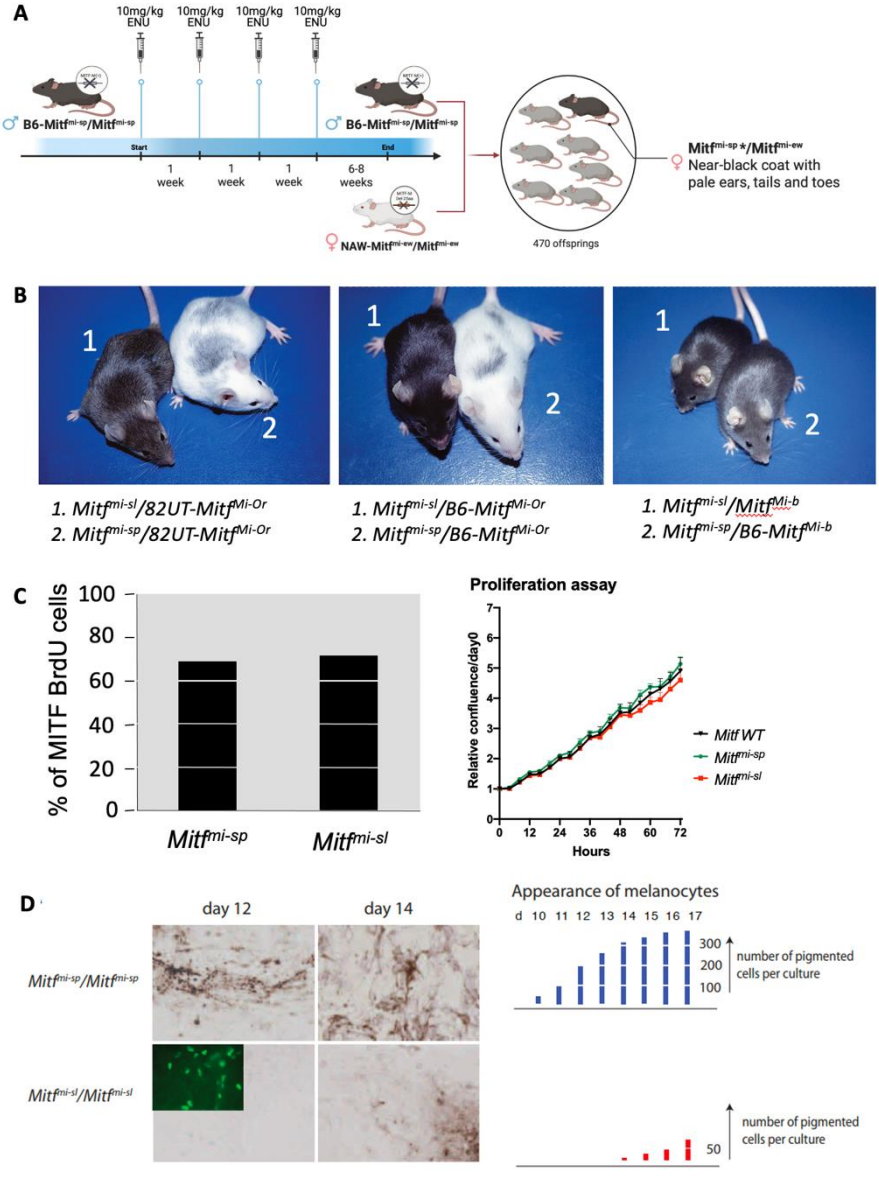
A
10mg/kg ENU
10mg/kg ENU
10mg/kg ENU
10mg/kg ENU
♂ B6-Mitf^mi-sp/Mitf^mi-sp
Start
End
1 week
1 week
1 week
6-8 weeks
♀ NAW-Mitf^mi-ew/Mitf^mi-ew
470 offsprings
Mitf^mi-sp */Mitf^mi-ew
Near-black coat with pale ears, tails and toes
B
1. Mitf^mi-sl/82UT-Mitf^Mi-Or
2. Mitf^mi-sp/82UT-Mitf^Mi-Or
1. Mitf^mi-sl/B6-Mitf^Mi-Or
2. Mitf^mi-sp/B6-Mitf^Mi-Or
1. Mitf^mi-sl/Mitf^Mi-b
2. Mitf^mi-sp/B6-Mitf^Mi-b
C
% of MITF BrdU cells
Mitf^mi-sp
Mitf^mi-sl
Proliferation assay
Relative confluence/day0
Hours
Mitf WT
Mitf^mi-sp
Mitf^mi-sl
D
day 12
day 14
Mitf^mi-sp/Mitf^mi-sp
Mitf^mi-sl/Mitf^mi-sl
Appearance of melanocytes
d 10 11 12 13 14 15 16 17
number of pigmented cells per culture
number of pigmented cells per culture

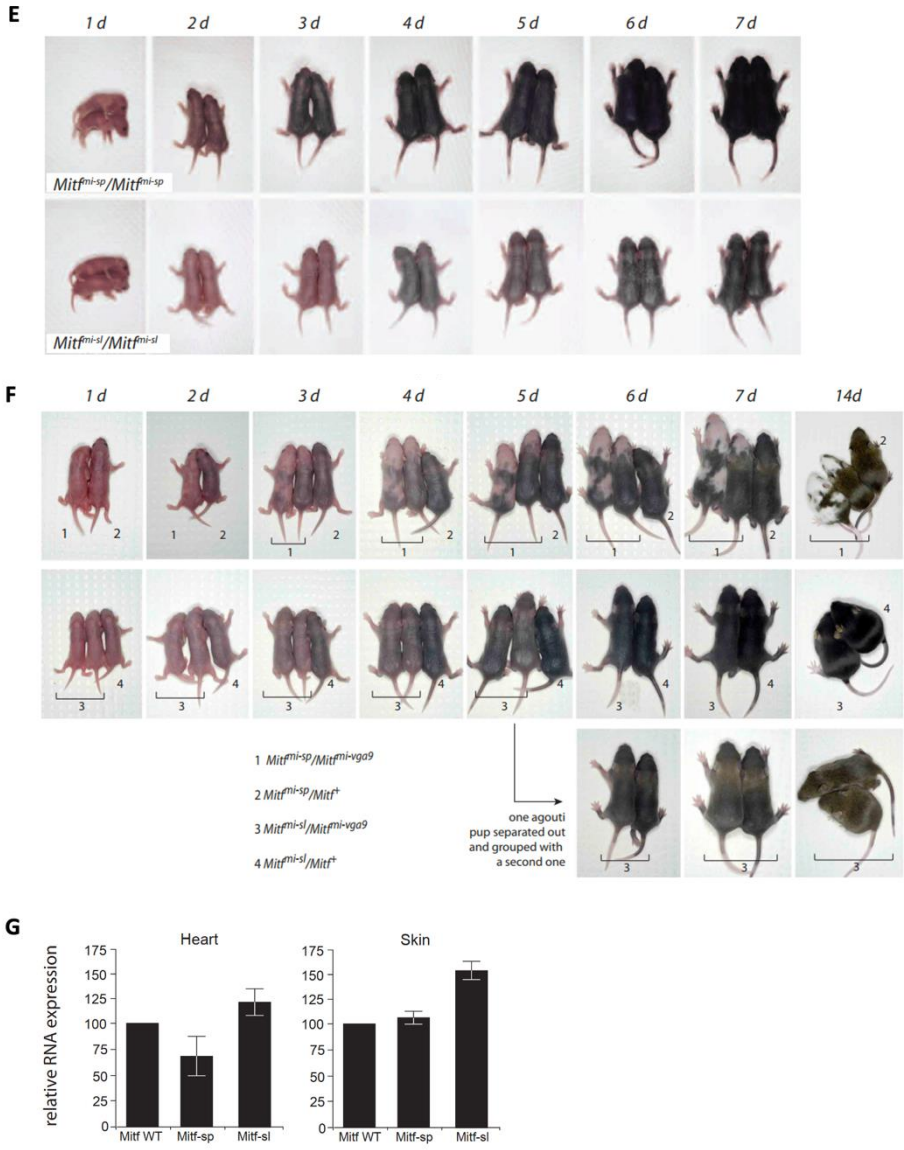

(A) Schematic of generation of a *Mitf* suppressor mutation in mouse **(B)** 82UT-*Mitf*$^{Mi\text{-}Or}$/B6-*Mitf*$^{mi\text{-}sp*}$ and 82UT-*Mitf*$^{Mi\text{-}Or}$/B6-*Mitf*$^{mi\text{-}sp}$ compound heterozygotes. B6-*Mitf*$^{mi\text{-}sp*}$/B6-*Mitf*$^{Mi\text{-}Or}$ *and B6-Mitf*$^{mi\text{-}sp}$/B6-*Mitf*$^{Mi\text{-}Or}$ compound heterozygotes. B6-*Mitf*$^{mi\text{-}sp*}$/B6-*Mitf*$^{Mi\text{-}b}$ and B6-*Mitf*$^{mi\text{-}sp}$/B6-*Mitf*$^{Mi\text{-}b}$ animals. **(C)** Percentage of BrdU-positive cells was assessed. Error bars represent SEM of three independent experiments and relative cell confluence compared to day 0 obtained from IncuCyte proliferation assay was plotted for A375P

expressing either *Mitf-WT, Mitf$^{mi\text{-}sp,}$ or Mitf$^{mi\text{-}sl}$*. Error bars represent SEM of three independent experiments. **(D)** Melanocytes differentiating from neural crest cultures from *Mitf$^{mi\text{-}sl}$* and *Mitf$^{mi\text{-}sp}$* animals show that pigmentation is severely delayed in *Mitf$^{mi\text{-}sl}$* homozygotes compared to *Mitf$^{mi\text{-}sp}$* homozygotes. Nevertheless, melanoblasts are present, as evidenced by anti-MITF antibody staining (inset). **(E)** Homozygous *Mitf$^{mi\text{-}sl}$* newborns show delayed onset of pigmentation compared to *Mitf$^{mi\text{-}sp}$* homozygotes, particularly clearly visible at postnatal day-2 and 3. **(F)** No difference in the onset of pigmentation in compound heterozygous condition with *Mitf$^{mi\text{-}vga9}$*. Compare mice labeled #1 (*Mitf$^{mi\text{-}sp}$/Mitf$^{mi\text{-}vga9}$*) with mice labeled #3 (*Mitf$^{mi\text{-}sl}$/Mitf$^{mi\text{-}vga9}$*). **(G)** Relative RNA expression levels in wild type, *Mitf$^{mi\text{-}sp,}$* and *Mitf$^{mi\text{-}sl}$* heart and skin, as determined by qPCR.

Appendix 2

Splicing variants of human PRDM7 and PRDM9 (Fumasoni et al., 2007)

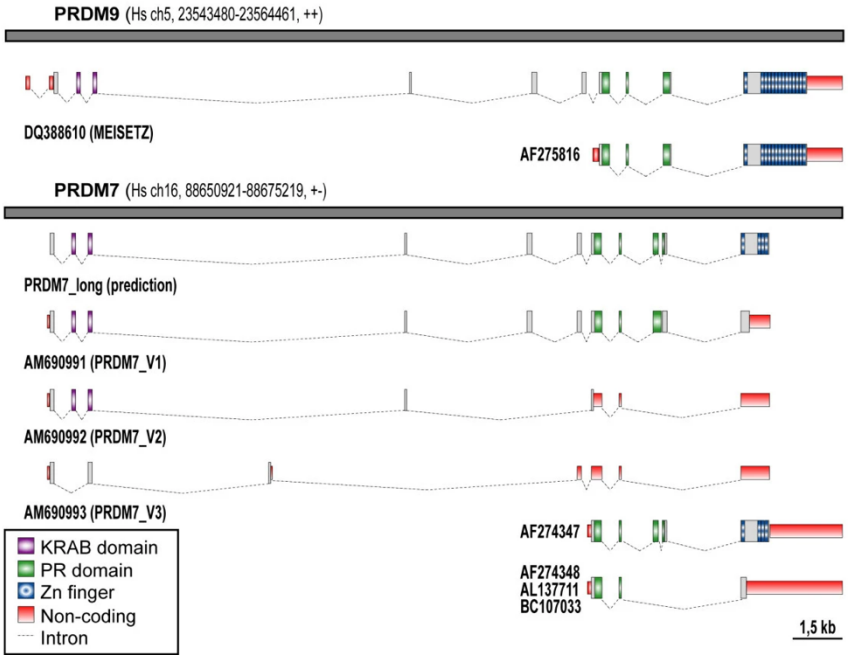

Appendix 3

ChIP-seq track of MITF ChIP-seq performed in 501Mel cells (Laurette et al., 2015) taken from UCSC genome browser.

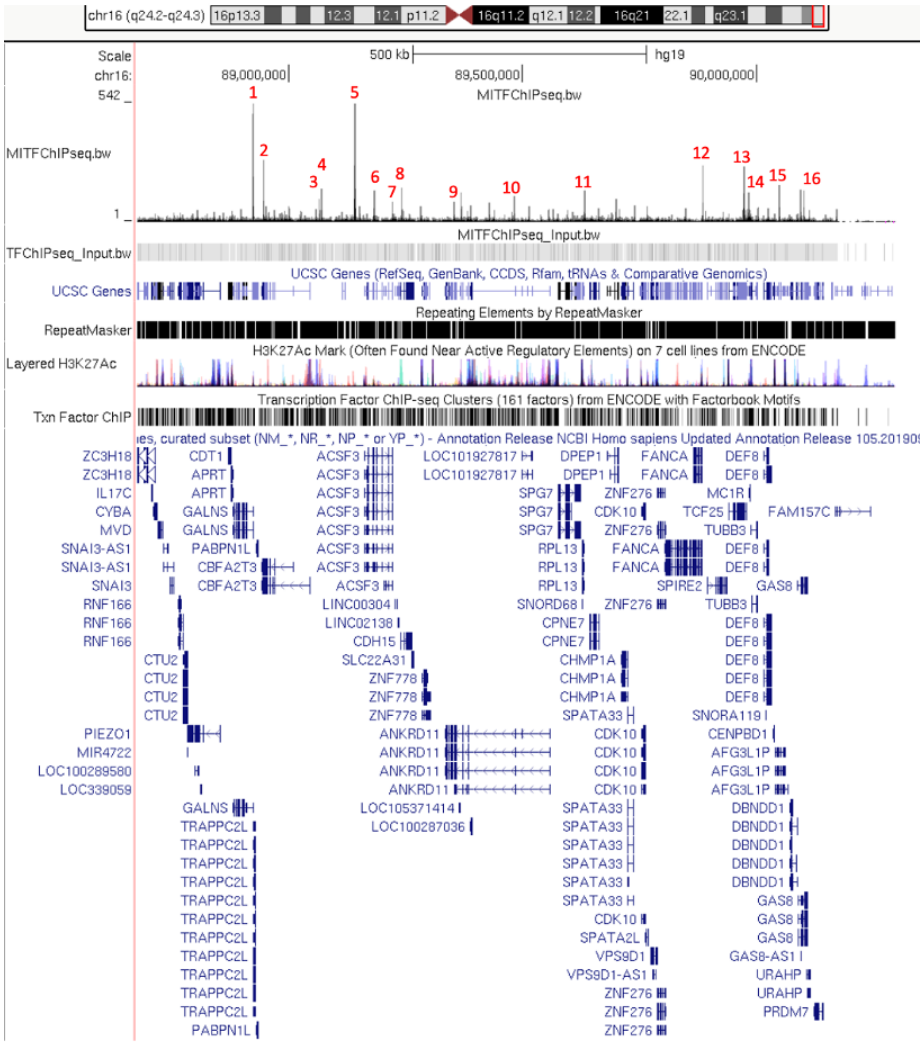

Hi-C data from SKMel5 melanoma cells suggests long-range interactions between the areas containing MITF-Chip-peaks and the PRDM7 promoter region (http://3dgenome.fsm.northwestern.edu/view.php).

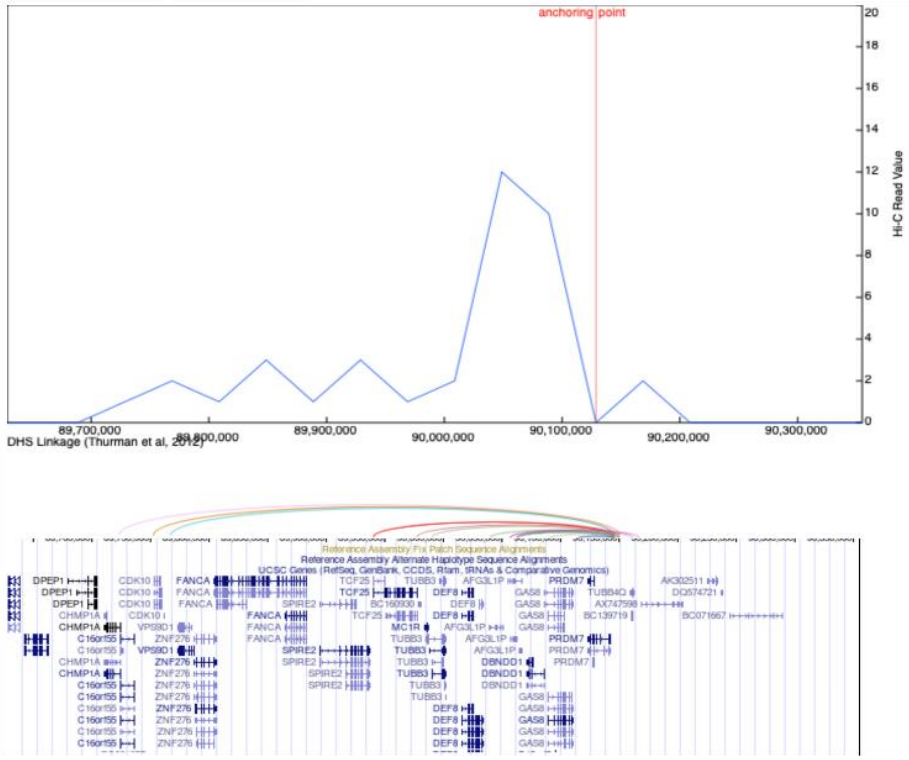

Appendix 4

Predicted transcripts based on RNA-seq data using Stringtie (de novo and reference guide)

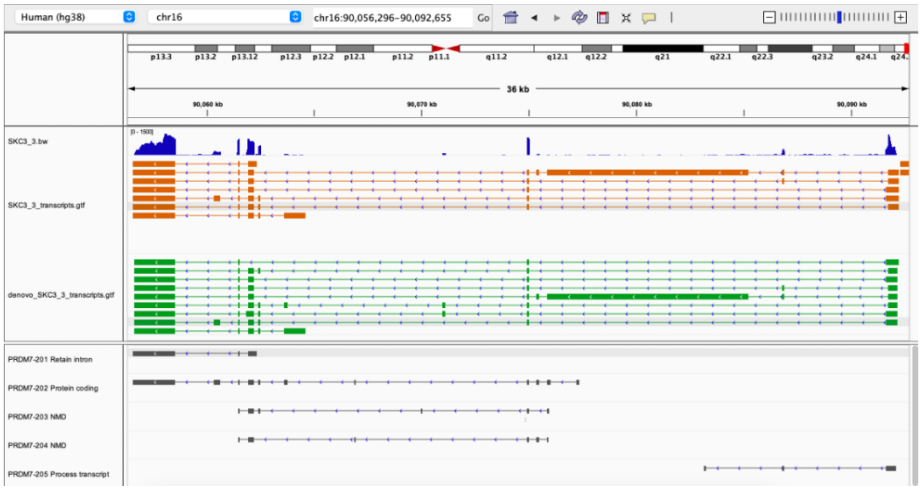

Predicted Junction between exon based on RNA-seq data using StringTie

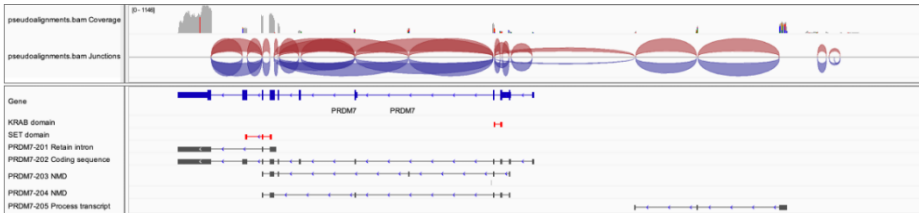

Novel identity sequence PRDM7 isoforms

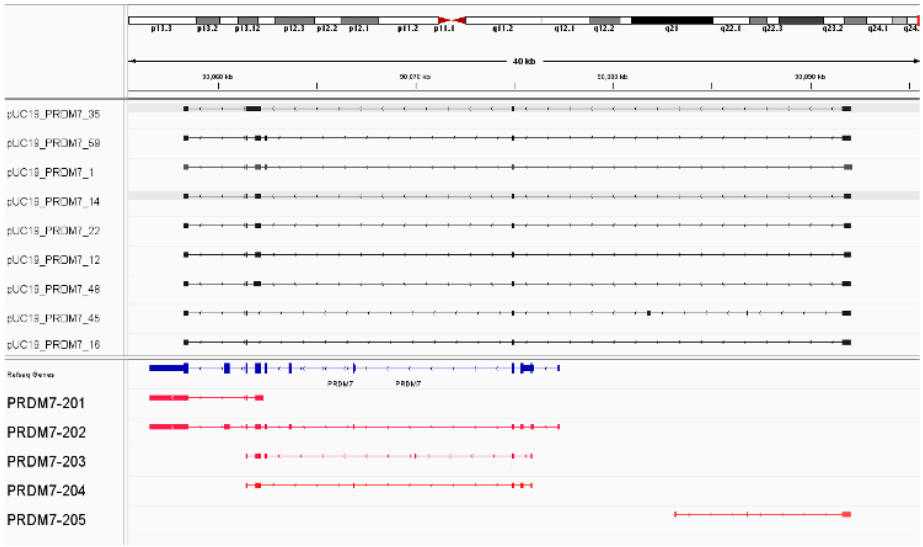

Appendix 5

Clustal O multiple sequence alignment of KRAB and SET domains of PRDM7 and PRD

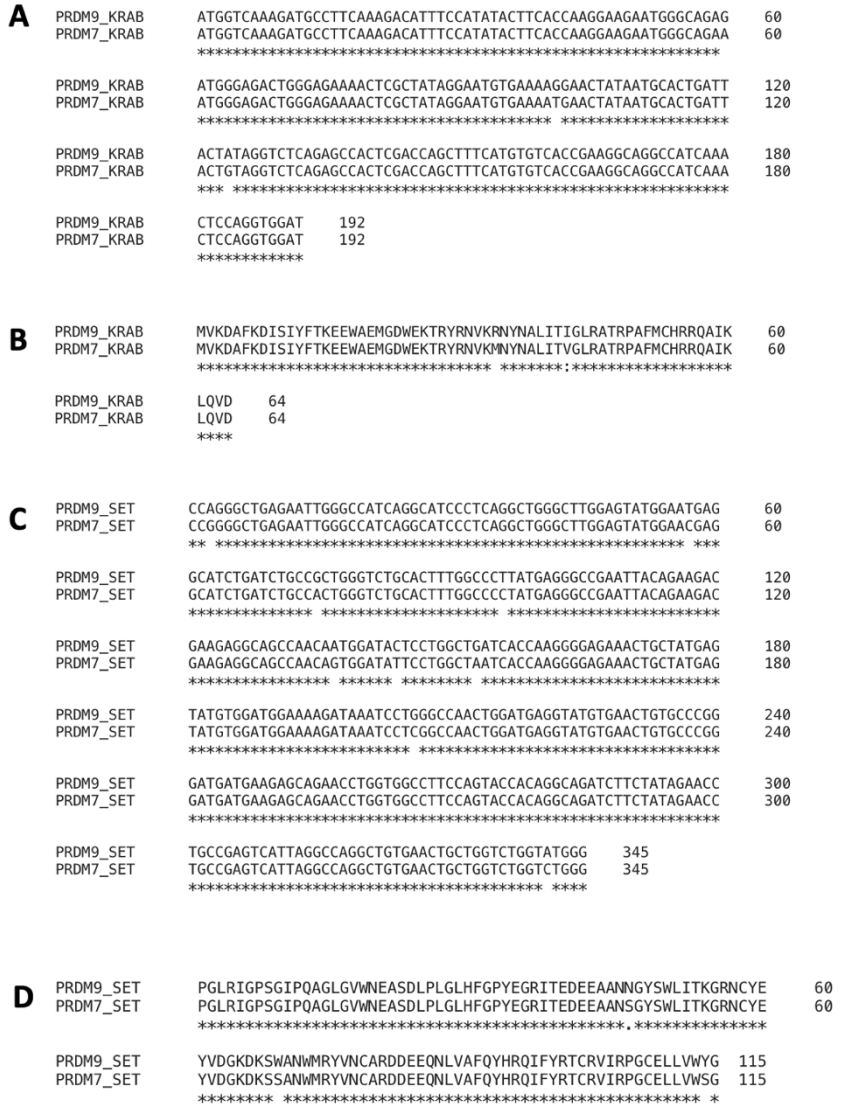

Appendix 6

Primers used for qPCR

Primer name	Sequence
PRDM7-cDNA-qPCR_F	CCTGGCTAATCACCAAGGGG
PRDM7-cDNA-qPCR_R	CGGGCACAGTTCACATACCT
PRDM9-cDNA-qPCR-F	GTTTGAAAGAATTGTCAAGAACAGC
PRDM9-cDNA-qPCR-R	TCCTTCTTCCTGAGTTCCAGTTT
PRDM9_cDNA_Zin_Fwd	TAGCGATAGGTCAAGCCTCTG
PRDM9_cDNA_Zin_Rev	ACTTACTCATCCTCCCTGCAGAC

The alignment of 501Mel-PRDM7-KO cell lines and their corresponding control confirm the acquired mutations in PRDM7-KO cell lines.

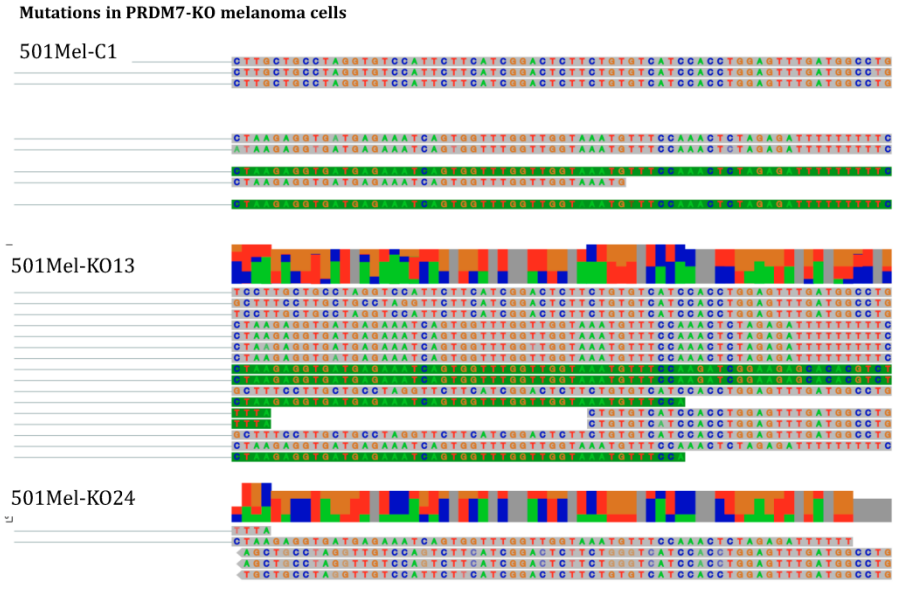

The alignment of SKmel28-PRDM7-KO cell lines and their corresponding control confirm the acquired mutations in PRDM7-KO cell lines.